# Appendix A

## Bearing capacity formulae

The drained bearing capacity formula is as follows,

$$V_{max} = A'\left( \tfrac{1}{2}\gamma\, B'\, N_\gamma\, s_\gamma\, d_\gamma\, i_\gamma + q\, N_q\, s_q\, d_q\, i_q \right) \qquad [A.1]$$

where

| | |
|---|---|
| $V_{max}$ | vertical failure load |
| $\gamma'$ | effective unit weight |
| $q$ | overburden pressure, $q = z\gamma'$ where $z$ is foundation embedment |
| $A'$ | effective foundation area |
| $B'$ | minimum effective foundation dimension |
| $N_\gamma$, $N_q$ | bearing capacity factors |
| $s_\gamma$, $s_q$ | shape factors |
| $d_\gamma$, $d_q$ | depth factors |
| $i_\gamma$, $i_q$ | load inclination factors |

The definitions of the factors in Equation A.1 - suggested by Brinch Hansen (1970), Meyerhof (1963) and Vesic (1975) - are listed in Table A.1. The API (1993) procedure for determining the effective foundation dimensions (see Figure 2.6) gives

$$A' = B'L' = \pi R^2 - 2e\sqrt{R^2 - e^2} - 2R^2 \sin^{-1}_{\text{radians}}\left(\frac{e}{R}\right) \qquad [A.2a]$$

$$\frac{L'}{B'} = \sqrt{\frac{R+e}{R-e}} \qquad [A.2b]$$

In the case of a central load (*i.e.* when $e = 0$), using $B'$ derived from Equations A.2a and A.2b instead of $2R$ results in a reduction of 13% in the ultimate load. De Beer (1970) used $B' = 2R$ when developing the shape factors.

# Appendix B

## Footing displacements from small LVDTs

An arrangement of three small LVDTs was used to measure the displacement of the footing relative to the specimen container. This is discussed in Section 3.3.3 and the LVDT frame is shown in Figure 3.11. A calculation procedure for deriving the displacements of the footing from the measurements of the three small LVDTs is given below.

The parameters used in the calculation are shown in Figure B.1. Points *A*, *B*, and *C* represent the ends of the LVDTs that were fixed to the LVDT frame, which was fixed to the specimen container. Points *D* and *E* represent the ends of the LVDTs that were fixed to the footing. The thick dotted lines in Figure B.1 represent the three LVDTs. These lengths change as the footing displaces. Point *G* represents the load and displacement reference point at the centre of the bottom of the footing. Point *A* is set as the origin and the downward ($y$) and rightward ($x$) directions are taken as positive. The position of point *E* is determined from transducers DSV2 and DSH. Points *D* and *G* are then determined by considering DSV1. The length of *DE* and *GH* are fixed, and point *H* is located midway along *DE*.

<u>Point *E*</u>

Consider the triangle *BCE* in Figure B.1. By the cosine rule,

$$\angle BCE = \cos^{-1}\left(\frac{BC^2 + CE^2 - BE^2}{2(BC)(CE)}\right) \qquad [B.1]$$

where *BE* and *CE* are given by DSV2 and DSH respectively, and *BC* is fixed and known from the geometry of the frame. Angle *BCE* is used to deduce the co-ordinates of *E*,

$$\begin{aligned} x_E &= x_C - (CE)\sin(\pi - \angle BCE - \angle BCF) \\ y_E &= y_C + (CE)\cos(\pi - \angle BCE - \angle BCF) \end{aligned} \qquad [B.2a;B.2b]$$

where the co-ordinates of *C* and the angle *BCF* are known.

<u>Point *D*</u>

The length *AE* and angle *DAB* are needed to find the co-ordinates of *D*. From the co-ordinates of *A* and *E*,

$$AE = \sqrt{x_E^{\,2} + y_E^{\,2}} \qquad [B.3]$$

since $A$ is taken as the origin. The angle $DAB$ is equal to the sum of angles $BAE$ and $DAE$, and is given by,

$$\angle DAB = \cos^{-1}\left(\frac{AB^2 + AE^2 - BE^2}{2(AB)(BE)}\right) + \cos^{-1}\left(\frac{AD^2 + AE^2 - DE^2}{2(AD)(AE)}\right) \qquad [B.4]$$

Angle $DAB$ is used to deduce the co-ordinates of $D$,

$$\begin{aligned} x_D &= (AD)\cos\angle DAB \\ y_D &= (AD)\sin\angle DAB \end{aligned} \qquad [B.5a;B.5b]$$

Point $G$

The rotation of the $G$ about the vertical is equivalent to the rotation of the footing ($\theta$) and is given by,

$$\theta = \tan^{-1}\left(\frac{y_E - y_D}{x_E - x_D}\right) \qquad [B.6]$$

The co-ordinates of $G$ are,

$$\begin{aligned} x_G &= x_D + (DG)\sin\left(\frac{\pi}{2} - \angle GDH - \theta\right) \\ y_G &= y_D + (DG)\cos\left(\frac{\pi}{2} - \angle GDH - \theta\right) \end{aligned} \qquad [B.7]$$

where length $DG$ and angle $GDH$ are known from the geometry of the footing and the footing/LVDT connecting beam shown in Figure 3.11.

The co-ordinates of G ($x_G$, $y_G$) represent the linear displacements of the footing ($w$, $u$) and the angle $\theta$ represents the rotation. The footing tests were initialised with the LVDT frame and the footing level ($y_A = y_B = 0$ and $y_D = y_E$ respectively), and with DSV1 and DSV2 vertical.

# References


Aas, P. M. & Andersen, K. H. (1992). Skirted foundations for offshore structures. *Proc. 9th Offshore South East Asia Conf., Singapore*, 1-8.

Allard, M. A., Andersen, K. H. and Hermstad, J. (1994). Centrifuge model tests of a gravity platform on very dense sand. I: Testing technique and results. *Proc. 7th Conf. on Behaviour of Offshore Structures, Boston*, **1**, pp. 231-254.

Altaee, A. & Fellenius, B. H. (1994). Physical modeling in sand. *Canadian Geotechnical Journal* **31**(3), 420-431.

Americam Petroleum Institute (1993). *Recommended practice for planning, designing and constructing fixed offshore platforms - load and resistance factor design*. RP 2A-LRFD, 1st ed. Washington DC: American Petroleum Institute.

Andersen, K. H. (1972). Bearing capacity of shallow foundations on cohesionless soils. *Internal report 51404-1*.Oslo: Norwegian Geotechnical Institute.

API (1993). *See* American Petroleum Institute (1993).

Atkinson, J. H. (1992). A note on modelling small strain stiffness in Cam-Clay. *Predictive Soil Mechanics (Proc. Wroth Memorial Sym., Oxford)*, 34-39. London: Thomas Telford.

Barltrop, N. D. P. & Adams, A. J. (1991). *Dynamics of fixed marine structures*. 3rd ed. UK: Butterworth-Heinemann Ltd.

Basma, A. A. (1994). Risk-reduction factor for bearing capacity of shallow foundations. *Canadian Geotechnical Journal* **31**(1), 12-16.

Been, K., and Jefferies, M. G. (1985). A state parameter for sands. *Géotechnique* **35**(2), 99-112.

Been, K., Jefferies, M. G. and Hachey, J. (1991). The critical state of sands. *Géotechnique* **41**(3), 365-381.

Bell, R. W. (1991). *The analysis of offshore foundations subjected to combined loading*. M.Sc. thesis, University of Oxford.

Bielby, F. (1989). *Triaxial tests on oil saturated sand*. Part II project report, Cambridge University Engineering Department.

Biot, M. A. (1941). General theory of three-dimensional consolidation. *J. Applied Physics* **12**, 155.

Bolton, M. D. (1986). The strength and dilatancy of sands. *Géotechnique* **36**(1), 65-78.

Bolton, M. D. (1987). The strength and dilatancy of sands (discussion). *Géotechnique* **37**(2), 219-226.

Bolton, M. D. and Lau, C. K. (1993). Vertical bearing capacity factors for circular and strip footings on Mohr-Coulomb soil. *Canadian Geotechnical Journal* **30**(6), 1024-1033.

Bossinesq, J (1885). Application des potentiels à l' équilibre et du mouvements des solides élastiques. Paris: Gauthier-Villars.

Bransby, P. L. (1973). Cambridge contact stress transducers. *Report no. CUED/C-SOILS/LN2*, Cambridge University Engineering Deparment.

Brinch Hansen, J. (1970). A revised and extended formula for bearing capacity. *Bulletin no. 28*, 5-11. Copenhagen: Danish Geotechnical Institute.

Butterfield, R. (1981). Another look at gravity platform foundations. Presented at CISM course *Soil Mech. and Foundation Eng. in Offshore Technology, Udine*.

Butterfield, R. & Gottardi, G. (1994). A complete three-dimensional failure envelope for shallow footings on sand (technical note). *Géotechnique* **44**(1), 181-184.

Butterfield, R., Houlsby, G. T. & Gottardi, G. (1997). Standardised sign conventions and notation for generally loaded foundations. *Géotechnique* **47**(5), 1051-1054.

Butterfield, R. & Ticof, J. (1979). Design parameters for granular soils (discussion contribution). *Proc. 7th European Conf. on Soil Mech. and Foundation Eng., Brighton*, **4**, 259-261.

Bye, A., Erbrich, C., Rognlien, B. & Tjelta, T. (1995). Geotechnical design of bucket foundations. *Proc. 27th Offshore Technology Conf., Houston*, OTC 7793.

Byrne, P. M. & Finn, W. D. L. (1978). Breakout of submerged structures buried to a shallow depth. *Canadian Geotechnical Journal* **15**(2), 146-154.

Byrne, B. W. & Houlsby, G. T. (1999). Drained behaviour of suction caisson foundations on very dense sand. *Proc. 31st Offshore Technology Conf., Houston*, OTC 10994.

Cassidy, M. J. (1996). *The behaviour of jack-up platforms*. First year report, University of Oxford.

Cassidy, M. J. (1999). *The non-linear dynamic response of jack-up units subjected to random wave loading*. D.Phil. thesis (to be published), University of Oxford.

Chiarella, C. & Booker, J. R. (1975). The time-settlement behaviour of a rigid elastic die resting on a deep clay layer. *Q. J. Mech. Appl. Math.* **28**(3), 317-328.

Chu, J. (1995). An Experimental examination of the critical state and other similar concepts for granular soils. *Canadian Geotechnical Journal* **32**(6), 1065-1075.

Corté, J. F. (1989). Model testing - geotechnical model tests (general report, discussion session 11). *Proc. 12th Int. Conf. on Soil Mech. and Foundation Eng., Rio de Janeiro*, **3**, 2553-2571.

Cox, A. D. (1962). Axially symmetric plastic deformations in soils - II. Indentation of ponderable soils. *Int. J. Mech. Sciences* **4**, 371-380.

Cox, A. D., Eason, G. & Hopkins, H. G. (1961). Axially symmetric plastic deformations in soils. *Phil. Trans. Royal Soc. London*, Series A, **25**, 1-45.

Craig, R. F. (1987). *Soil mechanics*. 4th ed. London: Van Nostrand Reinhold.

Davis, E. H. & Poulos, H. G. (1963). Triaxial testing and three-dimensional settlement analysis. *Proc. 4th Aust.-N.Z. Conf. on Soil Mech.* 233.

Davis, E. H. & Poulos, H. G. (1968). The use of elastic theory for settlement prediction under three-dimensional conditions. *Géotechnique* **18**(1), 67-91.

Davis, E. H. & Poulos, H.G. (1972). Rate of settlement under two- and three-dimensional conditions. *Géotechnique* **22**(1), 95-114.

de Beer, E. E. (1965a). Influence of the mean normal stress on the shear strength of sand. *Proc. 6th Int. Conf. on Soil Mech. and Foundation Eng., Montreal*, **1**, 165-169.

de Beer, E. E. (1965b). The scale effect on the phenomenon of progressive rupture in cohesionless soils. *Proc. 6th Int. Conf. on Soil Mech. and Foundation Eng., Montreal*, **2**, 13-17.

de Beer, E. E. (1970). Experimental determination of the shape factors and the bearing capacity factors of sand. *Géotechnique* **20**(4), 387-411.

Dean, E. T. R. (1991). Some potential approximate methods for the preliminary estimation of excess pore pressures and settlement-time curves for submerged circular spud foundations subjected to time-dependent loading. *Report no. CUED/D-Soils/TR240*, Cambridge University Engineering Department.

Dean *et al.* (1992a). *See* Dean, E. T. R., James, R. G., Schofield, A. S., Tan, F. S. C. & Tsukamoto, Y. (1992).

Dean *et al.* (1992b). *See* Dean, E. T. R., James, R. G., Schofield, A. S. & Tsukamoto, Y. (1992).

Dean, E. T. R., James, R. G., Schofield, A. S., Tan, F. S. C. & Tsukamoto, Y. (1992). The bearing capacity of conical footings on sand in relation to the behaviour of spudcan footings of jack-ups. *Predictive Soil Mechanics (Proc. Wroth Memorial Sym., Oxford)*, 230-253. London: Thomas Telford.

Dean, E. T. R., James, R. G., Schofield, A. S. & Tsukamoto, Y. (1992). Combined vertical, horizontal, and moment loading of circular spuds on dense sand foundations. *Report no. CUED/D-Soils/TR244*, Cambridge University Engineering Department.

Douglas, J. F., Gasiorek, J. M. & Swaffield, J. A. (1985). *Fluid mechanics*. 2nd ed. New York: John Wiley and Sons.

Erbrich, C. (1996). Bucket Foundations. *Aust. Centre for Geomech. News Letter* **5**, 1-2.

Eyton, D. G. P. (1982). *Triaxial tests on sands with viscous pore fluid*. Project report, Cambridge University Engineering Department.

Faber, O. (1933). Pressure distribution under bases and the stability of foundations. *Struct. Eng.* **11**(3), 116-125.

Finnie, I. M. S. (1993). *Performance of shallow foundations in calcareous soil*. Ph.D. thesis, University of Western Australia.

Gazetas, G., Dobry, R. & Tassoulas, J. L. (1985). Vertical response of arbitrarily shaped embedded foundations. *Proc. ASCE, J. of the Geotechnical Eng. Div.* **111**(6), 750-771.

Gazetas, G. & Tassoulas, J. L. (1987). Horizontal stiffness of arbitrarily shaped embedded foundations. *Proc. ASCE, J. of the Geotechnical Eng. Div.* **113**(5), 440-457.

Georgiadis, M. & Butterfield, R. (1988). Displacements of footings on sand under eccentric and inclined loads. *Canadian Geotechnical Journal*. **25**(2), 199-212.

Goodman, L. J., Lee, C. N. & Walker, F. J. (1961). The feasibility of vacuum anchorage in soil (correspondence). *Géotechnique* **11**(3), 356-359.

Gottardi, G. & Butterfield, R. (1993). On the bearing capacity of surface footings on sand under general planar loads. *Soils and Foundations* **33**(3), 68-79.

Gottardi, G. & Butterfield, R. (1995). The displacement of a model rigid surface footing on dense sand under general planar loading. *Soils and Foundations* **35**(3), 71-82.

Gottardi, G. & Houlsby, G. T. (1995). Model Tests of Circular Footings on Sand Subjected to Combined Loading. *Report no. OUEL 2071/95*, Oxford University Engineering Laboratory.

Gottardi, G., Houlsby, G. T. & Butterfield, R. (1997). The plastic response of circular footings on sand under general planar loading. *Report no. OUEL 2143/97*, Oxford University Engineering Laboratory.

Griffiths, D. V. (1982). Computation of bearing capacity factors using finite elements. *Géotechnique* **32**(3), 195-202.

Gue, S. S. (1984). *Ground heave around driven piles in clay*. D.Phil. thesis, University of Oxford.

Han, C. & Vardoulakis, I. G. (1991). Plane-strain compression experiments on water-saturated fine-grained sand. *Géotechnique* **41**(1), 49-78.

Hettler, A. & Gudehus, G. (1985). A pressure-dependent correction for displacement results from 1-g model tests with sand. *Géotechnique* **35**(4), 497-510.

Hettler, A. & Gudehus, G. (1988). Influence of the foundation width on the bearing capacity factor. *Soils and Foundations* **28**(4), 81-92.

Hicher, P. Y. (1996). Elastic properties of soils. *Proc. ASCE, J. of the Geotechnical Eng. Div.* **122**(8), 641-648.

Hicks, M. A. & Smith, I. M. (1988). Class A prediction of arctic caisson performance. *Géotechnique* **38**(4), 589-612.

Holubec, I. & D'Appolonia, E. (1973). Effect of particle shape on the engineering properties of granular soils. In *Evaluation of relative density and its role in geotechnical projects involving cohesionless soils*, ASTM STP 523, American Society for Testing and Materials, 304-318.

Houlsby, G. T. (1995). *Geotechnical model testing - Sleipner Vest project*. Main report 1-3 (draft), Civil Engineering Group, University of Oxford.

Houlsby, G. T. & Hitchman, R. (1988). Calibration chamber tests of a cone penetrometer in sand. *Géotechnique* **38**(1), 39-44.

Isaacson, E. de St. Q. & Isaacson, M. de St. Q. (1975). *Dimensional analysis*. London: Edward Arnold.

Ingra, T. S. & Baecher, G. B. (1983). Uncertainty in bearing capacity of sands. *Proc. ASCE, J. of the Geotechnical Eng. Div.* **109**(7), 899-914.

Iwasaki, T., Tatsuoka, F. & Takagi, Y. (1978). Shear moduli of sands under cyclic torsional shear loading. *Soils and Foundations* **18**(1), 39-56.

Jackson, N. & Dhir, R. K. (1988). *Civil engineering materials*. 4th ed. London: MacMillan Education.

Janbu, N. (1985). Soil models in offshore engineering. *Géotechnique* **35**(3), 239-281.

Kerr, A. D. (1989). Tests and analyses of footings on a sand base. *Soil and Foundations* **29**(3), 83-94.

Kolbuszewski, J. (1948). An experimental study of the maximum and minimum porosities of sand. *Proc. 2nd Int. Conf. on Soil Mech. and Foundation Eng., Rotterdam*, **1**, 158-165.

Kolk, H. J. & Campbell, K. J. (1997). Significant developments in offshore geosciences. *Proc. 8th Int. Conf. on Behaviour of Offshore Structures, Delft*, **1**, 3-40.

Lambe, T. W. & Whitman, R. V. (1969). *Soil mechanics - SI version*. New York: John Wiley and Sons.

Lau, C. K. (1988). *Scale effects in tests on footings*. Ph.D. thesis, University of Cambridge.

Lo Presti, D. (1987). *Mechanical behaviour of Ticino sand from resonant column tests.* Ph.D. thesis, Politecnico di Torino.

Luong, M. P. (1980). Stress-strain aspects of cohesionless soils under cyclic and transient loadings. *Proc. Int. Sym. on Soils under Cyclic and Transient Loading, Swansea*, 315-324.

McBean, H. F. & West, C. G. (1987). *The miniature cone penetrometer.* Third year project report, Department of Engineering Science, University of Oxford.

McManus, K. J. & Davis, R. O. (1997). Dilation-induced pore fluid cavitation in sands. *Géotechnique* **47**(1), 173-177.

McNeilan, T. W. (1985). Jack-up rig performance in predominantly silty soils, offshore california. *Proc. 17th Offshore Technology Conf., Houston*, OTC 5082.

Mangal, J. (1994). *Transient loading of offshore foundations.* First year report, Department of Engineering Science, University of Oxford.

Martin, C. M. (1994). *Physical and numerical modelling of offshore foundations under combined loads.* D.Phil. thesis, University of Oxford.

Meyerhof, G. G. (1953). The bearing capacity of foundations under eccentric and inclined loads. *Proc. 3rd Int. Conf. on Soil Mech. and Foundation Eng., Zurich*, **1**, 440-445.

Meyerhof, G. G. (1961). The ultimate bearing capacity of wedge shaped foundations. *Proc. 5th Int. Conf. on Soil Mech. and Foundation Eng., Paris*, **2**, 105-109.

Meyerhof, G. G. (1963). Some recent research on the bearing capacity of foundations. *Canadian Geotechnical Journal* **1**(1), 16-26.

Mitchell, J. K. (1976). *Fundamentals of soil behaviour.* New York: John Wiley and Sons.

Montrasio, L. & Nova, R. (1997). Settlements of shallow foundations on sand: geometrical effects. *Géotechnique* **47**(1), 49-60.

NGI (1993). *see* Norwegian Geotechnical Institute (1993).

NGI (1994a). *see* Norwegian Geotechnical Institute (1994a).

NGI (1994b). *see* Norwegian Geotechnical Institute (1994b).

Ngo-Tran, C. L. (1996). *The analysis of offshore foundations subjected to combined loading.* D.Phil. thesis, University of Oxford.

Noble Denton & Associates (1987). *Foundation fixity of jack-up units: a joint industry study.* London: Noble Denton & Associates.

Norwegian Geotechnical Institute (1993). Model testing of plated skirt foundation in sand - pilot study. *Report no. 933006-1*, 4th August. Oslo: Norwegian Geotechnical Institute.

Norwegian Geotechnical Institute (1994a). Statoil model tests - preliminary results. *Report no. 933013.* Oslo: Norwegian Geotechnical Institute.

Norwegian Geotechnical Institute (1994b). Sleipner T - special laboratory testing. *Report no. 932514-1*, 5th April. Oslo: Norwegian Geotechnical Institute.

Nova, R. & Montrasio, L. (1991). Settlements of shallow foundations on sand. *Géotechnique* **41**(2), 243-256.

Os, A. G. van & Van Leussen, W. (1987). Basic research on cutting forces in saturated sand. *Proc. ASCE, J. of the Geotechnical Eng. Div.* **113**(12), 1501-1516.

Ovesen, N. K. (1979). The use of physical models in design (discussion contribution). *Proc. 7th European Conf. on Soil Mech. and Foundation Eng., Brighton*, **4**, 319-323.

Poorooshasb, H. B. (1995). One gravity model testing. *Soils and Foundations* **35**(3), 55-59.

Poulos, H. G. (1988). *Marine geotechnics*. London: Unwin Hyman.

Poulos, H. G. & Davis, E. H. (1974). *Elastic solutions for soil and rock mechanics*. New York: John Wiley and Sons.

Prandtl, L. (1921). Uber die eindringungfestigkeit plastisher baustoffe und die festigkeit von schneiden. *Zeitschrift fur Angewandte Mathematik und Mechanik*, **1**(1). Basel, Switzerland.

Ricceri, G. & Simonini, P. (1989). Interaction diagrams for shallow footings on sand. *Proc. 12th Int. Conf. on Soil Mech. and Foundation Eng., Rio de Janeiro*, **2**, 967-972.

Roscoe, K. H. & Poorooshasb, H. (1963). A fundamental principle of similarity in model tests for earth pressure problems. In *Proc. 2nd Asian Regional Conf. on Soil Mech., Bangkok*, **1**, 134-140.

Roscoe, K. H. & Schofield, A. N. (1956). The stability of short pier foundations on sand. *British Welding Journal*, January, 12-18.

Scott, C. R. (1980). *An introduction to soil mechanics and foundations*. 3rd ed. London: Applied Science Publishers.

Selvadurai, A. P. S. (1979). Elastic analysis of soil-foundation interaction. Asterdam: Elsevier.

Shi, Q. (1988). *Centrifugal modelling of surface footings subjected to combined loading*. Ph.D. thesis, University of Cambridge.

Shield, R. T. (1955). On the plastic flow of metals under conditions of axial symmetry. *Proc. Royal Soc. London*, Series A, **233**, 267-287.

Simonini, P. (1993). Influence of relative density and stress level on the bearing capacity of sands. *Int. J. Numerical and Analytical Methods in Geomechanics* **17**, 871-890.

SINTEF (1992). Model development for light skirt foundations. *Report no. STF69 F92031*. Norway: SINTEF.

Small, J. C., Booker, J. R. & Davies, E. H. (1976). Elasto-plastic consolidation of soil. *Int. J. Solids and Structures* **12**, 431-448.

Spence, D. A. (1968). Self similar solutions to adhesive contact problems with incremental loading. *Proc. Royal Soc. London*, Series A, **305**, 55-80.

Stephens, R. C. (1970). *Strength of Materials*. London: Edward Arnold.

Tan, F. S. C. (1990). *Centrifuge and theoretical modelling of conical footings on sand*. Ph.D thesis, University of Cambridge.

Taylor, D. W. (1948). *Fundamentals of soil mechanics*. New York: John Wiley and Sons.

Terzaghi, K. (1943). *Theoretical soil mechanics*. New York: John Wiley and Sons.

Vesic, A. S. (1975). Bearing capacity of shallow foundations. In *Foundation Engineering Handbook* (ed. H. F. Winterkorn & H. Y. Fang), 121-147. New York: Van Nostrand

Vesic, A. S., Banks, D. C. & Woodard, J. M. (1965). An experimental study of dynamic bearing capacity of footings on sand. *Proc. 6th Int Conf. on Soil Mech. and Foundation Eng., Montreal*, **2**, 209-213.

Wang, M. C., Demars, K. R. & Nacci, V. A. (1977). Breakout capacity of model suction anchors in soil. *Canadian Geotechnical Journal*. **14**(2), 246-257.

Watson, P. G. & Randolph, M. F. (1997). A yield envelope design approach for caisson foundations in calcarreous sediments. *Proc. 8th Int. Conf. on Behaviour of Offshore Structures, Delft*, **1**, 259- 689.

Wood, D. M. (1990). *Soil behaviour and critical state soil mechanics*. Cambridge: Cambridge University Press.

Wroth, C. P. & Houlsby, G. T. (1985). Soil mechanics - property characterization and analysis procedures. *Proc. 11th Int. Conf. on Soil Mech. and Foundation Eng., San Francisco*, **1**, 1-50.

Yamaguchi, H., Kimura, T. & Fujii, N. (1977). On the scale effect of footings in dense sand. *Proc. 9th Int. Conf. on Soil Mech. and Foundation Eng., Tokyo*, **1**, 795-798.

Yamamuro, J. A. & Lade, P. V. (1998). Steady-state concepts and static liquefaction of silty sands. *Proc. ASCE, J. Geotechnical and Geoenvironmental Eng*. **122**(8), 641-648.

Youd, T. L. (1972). Compaction of sand by repeated shear straining. *Proc. ASCE, J. Soil Mech. and Foundations Div*. **98**(7), 709-725.

Yue, Z. Q., Selvadurai, A. P. S. & Law, K. T. (1994). Excess pore pressure in a poroelastic seabed saturated with a compressible fluid. *Canadian Geotechnical Journal* **31**(6), 898-1003.

**Table 1.1** Failure mechanisms of shallow footings

| | Sand | | Clay | |
|---|---|---|---|---|
| | Drained | Undrained | Drained | Undrained |
| Dense sand or Stiff clay | general shear | punching shear | general shear | punching shear |
| Loose sand or Soft clay | punching shear | *general shear* | punching shear | general shear |

Note:

Normal letters Based on experimental evidence

Italic letters Postulated

**Table 2.1** Elastic stiffness factors of Ngo-Tran (1996) for a rough flat circular footing embedded in an isotropic homogeneous elastic material

| $w/R$ | $\nu = 0.2$ | | | | $\nu = 0.49$ | | | |
|---|---|---|---|---|---|---|---|---|
| | $K_1$ | $K_2$ | $K_3$ | $K_4$ | $K_1$ | $K_2$ | $K_3$ | $K_4$ |
| 0.0 | 5.406 | 4.652 | 3.816 | -0.573 | 8.197 | 5.554 | 5.563 | -0.015 |
| 0.5 | 5.951 | 6.117 | 4.586 | -0.843 | 8.810 | 7.226 | 6.583 | -0.402 |

**Table 2.2** Scaling factors for different modelling scenarios

| Quantity | Prototype<br>P | Equivalent Void Ratio Model<br>M2 | Centrifuge Model<br>M3 | Equivalent State Parameter Model<br>M1 |
|---|---|---|---|---|
| Length | 1 | $1/n$ | $1/n$ | $1/n$ |
| Area | 1 | $1/n^2$ | $1/n^2$ | $1/n^2$ |
| Volume | 1 | $1/n^3$ | $1/n^3$ | $1/n^3$ |
| Acceleration | 1 | 1 | $n$ | 1 |
| Stress | 1 | $\sim 1/n$ | 1 | $1/n$ |
| Strain | 1 | ? | 1 | 1 |
| Displacement | 1 | ? | $1/n$ | $1/n$ |
| Force | 1 | $\sim 1/n^3$ | $1/n^2$ | $1/n^3$ |
| Moment | | $\sim 1/n^4$ | $1/n^3$ | $1/n^4$ |
| Void Ratio | $e_P$ | $e_M = e_P$ | $e_M = e_P$ | $e_M > e_P$ |
| State Parameter | $\psi_P$ | $\psi_M > \psi_P$ | $\psi_M = \psi_P$ | $\psi_M = \psi_P$ |
| Undrained strength | 1 | $1/n$ to 1 | 1 | $1/n$ |
| Soil stiffness | 1 | $\sim 1/n^{1/2}$ | 1 | $\sim 1/n^{1/2}$ |
| Vertical and horizontal footing stiffness | 1 | $\sim 1/n^{3/2}$ | $1/n$ | $\sim 1/n^{3/2}$ |
| Moment footing stiffness | 1 | $\sim 1/n^{7/2}$ | $1/n^3$ | $\sim 1/n^{7/2}$ |
| Scaling factors below include an additional viscosity scaling factor of $n$ | | | | |
| Permeability | 1 | $1/n$ | $1/n$ | $1/n$ |
| $M'$ (elastic) | 1 | $\sim 1/n^{1/2}$ | 1 | $\sim 1/n^{1/2}$ |
| $M'$ (plastic) | 1 | $\sim 1/n$ | 1 | $1/n$ |
| $c_v$ (elastic) | 1 | $\sim 1/n^{3/2}$ | $1/n$ | $\sim 1/n^{3/2}$ |
| $c_v$ (plastic) | 1 | $\sim 1/n^2$ | $1/n$ | $\sim 1/n^2$ |
| $t$ (elastic) | 1 | $\sim 1/n^{1/2}$ | $1/n$ | $\sim 1/n^{1/2}$ |
| $t$ (plastic) | 1 | $\sim 1$ | $1/n$ | $\sim 1$ |

**Table 3.1** Stepper motor specifications

| Control axis | Type of displacement | Step count conversion | Velocity range |
|---|---|---|---|
| 1 | rotational | 1 deg = 47,240 steps | 0.001 - 0.2 deg/s |
| 2 | horizontal | 1 mm = 50,340 steps | 0.001 - 0.4 mm/s |
| 3 | vertical | 1 mm = 10,000 steps | 0.001 - 1 mm/s |
| 3 | vertical (fast) | 1 mm = 200 steps | 1 - 5 mm/s |

**Table 3.2** Details of preliminary tests

| Test | Diameter of footing (mm) | Loading apparatus | Position and type of pore pressure transducer [a] | Hydraulic surcharge | Rate of penetration (mm/s) | $\frac{\Delta U}{\Delta V}$ [b] (%) |
|---|---|---|---|---|---|---|
| TP01 | 100 | rig | external, Druck | — | 0.3 | 10 |
| TP02 | 100 | rig | external, Druck | — | 0.8 | 4 |
| TP03 | 100 | rig | external, Druck | -3.8 | 1.4 | 2 |
| TP04 | 100 | hanger & weights | external, Druck | — | 9.3 | 2 |
| TP05 | 100 | hanger & weights | internal, Druck | — | 7.9 | 3 |
| TP06 | 100 | hanger & weights | internal, Gaeltec | — | 3 | 27 |
| TP07 | 100 | hanger & weights | internal, Gaeltec | — | 7 | 22 |
| TP08 | 150 | hanger & weights | internal, Gaeltec | — | 10.0 | 64 |
| TP09 | 150 | hanger & weights | internal, Gaeltec | -4.0 | 6.8 | 62 |

Note:

a *External* indicates that the transducer was connected to the centre of the footing via tubing and *internal* indicates that the transducer was connected directly to the centre of the footing.

b A uniform pore pressure distribution assumed.

**Table 3.3** Verification of the load cell calibration and errors involved

| Applied loads | | | Measured loads | | | Absolute errors | | | Relative errors (%) | | |
|---|---|---|---|---|---|---|---|---|---|---|---|
| $V$ (N) | $H$ (N) | $M$ (Nm) | $V$ (N) | $H$ (N) | $M$ (Nm) | $V$ (N) | $H$ (N) | $M$ (Nm) | $V$ | $H$ | $M$ |
| 656.1 | 0 | 0 | 657.1 | -0.9 | -0.06 | 1.0 | -0.9 | -0.06 | 0.15 | - | - |
| 656.1 | 457.9 | 0 | 657.4 | 461.2 | 0.18 | 1.3 | 3.3 | 0.18 | 0.20 | 0.72 | - |
| 656.1 | 0 | 26.24 | 655.3 | -0.13 | 26.42 | -0.8 | -0.13 | 0.18 | 0.12 | - | 0.69 |
| 656.1 | 287.75 | 26.24 | 652.5 | 287.7 | 26.41 | -3.6 | -0.1 | 0.17 | 0.55 | 0.04 | 0.65 |
| 656.1 | 287.75 | -26.24 | 660.3 | 289.9 | -26.35 | 4.2 | 2.2 | 0.11 | 0.64 | 0.76 | 0.42 |
| 656.1 | 0 | -26.24 | 661.2 | 0.32 | -26.50 | 5.1 | 0.32 | -0.26 | 0.78 | - | 0.99 |

**Table 3.4** LVDT specifications

| LVDT | Displacement | | Type | Range (mm) | Standard error in calibration coefficient (%) |
|---|---|---|---|---|---|
| DLV | vertical ($w$) | coarse measurements | ACT600C | ±150 | 0.08 |
| DLH | horizontal ($u$) | | D5/1000A | ±25 | 0.05 |
| DLM | rotational ($\theta$) | | ACT2000C | ±50 | 0.04 |
| DSV1 | transformed to $w$, $u$, and $\theta$ | fine measurements | D5/200AG | ±5 | 0.04 |
| DSV2 | | | D5/200AG | ±5 | 0.12 |
| DSH | | | D5/200AG | ±5 | 0.03 |

Note: All LVDTs supplied by RDP Electronics.

**Table 3.5** Pore pressure transducer specifications

| Pore pressure transducer | Location | Type | Range (kPa) | Standard error in calibration coefficient (%) |
|---|---|---|---|---|
| $pp_1$ | centre of footing | custom built (Gaeltec Ltd.) | ±100 | 0.10 |
| $pp_2$ | wall of specimen container (upper) | PDCR910 (Druck Ltd.) | ±70 | 0.06 |
| $pp_3$ | wall of specimen container (lower) | PDCR910 (Druck Ltd.) | ±70 | 0.04 |

Note: Pressures were referenced to atmospheric pressure.

**Table 3.6** Methods used in the preparation of the sand specimens

| Test | Specimen | Method of densification | Fully fluidised before densification ? |
|---|---|---|---|
| T101 | 1 | dhg/vibration, manual | yes |
| T102 | 1 | dhg/vibration, manual | no |
| T103 | 1 | dhg/vibration, manual | no |
| T204 | 2 | poured and vibrated | no |
| T105 | 1 | dhg/vibration, manual | no |
| T106 | 1 | dhg/vibration, automatic | no |
| T107 | 1 | dhg/vibration, automatic, surcharge | no |
| T108 | 1 | dhg/vibration, automatic | no |
| T309 | 3 | dhg/vibration, automatic, surcharge | yes |
| T110 | 1 | dhg/vibration, automatic | yes |
| T311 | 3 | dhg/vibration, automatic | yes |
| T112 | 1 | dhg/vibration, automatic | yes |
| T313 | 3 | dhg/vibration, automatic | yes |
| T114 | 1 | dhg/vibration, automatic | yes |
| T315 | 3 | dhg/vibration, automatic | yes |
| T116 | 1 | dhg/vibration, automatic | yes |
| T317 | 3 | dhg/vibration, automatic | yes |
| T118 | 1 | dhg/vibration, automatic | yes |
| T319 | 3 | dhg/vibration, automatic | yes |
| T120 | 1 | dhg/vibration, automatic | yes |

Note:
- *dhg* abbreviates downward hydraulic gradient.
- *manual* indicates that the switching between the densification components was done manually, and *automatic* indicates that the asynchronous switch and solenoid valve apparatus was used.
- *surcharge* indicates a weight was applied to the surface of the sand during the densification process.

**Table 4.1** Permeability tests on oil-saturated Baskarp Cyclone sand

| Test | Time (min) | Head difference in manometer tubes (m) | Flow (ml) | Flow rate ($m^3/s$) | Permeability $k$ (m/s) |
|---|---|---|---|---|---|
| 1 | 123 | 0.855 ± 0.005 | 51.0 | $6.91 \times 10^{-9}$ | $1.77 \times 10^{-7}$ |
| 2 | 85 | 0.863 ± 0.003 | 35.5 | $6.96 \times 10^{-9}$ | $1.77 \times 10^{-7}$ |
| 3 | 214 | 0.865 | 93.0 | $7.24 \times 10^{-9}$ | $1.83 \times 10^{-7}$ |

**Table 4.2** Elastic and consolidation parameters derived from NGI (1994b) element tests

| Test Number | Type of test | $R_D$ (%) | $p'$ (kPa) | $k \times 10^{-5}$ (m/s) | Loading | | | Unloading | | |
|---|---|---|---|---|---|---|---|---|---|---|
| | | | | | $\varepsilon_q$ (%) | $G$ (MPa) | $c_v$ (m²/s) | $\varepsilon_q$ (%) | $G$ (MPa) | $c_v$ (m²/s) |
| BC10 | $CIU_{Oedo}$ | 60 | 87 | 2.0 | 0.53 | 5 | 0.04 | -0.04 | 57 | 0.54 |
| BC11 | $CIU_{Oedo}$ | 70 | 87 | 1.6 | 0.33 | 7 | 0.05 | -0.04 | 64 | 0.42 |
| BC12 | $CIU_{Oedo}$ | 90 | 87 | 0.8 | 0.15 | 17 | 0.04 | -0.04 | 101 | 0.23 |
| BC13 | Oedo | 60 | 30 | 2.0 | 0.23 | 4 | 0.02 | -0.04 | 22 | 0.12 |
| BC14 | Oedo | 90 | 30 | 0.8 | 0.03 | 27 | 0.06 | -0.02 | 45 | 0.09 |
| NTH93-1 | $CAD_{Oedo}$ | 60 | 136 | 1.8 | 1.08 | 3 | 0.02 | -0.06 | 57 | 0.35 |
| NTH93-2 | $CAD_{Oedo}$ | 85 | 98 | 0.9 | 0.70 | 8 | 0.02 | -0.02 | 66 | 0.16 |

Note:
$\sigma'_{consol}$ = 10 kPa and $\Delta\varepsilon_r \neq 0$ in tests BC10 to BC12.
$\sigma'_{consol}$ = 0 kPa and $\Delta\varepsilon_r = 0$ in tests NTH93-1 and NTH93-2.

**Table 4.3** Drained triaxial test parameters of Baskarp Cyclone sand (NGI, 1994b)

| Test | Type of Test | Pore Fluid | $R_D$ (%) | Consol. $p'$ (kPa) | Peak State | | Critical State | |
|---|---|---|---|---|---|---|---|---|
| | | | | | $\phi'_{max}$ (deg) | $p'$ (kPa) | $\phi'_{crit}$ (deg) | $p'$ (kPa) |
| BC15 | $CID_c$ | water | 79 | 10 | 44.0 | 27.1 | 33.4 | 21.8 |
| BC16 | $CID_c$ | water | 81 | 50 | 42.5 | 124.0 | 34.9 | 98.4 |
| BC17 | $CID_c$ | water | 80 | 200 | 36.4 | 400.7 | 31.1 | 348.3 |
| BC23 | $CID_c$ | oil | 81 | 10 | 41.9 | 26.2 | 33.1 | 21.7 |
| BC18 [a] | $CID_{cy}$ | water | 79 | 10 | 44.2 | 28.3 | 34.5 | 24.7 |
| BC20 [a] | $CID_{cy}$ | water | 80 | 8 [b] | 43.1 | 26.8 | 31.8 | 23.5 |

Note:
a Undrained cyclic test performed before drained static test.
b Anisotropic consolidation, $\sigma'_{ac}$ = 4.6 kPa and $\sigma'_{rc}$ = 9.7 kPa

**Table 4.4** Undrained triaxial test parameters of Baskarp Cyclone sand (NGI, 1994b)

| Test | Type of Test | Pore Fluid | $R_D$ (%) | $p'_{con}$ (kPa) | Back Pressure (kPa) | Critical State | |
|---|---|---|---|---|---|---|---|
| | | | | | | $\phi'_{crit}$ (deg) | $p'$ (kPa) |
| BC1 | $CIU_c$ | water | 50 | 10 | 1471 | 35.0 | 185 |
| BC2 | $CIU_c$ | water | 79 | 20 | 1471 | 35.3 | 1913 |
| BC24 | $CIU_c$ | oil | 82 | 20 | 1569 | 32.6 | 1778 |
| BC3 [a] | $CIU_{cy}$ | water | 90 | 20 | 1471 | 31.6 | 2258 |
| BC6 [a] | $CIU_{cy}$ | water | 70 | 20 | 1569 | 33.6 | 840 |
| BC8 [a] | $CIU_{cy}$ | water | 80 | 20 | 1471 | 32.9 | 1824 |
| BC9 [a] | $CIU_{cy}$ | water | 90 | 18 [b] | 1765 | 34.2 | 3120 |

Note:
a Undrained cyclic test performed before drained static test.
b Anisotropic consolidation, $\sigma'_{ac}$ = 13.5 kPa and $\sigma'_{rc}$ = 20.0 kPa

**Table 4.5** Properties of Baskarp Cyclone sand specimens

| Specimen | Type | Mass of sand (kg) |
|---|---|---|
| 1 | oil-saturated | 67.052 |
| 2 | dry | 65.069 |
| 3 | oil-saturated | 66.997 |

**Table 4.6** Cone penetrometer test results

| Test | Bulk $R_D$ (%) | $K_{ch}$ (N/mm) | $q_c$ [a] (kPa) | | | | Local $\phi'_{max}$ [d] (deg) | Local $R_D$ [e] (%) |
|---|---|---|---|---|---|---|---|---|
| | | | Before footing test | | After footing test | | | |
| | | | Centre | Side | Centre | Side | | |
| T101 | 87 | 144 | | | | | | |
| T102 | 86 | 180 | 332 [b] | | **200** | **230** | 43.9 | 81 |
| T103 | 81 | 112 | 66 [b] | | **40** | **130** | 41.3 | 67 |
| T204 | 84 | 628 | 1162 [b] | | **700** | **1000** | 45.3 | 80 |
| T105 | 89 | 156 | 199 [b] | | **120** | **200** | 43.1 | 77 |
| T106 | 91 | 337 | 664 [b] | | **400** | **400** | 45.1 | 88 |
| T107 | 84 | 173 | 166 [b] | | **100** | **140** | 42.8 | 75 |
| T108 | 82 | 99 | 17 [b] | | **10** | **50** | 39.0 | 54 |
| T309 | 90 | 476 | 996 [b] | | **600** | **950** | 45.7 | 91 |
| T110 | 94 | 483 | 747 [b] | | **450** | **550** | 45.2 | 89 |
| T311 | 73 | 259 | 116 [b] | | **70** | **100** | 42.3 | 72 |
| T112 | 88 | 350 | 315 [c] | **450** | **180** | **300** | 43.8 | 81 |
| T313 | 91 | 480 | 996 [b] | **600** | **600** | **500** | 45.7 | 91 |
| T114 | 91 | 234 | 399 [c] | **570** | **100** | | 44.2 | 83 |
| T315 | 92 | 470 | 840 [c] | **1200** | **250** | | 45.5 | 90 |
| T116 | 96 | 385 | 634 [c] | **905** | **200** | | 45.0 | 87 |
| T317 | 88 | 481 | 770 [c] | **1100** | **450** | | 45.3 | 89 |
| T118 | 100 | 409 | 823 [c] | **1175** | | | 45.4 | 89 |
| T319 | 102 | 342 | 665 [c] | **950** | | | 45.0 | 88 |
| T120 | 98 | 345 | 543 [c] | **775** | | | 44.7 | 86 |

Note:
$q_c$ values in bold font refer to measured values.
$q_c$ values in normal font refer to estimated values.
a $q_c$ measured between 50 mm and 100 mm of penetration.
b Estimated from after-centre measured values, *i.e.* equal to measured value multiplied by 1.66.
c Estimated from before-side measured values, *i.e.* equal to measured value multiplied by 0.70
d Estimated from before-centre cone penetrometer results using Equation 4.11.
e Estimated from before-centre cone penetrometer results using Equation 4.12 for the dry specimens and Equation 4.13 for the oil-saturated specimens.

**Table 5.1** Chronological list of tests (page 1 of 4)

| Test name | Main-test files [a] | Sub-Tests | | | | | Notes |
|---|---|---|---|---|---|---|---|
| | | Input files [b] | Output files [c] | Type of test | Intended displacement rate (mm/s) | Initial vertical load (N) | |
| T101 | T101 | | *T101_U* | ULRL | ±0.001 | 1000 | |
| | | | *T101_1* | HSS | 0.001 | 1630 | |
| T102 | T102 | T102_A | T102_1 | VP | 1 | 500 | |
| | T102A | T102_B | T102A_1 | VP | 1 | 1000 | |
| | | | *T102A_2* | MSS | 0.0026 | 1500 | |
| T103 | T103 | | | | | | |
| | T103A | T103_A | T103A_1 | VP | 0.1 | 500 | |
| | | T103_B | T103A_2 | VP | 0.1 | 1000 | |
| | | T103_C | T103A_3 | HSS | 0.1 | 1340 | |
| T204 | T204 | | *T204_U* | ULRL | ±0.001 | 1000 | |
| | | | *T204_1* | HSS | 0.001 | 1500 | |
| T105 | T105 | T105_A | T105_1 | VP | 0.01 | 500 | |
| | | T105_B | T105_2 | VP | 0.01 | 1000 | |
| | | T105_C | T105_3 | MSS | 0.26 | 1500 | |
| T106 | T106 | T106_A | T106_1 | VP | 2 | 500 | motor stalled |
| | | T106_A | T106_2 | VP | 2 | 500 | reduced acceleration in input file but motor still stalled |
| | | T106_A | T106_3 | VP | 1 | 500 | reduced velocity in input file |
| | | T106_B | T106_4 | VP | 1 | 1000 | |
| | | T106_C | T106_5 | HSS | 0.4 | 1500 | |
| T107 | T107 | T107_A | T107_1 | VP | 1 | 500 | |
| | | T107_B | | VP | 1 | 1000 | no activity |
| | | T107_B | | VP | 1 | 1000 | no activity, error in control program, program stopped |
| | T107A | T107_B | T107A_1 | VP | 1 | 1000 | |
| | | T107_C | T107A_2 | HSS | 0.4 | 1500 | motor stalled, error in input file |
| | | T107_D | T107A_3 | HSS | 0.4 | 1500 | |
| T108 | T108 | | | | | | |
| | T108A | | | | | | |
| | T108B | | | | | | |
| | T108C | | | | | | |
| | T108D | | | | | | |
| | T108E | | *T108E_U* | ULRL | ±0.001 | 1000 | |
| T309 | T309 | | *T309_U* | ULRL | ±0.001 | 1000 | |
| | | | *T309_1* | HSS | 0.001 | 1500 | |
| T110 | T110 | T110_A | T110_1 | VP | 1 | 500 | |
| | | T110_B | T110_2 | VP | 1 | 1000 | |
| | | T110_C | T110_3 | HSS | 0.4 | 1500 | |

Table continued on next page.
See notes on page three.

**Table 5.1 (cont.)** Chronological list of tests (page 2 of 4)

| Test name | Main-test files [a] | Sub-Tests | | | | | Notes |
|---|---|---|---|---|---|---|---|
| | | Input files [b] | Output files [c] | Type of test | Intended displacement rate (mm/s) | Initial vertical load (N) | |
| T311 | T311 | T311_A | T311_1 | VP | 0.1 | 500 | |
| | | T311_B | T311_2 | VP | 0.1 | 1000 | |
| | | | *T311_3* | MSS | 0.0026 | 1500 | |
| T112 | T112 | | | | | | |
| | T112A | | | | | | |
| | T112B | T112_A | T112B_1 | VP | 1 | 500 | |
| | T112C | | | | | | |
| | T112D | T112_B | T112D_1 | VP | 1 | 1000 | |
| | T112E | T112_C | T112E_1 | MSS | 0.524 | 1500 | |
| T313 | T313 | | | | | | |
| | T313A | T313_A | T313A_1 | VP | 5 | 500 | |
| | T313B | | | | | | |
| | T313C | T313_B | T313C_1 | VP | 5 | 1000 | |
| | T313D | T313_C | T313D_1 | MSS | 0.524 | 1500 | |
| T114 | T114 | | | | | | |
| | T114A | | | | | | |
| | T114B | T114_A | T114B_1 | VP | 5 | 500 | |
| | T114C | | | | | | |
| | T114D | T114_B | T114D_1 | VP | 5 | 1000 | |
| | T114E | T114_C | T114E_1 | MSS | 0.524 | 1500 | |
| T315 | T315 | T315_A | T315_1 | VP | 0.1 | 500 | |
| | | T315_B | T315_2 | VP | 0.1 | 1000 | |
| | | T315_C | T315_3 | HSS | 0.4 | 1500 | error in input file |
| | T315A | | | | | | |
| | T315B | T315_D | T315B_1 | HSS | 0.4 | 1500 | new input file, motor stalled |
| | | T315_D | T315B_2 | HSS | 0.4 | 1500 | motor stalled |
| | T315C | T315_E | T315C_1 | HSS | 0.1 | 1500 | new input file with reduced velocity |
| | T315D | | | | | | |
| | T315E | | | | | | |
| T116 | T116 | T116_A | T116_1 | VP | 0.01 | 500 | |
| | | T116_B | | VP | 0.01 | 1000 | error in control program, file not retrieved |
| | T116A | T116_B | T116A_1 | VP | 0.01 | 1000 | |
| | | T116_C | *T116A_2* | HSS | 0.1 | 1500 | test not logged on ADU, file T116A_2 created from background data |
| | T116B | | | | | | |
| | T116C | | | | | | |
| | T116D | | | | | | |
| | T116E | | | | | | |
| | T116F | | | | | | |

Table continued on next page.
See notes on page three.

**Table 5.1 (cont.)** Chronological list of tests (page 3 of 4)

| Test name | Main-test files [a] | Sub-Tests: Input files [b] | Output files [c] | Type of test | Intended displacement rate (mm/s) | Initial vertical load (N) | Notes |
|---|---|---|---|---|---|---|---|
| T317 | T317 | T317_A | T317_1 | VP | 0.01 | 500 | |
| | | T317_B | T317_2 | VP | 0.01 | 500 | |
| | | T317_C | T317_3 | MSS | 0.026 | 1500 | the limit on the moment load in the input file was set too low |
| | T317A | T317_D | T317A_1 | MSS | 0.026 | 1800 | new input file |
| T118 | T118 | | | | | | |
| | T118A | T118_A | T118A_1 | VP | 5 | 500 | |
| | T118B | T118_B | T118B_1 | CONSL | | 700 | |
| | | | T118B_2 | CONSL | | 900 | |
| | | | T118B_3 | CONSL | | 700 | |
| | T118C | T118_C | T118C_1 | VP | 5 | 1000 | |
| | T118D | | *T118D_1* | HSS | 0.001 | 1500 | |
| | | | *T118D_2* | HSS | -0.001 | 1700 | |
| | T118E | | *T118E_U* | ULRL | ±0.001 | 1900 | |
| | T118F | | | | | | |
| | T118G | | | | | | |
| T319 | T319 | | | | | | |
| | T319A | T319_A | T319A_1 | VP | 5 | 500 | |
| | T319B | T319_B | T319B_1 | CONSL | | 700 | |
| | | | T319B_2 | CONSL | | 900 | |
| | | | T319B_3 | CONSL | | 700 | |
| | T319C | T319_C | T319C_1 | VP | 5 | 1000 | |
| | T319D | | *T319D_1* | MSS | 0.0026 | 1500 | |
| | | | *T319D_2* | MSS | -0.0026 | 1700 | |
| | | | *T319D_3* | MSS | 0.0026 | 2000 | |

Table continued on next page.

Note:

a The main-test files are the background logging files that were logged directly onto the host PC. The filename extension of these files is .OUT.

b The filename extension of the input files is .INP.

c The filename extension of the output files is .DAT. Output files shown in italic were created from the background logging data.

ULRL Vertical unload-reload test.
HCYC Horizontal load-unload-reload test.
MCYC Moment load-unload-reload.
VP Vertical partially-drained test.
HSS Horizontal sideswipe test.
MSS Moment sideswipe test.
CONSL Vertical consolidation test.
VPM Vertical partially-drained test with alternating slow and fast rates.
HSSM Horizontal sideswipe test with alternating slow and fast rates.
MSSM Moment sideswipe test with alternating slow and fast rates.

**Table 5.1 (cont.)** Chronological list of tests (page 4 of 4)

| Test name | Main-test files [a] | Sub-Tests: Input files [b] | Sub-Tests: Output files [c] | Sub-Tests: Type of test | Sub-Tests: Intended displacement rate (mm/s) | Sub-Tests: Initial vertical load (N) | Notes |
|---|---|---|---|---|---|---|---|
| T120 | T120 | | | | | | |
| | T120A | T120_A | T120A_1<br>T102A_2<br>T120A_3 | VPM | 0.01<br>1 | 500 | |
| | T120B | | *T120B_HC* | HCYC | 0.001 | 1000 | |
| | | | *T120B_MC* | MCYC | 0.0026 | 1000 | |
| | T120C | T120_A | T120C_1<br>T120C_2<br>T120C_3 | VPM | 0.01<br>1 | 1000 | |
| | T120D | T120_B | T120D_1<br>to<br>T120D_5 | HSSM | 0.001<br>0.1 | 1500 | the data files of this sideswipe were merged into a single file labelled T120D_H1 |
| | | | *T120D_5A* | | | | |
| | | | *T120D_HC* | HCYC | 0.001 | 1500 | |
| | | | *T120D_MC* | MCYC | 0.0026 | 1500 | |
| | | T120_C | T120D_6<br>to<br>T120D_11 | HSSM | -0.001<br>-0.1 | 1700 | the data files of this sideswipe were merged into a single file labelled T120D_H2 |
| | | | *T120D_11A* | | | | |
| | | T120_C | T120D_12<br>to<br>T120D_17 | | | | |
| | | T120_D | T120D_18<br>to<br>T120D_22 | MSSM | 0.0026<br>0.26 | 1900 | the data files of this sideswipe were merged into a single file labelled T120D_M1 |
| | | | *T120D_22A* | | | | |
| | | T120_D | T120D_23<br>to<br>T120D_27 | | | | |
| | T120E | T120_E | T120E_1<br>to<br>T120E_8 | MSSM | -0.0026<br>-0.26 | 2100 | the data files of this sideswipe were merged into a single file labelled T120E_M2 |
| | T120F | | | | | | |
| | T120G | | | | | | |

See notes on page three.

**Table 5.2** Details of the miniature cone penetration tests

| Sample | Specimen | Cone test [a] | Timing [b] | Rate (mm/s) |
|---|---|---|---|---|
| 2 | 1 | CP02C | after | 0.3 |
| | | CP02L | after | 0.3 |
| 3 | 1 | CP03C | after | 0.3 |
| | | CP03L | after | 0.3 |
| 4 | 2 | CP04C | after | 0.3 |
| | | CP04L | after | 0.3 |
| 5 | 1 | CP05C | after | 0.3 |
| | | CP05L | after | 0.3 |
| 6 | 1 | CP06C | after | 0.3 |
| | | CP06L | after | 0.1 |
| 7 | 1 | CP07C | after | 0.1 |
| | | CP07L | after | 0.1 |
| 8 | 1 | CP08C | after | 0.1 |
| | | CP08L | after | 0.1 |
| 9 | 3 | CP09C | after | 0.1 |
| | | CP09L | after | 0.1 |
| 10 | 1 | CP10C | after | 0.1 |
| | | CP10L | after | 0.1 |
| 11 | 3 | CP10C | after | 0.1 |
| | | CP10L | after | 0.1 |
| 12 | 1 | CP12C | after | 0.1 |
| | | CP12F | before | 0.1 |
| | | CP12L | after | 0.1 |
| 13 | 3 | CP13B | before | 0.1 |
| | | CP13C | after | 0.1 |
| | | CP13F | before | 0.1 |
| | | CP13L | after | 0.1 |
| | | CP13R | before | 0.1 |
| 14 | 1 | CP14B | before | 0.1 |
| | | CP14C | after | 0.1 |
| | | CP14F | before | 0.1 |
| | | CP14L | before | 0.1 |
| | | CP14R | before | 0.1 |
| 15 | 3 | CP15B | before | 0.1 |
| | | CP15C | after | 0.1 |
| | | CP15F | before | 0.1 |
| | | CP15L | before | 0.1 |
| | | CP15R | before | 0.1 |

| Sample | Specimen | Cone test [a] | Timing [b] | Rate (mm/s) |
|---|---|---|---|---|
| 16 | 1 | CP16B | before | 0.1 |
| | | CP16C | after | 0.1 |
| | | CP16F | before | 0.1 |
| | | CP16L | before | 0.1 |
| | | CP16R | before | 0.1 |
| 17 | 3 | CP17B | before | 0.1 |
| | | CP17C | after | 0.1 |
| | | CP17F | before | 0.1 |
| | | CP17L | before | 0.1 |
| | | CP17R | before | 0.1 |
| 18 | 1 | CP18B | before | 0.1 |
| | | CP18F | before | 0.1 |
| | | CP18L | before | 0.1 |
| | | CP18R | before | 0.1 |
| 19 | 3 | CP19B | before | 0.1 |
| | | CP19F | before | 0.1 |
| | | CP19L | before | 0.1 |
| | | CP19R | before | 0.1 |
| 20 | 1 | CP20B | before | 0.1 |
| | | CP20F | before | 0.1 |
| | | CP20L | before | 0.1 |
| | | CP20R | before | 0.1 |

Note:

a The last character of the test name indicates the position of the test in the tank:
- B back
- C centre
- F front
- L left
- R right

b Indicates whether the cone tests were performed *before* or *after* the main-test.

**Table 6.1** Virgin-penetration stiffness and estimated bearing capacity values

| Test | Virgin-penetration stiffness (N/mm) | | | | Local [e] $R_D$ (%) | $V_m$ [f] (kN) |
|---|---|---|---|---|---|---|
| | 100 - 200 N | 400 - 500 N [a] | 900 - 1000 N | 1400 - 1500 N | | |
| T101 | 111 | 144 | 160 | 166 | | |
| T102 | 116 | 180 | 255 | 408 | 81 | 5.5 |
| T103 | 90 | 112 | 136 | 136 | 67 | 3.2 |
| T204 | 670 | 628 | 766 | 890 | 80 | 9.8 |
| T105 | 87 | 156 | 223 | 233 | 77 | 4.6 |
| T106 | 267 | 337 | 514 [b] | 600 [b] | 88 | 6.9 |
| T107 | 133 | 173 | 220 [c] | 248 | 75 | 4.3 |
| T108 | 108 | 99 | 110 | [d] | 54 | 2.0 |
| T309 | 328 | 476 | 603 | 702 | 91 | 7.9 |
| T110 | 313 | 483 | 925 [b] | 946 [b] | 89 | 7.2 |
| T311 | 189 | 259 | 264 | 250 | 72 | 3.8 |
| T112 | 294 | 350 | 412 | 459 | 81 | 5.4 |
| T313 | 333 | 480 | 657 | 803 | 91 | 7.9 |
| T114 | 135 | 234 | 354 | 445 | 83 | 5.8 |
| T315 | 322 | 470 | 593 | 682 | 90 | 7.5 |
| T116 | 263 | 385 | 517 | 599 | 87 | 6.8 |
| T317 | 313 | 481 | 659 | 731 | 89 | 7.3 |
| T118 | 322 | 409 | 910 [b] | 673 | 89 | 7.4 |
| T319 | 167 | 342 | 661 [b] | 536 | 88 | 6.9 |
| T120 | 225 | 345 | 638 [b] | 582 | 86 | 6.4 |

Note:

a The 400-500 N stiffness was equivalent to the characterisation stiffness, $K'_{ch}$.

b The sample was most probably overconsolidated at this stage.

c The value was estimated from Figure 6.6.

d The maximum vertical load of the test was less than 1400 N.

e The relative density of the top layer of the specimens was estimated from the cone penetrometer tests, see Table 4.6.

f The bearing capacity was estimated from the local $R_D$ values, see Section 6.2.3.

**Table 6.2** Vertical stiffness parameters derived from unload-reload footing tests

| | | | | Type of stiffness measurement | | | |
|---|---|---|---|---|---|---|---|
| | | | | Initial section of unloading curve, $\varepsilon_a = 0.05$ % | | | Whole ULRL loop |
| Test number | $K'_{ch}$ (N/mm) | $K'_{eq}$ [a] (N/mm) | $V$ (N) | $K'_{ul}$ (N/mm) | $K'_{ul}/K'_{eq}$ | $G$ (MPa) | $K'_{ulrl}$ (N/mm) |
| T101 | 144 | 160 | 1000-200 | 6000 | 37.5 | 12.3 | 2500 |
| T204 | 628 | 766 | 1000-200 | 6667 | 8.6 | 13.7 | 4000 |
| T108 | 99 | 110 | 1000-200 | 5417 | 49.2 | 11.1 | 2597 |
| T309 | 476 | 603 | 1000-200 | 6750 | 11.2 | 13.8 | 3496 |
| T118 | 409 | 520 | 1900-190 | 11000 | 21.2 | 22.6 | 3448 |

Note: a $K'_{eq}$ measured over the 100 N of virgin-penetration preceding the loops.

**Table 6.3** Consolidation settlements

| Test | Type of loading | Load range (N) | Immediate (partially-drained) | | | | Primary (drained) | | | | | Theoretical undrained settlement [a] |
|---|---|---|---|---|---|---|---|---|---|---|---|---|
| | | | $dV$ (N) | $dw$ (mm) | $K$ (N/mm) | $dw/dt$ (mm/s) | $dV$ (N) | $dw$ (mm) | $K$ (N/mm) | $G$ (MPa) | $dw/dt$ (mm/s) | (mm) |
| T118b_1 | loading | 700 - 900 | 131 | 0.047 | 2787 | 0.0313 | 200 | 0.315 | 635 | 1.3 | 0.0035 | 0.007 |
| T118b_2 | unloading | 900 - 700 | -272 | -0.025 | 10880 | -0.0167 | -200 | -0.020 | 10000 | 20.5 | -0.0002 | -0.015 |
| T118b_3 | reloading | 700 - 900 | 218 | 0.035 | 6229 | 0.0233 | 200 | 0.050 | 4000 | 8.2 | 0.0017 | 0.012 |
| T319b_1 | loading | 700 - 900 | 123 | 0.036 | 3417 | 0.0240 | 200 | 0.345 | 580 | 1.2 | 0.0035 | 0.007 |
| T319b_2 | unloading | 900 - 700 | -230 | -0.017 | 13529 | -0.0113 | -200 | -0.020 | 10000 | 20.5 | -0.0002 | -0.013 |
| T319b_3 | reloading | 700 - 900 | 210 | 0.035 | 6000 | 0.0233 | 200 | 0.055 | 3636 | 7.5 | 0.0014 | 0.012 |

Note:

a Calculated using Equation 2.39 and elastic shear modulus from unloading tests, *i.e.* 20.5 MPa.

**Table 6.4** Dissipation times and coefficients of consolidation (unloading and reloading tests)

| Test | $t_{50}$ (s) | $c_v$ ($m^2/s$) |
|---|---|---|
| T118B_2 | 11.7 | $0.7 \times 10^{-3}$ |
| T118B_3 | 6.3 | $1.3 \times 10^{-3}$ |
| T319B_2 | 15.5 | $0.5 \times 10^{-3}$ |
| T319B_3 | 9.5 | $0.9 \times 10^{-3}$ |

Note:
A time factor $T_v$ of 0.135 was taken to be representative of $t_{50}$, see Figure 2.27.

**Table 6.5** Settlement and fluid flow data from unloading and reloading consolidation tests

| Test | $dt$ (s) | Settlement | | Flow | | | |
|---|---|---|---|---|---|---|---|
| | | $dw$ (mm) | $Adw/dt$ ($mm^3/s$) | $du_{average}$ (kPa) | $i$ | | $Aki$ ($mm^3/s$) |
| T118B_2 | 1.5 | -0.02 | -236 | -3.5 | Section 1 | -38.1 | -136 |
| | | | | | Section 2 | -4.8 | |
| T118B_3 | 2 | 0.04 | 353 | 3 | Section 1 | 32.6 | 117 |
| | | | | | Section 2 | 4.1 | |
| | 26 | 0.016 | 11 | 3 | | 4.1 | 26 |
| T319B_2 | 1.5 | -0.017 | -200 | -4.25 | Section 1 | -46.2 | -165 |
| | | | | | Section 2 | -5.8 | |
| T319B_3 | 1.5 | 0.033 | 389 | 4.25 | Section 1 | 46.2 | 165 |
| | | | | | Section 2 | 5.8 | |
| | 40 | 0.022 | 10 | 4.25 | | 5.8 | 37 |

Note:
Refer to Figure 6.32.

**Table 6.6** Displacement rates of vertical partially-drained tests

| Test | $K'_{ch}$ (N/mm) | $V_o$ (N) | $dw/dt$ (mm/s) Intended | $dw/dt$ (mm/s) Measured | Displacement rate ratio |
|---|---|---|---|---|---|
| T102_1 | 180 | 500 | 1 | 1.014 | 1.01 |
| T102A_1 | | 1000 | | 0.952 | 0.95 |
| T103A_1 | 112 | 500 | 0.1 | 0.101 | 1.01 |
| T103A_2 | | 1000 | | 0.102 | 1.02 |
| T105_1 | 156 | 500 | 0.01 | 0.009 | 0.91 |
| T105_2 | | 1000 | | 0.009 | 0.90 |
| T106_3 | 337 | 500 | 1 | 0.853 | 0.85 |
| T106_4 | | 1000 | | 0.808 | 0.81 |
| T107_1 | 173 | 500 | 1 | 0.920 | 0.92 |
| T107A_1 | | 1000 | | 0.918 | 0.92 |
| T110_1 | 483 | 500 | 1 | 0.963 | 0.96 |
| T110_2 | | 1000 | | 0.902 | 0.90 |
| T311_1 | 259 | 500 | 0.1 | 0.088 | 0.88 |
| T311_2 | | 1000 | | 0.088 | 0.88 |
| T112B_1 | 350 | 500 | 1 | 1.052 | 1.05 |
| T112D_1 | | 1000 | | 0.978 | 0.98 |
| T313A_1 | 480 | 500 | 5 | 4.611 | 0.92 |
| T313C_1 | | 1000 | | 3.800 | 0.76 |
| T114B_1 | 234 | 500 | 5 | 4.773 | 0.95 |
| T114D_1 | | 1000 | | 4.582 | 0.92 |
| T315_1 | 470 | 500 | 0.1 | 0.081 | 0.81 |
| T315_2 | | 1000 | | 0.075 | 0.75 |
| T116_1 | 385 | 500 | 0.01 | 0.009 | 0.85 |
| T116A_1 | | 1000 | | 0.008 | 0.82 |
| T317_1 | 481 | 500 | 0.01 | 0.008 | 0.77 |
| T317_2 | | 1000 | | 0.007 | 0.74 |
| T118A_1 | 409 | 500 | 5 | 4.479 | 0.90 |
| T118C_1 | | 1000 | | 4.028 | 0.81 |
| T319A_1 | 342 | 500 | 5 | 4.543 | 0.91 |
| T319C_1 | | 1000 | | [a] | [a] |
| T120A_1 | 345 | 500 | 0.01 | 0.006 | 0.55 |
| | | | 1 | 0.857 | 0.86 |
| T120A_2 | | | 0.01 | 0.009 | 0.93 |
| | | | 1 | [a] | [a] |
| T120A_3 | | | 0.01 | 0.009 | 0.93 |
| | | | 1 | 0.759 | 0.76 |
| T120C_1 | | 1000 | 0.01 | 0.006 | 0.61 |
| | | | 1 | 0.559 | 0.56 |
| T120C_2 | | | 0.01 | 0.009 | 0.86 |
| | | | 1 | 0.410 | 0.41 |
| T120C_3 | | | 0.01 | 0.009 | 0.88 |
| | | | 1 | 0.455 | 0.46 |

Note:

a Stepper motor stalled.

**Table 6.7** Measured parameters from the vertical partially-drained tests

| Test | $K^{/}_{eq}$ (N/mm) | $V_o$ (N) | Primary Section | | Secondary Section |
|---|---|---|---|---|---|
| | | | $K_{vp\text{-}p}$ (N/mm) | $\Delta V_{vp\text{-}p}$ (N) | $K_{vp\text{-}s}$ (N) |
| T102_1 | 180 | 500 | 3690 | 80 | 148 [c] |
| T102a_1 | 255 | 1000 | 3930 | 160 | 160 [c] |
| T103a_1 | 112 | 500 | 3260 | 65 | 82 [c] |
| T103a_2 | 136 | 1000 | 3770 | 100 | 70 [c] |
| T105_1 | 156 | 500 | 1700 | 50 | 171 |
| T105_2 | 223 | 1000 | 4290 | 60 | 230 [c] |
| T106_3 | 337 | 500 | 6290 | 75 | 357 |
| T106_4 | 514 [a] | 1000 | 8170 | 200 | 488 |
| T107_1 | 173 | 500 | 2450 | 100 | 132 |
| T107a_1 | 220 [b] | 1000 | 4680 | 175 | 159 |
| T110_1 | 483 | 500 | 2500 | 125 | 624 |
| T110_2 | 925 [a] | 1000 | 4820 | 250 | 832 |
| T311_1 | 259 | 500 | 3350 | 60 | 261 |
| T311_2 | 264 | 1000 | 3820 | 100 | 274 |
| T112b_1 | 350 | 500 | 2520 | 125 | 250 |
| T112d_1 | 412 | 1000 | 4980 | 210 | 291 |
| T313a_1 | 480 | 500 | 9140 | 150 | 469 |
| T313c_1 | 657 | 1000 | 23900 | 240 | 930 |
| T114b_1 | 234 | 500 | 7390 | 150 | 191 |
| T114d_1 | 354 | 1000 | 5420 | 250 | 248 |
| T315_1 | 470 | 500 | 4400 | 75 | 524 |
| T315_2 | 593 | 1000 | 5690 | 150 | 652 |
| T116_1 | 385 | 500 | 3000 | 60 | 410 |
| T116a_1 | 517 | 1000 | 6580 | 150 | 537 |
| T317_1 | 481 | 500 | 4000 | 50 | 582 |
| T317_2 | 659 | 1000 | 7000 | 100 | 715 |
| T118a_1 | 409 | 500 | 4590 | 125 | 414 |
| T118c_1 | 910 [a] | 1000 | 10290 | 300 | 397 |
| T319a_1 | 342 | 500 | 3000 | 150 | 310 |
| T319c_1 | 661 [a] | 1000 | 6970 | 300 | [d] |

Note:

a These values of $K^{/}_{eq}$ that were measured between 900 N and 1000 N may not have been representative of the virgin-penetration stiffness because of over-consolidation.

b Estimated value, see Table 6.1.

c Significant work softening was evident before the secondary section.

d Motor stalled.

**Table 7.1** Displacement rates of horizontal sideswipe tests

<table>
<tr><th colspan="2" rowspan="2">Name</th><th>$K'_{ch}$</th><th>$V_{oi}$</th><th colspan="2">d$u$/d$t$ (mm/s)</th></tr>
<tr><th>(N/mm)</th><th>(N)</th><th>Intended</th><th>Measured</th></tr>
<tr><td colspan="2">T101_1</td><td>144</td><td>1630</td><td>0.001</td><td>0.0008</td></tr>
<tr><td colspan="2">T103A_3</td><td>112</td><td>1340</td><td>0.1</td><td>0.0969</td></tr>
<tr><td colspan="2">T204_1</td><td>628</td><td>1500</td><td>0.001</td><td>0.0008</td></tr>
<tr><td colspan="2">T106_5</td><td>337</td><td>1500</td><td>0.4</td><td>0.3167</td></tr>
<tr><td colspan="2">T107A_3</td><td>173</td><td>1500</td><td>0.4</td><td>0.3464</td></tr>
<tr><td colspan="2">T309_1</td><td>476</td><td>1500</td><td>0.001</td><td>0.0008</td></tr>
<tr><td colspan="2">T110_3</td><td>483</td><td>1500</td><td>0.4</td><td>0.2128</td></tr>
<tr><td colspan="2">T315_3</td><td rowspan="2">470</td><td>1500</td><td>0.04</td><td>0.009</td></tr>
<tr><td colspan="2">T315C_1</td><td>1500</td><td>0.1</td><td>0.0617</td></tr>
<tr><td colspan="2">T116A_2</td><td>385</td><td>1500</td><td>0.1</td><td>0.0688</td></tr>
<tr><td colspan="2">T118D_1</td><td rowspan="2">409</td><td>1500</td><td>0.001</td><td>0.0009</td></tr>
<tr><td colspan="2">T118D_2</td><td>1700</td><td>-0.001</td><td>-0.001</td></tr>
<tr><td rowspan="2">T120D_1</td><td rowspan="11">T120D_H1</td><td rowspan="23">345</td><td rowspan="11">1500</td><td>0.001</td><td>0.0001</td></tr>
<tr><td>0.1</td><td>0.0165</td></tr>
<tr><td rowspan="2">T120D_2</td><td>0.001</td><td>0.0003</td></tr>
<tr><td>0.1</td><td>0.0029</td></tr>
<tr><td rowspan="2">T120D_3</td><td>0.001</td><td>0.0005</td></tr>
<tr><td>0.1</td><td>0.0115</td></tr>
<tr><td rowspan="2">T120D_4</td><td>0.001</td><td>0.0006</td></tr>
<tr><td>0.1</td><td>0.0186</td></tr>
<tr><td rowspan="2">T120D_5</td><td>0.001</td><td>0.0007</td></tr>
<tr><td>0.1</td><td>0.0044</td></tr>
<tr><td>T120D_5A</td><td>0.001</td><td>0.0001</td></tr>
<tr><td>T120D_6</td><td rowspan="12">T120D_H2</td><td rowspan="12">1700</td><td>-0.001</td><td>-0.0002</td></tr>
<tr><td>T120D_7</td><td>-0.1</td><td>-0.0167</td></tr>
<tr><td>T120D_8</td><td>-0.001</td><td>-0.0004</td></tr>
<tr><td>T120D_9</td><td>-0.1</td><td>-0.0291</td></tr>
<tr><td>T120D_10</td><td>-0.001</td><td>-0.0005</td></tr>
<tr><td>T120D_11</td><td>-0.1</td><td>-0.0219</td></tr>
<tr><td>T120D_11A</td><td>-0.001</td><td>-0.0006</td></tr>
<tr><td>T120D_12</td><td>-0.001</td><td>-0.0006</td></tr>
<tr><td>T120D_13</td><td>-0.1</td><td>-0.0297</td></tr>
<tr><td>T120D_14</td><td>-0.001</td><td>-0.0007</td></tr>
<tr><td>T120D_15</td><td>-0.1</td><td>-0.0195</td></tr>
<tr><td>T120D_16</td><td>-0.001</td><td>-0.0008</td></tr>
<tr><td>T120D_17</td><td>-0.1</td><td>-0.0359</td></tr>
</table>

Note:
Tests T120D_1 to T120D_5A composed a single sideswipe that was labelled T120D_H1.
Tests T120D_6 to T120D_17 composed a single sideswipe that was labelled T120D_H2.

**Table 7.2** Displacement rates of moment sideswipe tests

| Name | $K'_{ch}$ (N/mm) | $V_{oi}$ (N) | $d(2R\theta)/dt$ (mm/s) | |
|---|---|---|---|---|
| | | | Intended | Measured |
| T102A_2 | 180 | 1500 | 0.0026 | 0.0026 |
| T105_3 | 156 | 1500 | 0.26 | 0.2616 |
| T311_3 | 259 | 1500 | 0.0026 | 0.0026 |
| T112E_1 | 350 | 1500 | 0.524 | 0.4926 |
| T313D_1 | 480 | 1500 | 0.524 | 0.4639 |
| T114E_1 | 234 | 1500 | 0.524 | 0.5036 |
| T317_3 | 481 | 1500 | 0.026 | 0.0213 |
| T317A_1 | | 1800 | 0.026 | 0.0216 |
| T319D_1 | 342 | 1500 | 0.0026 | 0.0023 |
| T319D_2 | | 1700 | -0.0026 | -0.0022 |
| T319D_3 | | 2000 | 0.0026 | 0.0023 |
| T120D_18 | 345 | 1900 | 0.0026 | 0.0017 |
| | | | 0.26 | 0.1465 |
| T120D_19 | | | 0.0026 | 0.0019 |
| | | | 0.26 | 0.1833 |
| T120D_20 | | | 0.0026 | 0.0021 |
| | | | 0.26 | 0.2182 |
| T120D_21 | | | 0.0026 | 0.0022 |
| | | | 0.26 | 0.2121 |
| T120D_22 | | | 0.0026 | 0.0023 |
| | | | 0.26 | 0.2286 |
| T120D_22A T120D_M1 | | | 0.0026 | 0.0023 |
| T120D_23 | | | 0.0026 | 0.0026 |
| | | | 0.26 | 0.2339 |
| T120D_24 | | | 0.0026 | 0.0023 |
| | | | 0.26 | 0.1833 |
| T120D_25 | | | 0.0026 | 0.0022 |
| | | | 0.26 | 0.1676 |
| T120D_26 | | | 0.0026 | 0.0021 |
| | | | 0.26 | 0.1833 |
| T120D_27 | | | 0.0026 | 0.0026 |
| | | | 0.26 | 0.2294 |
| T120E_1 (T120E_M2) | | 2100 | -0.0026 | -0.002 |
| T120E_2 | | | -0.26 | -0.2755 |
| T120E_3 | | | -0.0026 | -0.0019 |
| T120E_4 | | | -0.26 | -0.2686 |
| T120E_5 | | | -0.0026 | -0.002 |
| T120E_6 | | | -0.26 | -0.313 |
| T120E_7 | | | -0.0026 | -0.0023 |
| T120E_8 | | | -0.26 | -0.2696 |

Note:
Tests T120D_18 to T120D_27 composed a single sideswipe that was labelled T120D_M1.
Tests T120E_1 to T120D_8 composed a single sideswipe that was labelled T120E_M2.

**Table A.1** Factors for bearing capacity formulae

| Factor | Brinch Hansen (1970) | Meyerhof (1963) | Vesic (1975) |
|---|---|---|---|
| $N_\gamma$ | $1.5(N_q - 1)\tan\phi$ | $(N_q - 1)\tan(1.4\phi)$ | $2(N_q + 1)\tan\phi$ |
| $N_q$ | $e^{\pi\tan\phi}\tan^2\left(45° + \frac{\phi}{2}\right)$ | $e^{\pi\tan\phi}\tan^2\left(45° + \frac{\phi}{2}\right)$ | $e^{\pi\tan\phi}\tan^2\left(45° + \frac{\phi}{2}\right)$ |
| $s_\gamma$ | $1 - 0.4 i_\gamma \frac{B'}{L'}$ | $1 + 0.1\tan^2\left(45° + \frac{\phi}{2}\right)\frac{B'}{L'}$ | $1 - 0.4\frac{B'}{L'}$ |
| $s_q$ | $1 + i_q \sin\phi \frac{B'}{L'}$ | $1 + 0.1\tan^2\left(45° + \frac{\phi}{2}\right)\frac{B'}{L'}$ | $1 + \tan\phi \frac{B'}{L'}$ |
| $d_\gamma$ | 1 | $1 + 0.1\tan\left(45° + \frac{\phi}{2}\right)\frac{z}{B'}$ | 1 |
| $d_q$ | $1 + 2\tan\phi(1 - \sin\phi)^2 \frac{z}{B'}$ | $1 + 0.1\tan\left(45° + \frac{\phi}{2}\right)\frac{z}{B'}$ | $1 + 2\tan\phi(1 - \sin\phi)^2 \frac{z}{B'}$ |
| $i_\gamma$ | $\left(1 - 0.7\frac{H}{V}\right)^5$ | $\left(1 - \frac{\alpha}{\phi}\right)^2$ | $\left(1 - \frac{H}{V}\right)^{m+1}$ |
| $i_q$ | $\left(1 - 0.5\frac{H}{V}\right)^5$ | $\left(1 - \frac{\alpha}{90}\right)^2$ | $\left(1 - \frac{H}{V}\right)^{m}$ |

Note:

See Appendix A for definitions not mentioned below.

$\phi$ in degrees.

For circular footings use the triaxial friction angle in Meyerhof's and Vesic's formulae but use the plane-strain friction angle in Brinch Hansen's formulae.

$L'$ is the maximum effective foundation dimension.

$\alpha = \tan^{-1}(H/V)$ where $H/V$ is the ratio of horizontal to vertical load and $\alpha < \phi$.

$$m = \frac{2 + B'/L'}{1 + B'/L'}$$

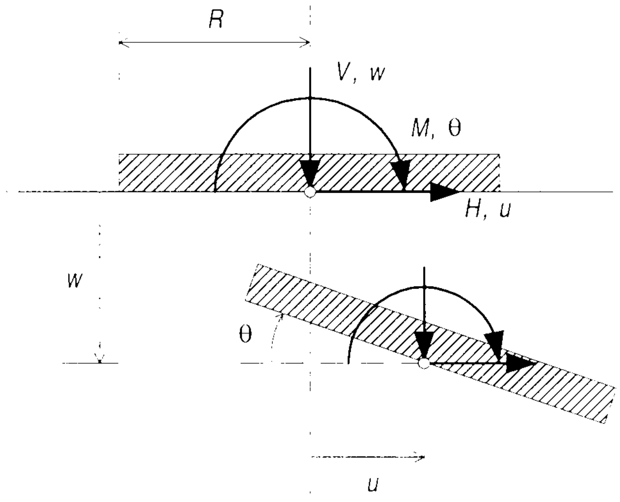


**Figure 2.1**
Sign convention for combined loads and displacements

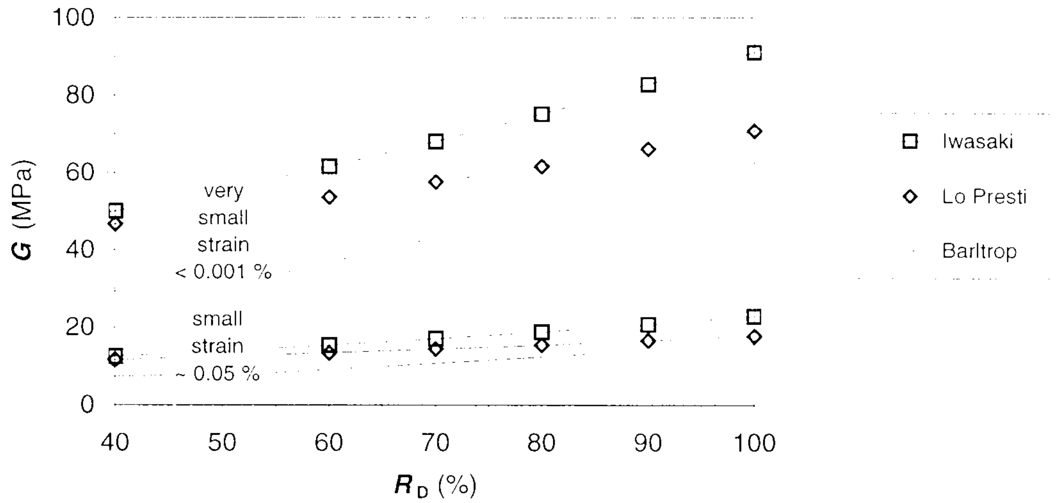


Notes:

Iwasaki et.al. (1978) :

$$\frac{G_0}{p_a} = 900\left(\frac{p'}{p_a}\right)^{0.4}\frac{(2.17-e)^2}{(1+e)}$$

Lo Presti (1987) :

$$\frac{G_0}{p_a} = 591\left(\frac{p'}{p_a}\right)^{0.246} e^{0.693 R_D}$$

Barltrop & Adams (1991) :

$$G_0 = 600\sqrt{p_a p'} \quad \text{for } e > 0.8$$

$$G_0 = 1300\sqrt{p_a p'} \quad \text{for } e < 0.5$$

$p' = 30$ kPa; $p_a = 100$ kPa; $G_{small\ strain} = 0.25 G_0$

**Figure 2.2** Elastic shear moduli from the literature

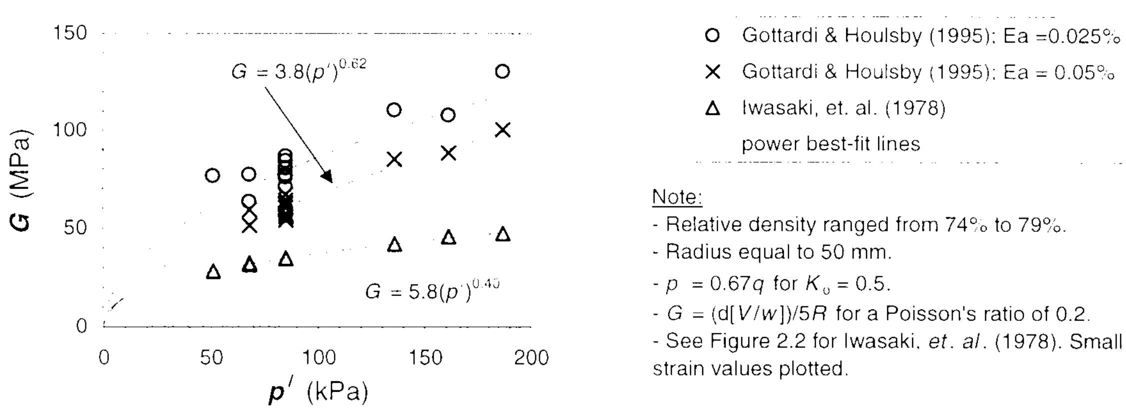


Note:
- Relative density ranged from 74% to 79%.
- Radius equal to 50 mm.
- $p' = 0.67q$ for $K_0 = 0.5$.
- $G = (d[V/w])/5R$ for a Poisson's ratio of 0.2.
- See Figure 2.2 for Iwasaki, *et. al.* (1978). Small strain values plotted.

**Figure 2.3** Elastic shear moduli from the footing tests of Gottardi and Houlsby (1995)

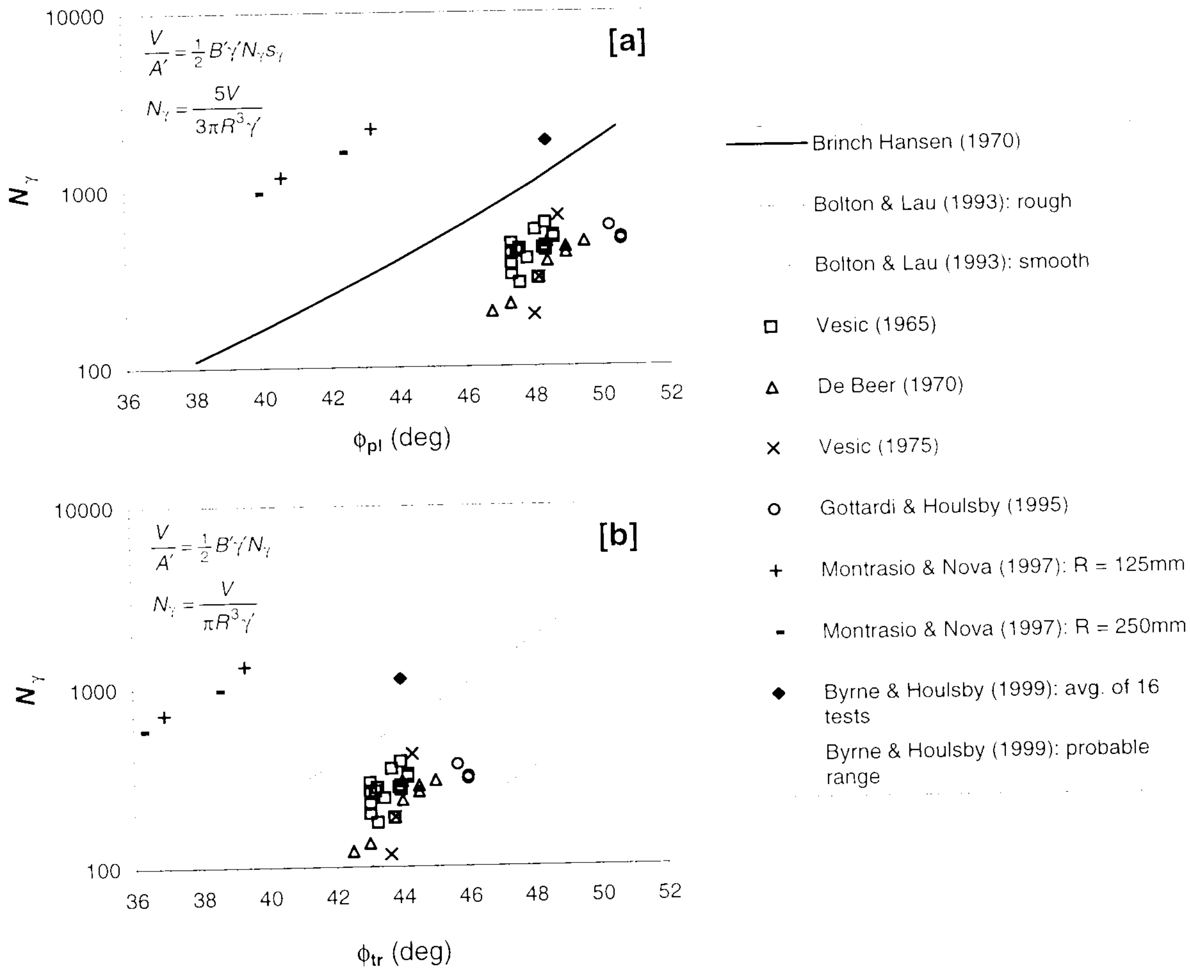


| Source | $R$ (mm) | $R_D$ (%) | $p'$ [a] (kPa) | Derivation of $\phi_{max}$ | $\phi_{crit}$ (deg) |
|---|---|---|---|---|---|
| Vesic (1965) | 50 | 76 - 82 | 14 - 30 | $\phi = \tan^{-1}(0.68/e)$ [b] | n/a |
| De Beer (1970) | 75 | 65 - 89 | 14 - 37 | $\phi = f(R_D, p')$ [c] | n/a |
| Vesic (1975) | 76 | 61 - 78 | 13 - 49 | Bolton (1986) | 33 [d] |
| Gottardi & Houlsby (1995) | 50 | 75 | 28 | Bolton (1986) | 34 |
| Montrasio & Nova (1997) | 125 & 500 | 45 & 70 | 132 - 382 | Bolton (1986) | 33 [d] |
| Byrne & Houlsby (1999) | 25 | 97 | 47 | Bolton (1986) | 32 [e] |

Note:

a Effective mean stress along shear plane at failure taken as one tenth of contact stress. see de Beer (1970).
b Relationship stated to be relevant for $p' < 70$ kPa.
c See Figure 10 in de Beer (1970).
d Value of $\phi_{crit}$ assumed.
e Byrne's tests were on Baskarp Cyclone sand, see Section 4.5 for relevant data.

All footings were classified as "rough".
Plane strain friction angles used in Brinch Hansen's method, $\phi_{pl} = 1.1\phi_{tr}$.

**Figure 2.4** A comparison of theoretical and experimental bearing capacity factors: **[a]** Brinch Hansen (1970); and **[b]** Bolton and Lau (1993)

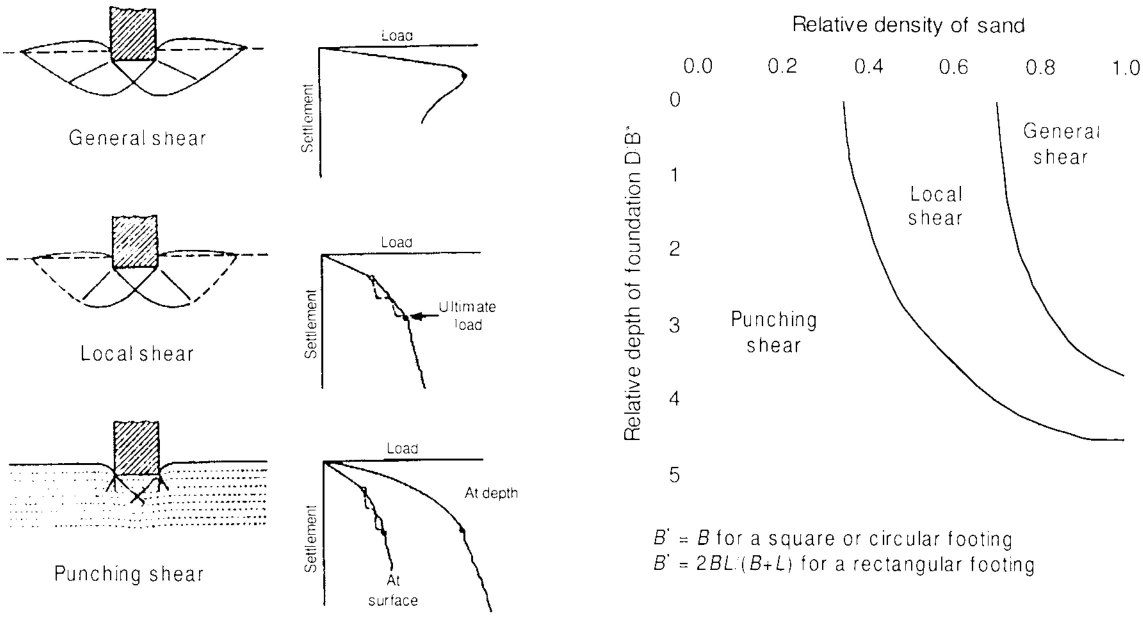


**Figure 2.5** Bearing capacity failure mechanisms (after Vesic, 1975)

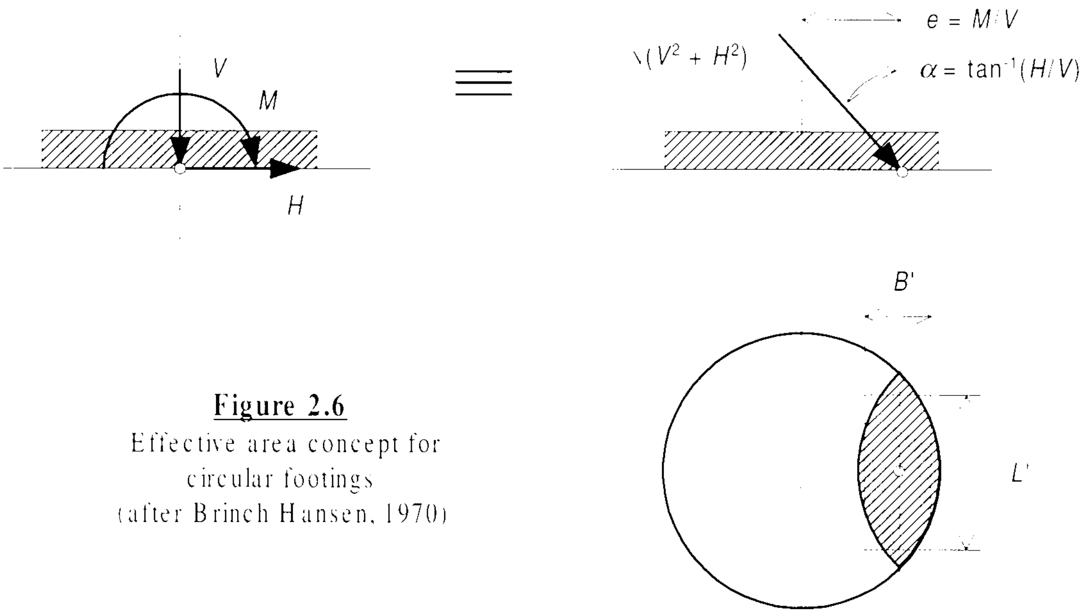


**Figure 2.6**
Effective area concept for circular footings
(after Brinch Hansen, 1970)

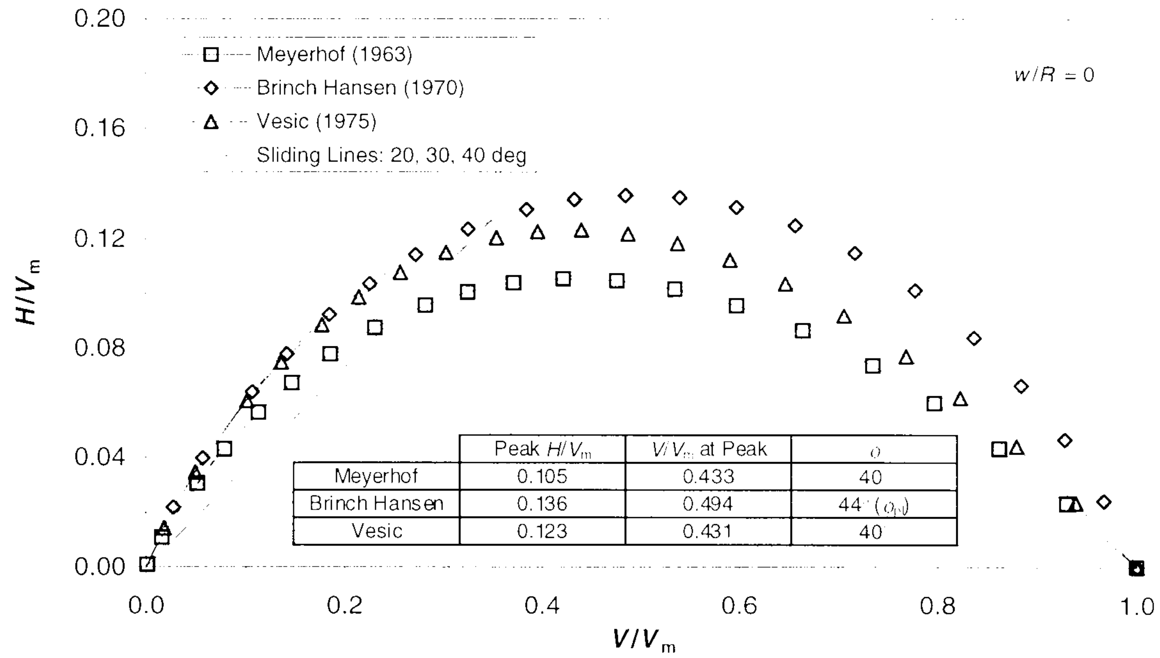


| | Peak $H/V_m$ | $V/V_m$ at Peak | $\phi$ |
|---|---|---|---|
| Meyerhof | 0.105 | 0.433 | 40 |
| Brinch Hansen | 0.136 | 0.494 | 44° ($\phi_{ps}$) |
| Vesic | 0.123 | 0.431 | 40 |

**Figure 2.7** $V{:}H$ yield surfaces deduced from the traditional bearing capacity methods

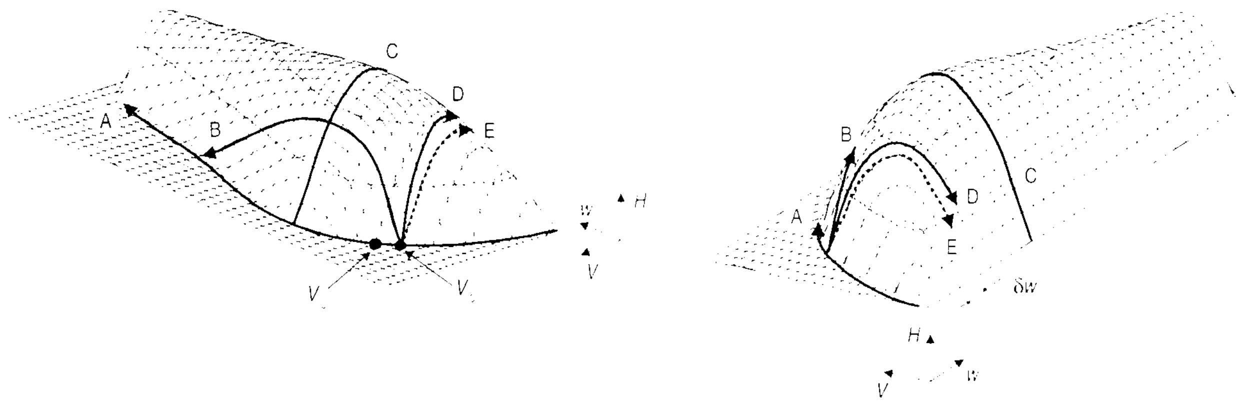


[a]

$V_c$ is the initial virgin-penetration load
$V_c$ is the extrapolated virgin-penetration load
$w_e$ is the elastic vertical displacement
$w_p$ is the plastic vertical displacement

A Virgin-penetration curve
B Constant-$V$ test
C $V_m{:}H$ failure envelope
D Sideswipe with $\delta w > 0$
E Sideswipe with $\delta w = 0$

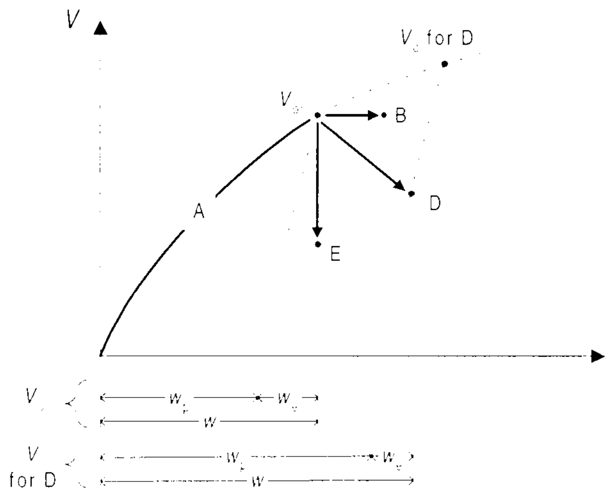


[b]

**Figure 2.8**
Illustration of sideswipe and constant-$V$ tests:
[a] in $w{:}V{:}H$ space; and
[b] in $w{:}V$ space

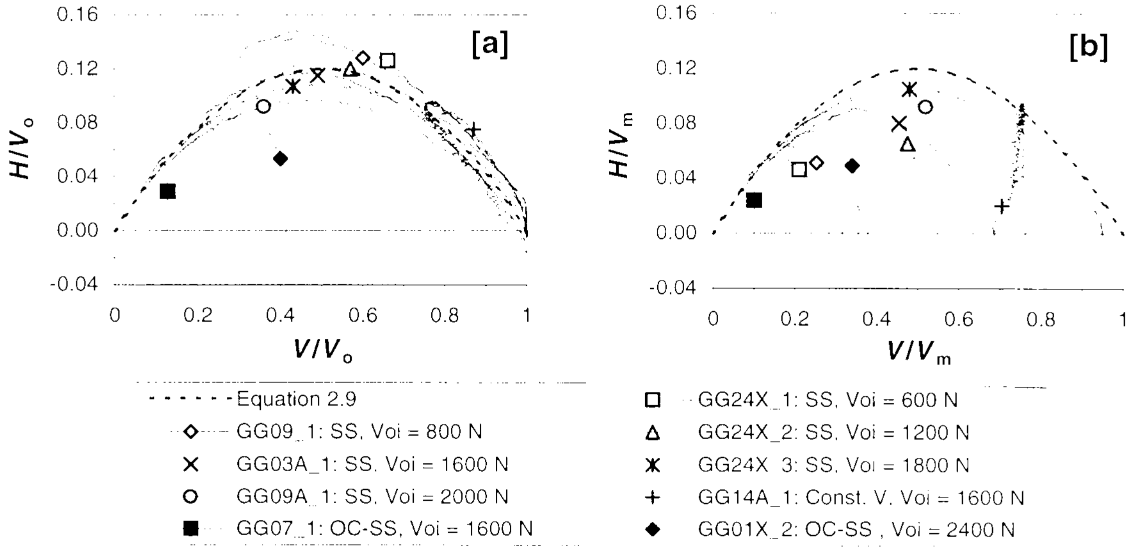


Note:
- SS = sideswipe test, Const. V = constant V test, and OC-SS = overconsolidated sideswipe test.
- In the OC-SS tests, the footing was loaded up to the indicated $V_{oi}$ values before unloading and performance of the sideswipes.

**Figure 2.9** Effect of normalisation on $V$:$H$ yield surfaces:
**[a]** $V_o$-normalised; and **[b]** $V_m$-normalised (data from Gottardi and Houlsby, 1995)

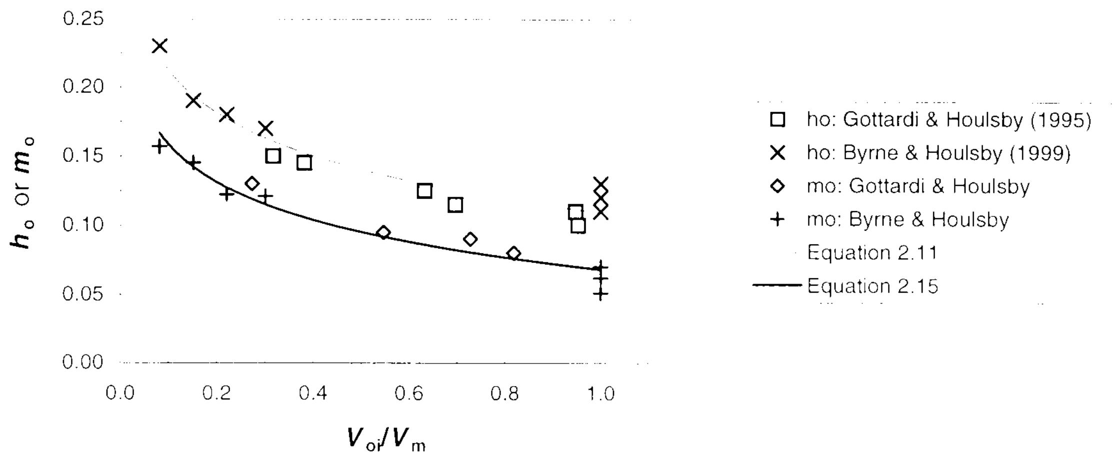


**Figure 2.10** Relationship between normalised peak loads and $V_{oi}/V_m$ ratio from sideswipe tests in the literature

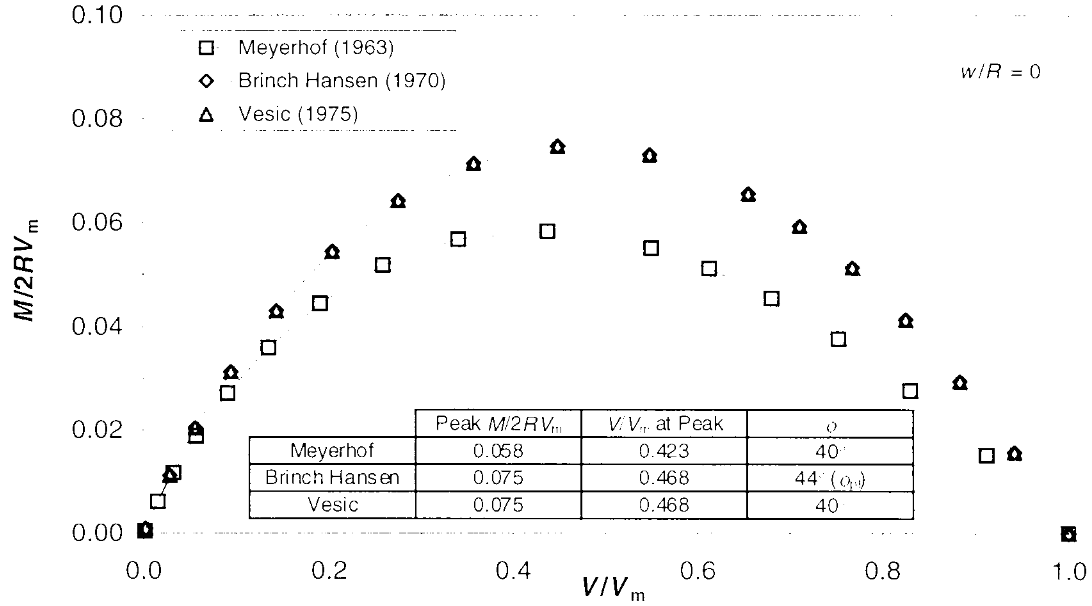


| | Peak $M/2RV_m$ | $V/V_m$ at Peak | $\phi$ |
|---|---|---|---|
| Meyerhof | 0.058 | 0.423 | 40° |
| Brinch Hansen | 0.075 | 0.468 | 44° ($\phi_{ps}$) |
| Vesic | 0.075 | 0.468 | 40° |

**Figure 2.11** $V:M$ interaction loci deduced from traditional bearing capacity methods

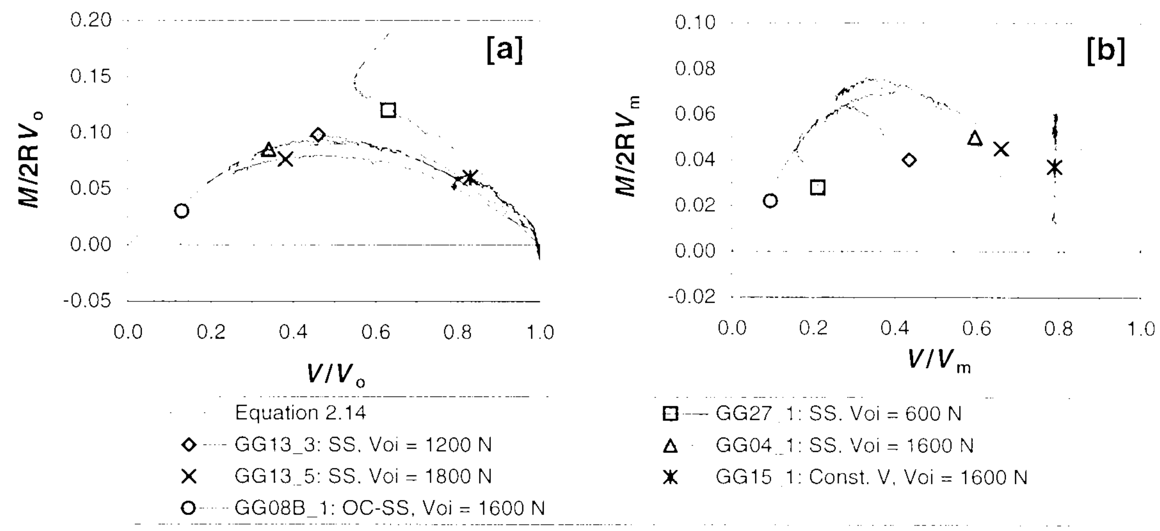


Note:
- SS = sideswipe test, Const. V = constant V test, and OC-SS = overconsolidated sideswipe test.
- In the OC-SS tests, the footing was loaded up to the indicated $V_o$ values before unloading and performance of the

**Figure 2.12** Effect of normalisation on $V:M$ yield surfaces:
**[a]** $V_o$-normalised; and **[b]** $V_m$-normalised (data from Gottardi and Houlsby, 1995)

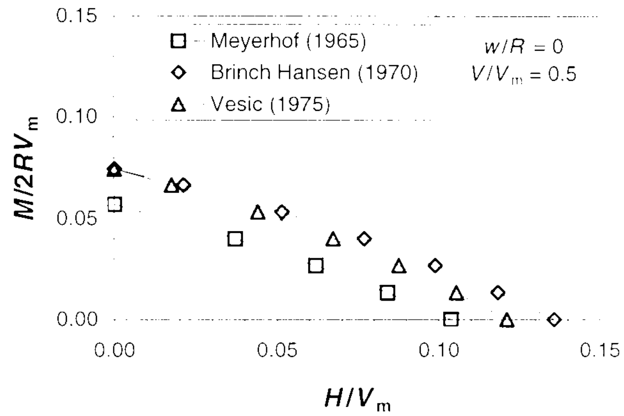


**Figure 2.13**
$H:M$ failure surfaces derived using the traditional bearing capacity methods (plotted in the $(+H):(+M)$ quadrant only)

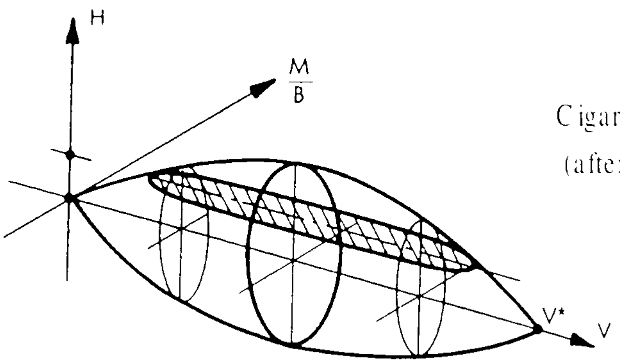


**Figure 2.14**
Cigar shaped $V$:$H$:$M$ failure surface
(after Butterfield and Ticof, 1979)

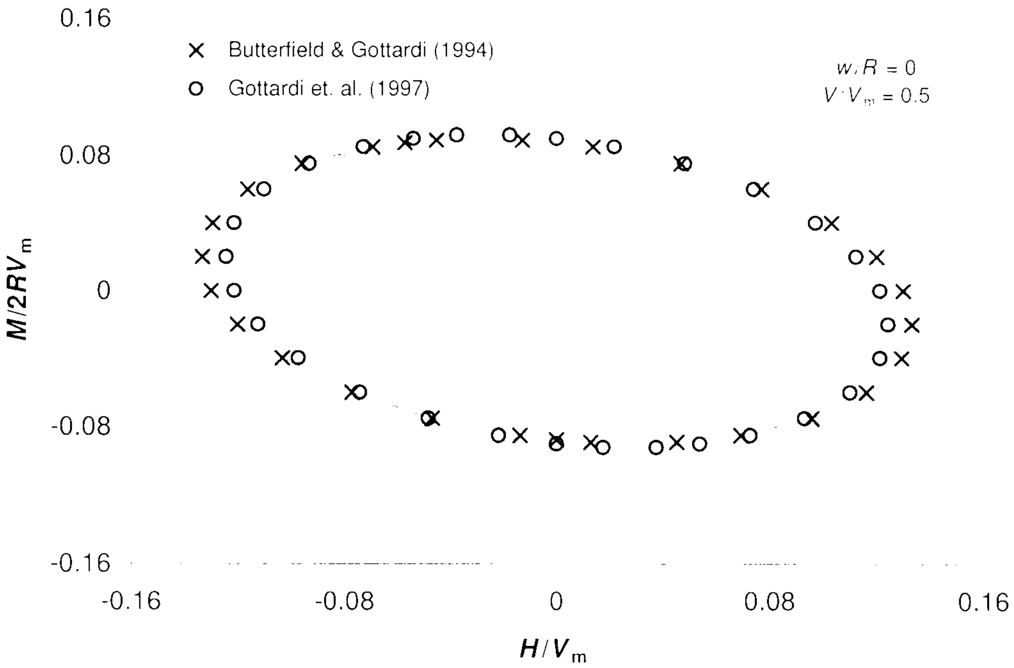


**Figure 2.15** $H$:$M$ failure surfaces derived from combined load tests

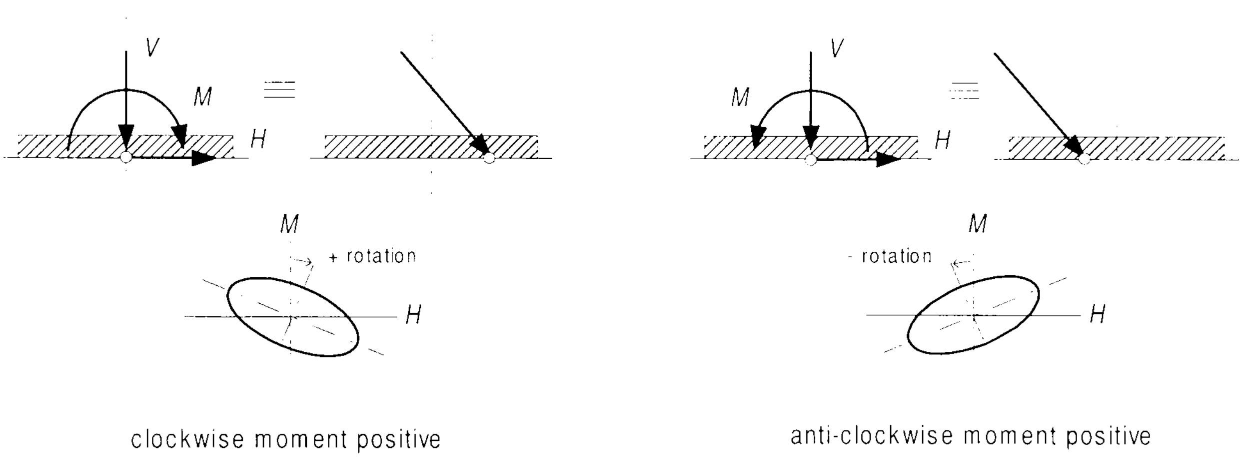


**Figure 2.16** Effect of sign convention on eccentricity of $H$:$M$ ellipse

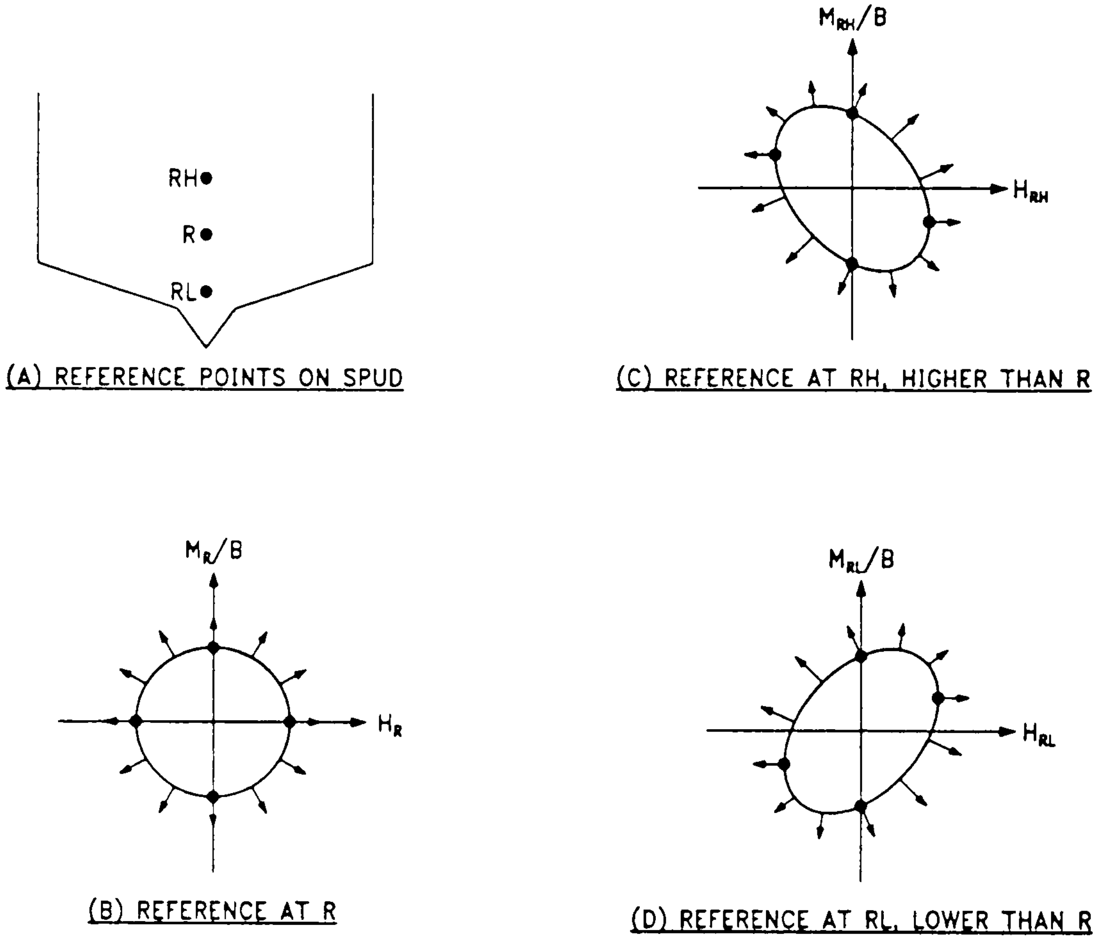


**Figure 2.17** Effect of the position of the load/displacement reference point (after Dean *et al.*, 1992b)

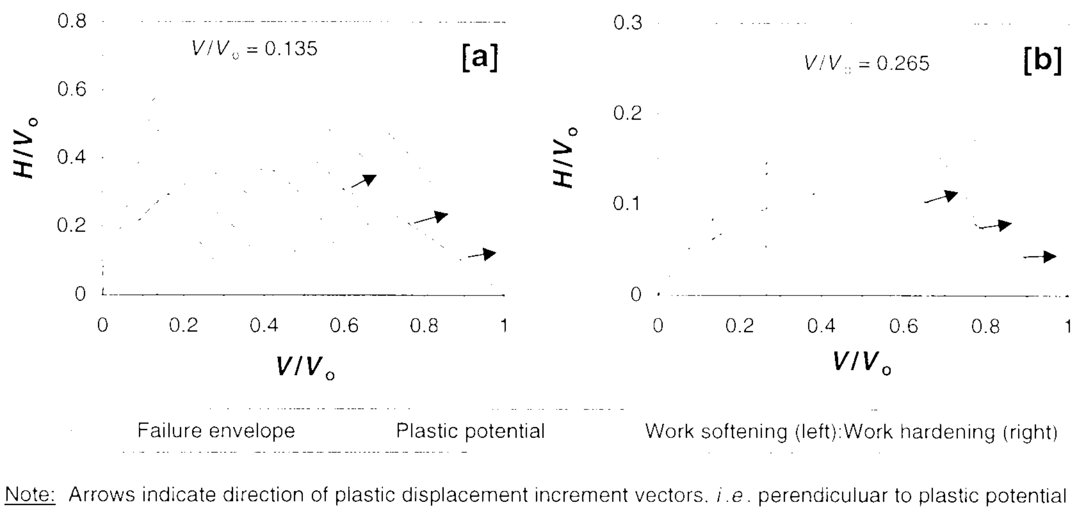


**Figure 2.18** Failure envelope, plastic potentials and work softening/work hardening regions: **[a]** Tan (1990); and **[b]** Cassidy (1996)

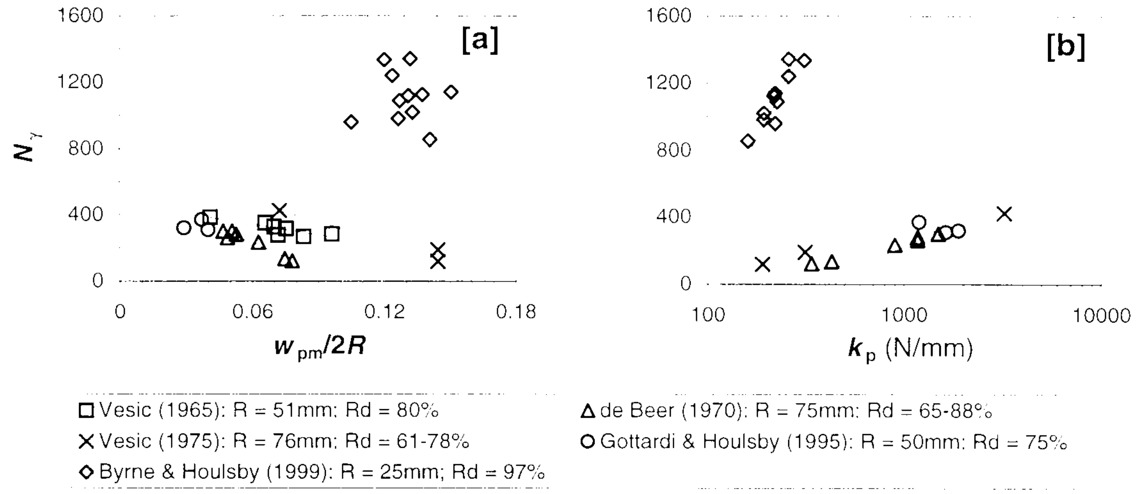


Note: Some linear trendlines shown. Intercepts set to zero in [b].

**Figure 2.19** Relationship between load:deformation parameters of experimental data in the literature: **[a]** bearing capacity factor against normalised displacement at failure: and **[b]** bearing capacity factor against initial virgin-penetration stiffness

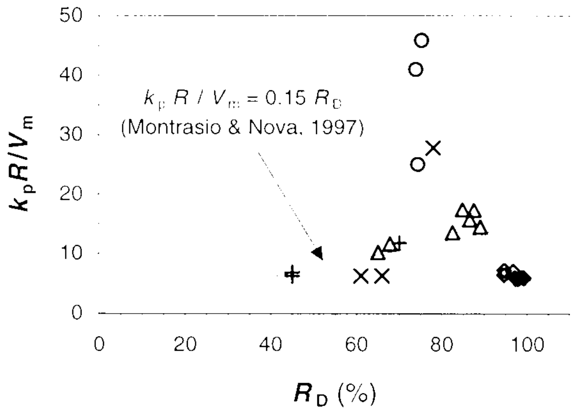


de Beer (1970): R = 75mm
Vesic (1975): R = 76mm
Gottardi & Houlsby (1995): R = 50mm
Montrasio & Nova (1997): R = 125 & 250mm
Byrne & Houlsby (1999): R = 25mm

**Figure 2.20** Normalised initial virgin-penetration stiffness; relationship suggested by Montrasio and Nova compared with other results

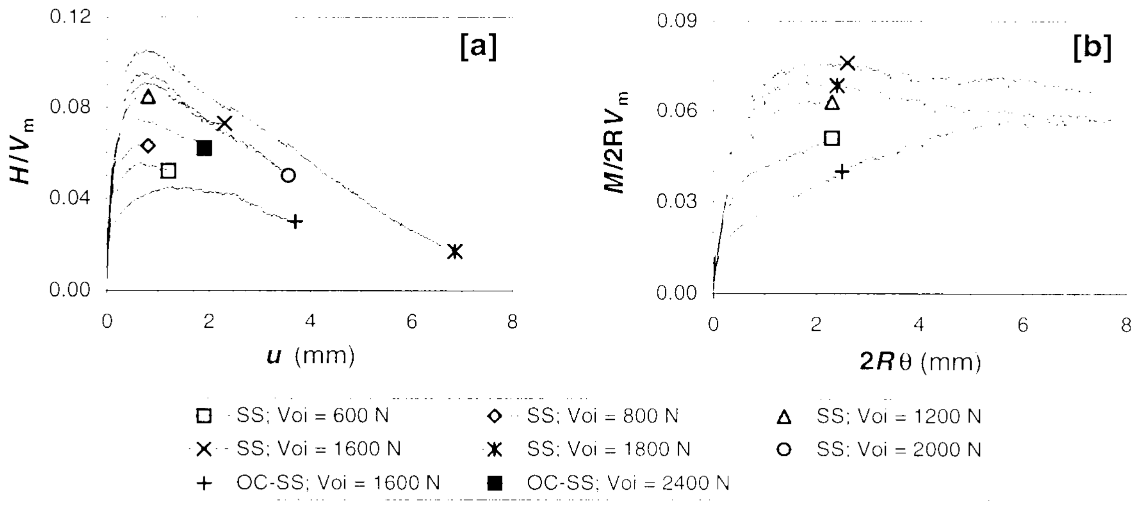


Note:
- SS = sideswipe test and OC-SS = overconsolidated sideswipe test.
- In the OC-SS tests, the footing was loaded up to the indicated $V_{oi}$ values before unloading and performance of the sideswipes.

**Figure 2.21** Normalised load:deformation response of sideswipe tests:
**[a]** horizontal sideswipes; and **[b]** moment sideswipes (data from of Gottardi & Houlsby, 1995)

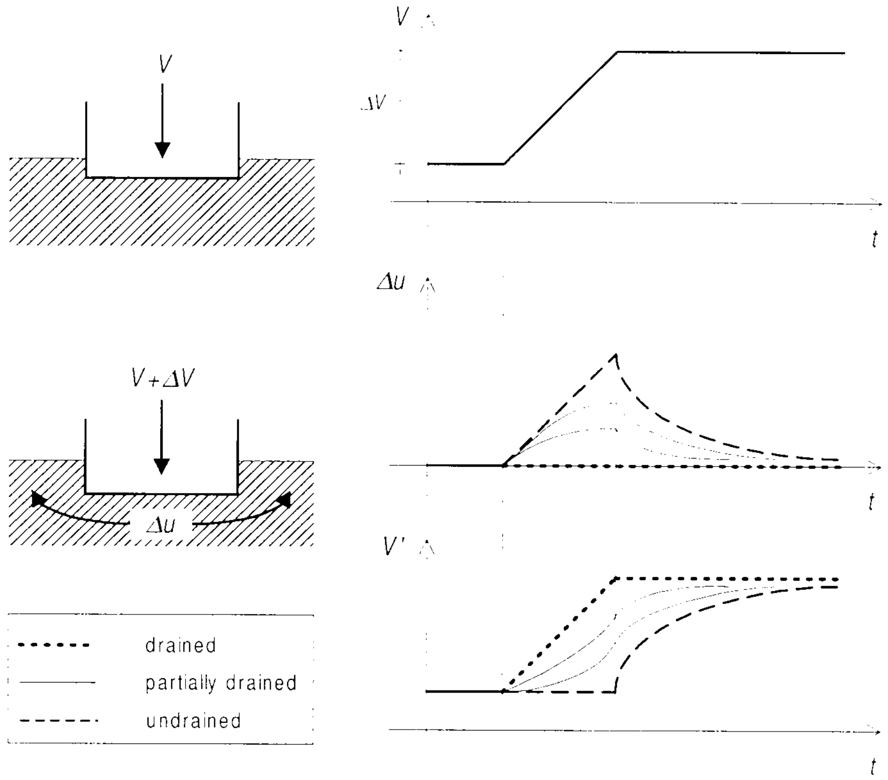


**Figure 2.22**
Effect of drainage conditions on a transient load increment

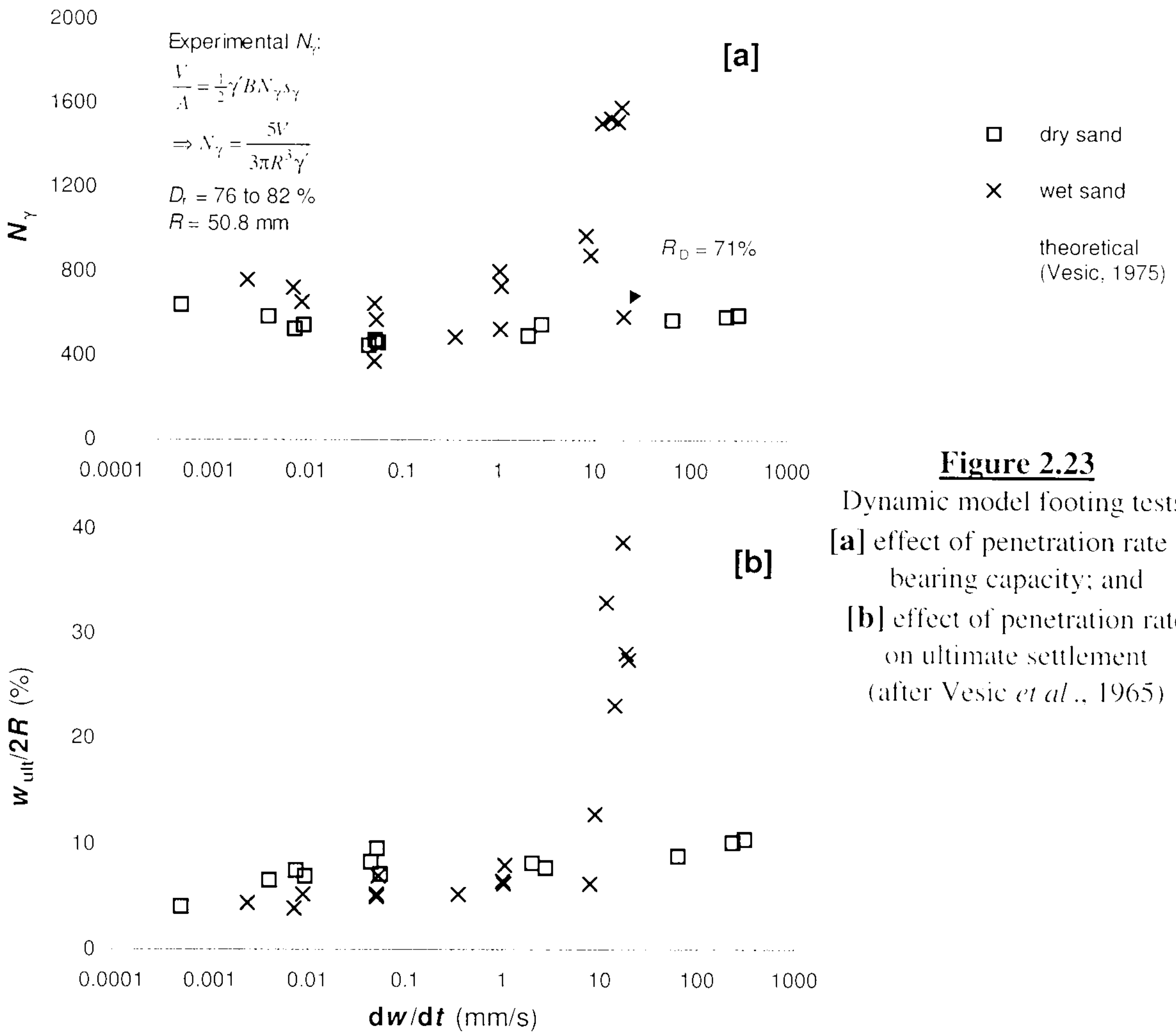


**Figure 2.23**
Dynamic model footing tests:
**[a]** effect of penetration rate on bearing capacity; and
**[b]** effect of penetration rate on ultimate settlement
(after Vesic *et al.*, 1965)

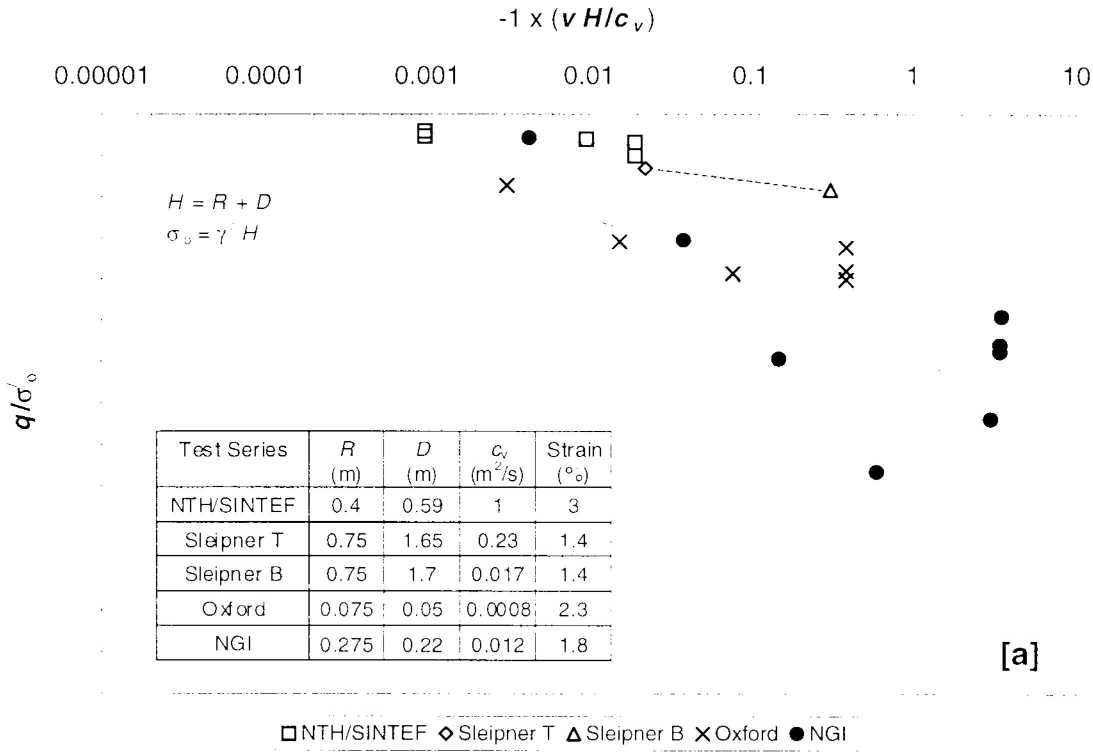


| Test Series | $R$ (m) | $D$ (m) | $c_v$ ($m^2/s$) | Strain (%) |
|---|---|---|---|---|
| NTH/SINTEF | 0.4 | 0.59 | 1 | 3 |
| Sleipner T | 0.75 | 1.65 | 0.23 | 1.4 |
| Sleipner B | 0.75 | 1.7 | 0.017 | 1.4 |
| Oxford | 0.075 | 0.05 | 0.0008 | 2.3 |
| NGI | 0.275 | 0.22 | 0.012 | 1.8 |

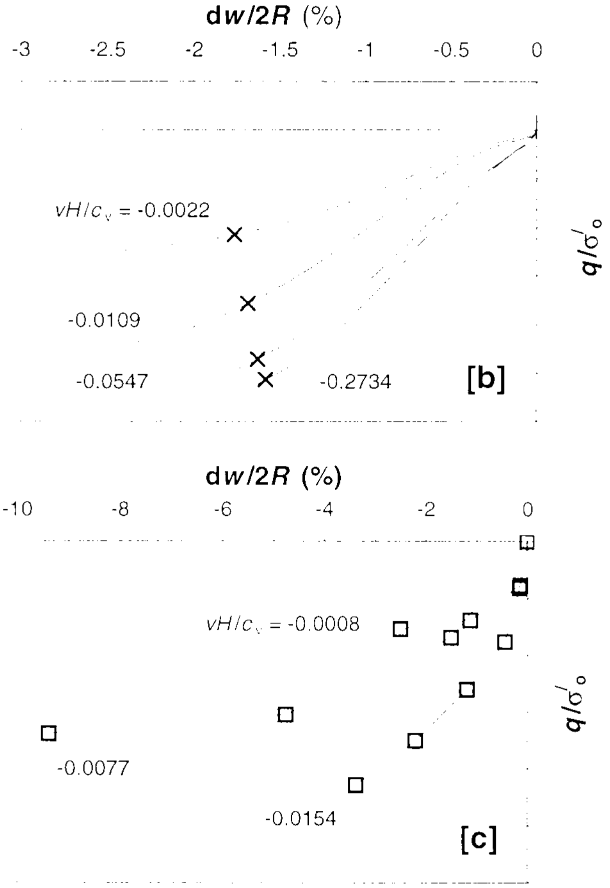


Note:
Vertical scales not labelled because of confidentiality restrictions.

NTH/SINTEF:
- SINTEF (1992)
- tests 2, 4, 6, 9, 12 & 16
- laboratory tests

Sleipner T & B:
- SINTEF (1992)
- offshore tests

Oxford:
- Houlsby (1995)
- test OX01
- laboratory test
- downward hydraulic gradient of 3.6
- Oxford tests scaled to NGI as geometric and effective stress scales were similar

NGI:
- NGI (1994a)
- tests LOAD 1L-1 to LOAD 1L-9
- laboratory tests

**Figure 2.24** Effect of pull-out rate on load:deformation behaviour of suction caisson foundations:
**[a]** trend of increasing load with increasing pull-out velocity;
**[b]** Oxford tests; and **[c]** NTH/SINTEF tests

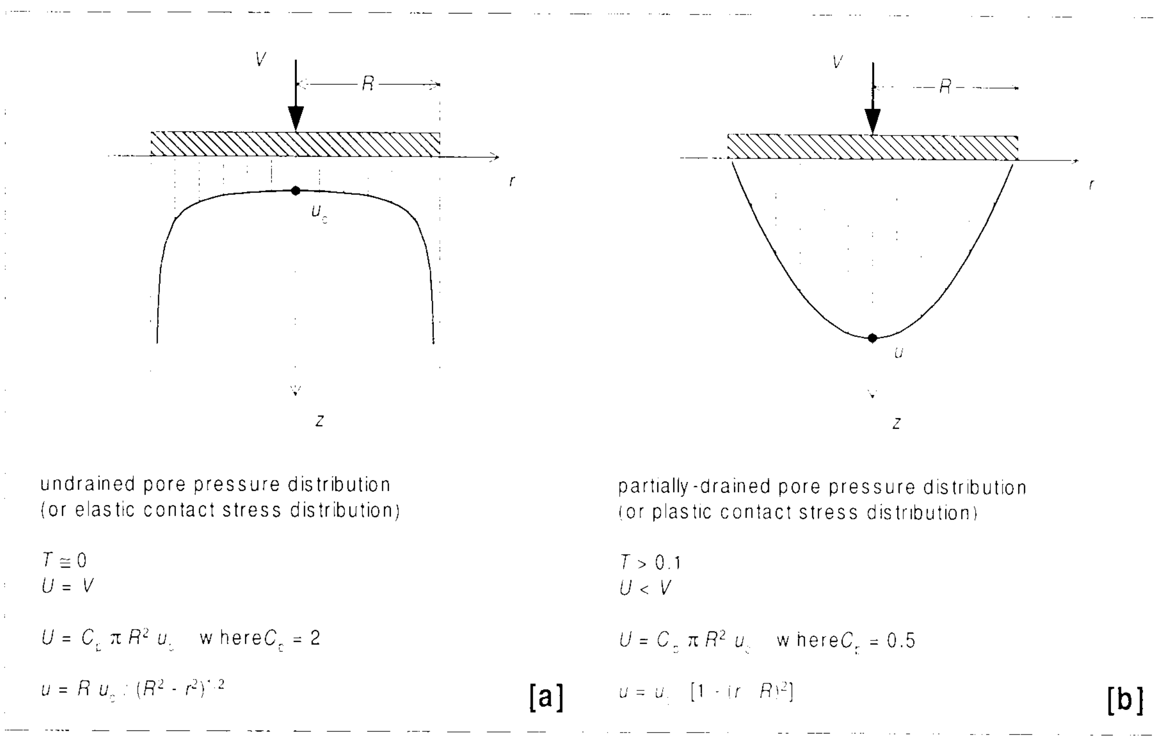


**Figure 2.25** Pore pressure distributions beneath a rigid circular footing: **[a]** undrained distribution; and **[b]** partially-drained distribution

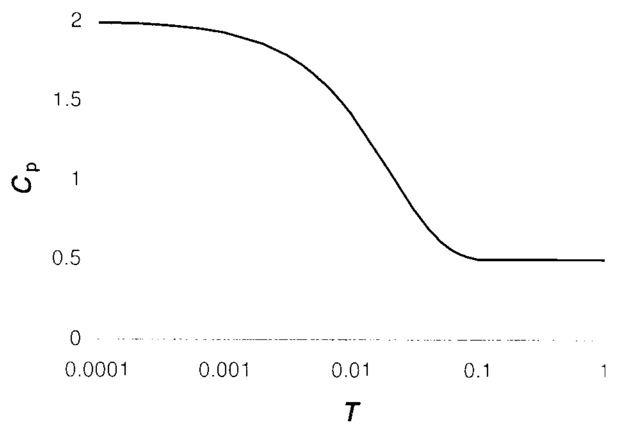


**Figure 2.26**
Variation of the coefficient of pore pressure distribution with the non-dimensional time factor

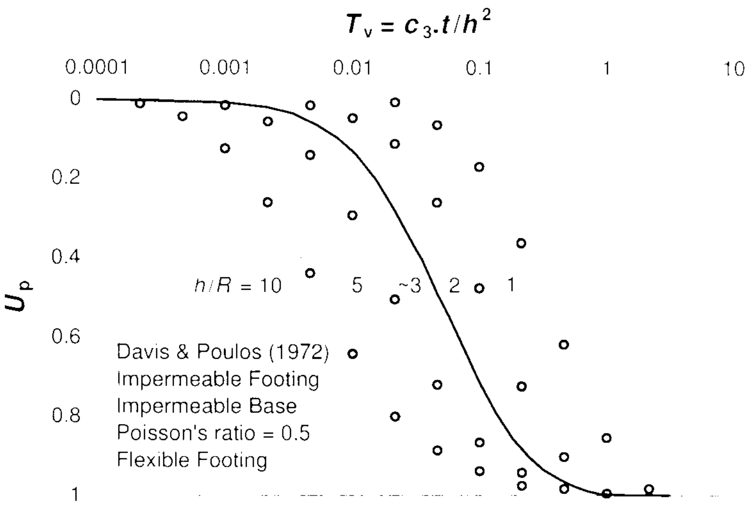


**Figure 2.27**
Rate of pore pressure dissipation

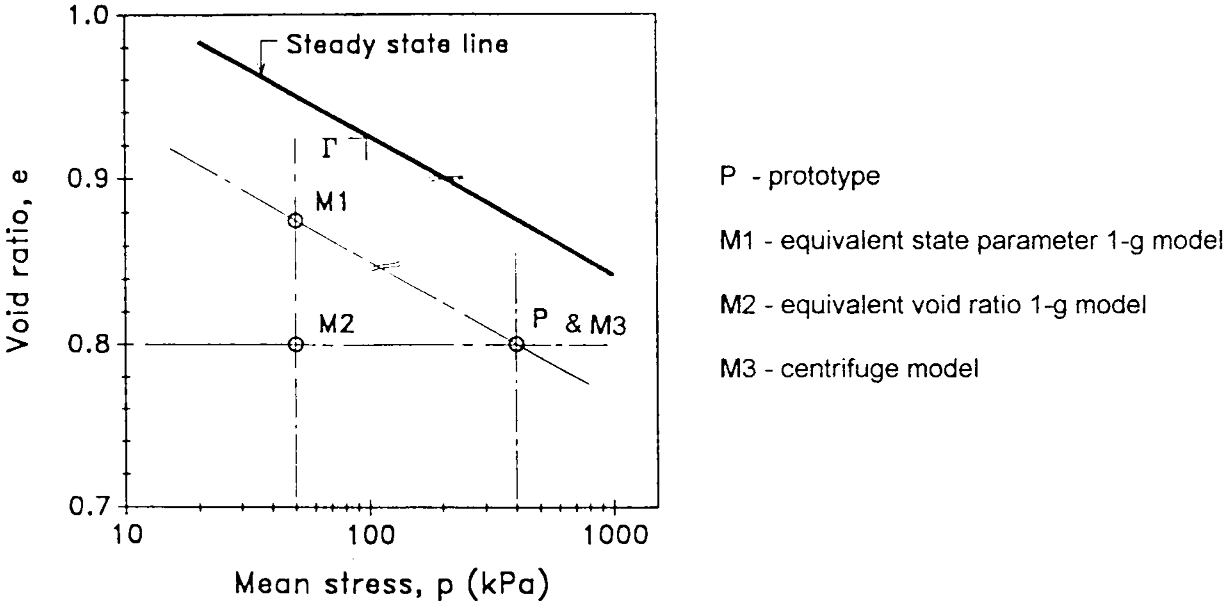


**Figure 2.28** Reference states of models and prototype
(after Altaee and Fellenius, 1994)

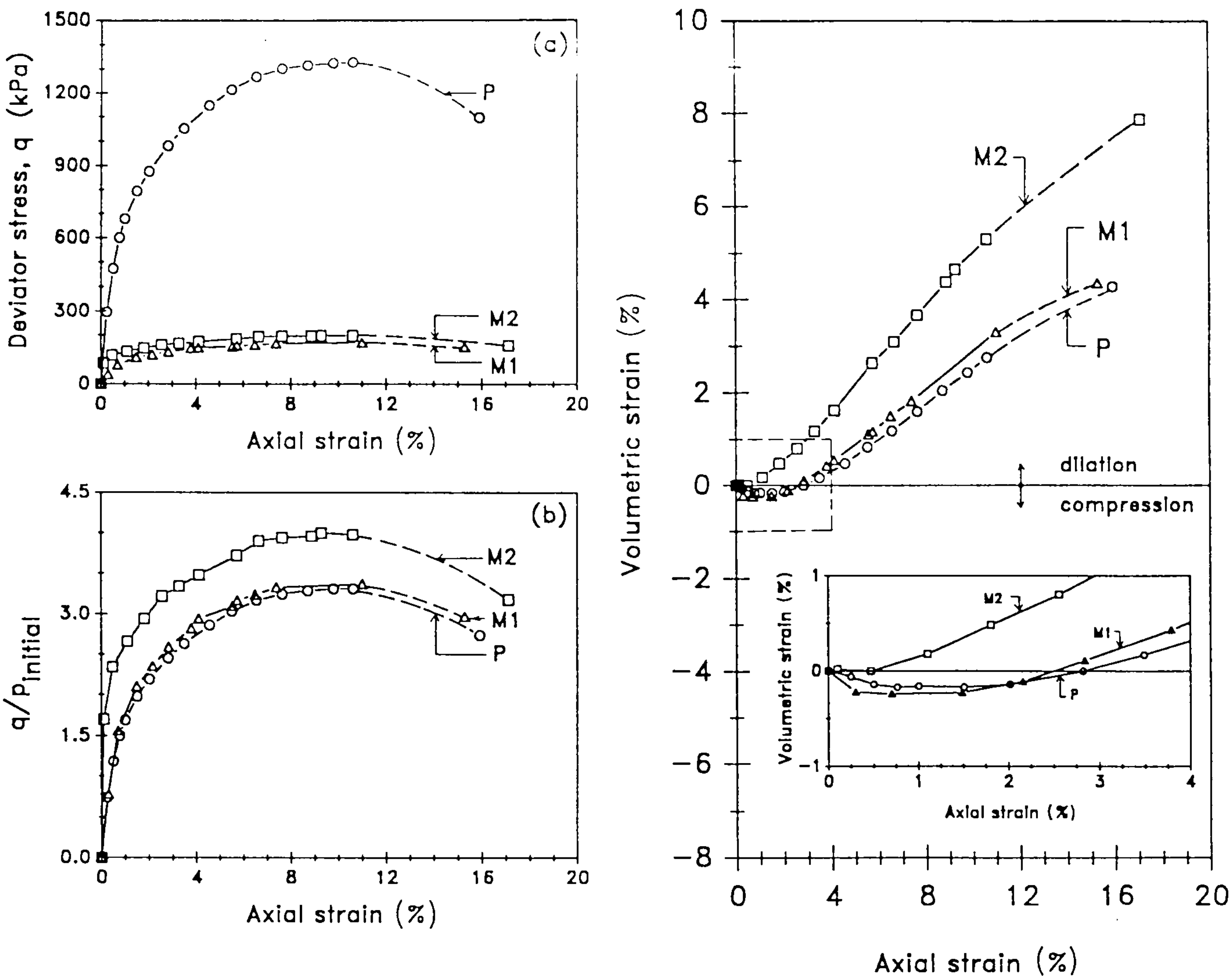


P - prototype; M1 - equivalent state parameter 1-g model; M2 - equivalent void ratio 1-g model

**Figure 2.29** Triaxial drained response of reference states P, M1, and M2
(after Altaee and Fellenius, 1994)

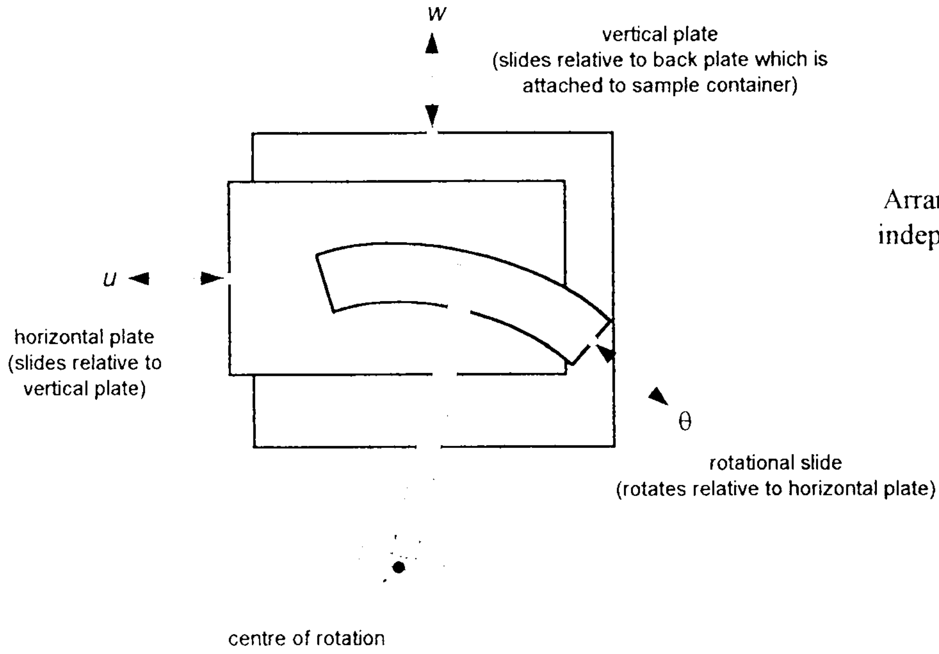


**Figure 3.1**
Arrangement of the three independent displacement systems

**Figure 3.2** Shaft connecting footing to rotational slide

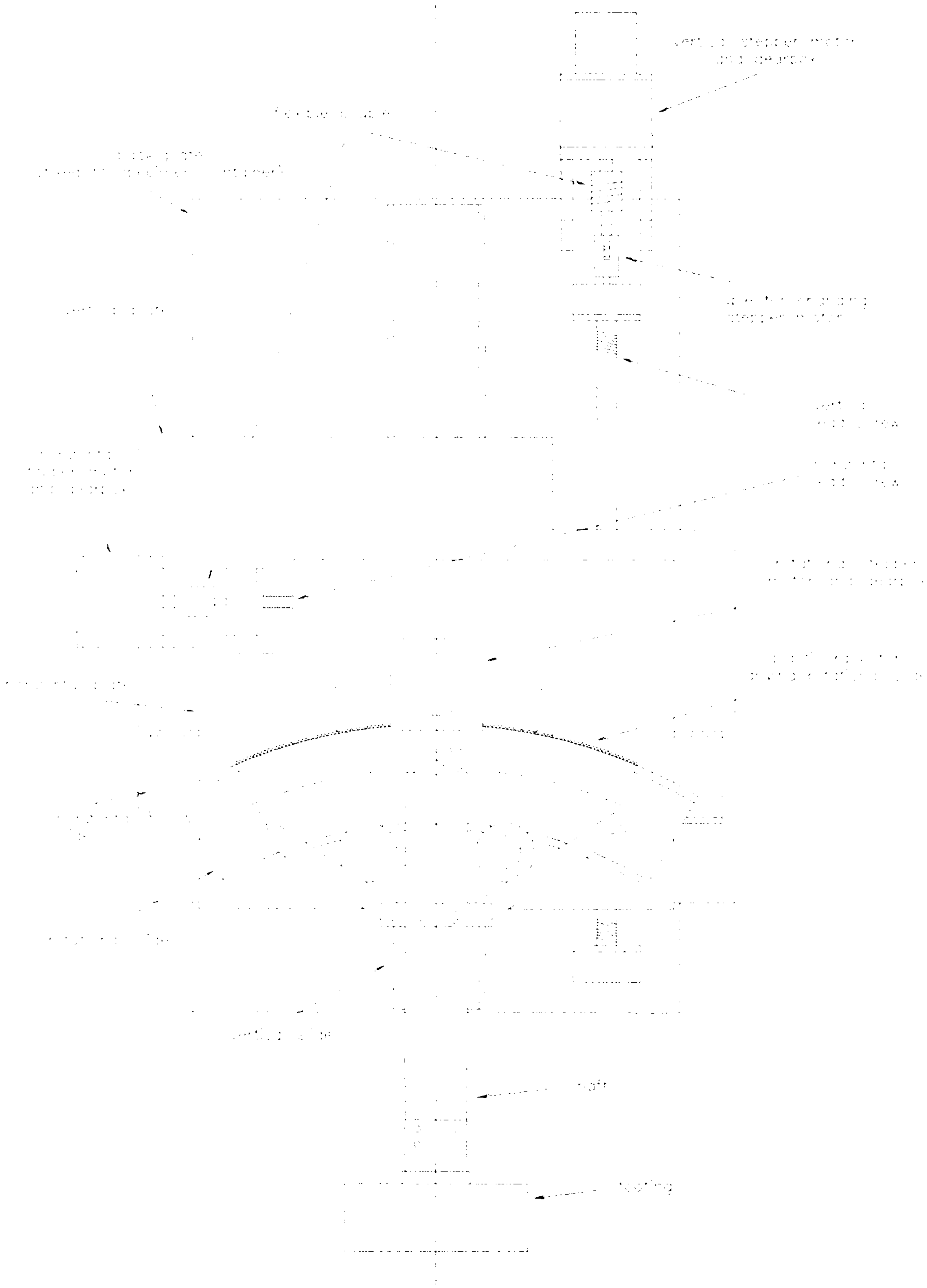

**Figure 3.3** Stepper motor arrangement and drive system

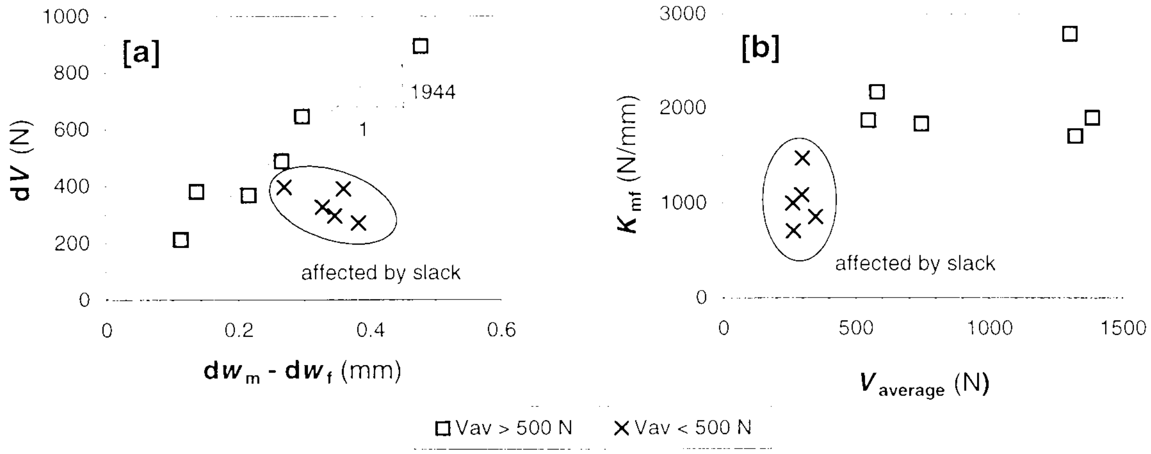


Note:
- $dw_m$ was the vertical displacement at the stepper motor.
- $dw_f$ was the vertical displacement at the footing.
- $K_{mf}$ was the vertical stiffness of the rig measured between the stepper motor and the footing.

**Figure 3.4** The vertical stiffness of the rig and slack in the vertical displacement system: **[a]** average vertical stiffness of rig; and **[b]** effect of slack on vertical rig stiffness

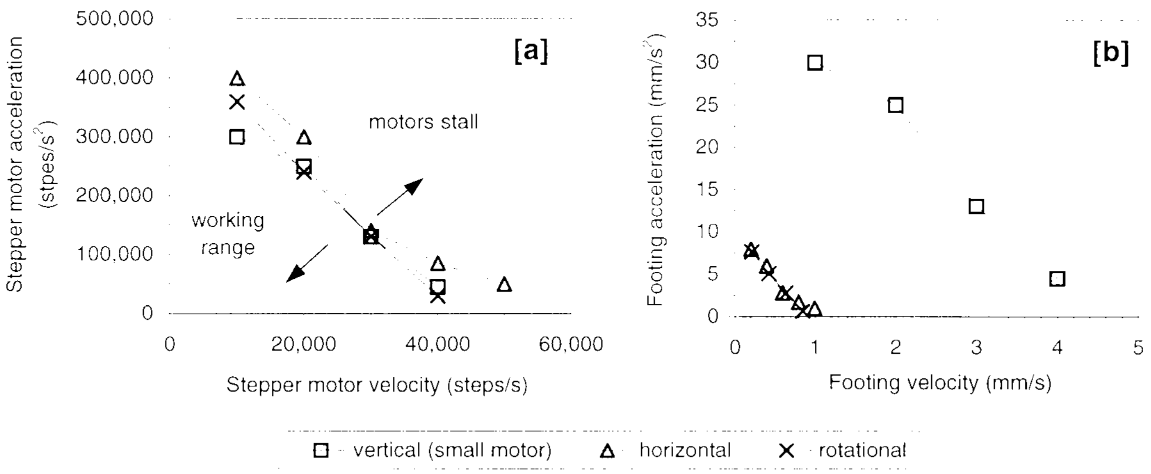


**Figure 3.5** Working range of the stepper motors under minimal load: **[a]** in steps; and **[b]** in millimeters

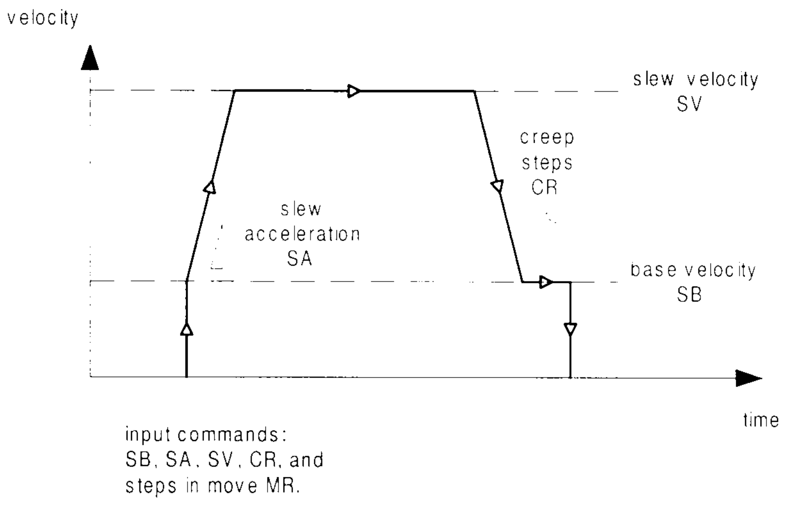


**Figure 3.6** Velocity path and stepper motor commands for a Move Relative (MR) event

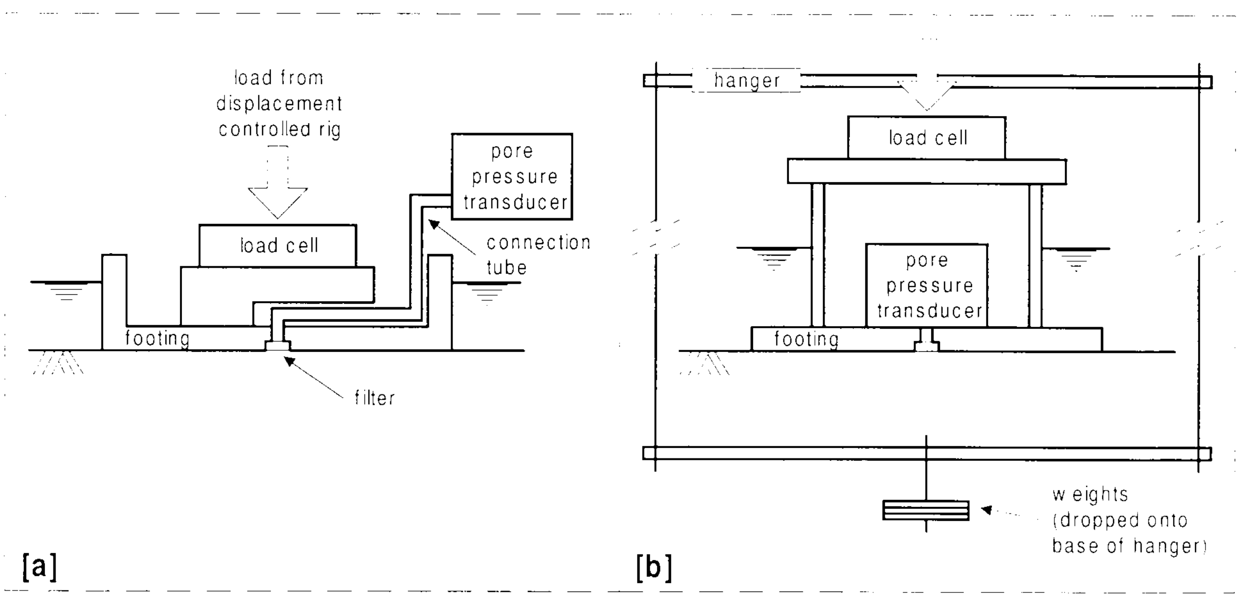


**Figure 3.7** Apparatus of preliminary tests:
[a] 100 mm diameter footing with external pore pressure transducer; and
[b] 150 mm diameter footing with internal pore pressure transducer

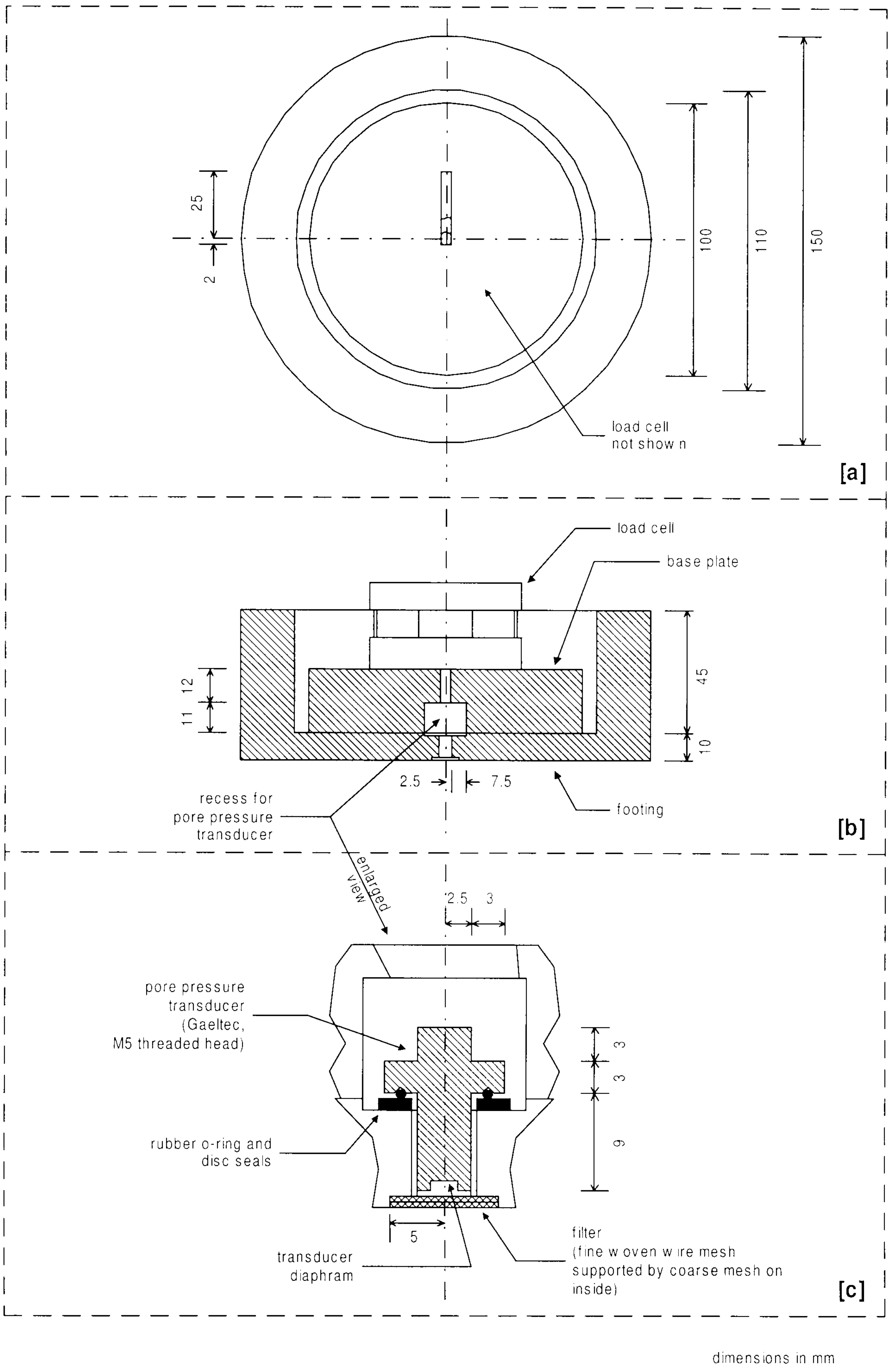


**Figure 3.8** The footing and base plate, and pore pressure transducer:
[a] plan view of footing and base plate; [b] section through footing and base plate; and
[c] detail of pore pressure transducer

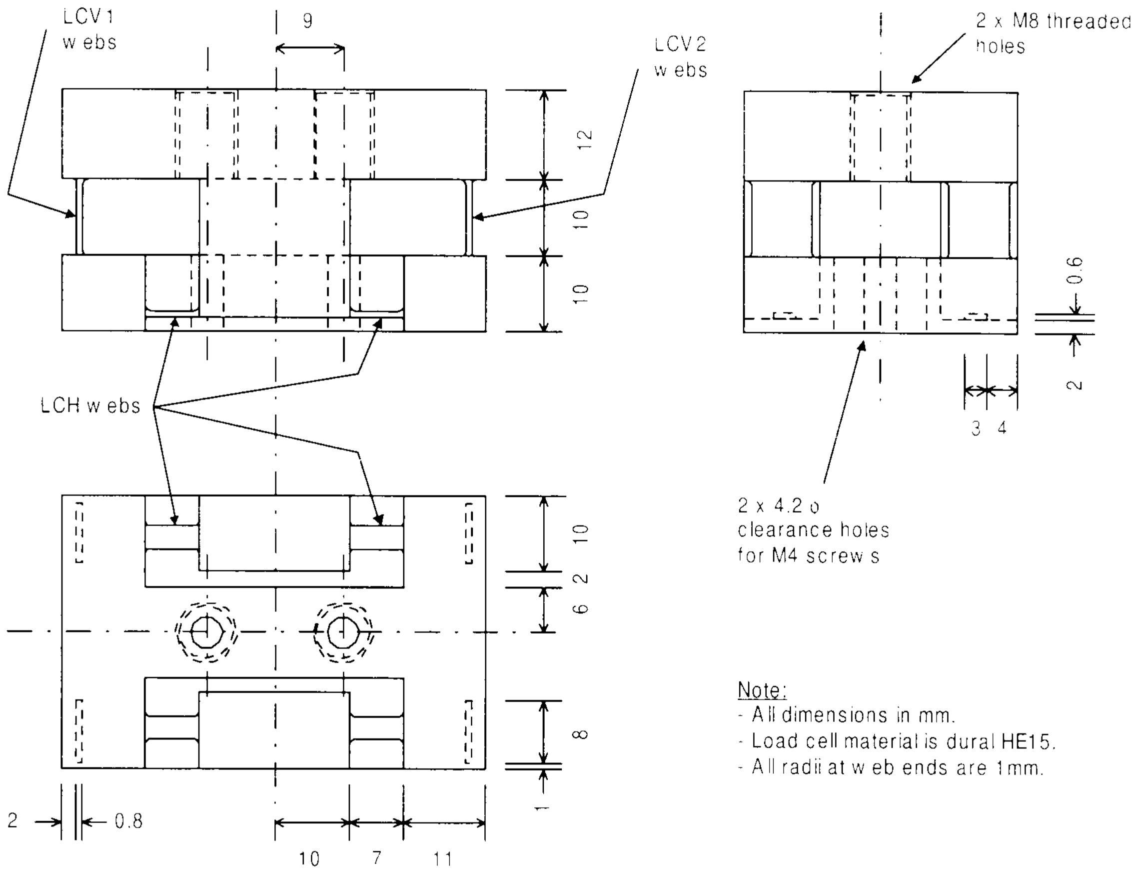


**Figure 3.9** Load cell for measuring $V$, $H$, and $M$ loads on footing

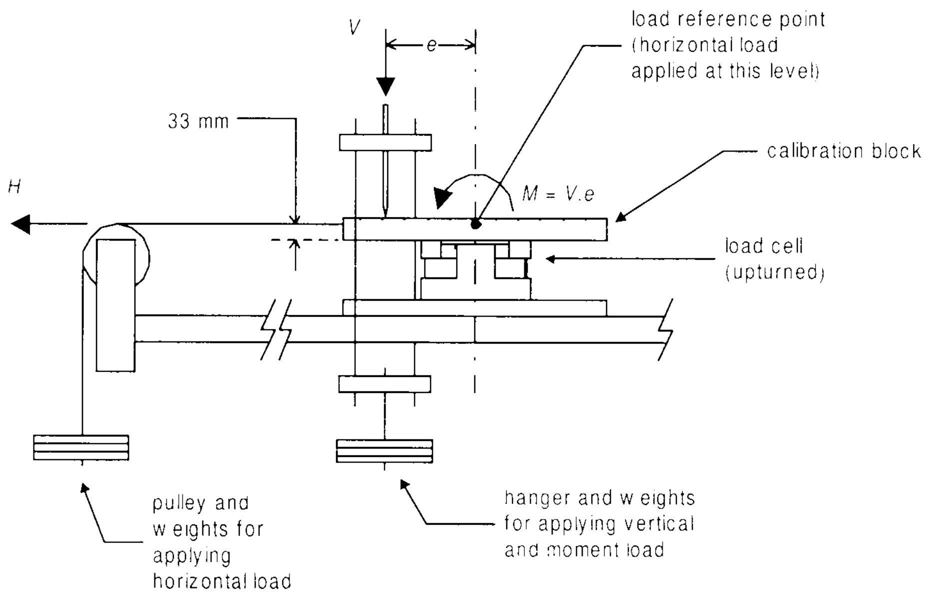


**Figure 3.10** Load cell calibration apparatus

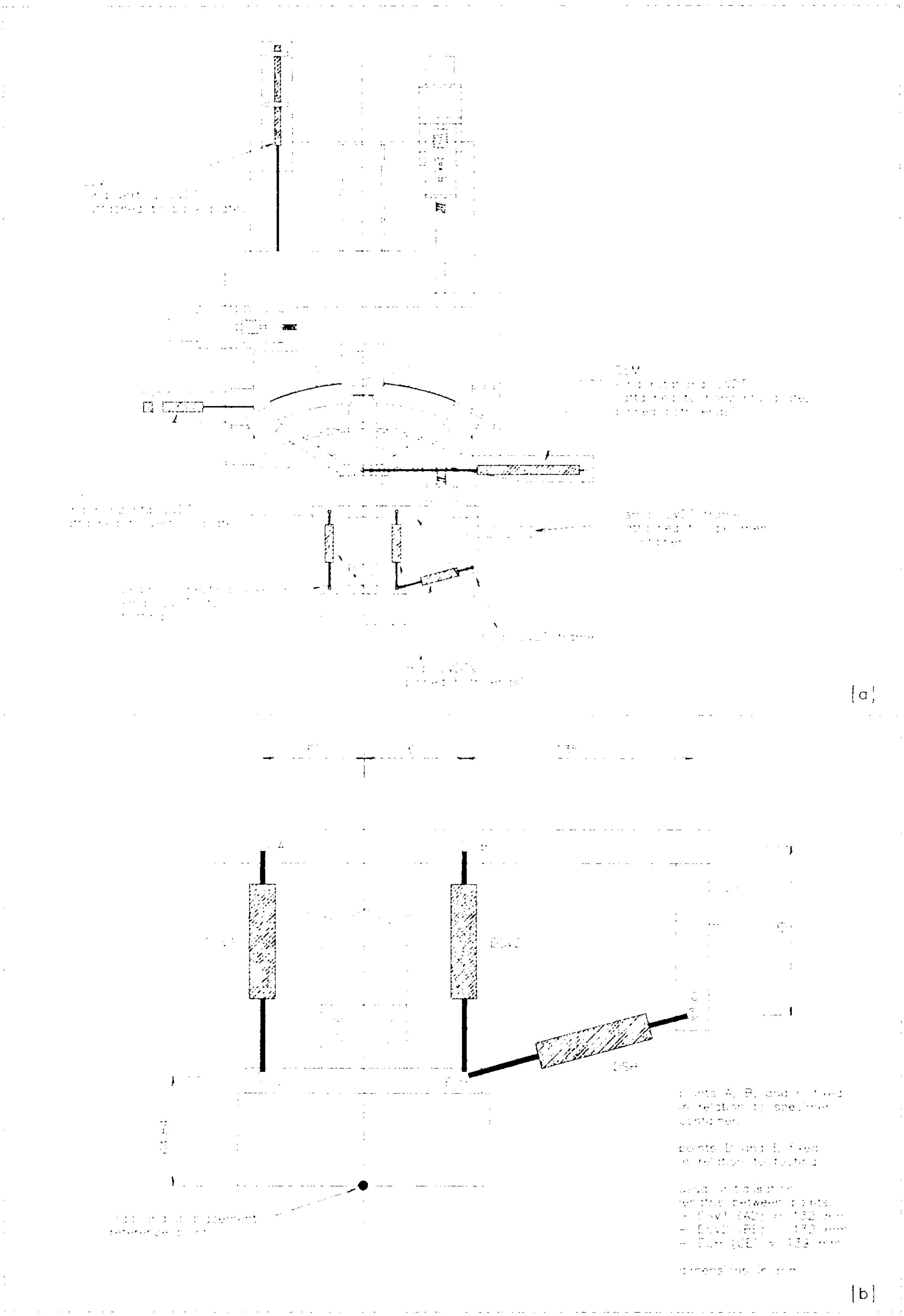

**Figure 3.11** Arrangement of long and small LVDTs:

**[a]** position of all LVDTs on rig; and **[b]** detail of LVDT frame

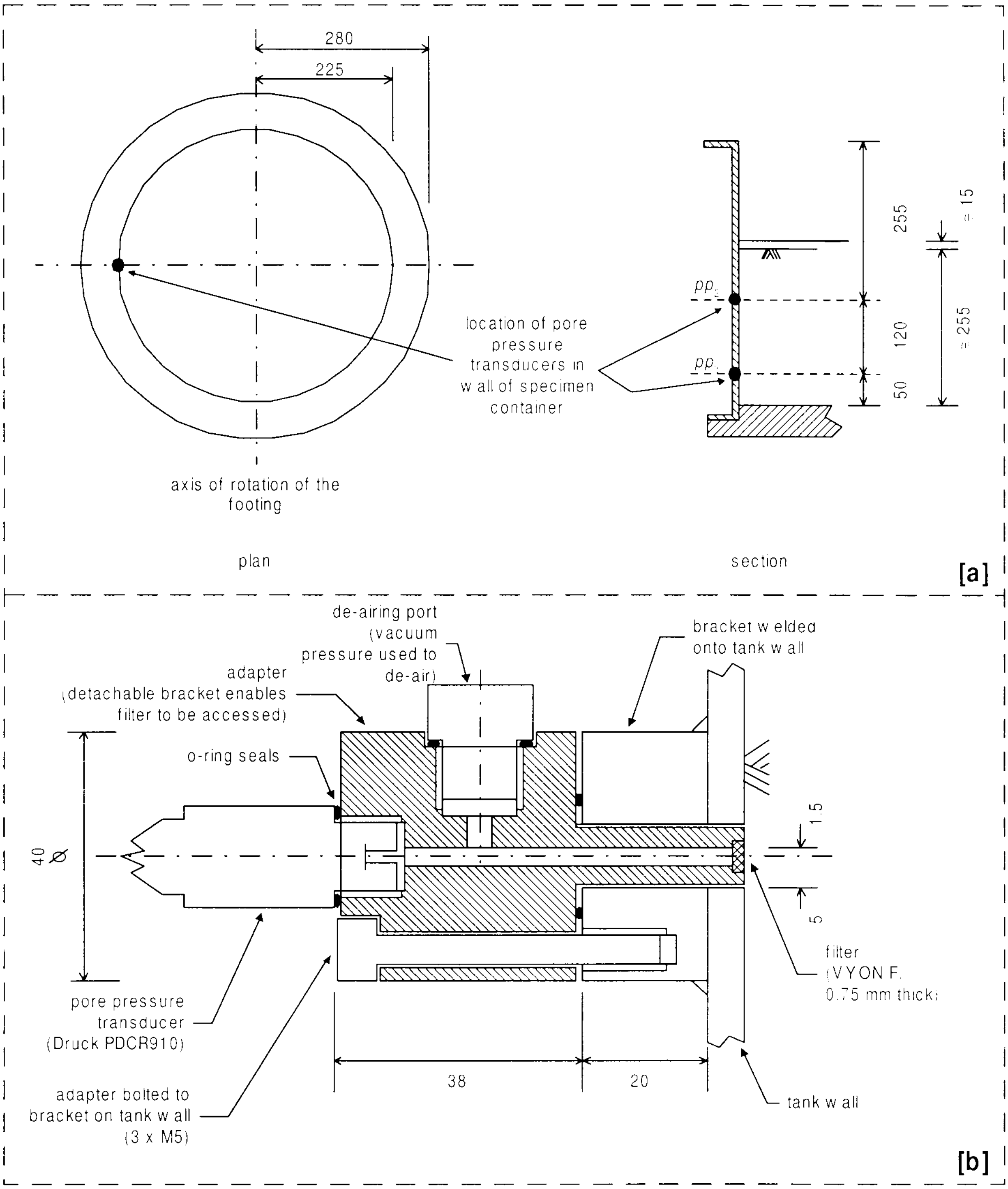


dimensions in mm

**Figure 3.12** Pore pressure transducers in the wall of the specimen container: [a] location of transducers; and [b] detail of connection

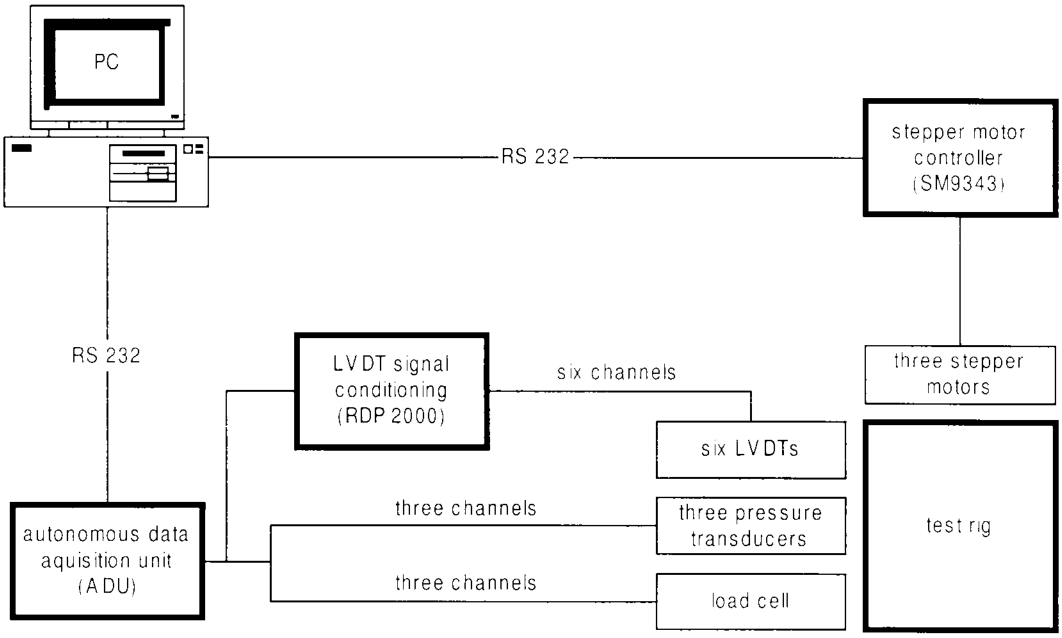


**Figure 3.13** Control and monitoring layout

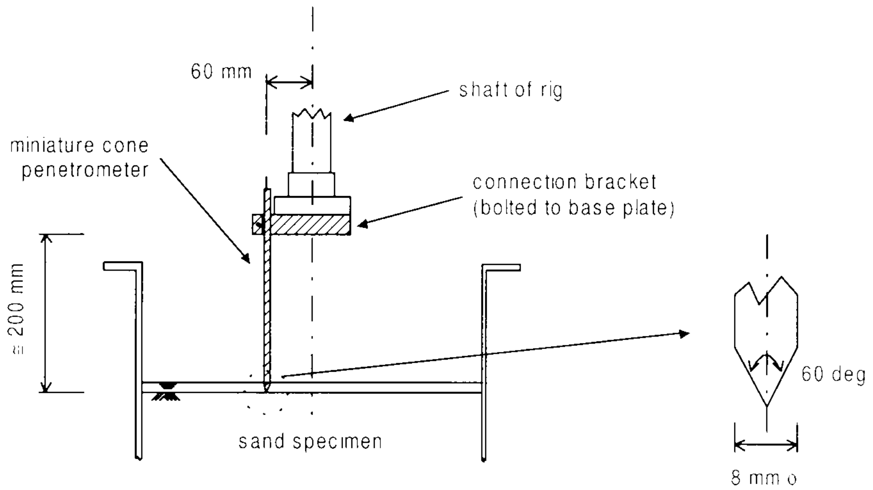


**Figure 3.14** Miniature cone penetrometer

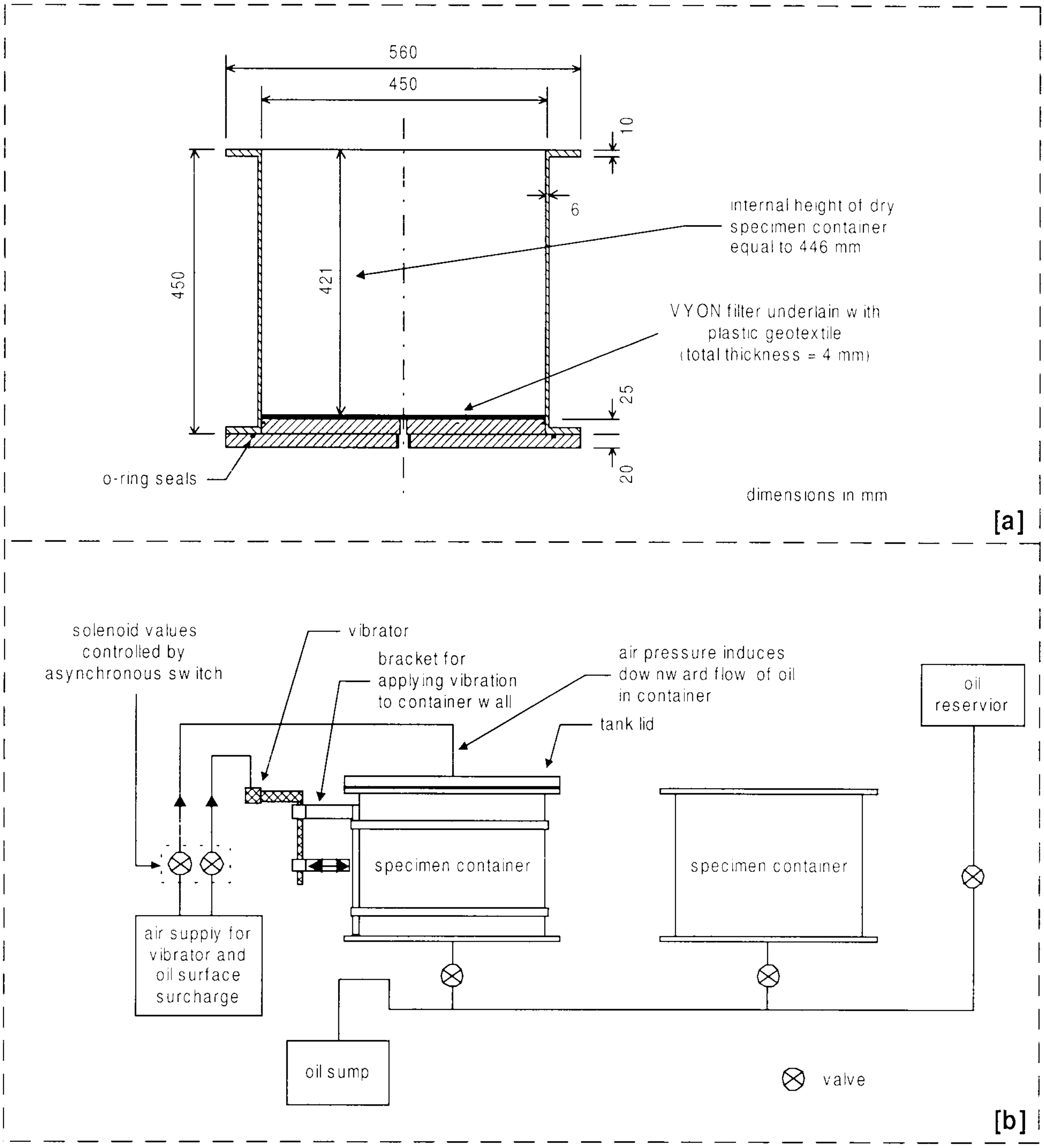


**Figure 3.15** Containers for saturated specimens: [a] dimensions of containers; and [b] hydraulics and densification apparatus

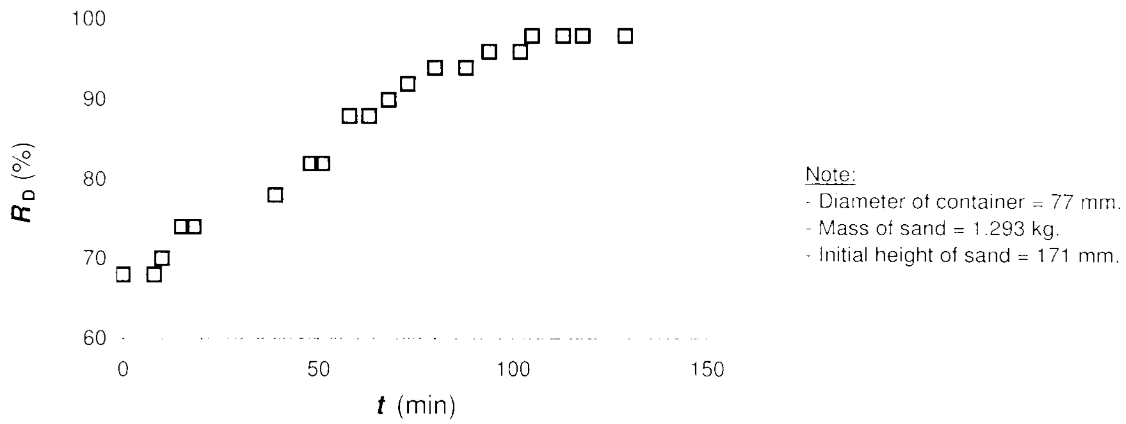


**Figure 3.16** Densification of sand using vibration and downward hydraulic gradient

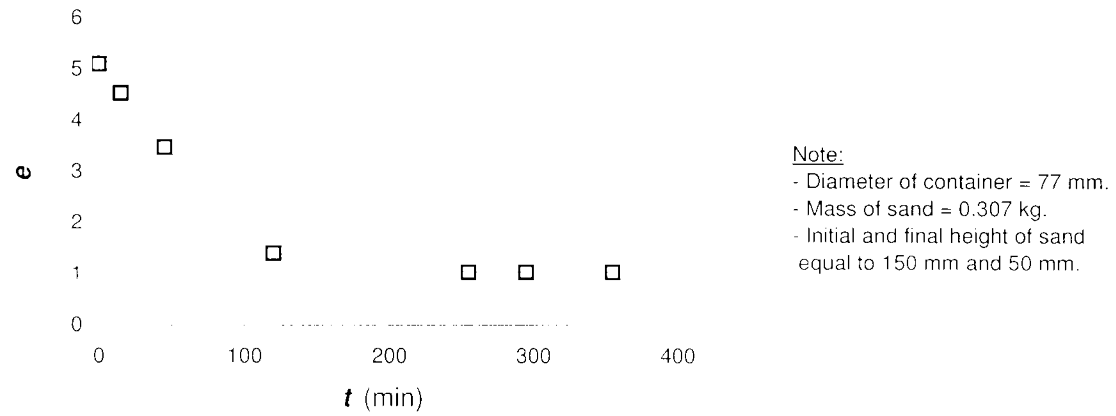


**Figure 3.17** Sedimentation of sand

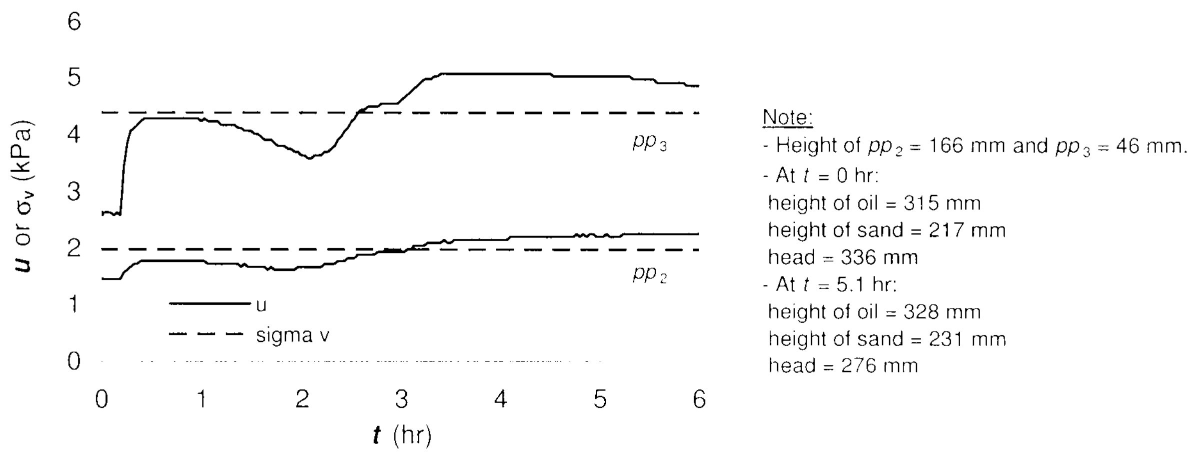


**Figure 3.18** Pore pressure and total stress during liquefaction of sand specimen

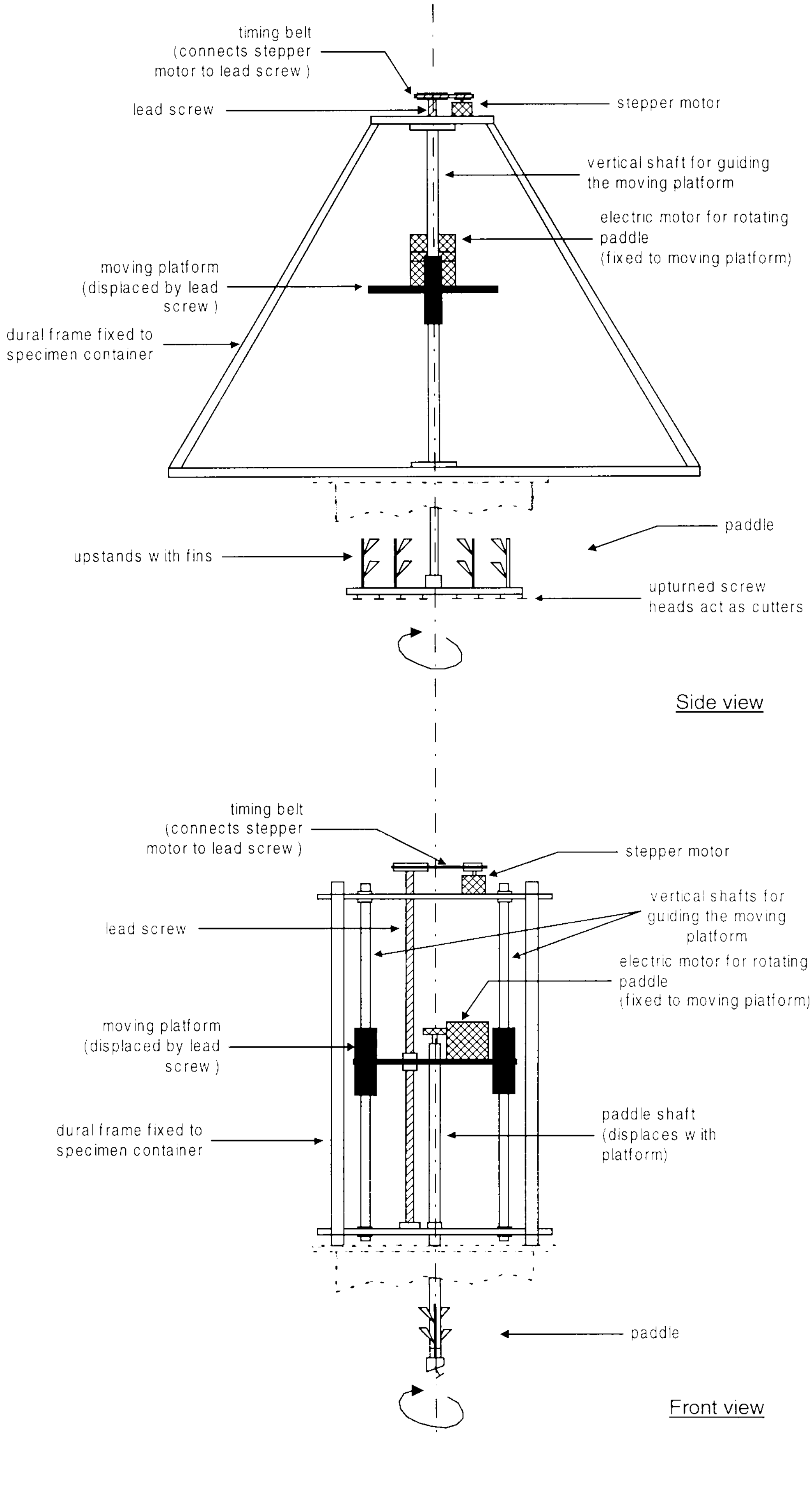


**Figure 3.19** Stirrer used to fluidise sand specimens

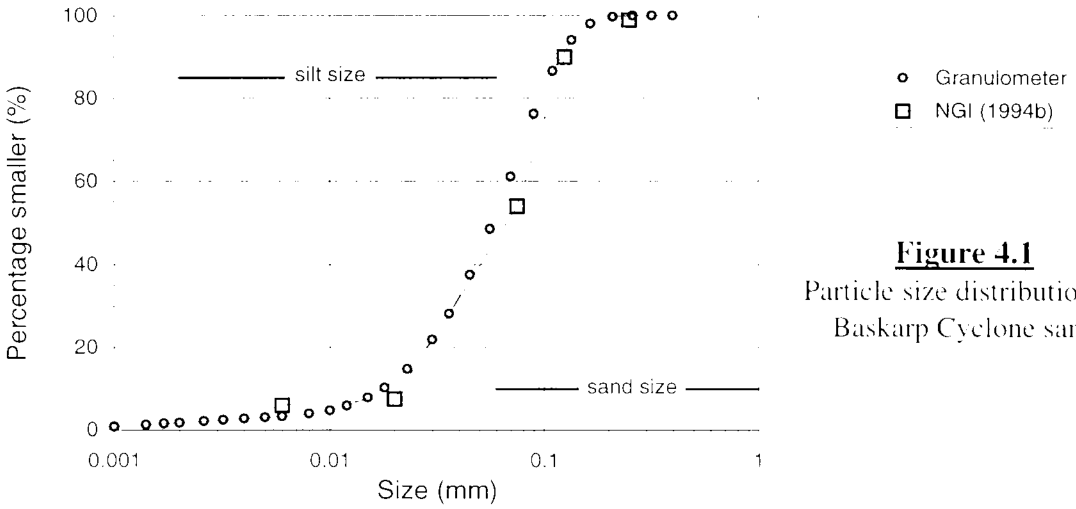


**Figure 4.1**
Particle size distribution of Baskarp Cyclone sand

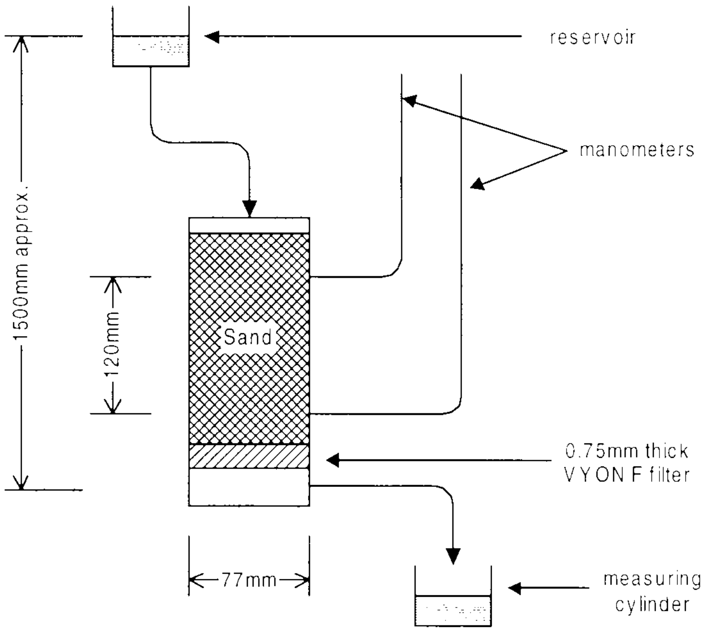


**Figure 4.2**
Apparatus for permeability tests

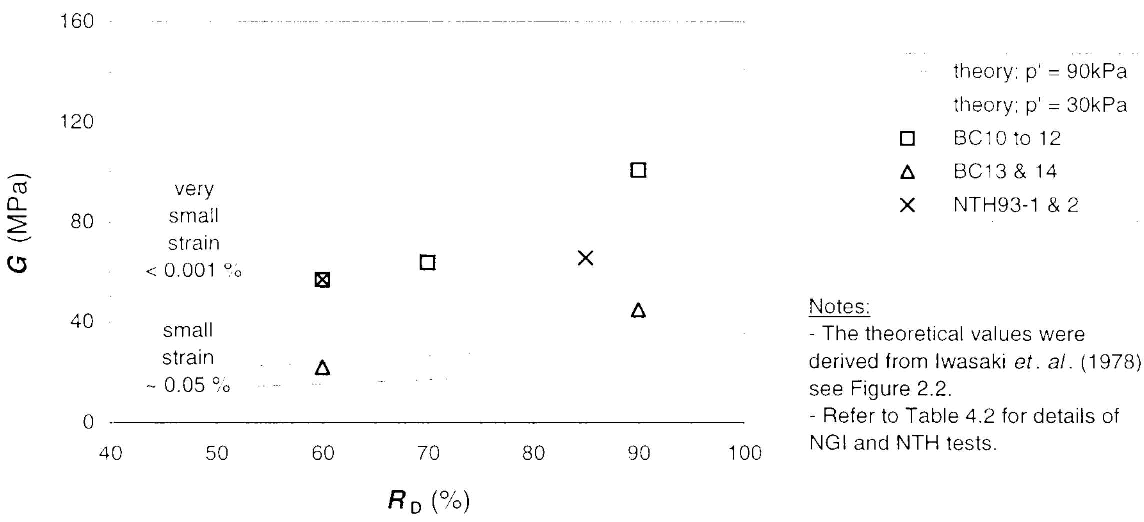


Notes:
- The theoretical values were derived from Iwasaki *et. al*. (1978), see Figure 2.2.
- Refer to Table 4.2 for details of NGI and NTH tests.

**Figure 4.3** Comparison of small-strain elastic shear moduli of Baskarp Cyclone sand, derived from NGI (1994b) element tests, with values from the literature

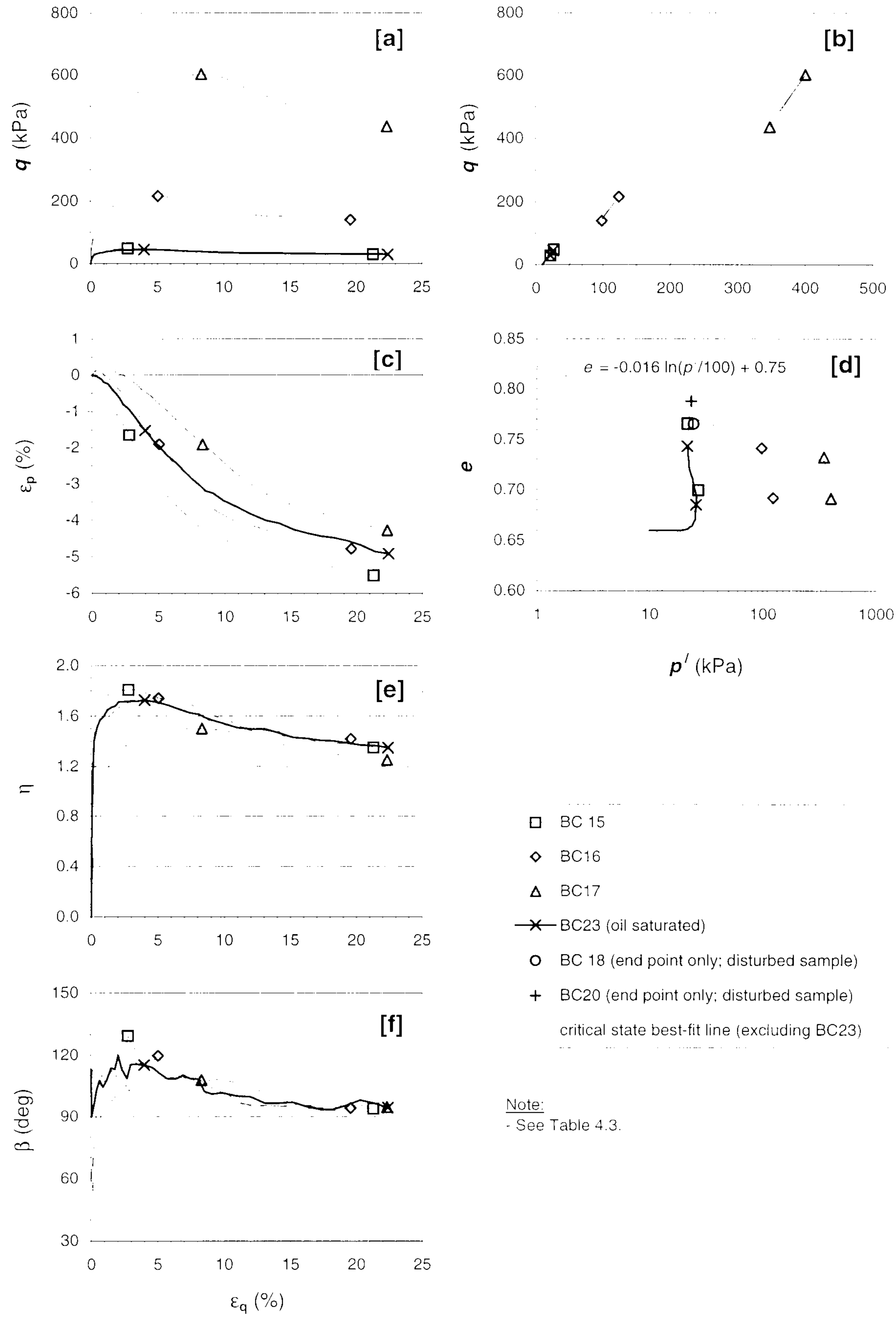


**Figure 4.4** Drained triaxial tests on Baskarp Cyclone sand

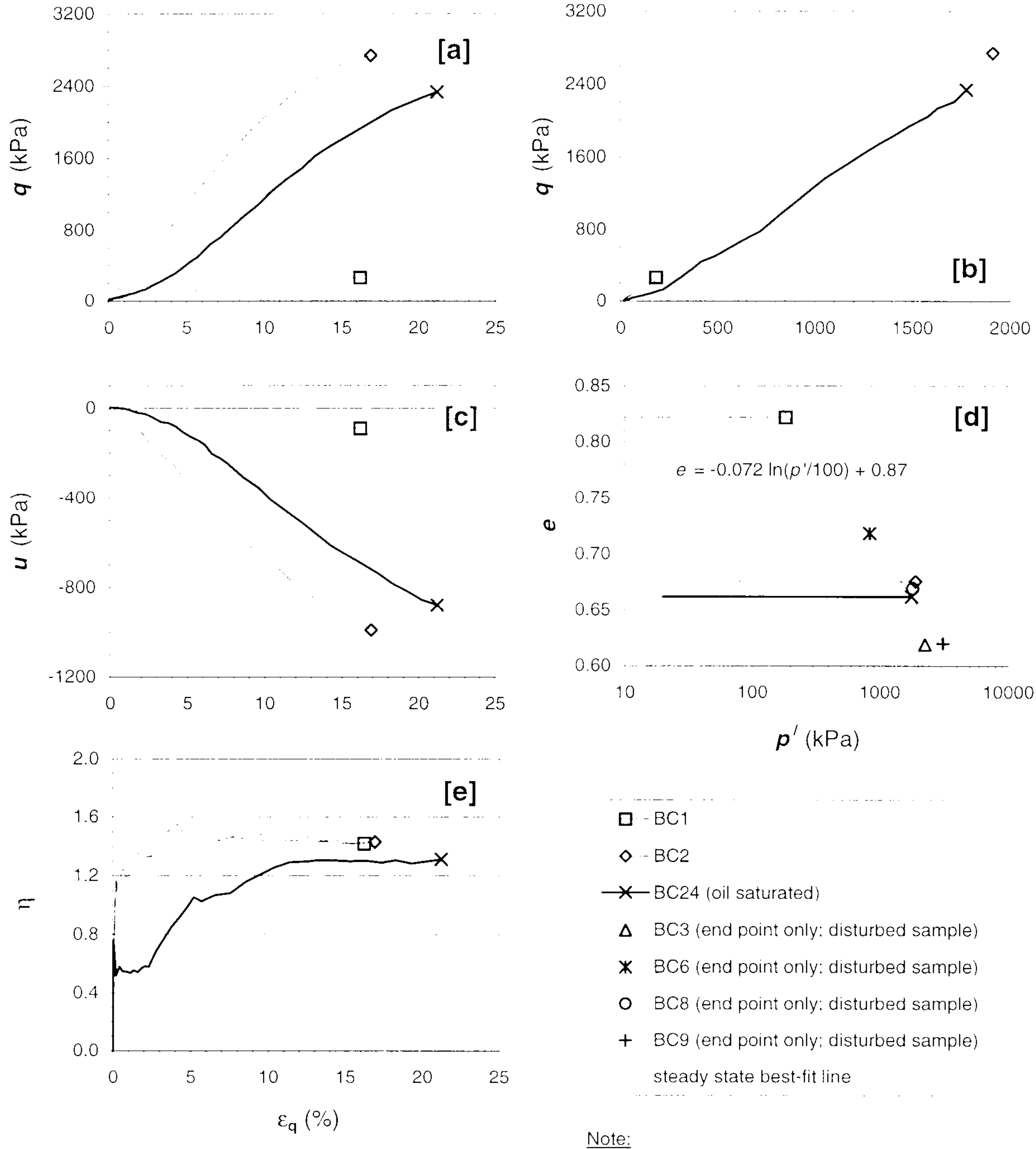


Note:
- See Table 4.4.

**Figure 4.5** Undrained triaxial tests on Baskarp Cyclone sand

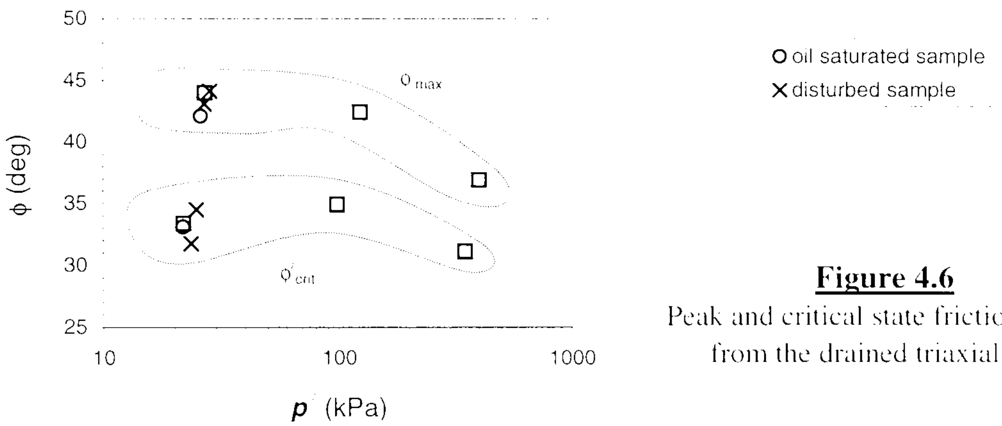


**Figure 4.6**
Peak and critical state friction angles from the drained triaxial tests

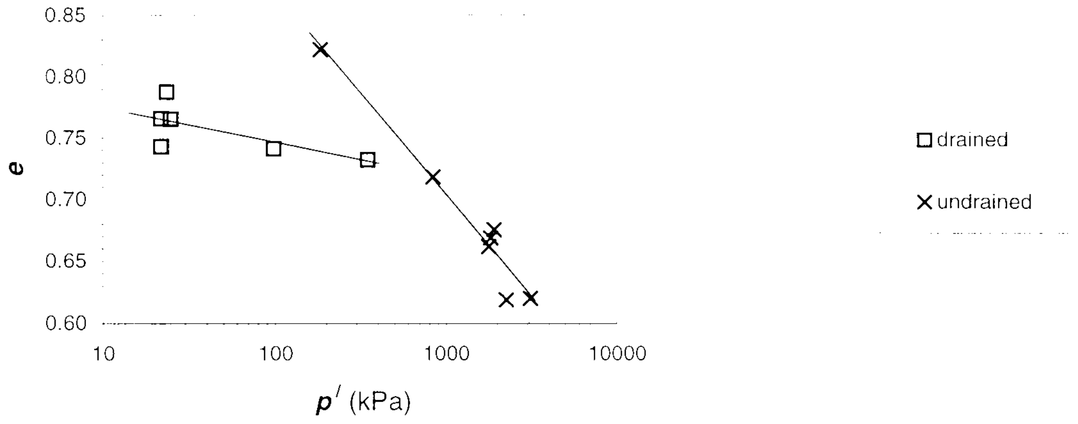


**Figure 4.7** Probable drained critical state and undrained steady state lines of Baskarp Cyclone sand

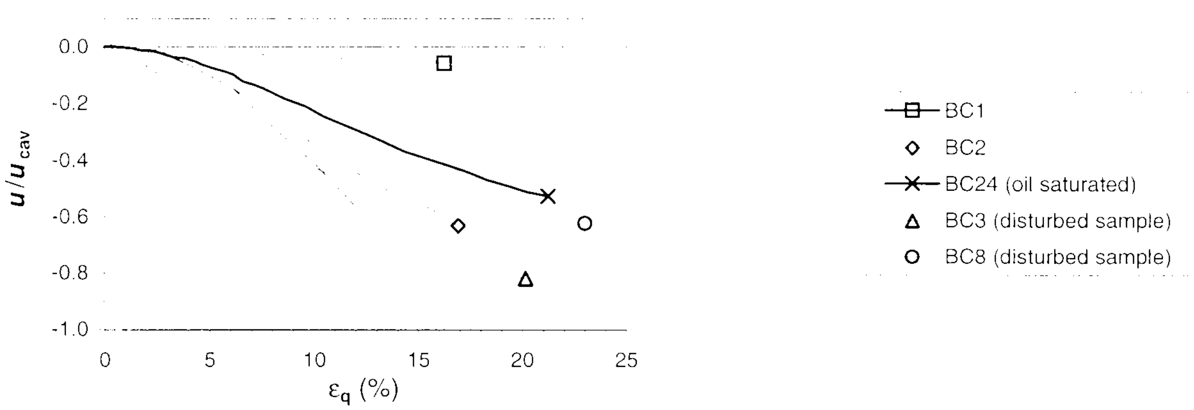


**Figure 4.8** Pore pressure normalised by cavitation increment

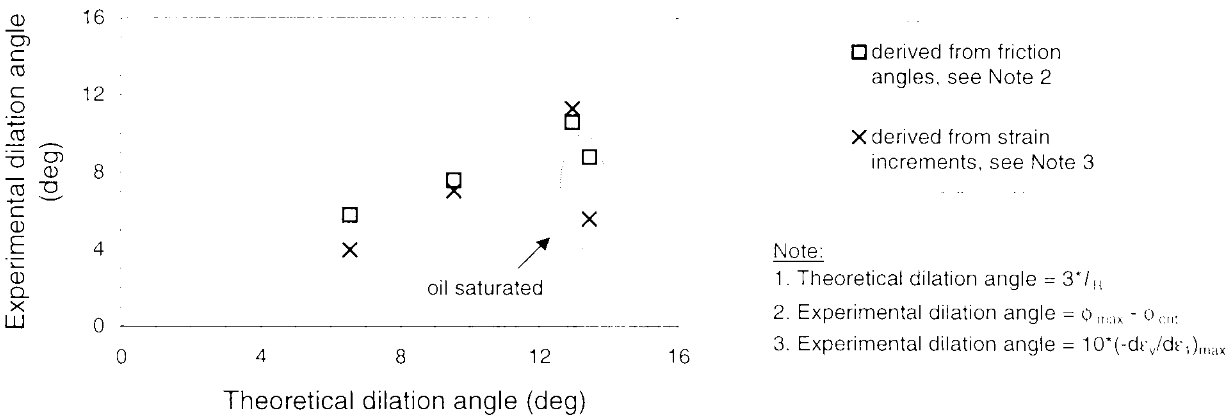


**Figure 4.9** Comparison of maximum theoretical and experimental dilation angles of Baskarp Cyclone sand

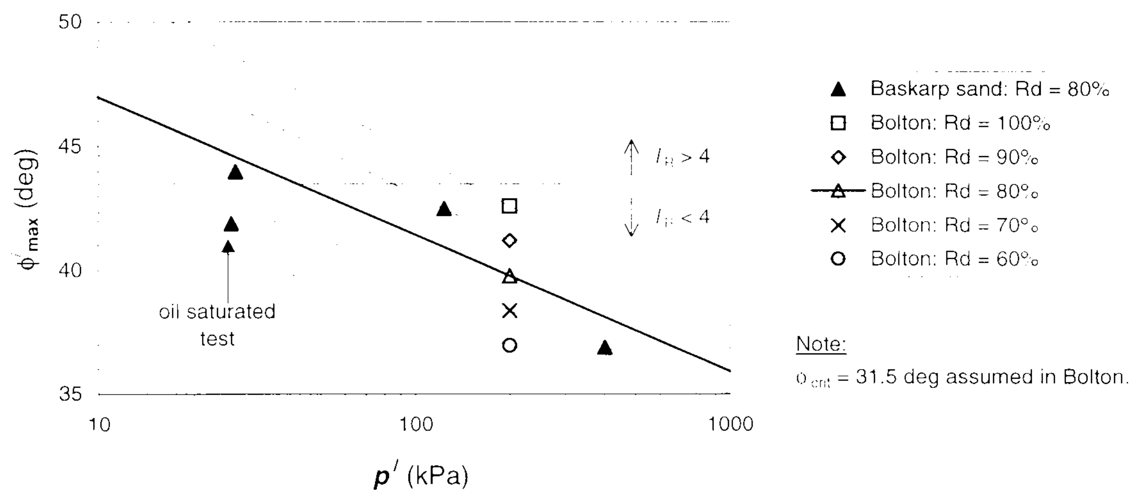


**Figure 4.10** Comparison of triaxial test results of Baskarp Cyclone sand with predictions using Bolton's method

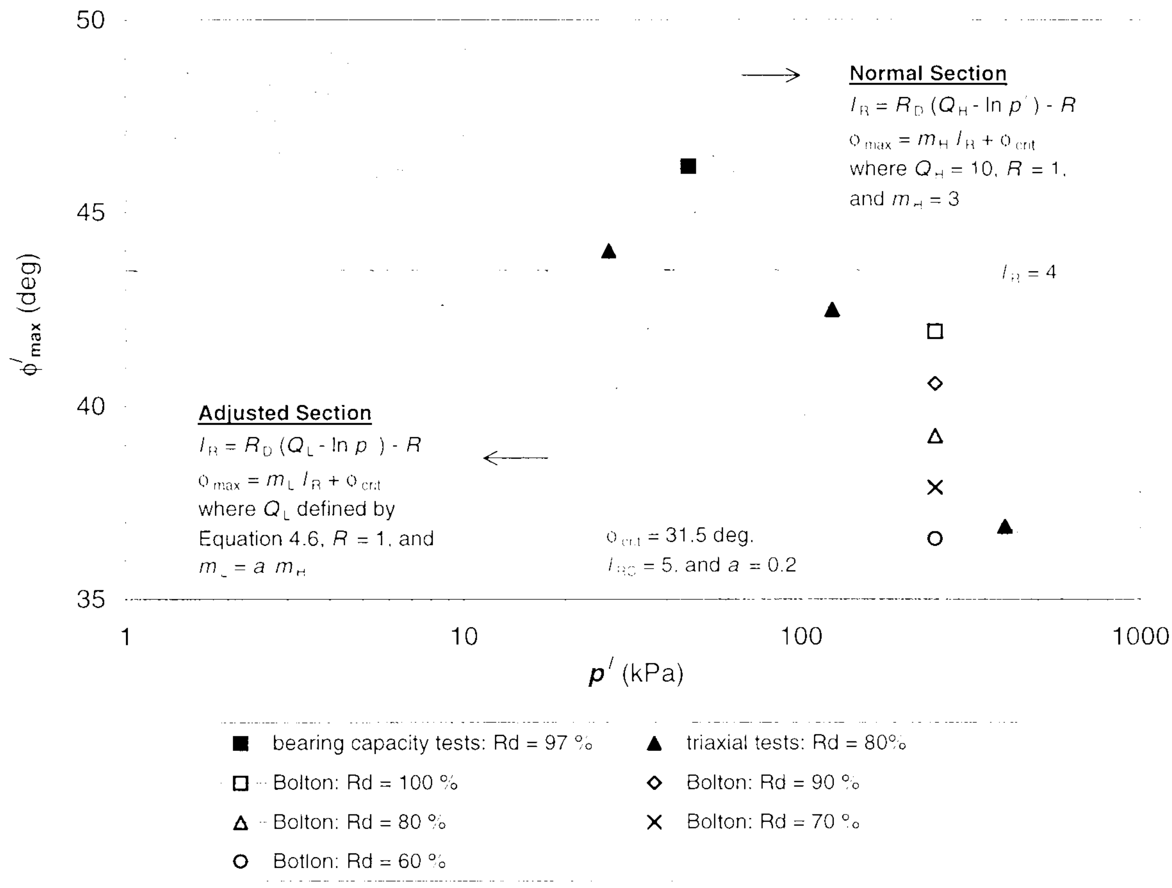


Note:
- The bearing capacity tests were performed by Byrne and Houlsby (1999), see Section 2.3.1 and Figure 2.4. The friction angle of the tests was derived from the $\phi$:$N_\gamma$ relationship of Bolton and Lau (1993).

**Figure 4.11** Bolton's (1986) $R_D$:$p'$:$\phi'_{max}$ relationship with low stress adjustment

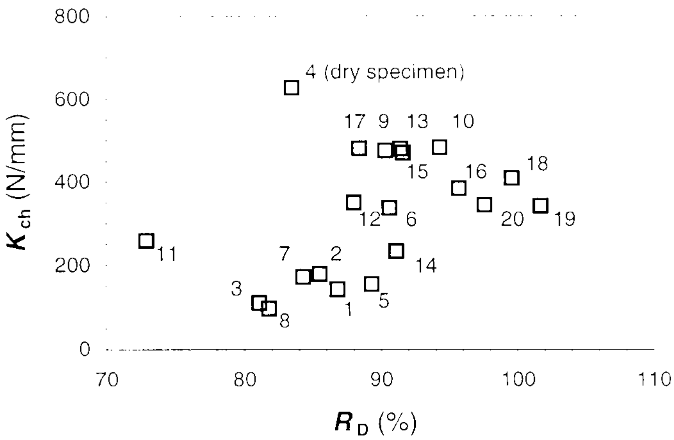


**Figure 4.12**
Distribution of the footing tests in terms of the characterisation stiffness and the bulk relative density of the samples

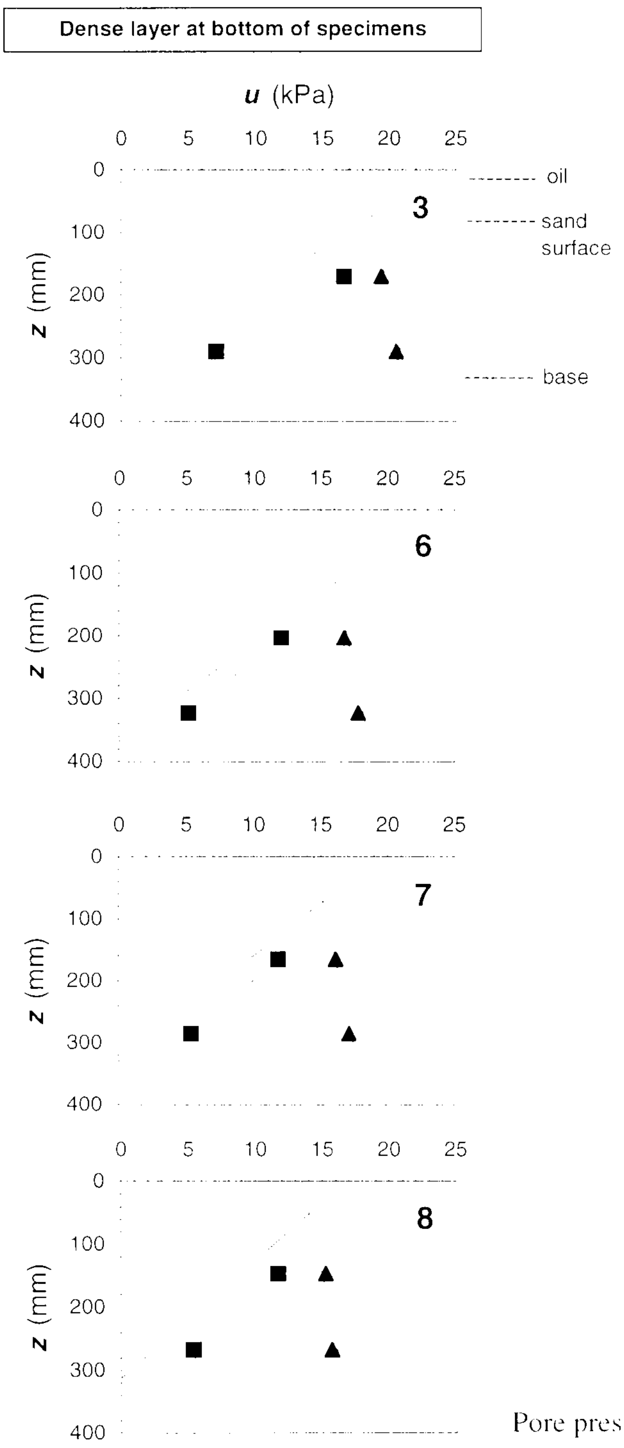


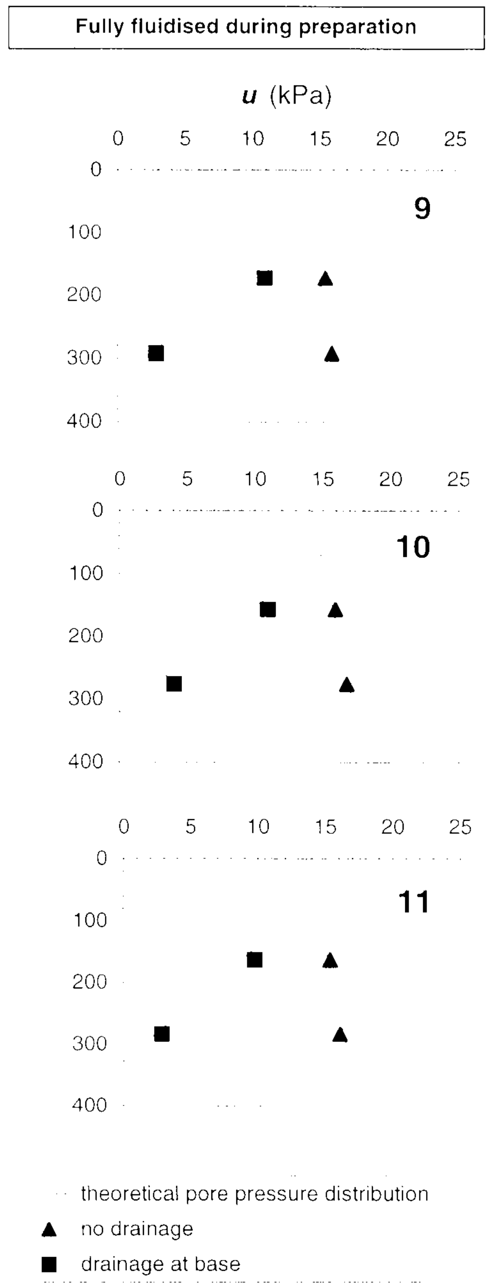


**Figure 4.13**
Pore pressures at the wall of the sample containers during the downward hydraulic gradient tests.

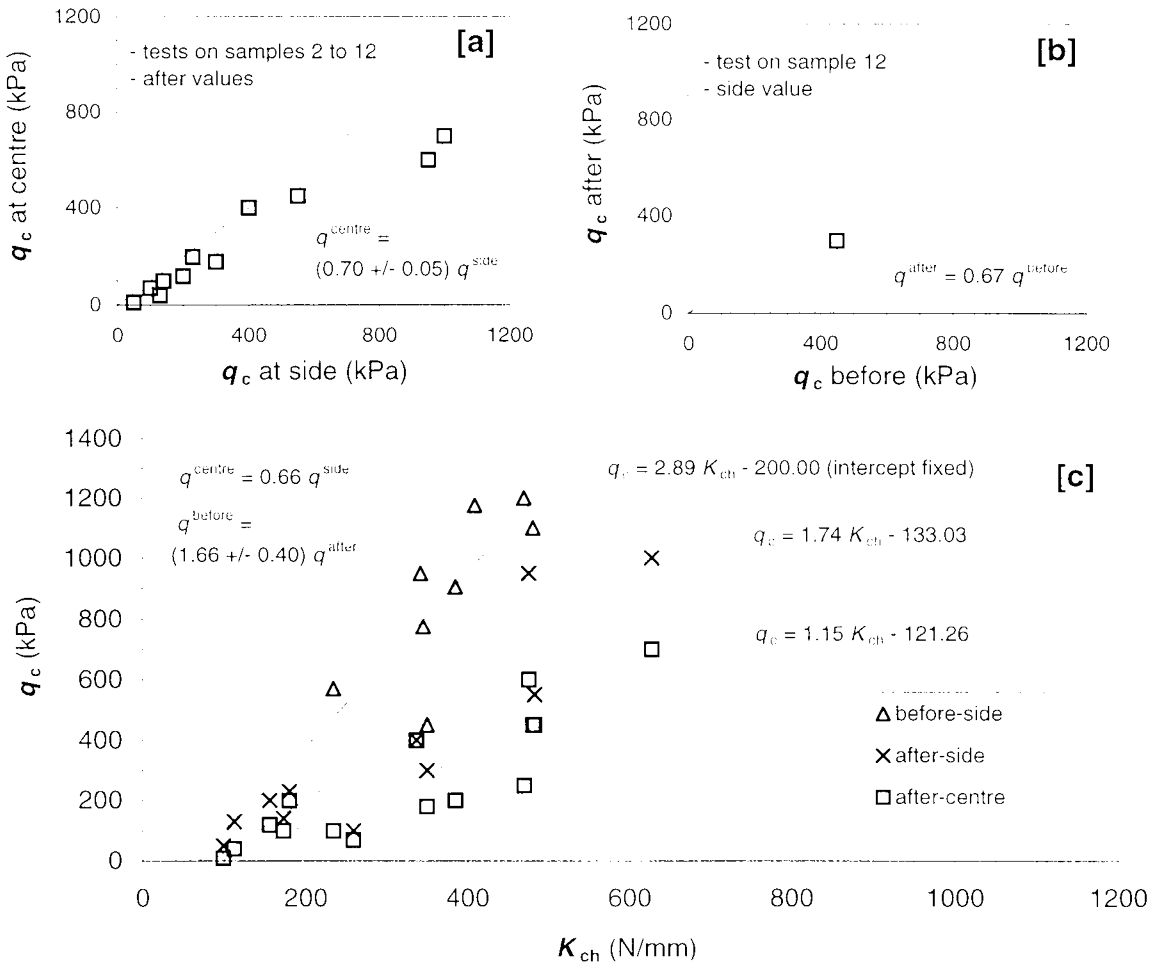


Note:
- Results from tests performed on sample 13 excluded.
- See Table 4.6.

**Figure 4.14** Correlation between the different types of cone penetrometer test: **[a]** tests performed at the centre of the samples versus those at the side; **[b]** tests performed after the footing tests versus those before; and **[c]** the three different types of $q_c$ result plotted against the characterisation stiffness

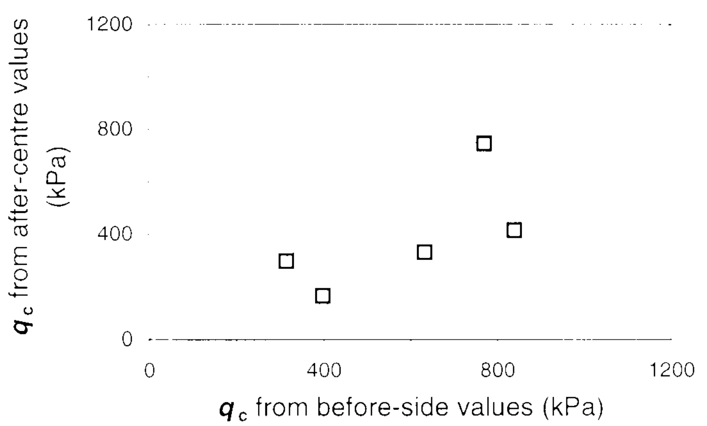


Note:
- see Table 4.6

**Figure 4.15** Comparison of before-centre $q_c$ values calculated from two different sets of measured values, from tests on samples 12 and 14 to 17

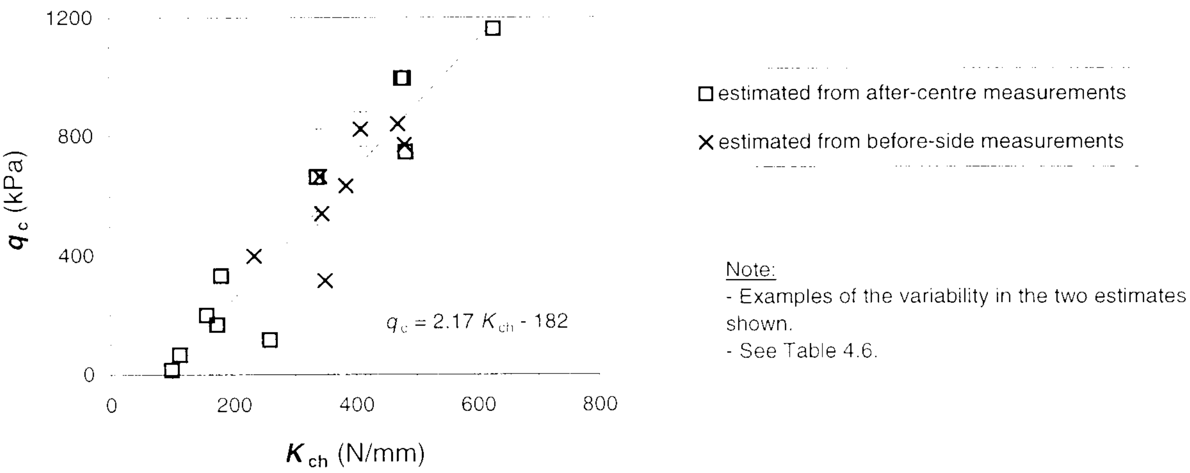


**Figure 4.16** Estimated before-centre $q_c$ values

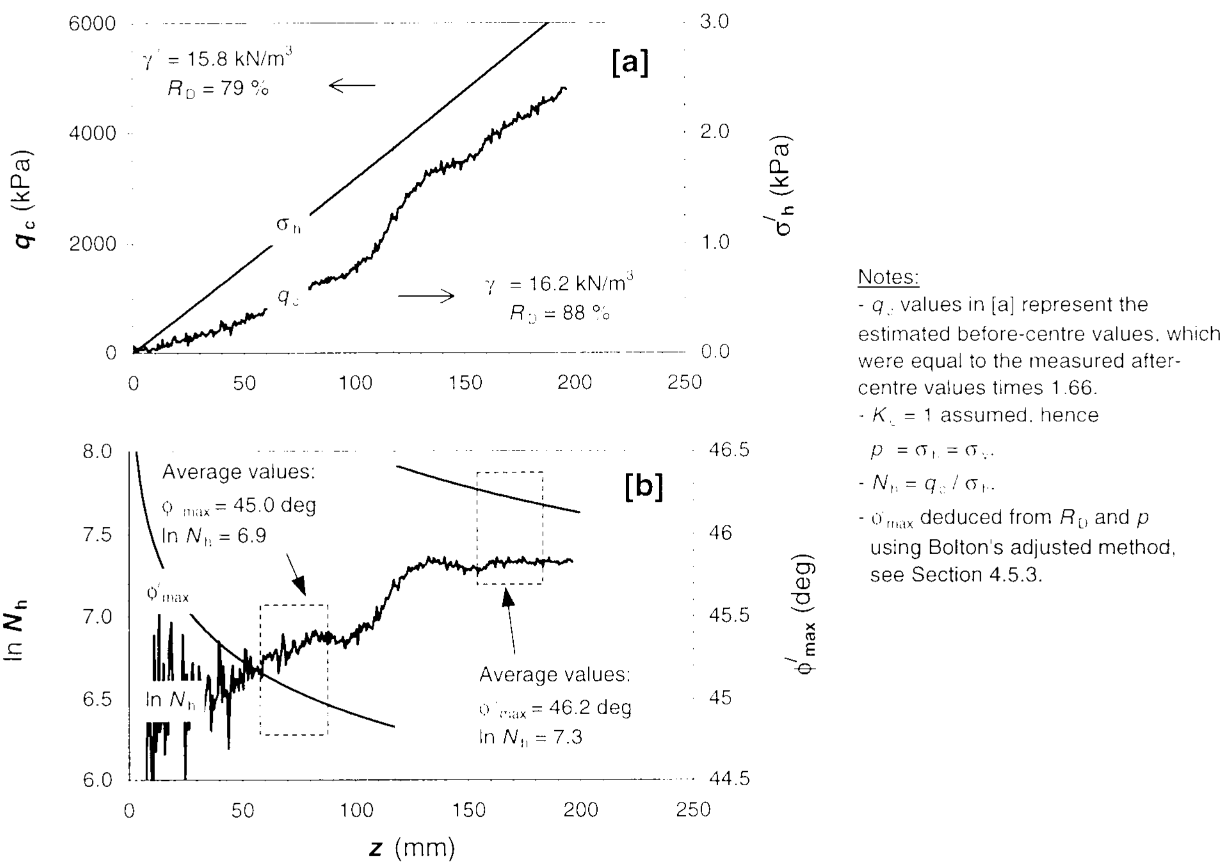


**Figure 4.17** Cone penetrometer results from CP04C, *i.e.* test at centre of sample T204:
**[a]** cone tip resistance and effective horizontal stress; and
**[b]** tip resistance factor and peak friction angle

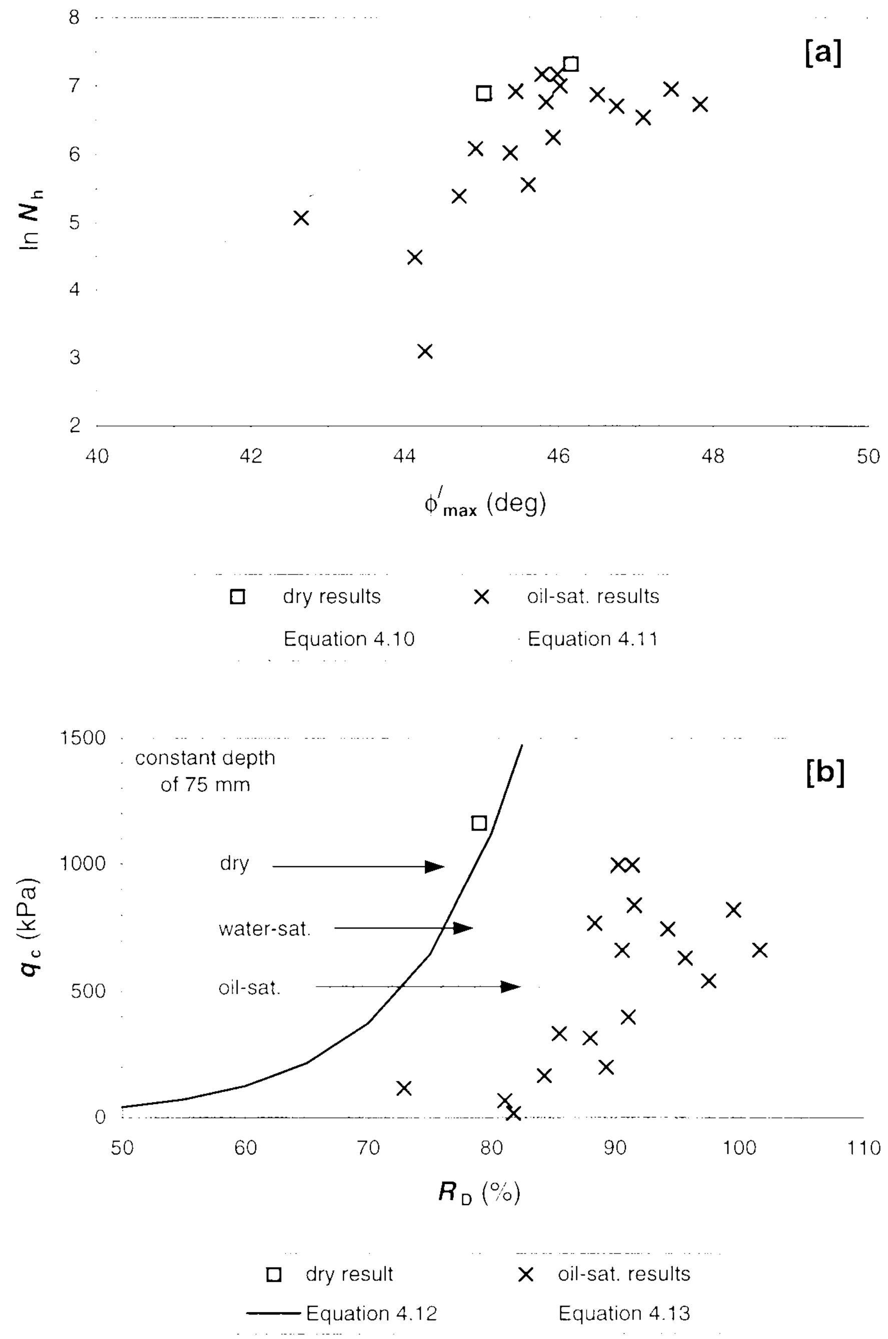


**Figure 4.18** Correlation between cone penetrometer results and sand properties:
**[a]** cone tip resistance factor versus peak friction angle; and
**[b]** cone tip resistance versus relative density

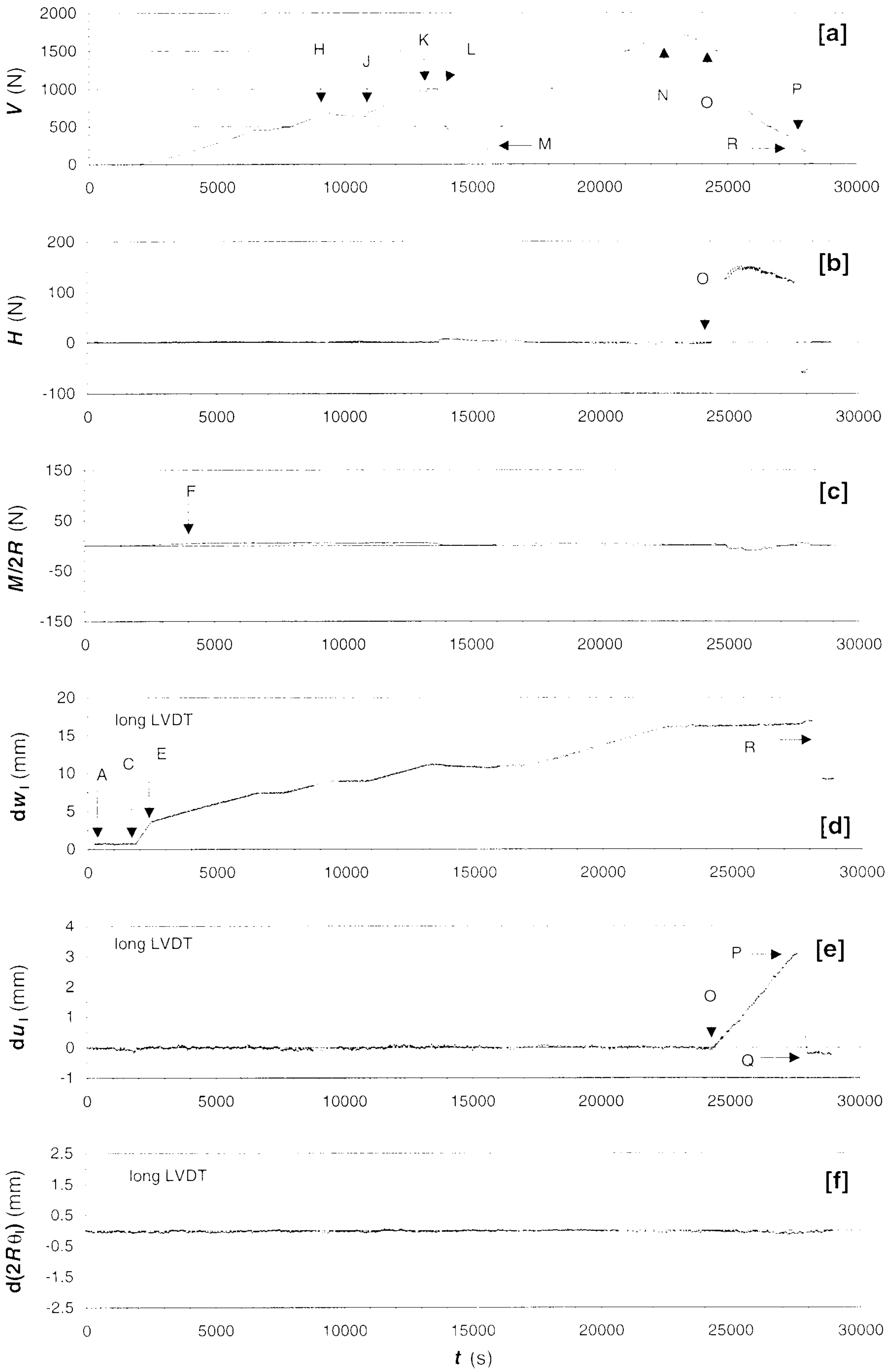


**Figure 5.1** Time history of test T101

(continued on next page)

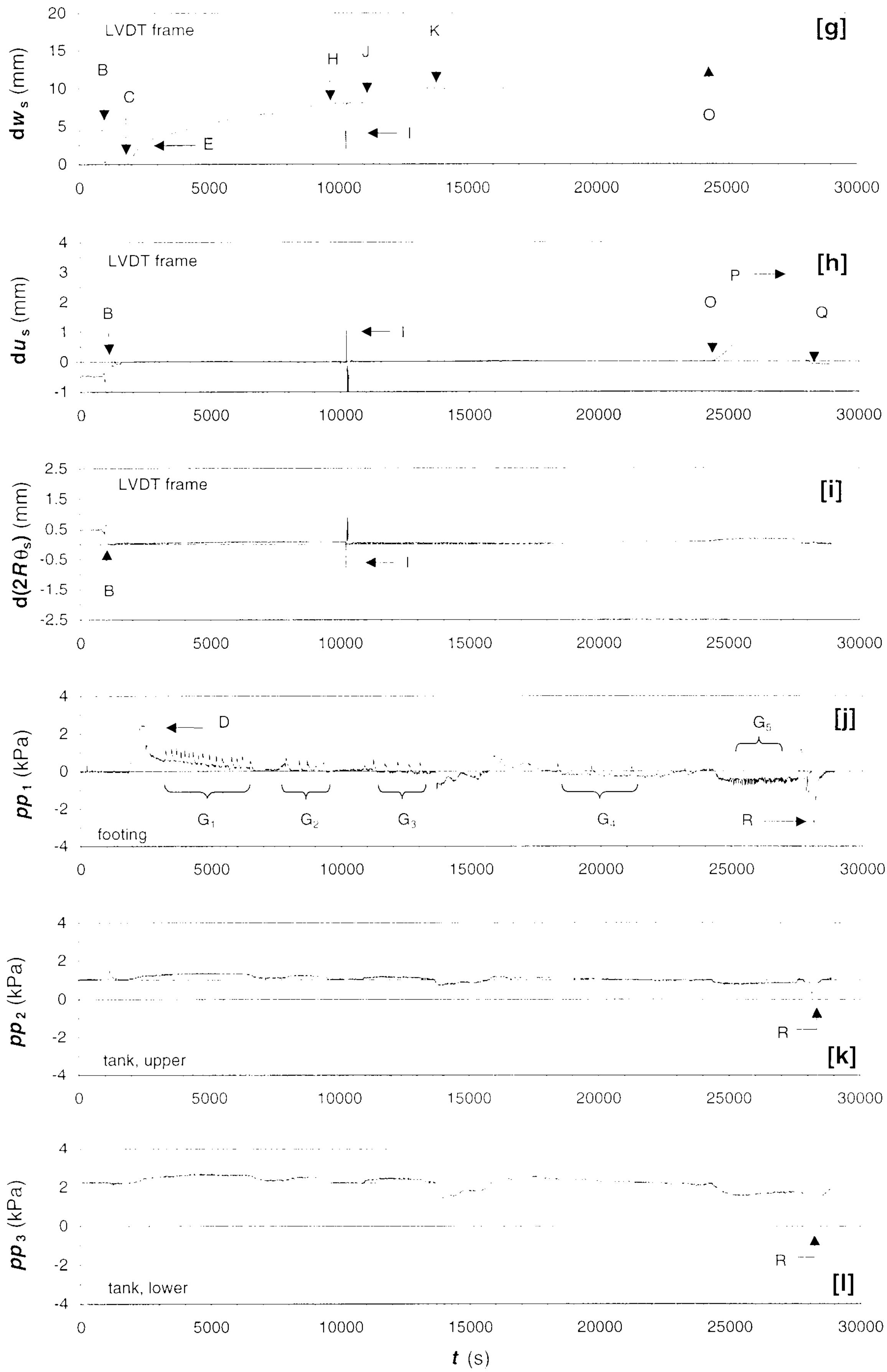


**Figure 5.1 (cont.)** Time history of test T101

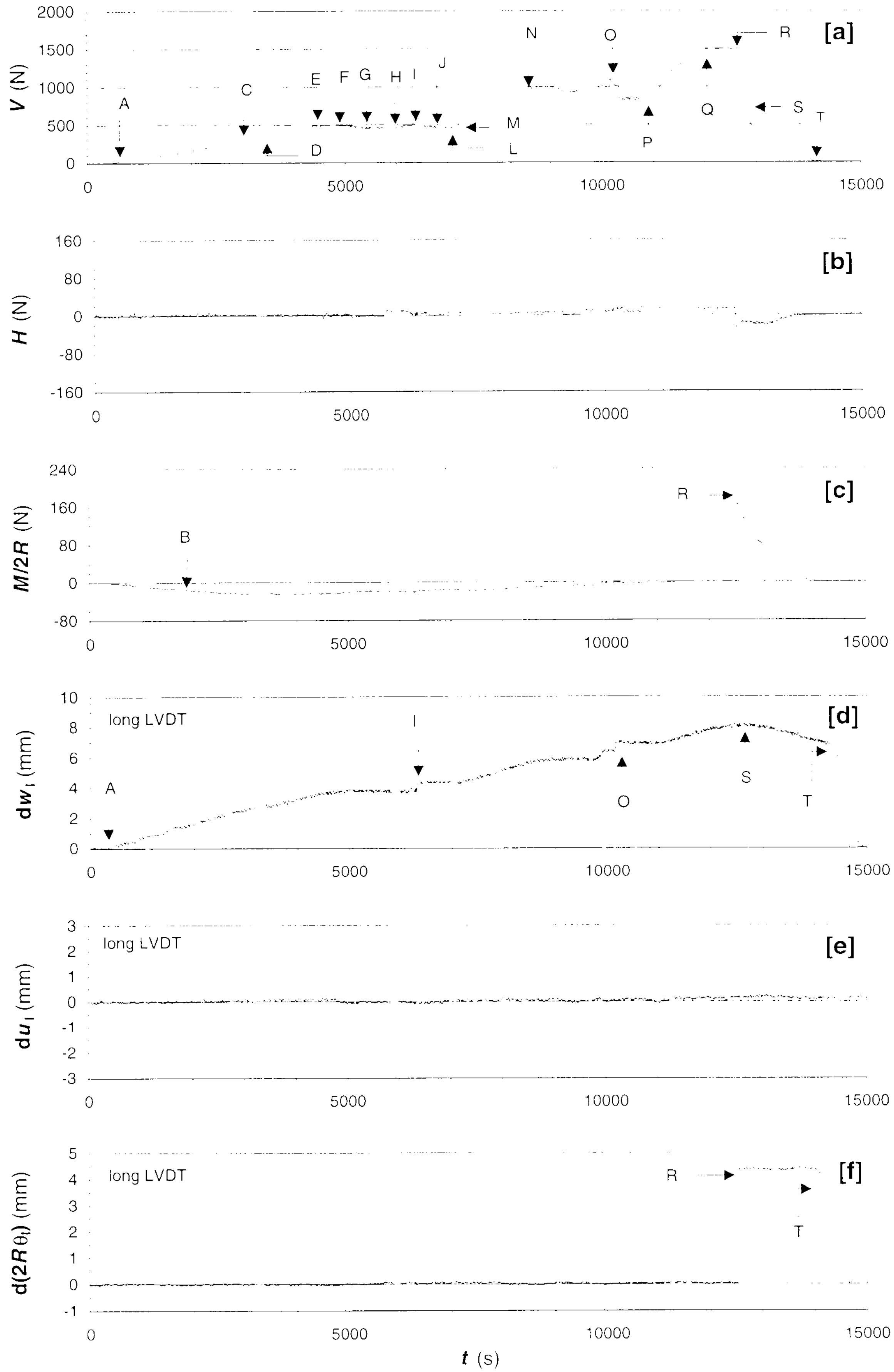


**Figure 5.2** Time history of test T114
(continued on next page)

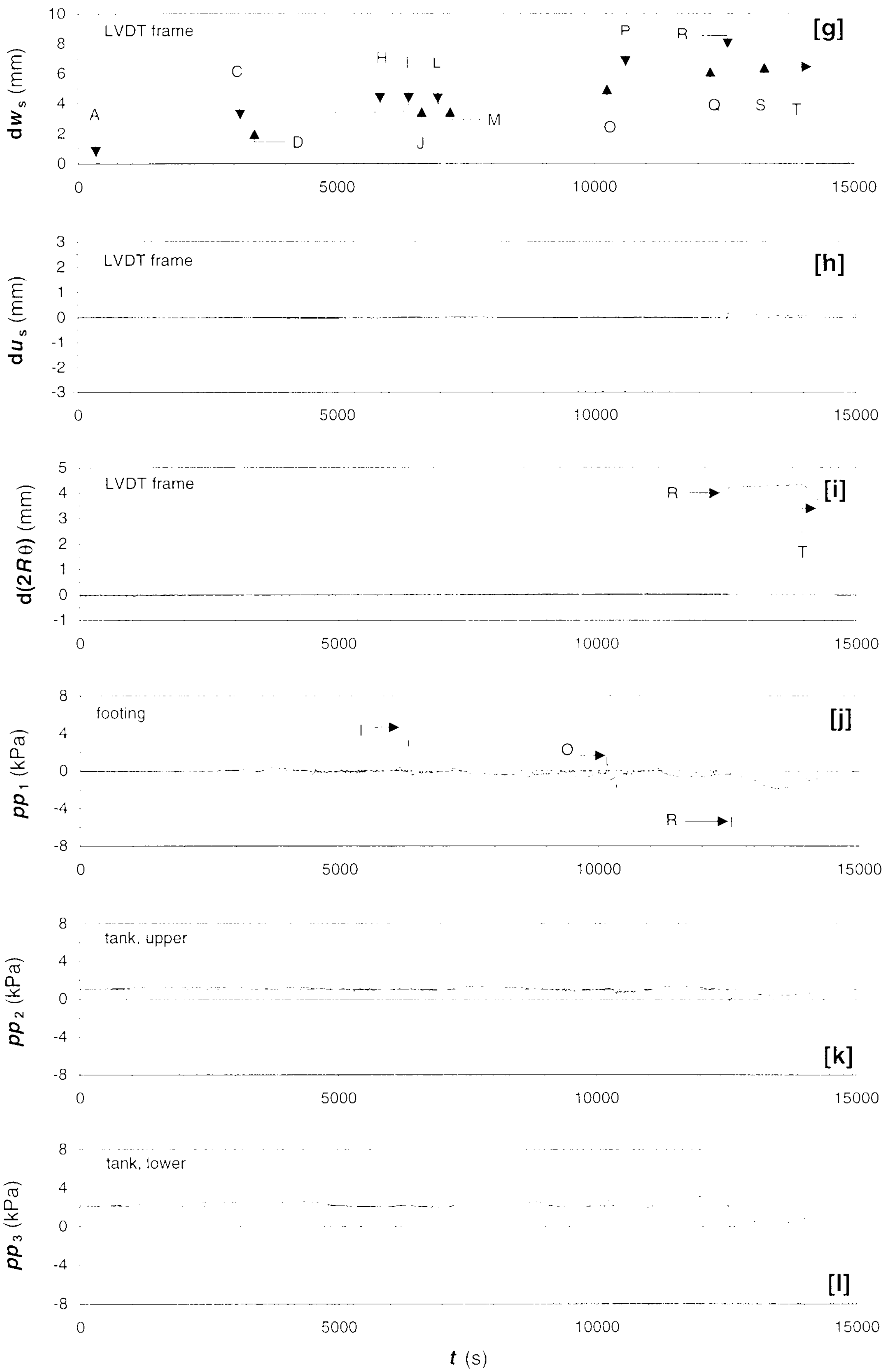


**Figure 5.2 (cont.)** Time history of test T114

| | input file | |
|---|---|---|
| command | **LIMITS** | sets the load soft limits that are active during the MTEST |
| parameters | -1000 900 | vertical load soft limits |
| | -100 100 | horizontal load soft limits |
| | -15 15 | moment load soft limits |
| command | **MTEST** | sets the move test data and activates the move |
| parameters | 4 100 1 | test allotment parameters for ADU (test time, scans per second, delay) |
| | 0.5 5 250 4 | vertical move parameters for stepper motor controller (displacement, velocity, acceleration, base speed) |
| | 0 0 0 | horizontal move parameters for stepper motor controller (displacement, velocity, acceleration) |
| | 0 0 0 | rotational move parameters for stepper motor controller (displacement, velocity, acceleration) |
| command | **LIMITS** | sets the load soft limits that are active after the MTEST |
| parameters | -1000 2000 | vertical load soft limits |
| | -200 200 | horizontal load soft limits |
| | -20 20 | moment load soft limits |
| command | **ADUSTORE** | transfers the test data stored on ADU to the host PC |
| command | **MOVE** | sets the move data; this is used to reset the base speed before control is returned to the interactive menu on the host PC |
| parameters | 0 0 0 0.005 | vertical move parameters for stepper motor controller (displacement, velocity, acceleration, base speed) |
| | 0 0 0 | horizontal move parameters for stepper motor controller (displacement, velocity, acceleration) |
| | 0 0 0 | rotational move parameters for stepper motor controller (displacement, velocity, acceleration) |
| command | **END** | returns control to the interactive menu on the host PC |

**Figure 5.3** Input file T114_A.INP

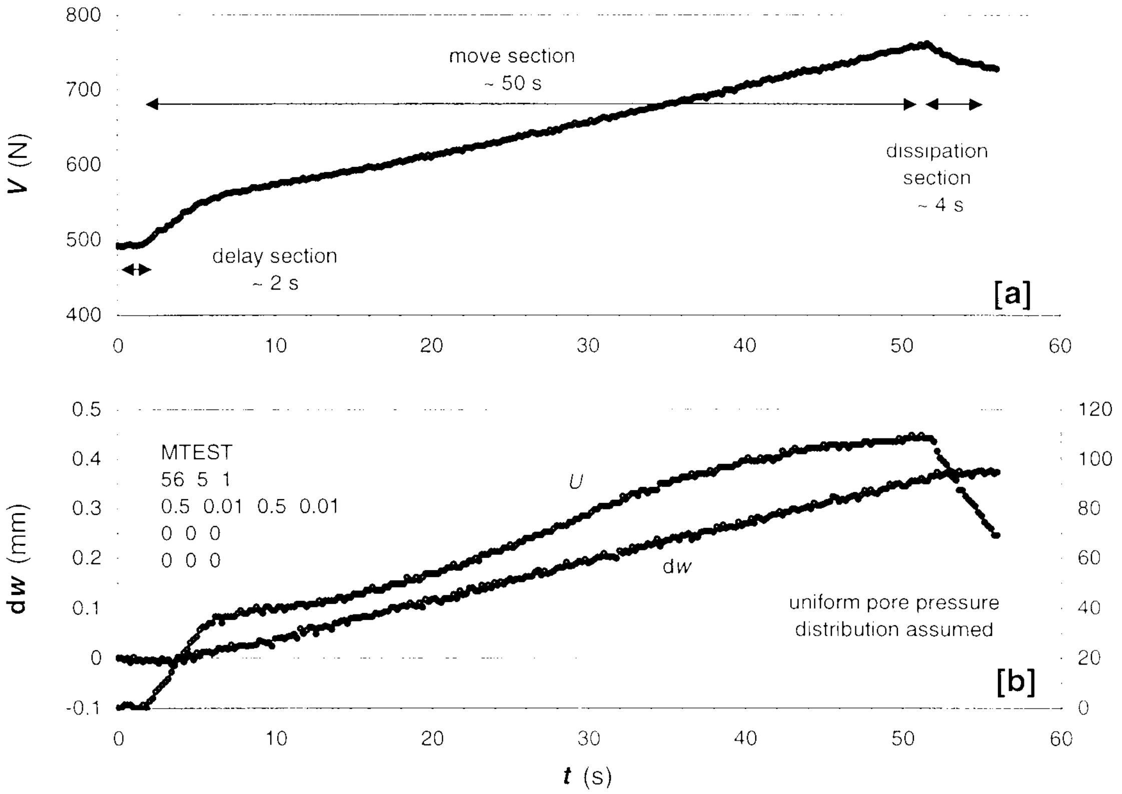


**Figure 5.4** Time history of a slow vertical partially-drained test (T317_1, d$w$/d$t$ = 0.01 mm/s)

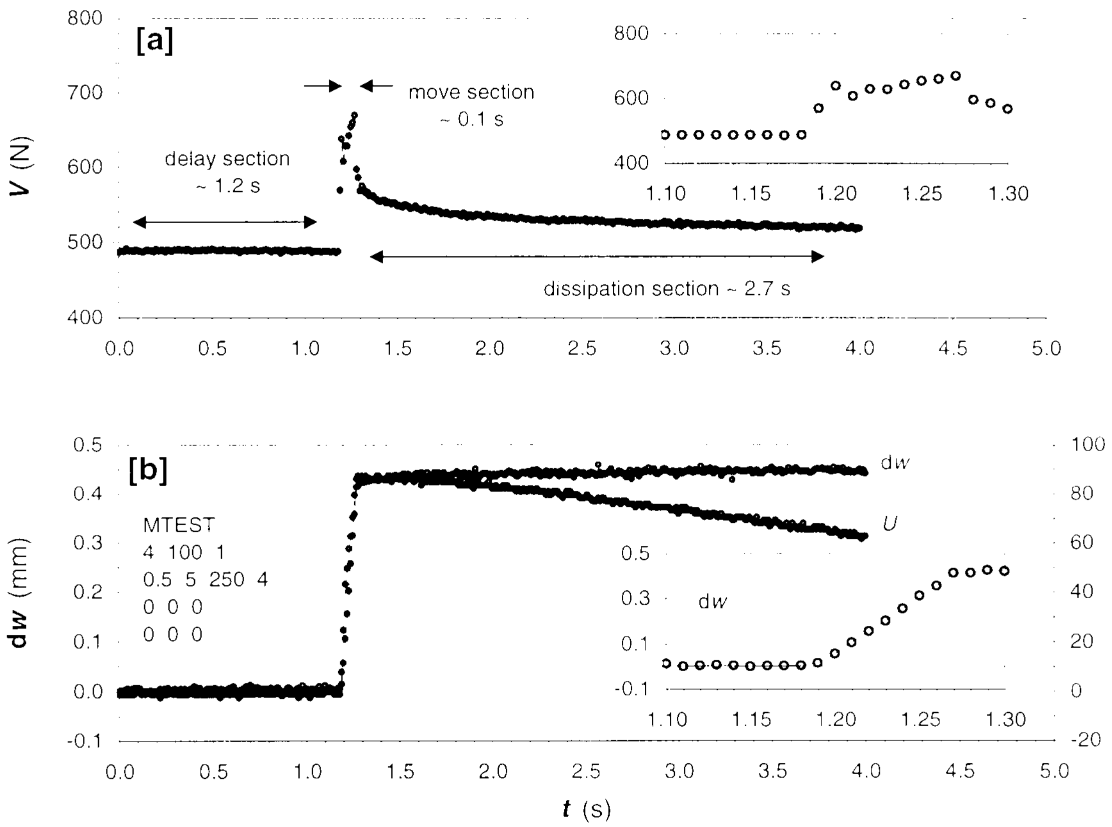


**Figure 5.5** Time history of a fast vertical partially-drained test (T114B_1, d$w$/d$t$ = 5 mm/s)

| | input file | |
|---|---|---|
| command | LIMITS | sets the load soft limits that are active during the SEQTEST1 events |
| parameters | -500 1400 | vertical load soft limits |
| | -100 100 | horizontal load soft limits |
| | -10 10 | moment load soft limits |
| command | SEQTEST1 | sets the sequence test data and activates subroutine SEQMOVE1 |
| parameters | 7.1 100 1 | test allotment parameters for ADU (test time, scans per second, delay) |
| command | SEQTEST1 | sets the sequence test data and activates subroutine SEQMOVE1 |
| parameters | 6.1 100 0 | test allotment parameters for ADU (test time, scans per second, delay) |
| command | SEQTEST1 | sets the sequence test data and activates subroutine SEQMOVE1 |
| parameters | 6.1 100 0 | test allotment parameters for ADU (test time, scans per second, delay) |
| command | LIMITS | sets the load soft limits that are active after the SEQTEST1 events |
| parameters | -500 2000 | vertical load soft limits |
| | -200 200 | horizontal load soft limits |
| | -15 15 | moment load soft limits |
| command | ADUSTORE | transfers the test data stored on ADU to the host PC |
| command | END | returns control to the interactive menu on the host PC |

[a]

subroutine

```
SEQMOVE1:
    PRINT #2,    "3DS"          start defining sequence
    PRINT #2,    "3SA2000"      set acceleration (0.2 mm/s^2)
    PRINT #2,    "3SV100"       set velocity (0.01 mm/s)
    PRINT #2,    "3SB100"       set base velocity (0.01 mm/s)
    PRINT #2,    "3MR600"       move relative (0.06 mm)
    PRINT #2,    "3SA200000"    set acceleration (20 mm/s^2)
    PRINT #2,    "3SV10000"     set velocity (1 mm/s)
    PRINT #2,    "3SB100"       set base velocity (0.01 mm/s)
    PRINT #2,    "3MR1000"      move relative (0.1 mm)
    PRINT #2,    "3SB10"        set base velocity (0.001 mm/s)
    PRINT #2,    "3ES"          end defining sequence
    PRINT #2,    "3XS"          execute sequence
RETURN
```

send to stepper motor controller (I/O channel two)

commands for stepper motor controller (3 is the vertical motor axis)

Note:
1 mm of displacement at the footing is equal to 10,000 steps of the stepper motor

[b]

**Figure 5.6** Control of multi-rate vertical partially-drained tests:
[a] input file T120_A.INP; and [b] subroutine SEQMOVE1 in control program

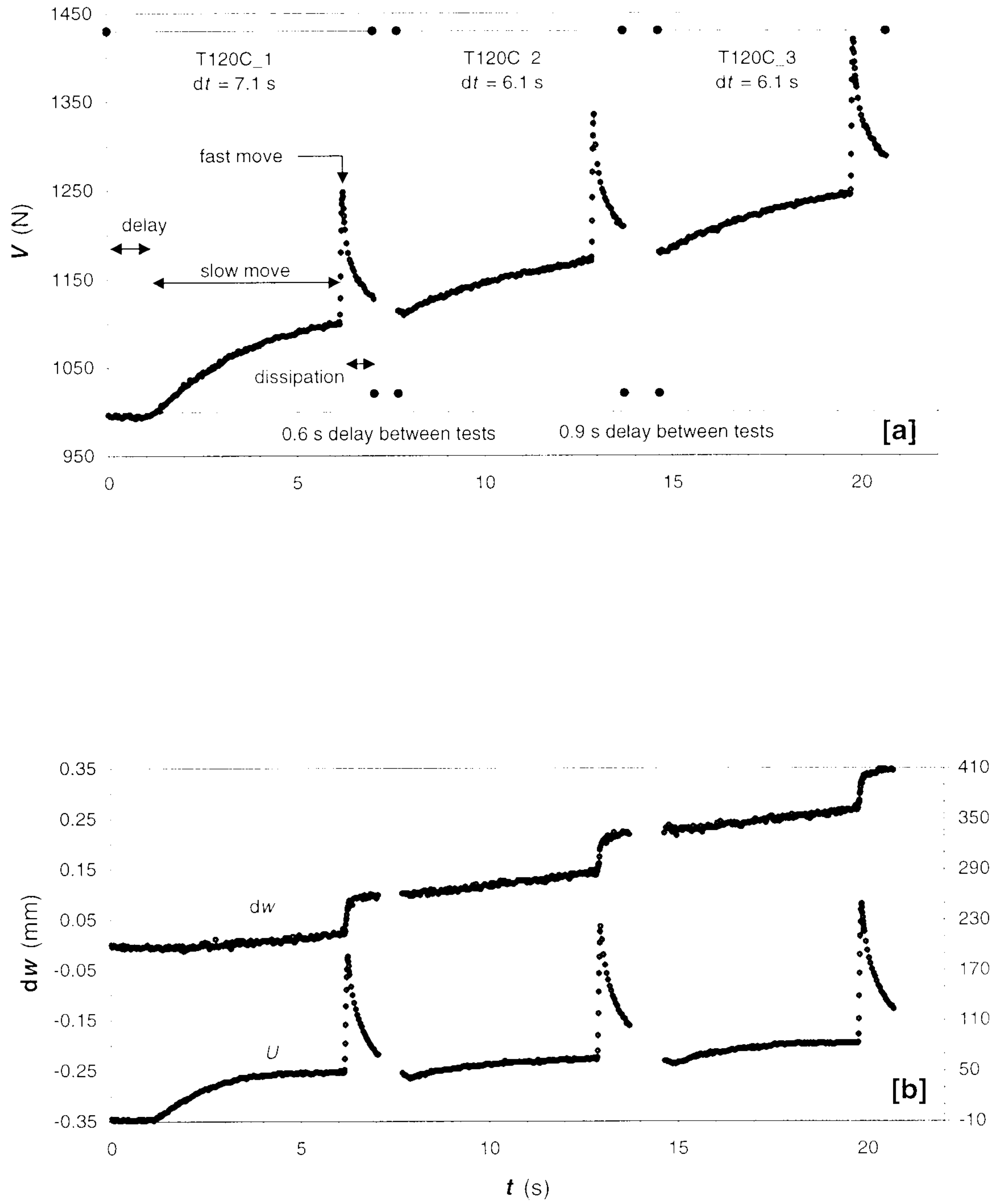


**Figure 5.7** Time history of the multi-rate vertical partially-drained test from 1000 N

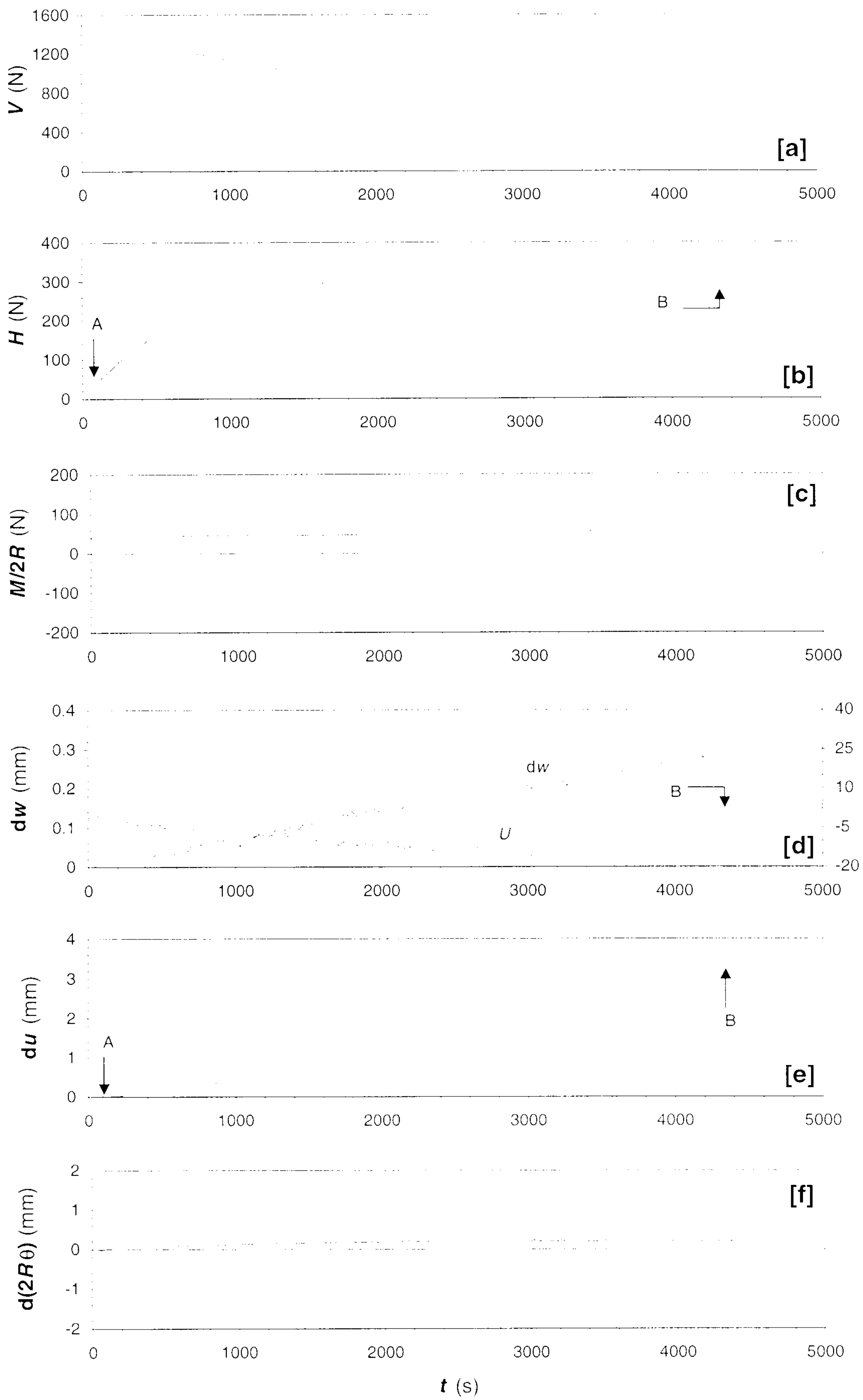


**Figure 5.8** Time history of a slow horizontal sideswipe test (T309_1, $du/dt$ = 0.001 mm/s)

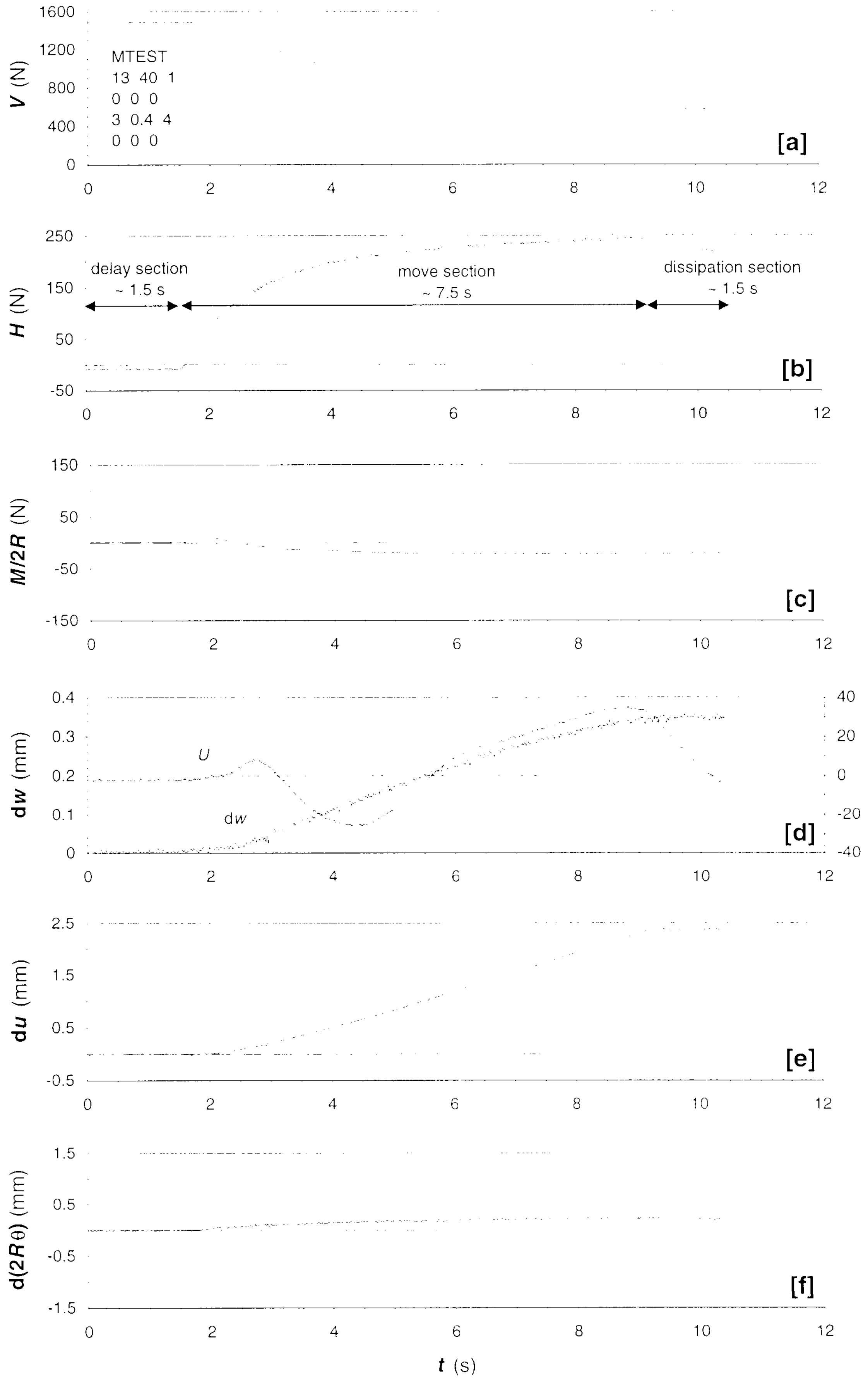


**Figure 5.9** Time history of a fast horizontal sideswipe test (T107A_3, $du/dt$ = 0.4 mm/s)

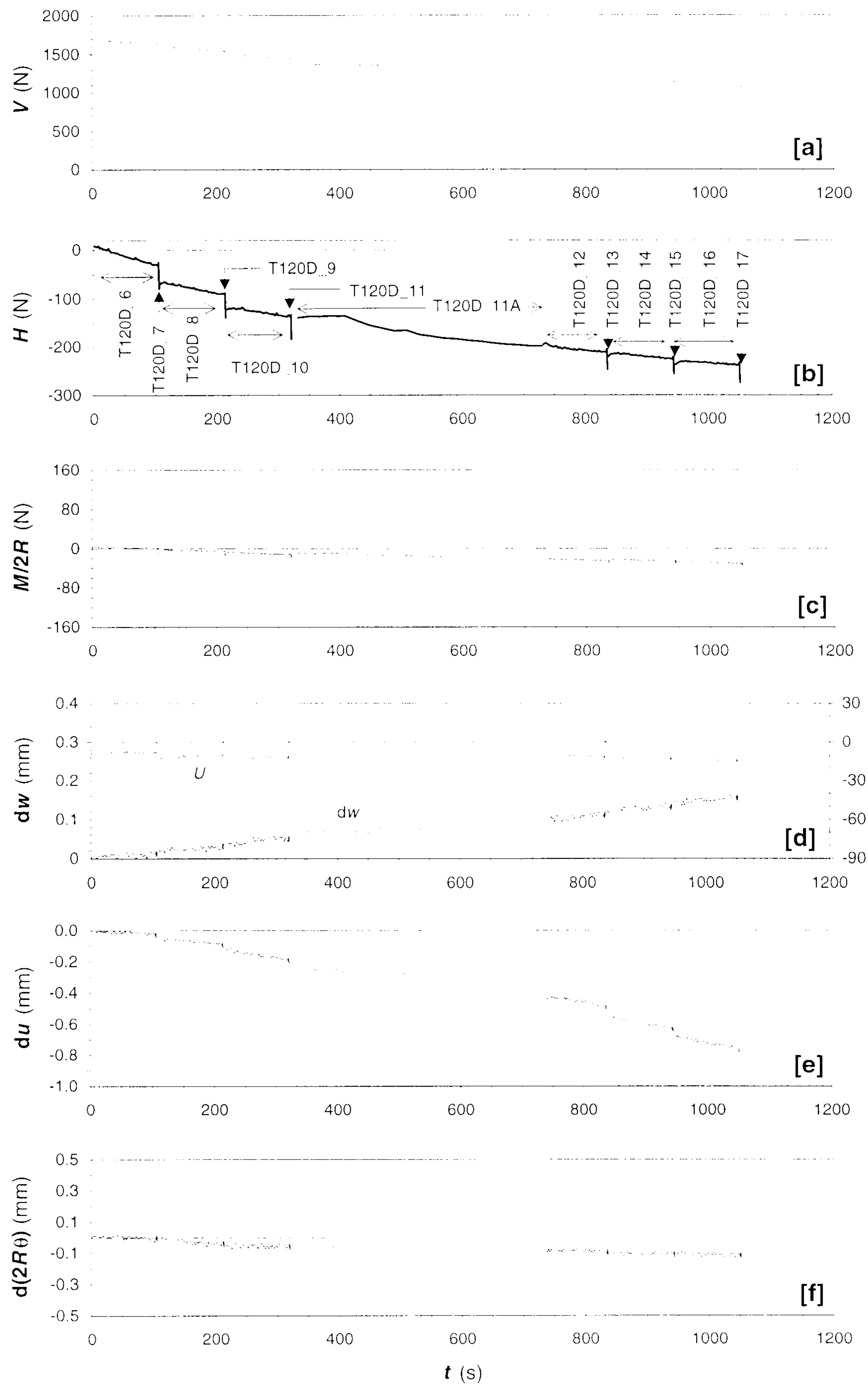


**Figure 5.10** Time history of the multi-rate horizontal sideswipe test from 1700 N

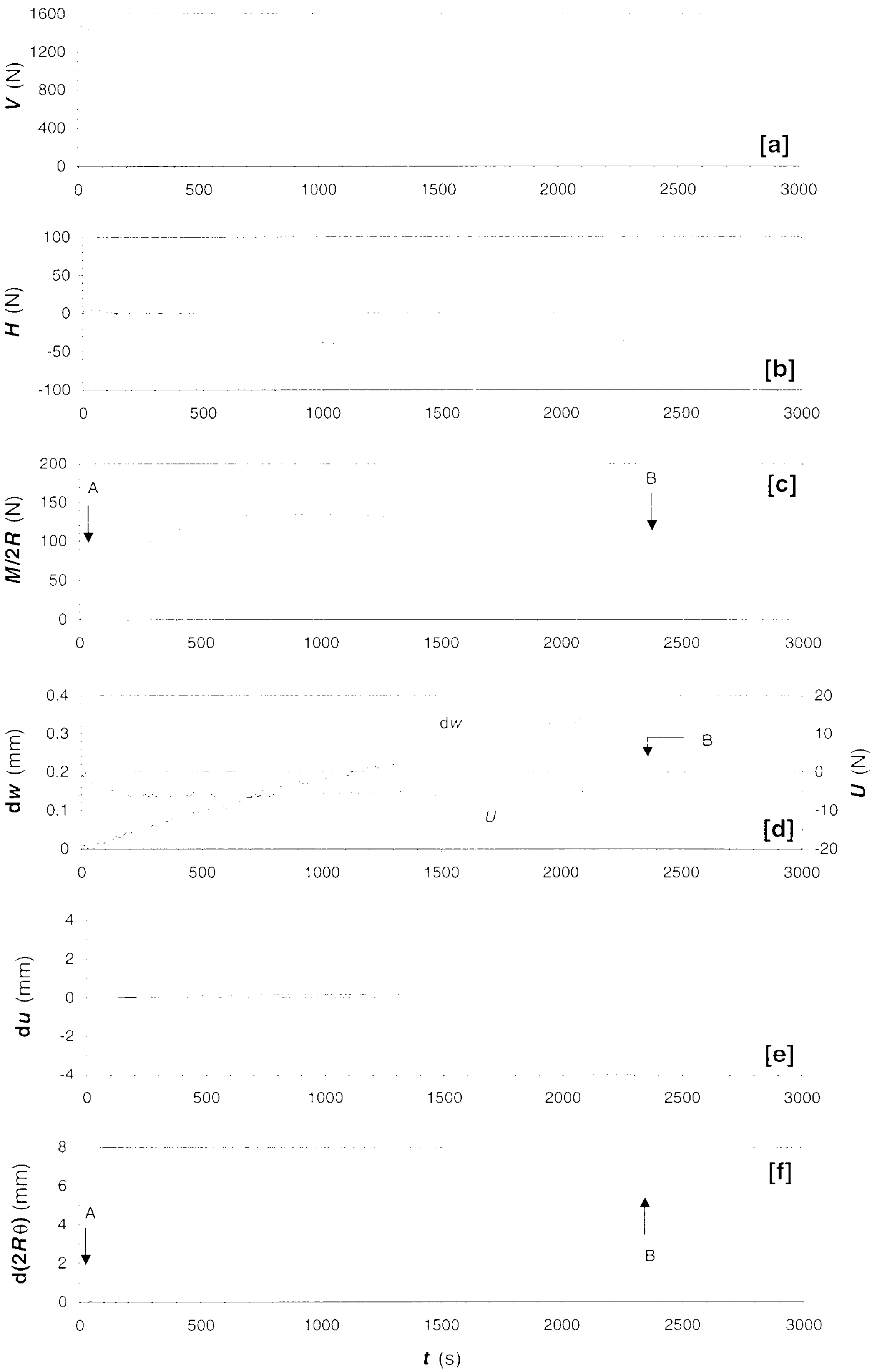


**Figure 5.11** Time history of a slow moment sideswipe test (T311_3, $d(2R\theta)/dt$ = 0.0026 mm/s)

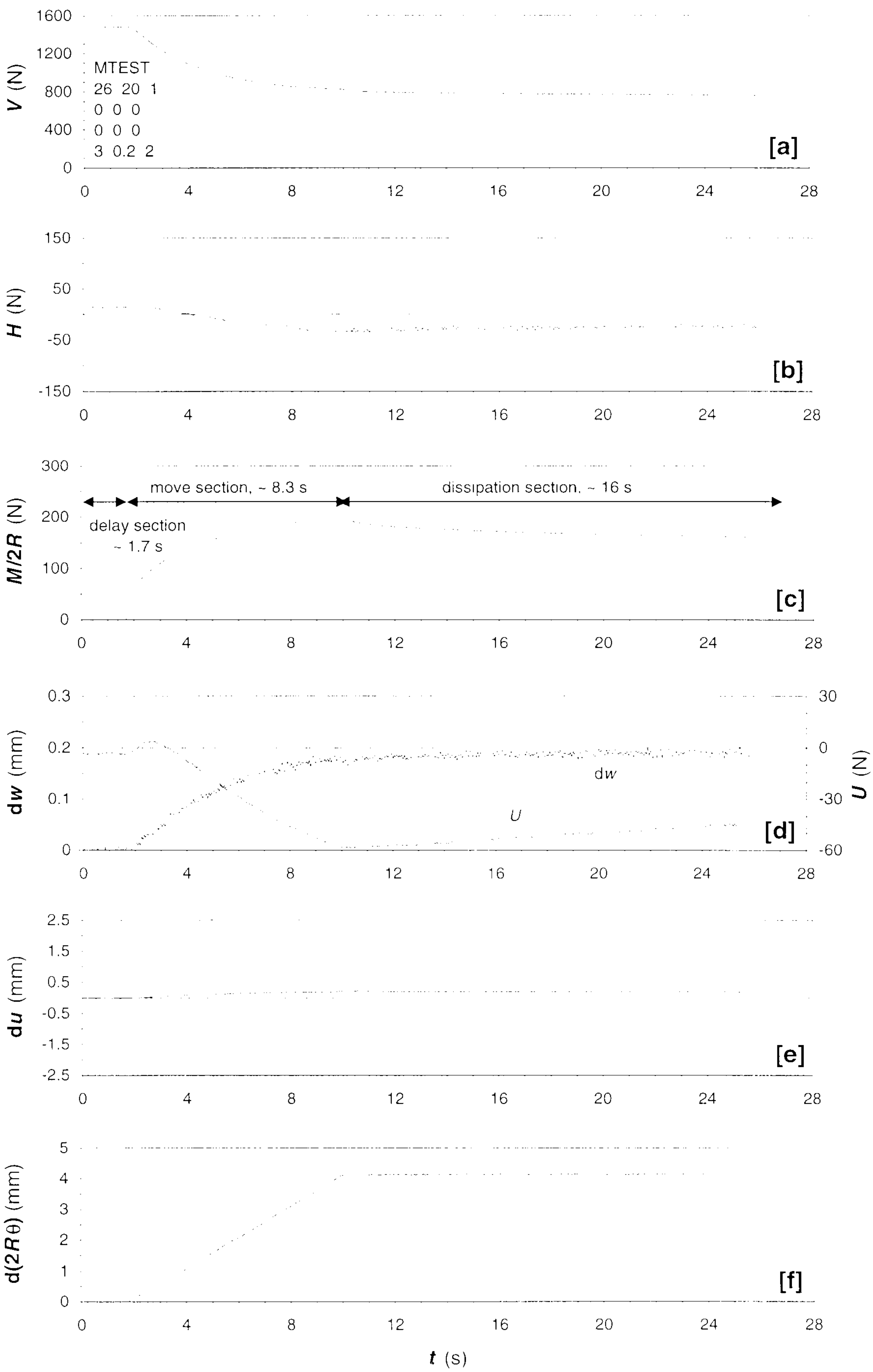


**Figure 5.12** Time history of a fast moment sideswipe test
(T114E_1, $d(2R\theta)/dt$ = 0.524 mm/s)

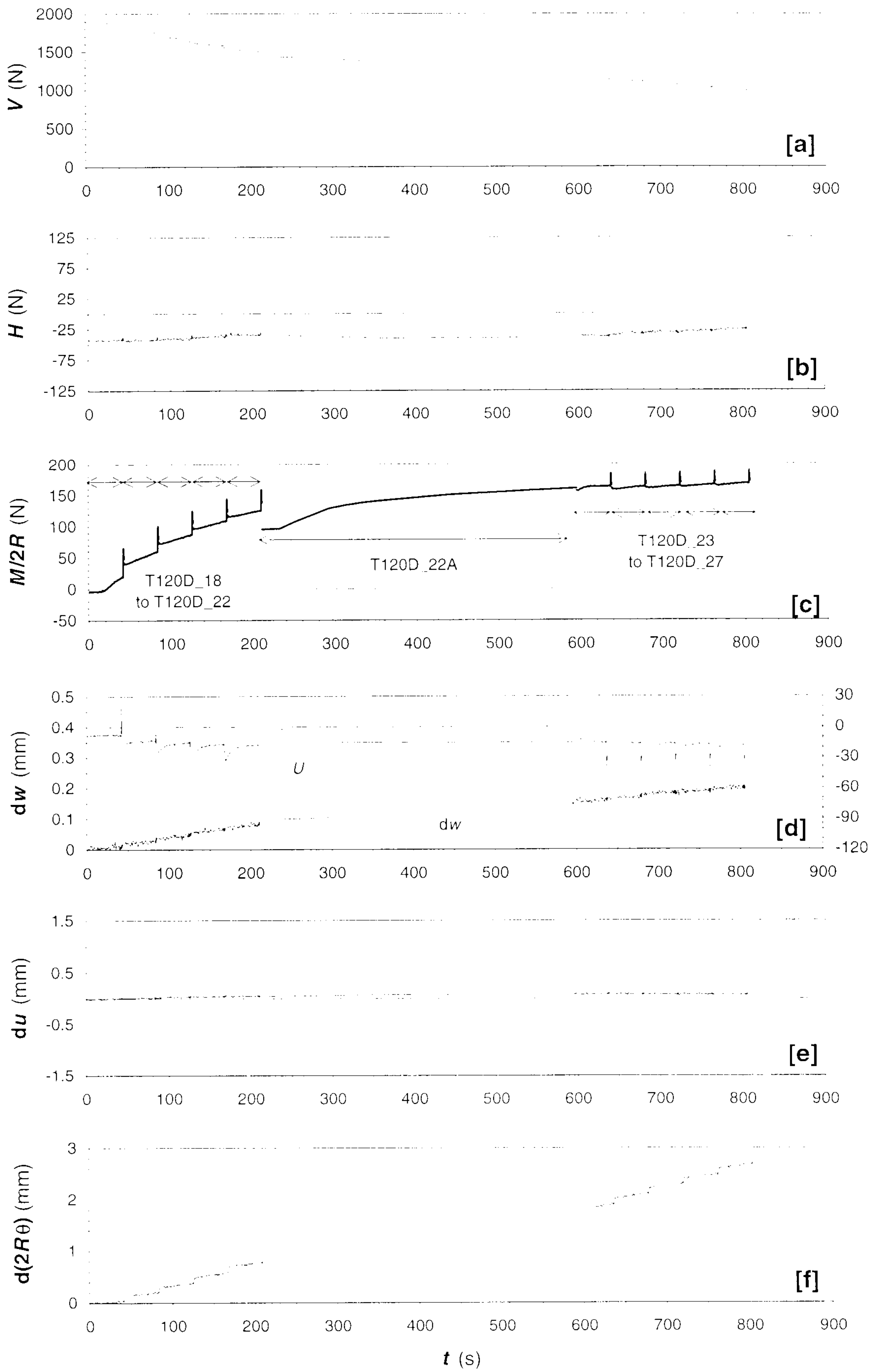


**Figure 5.13** Time history of the multi-rate moment sideswipe test from 1900 N

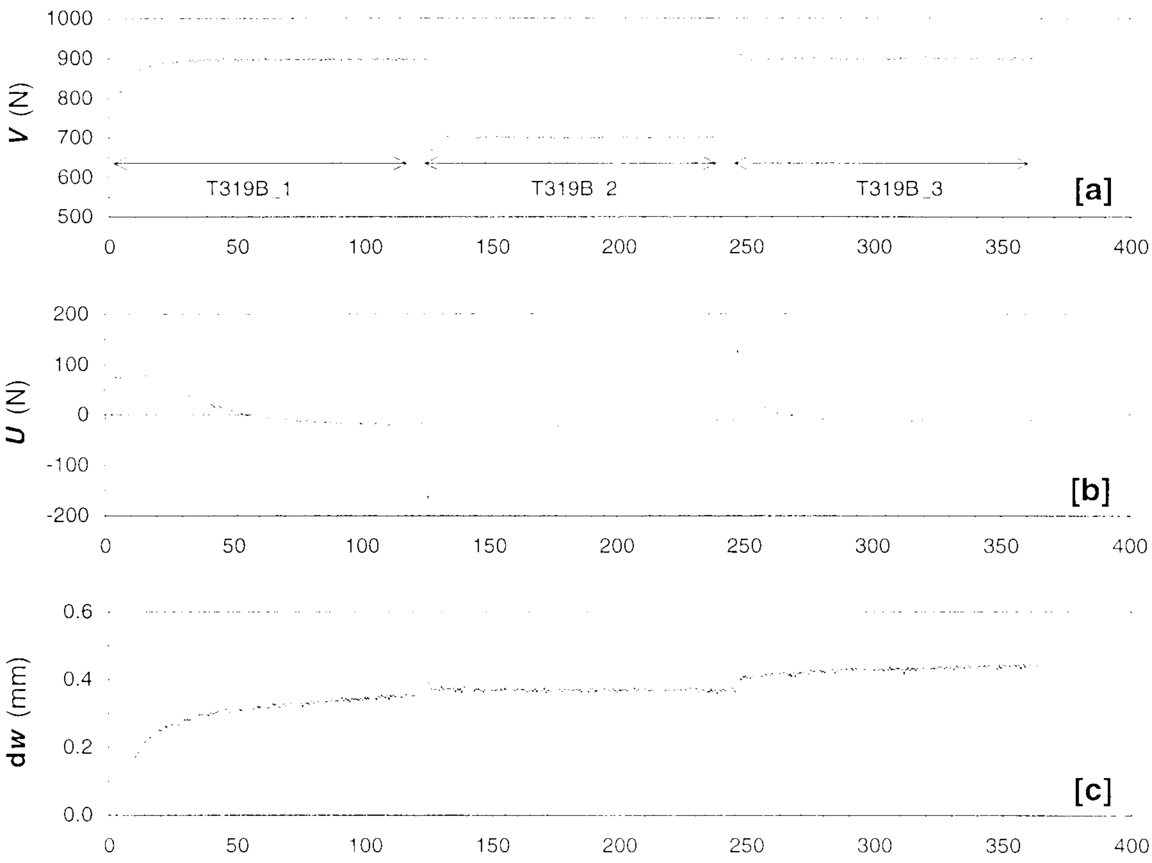


**Figure 5.14** Time history of the consolidation tests in T319

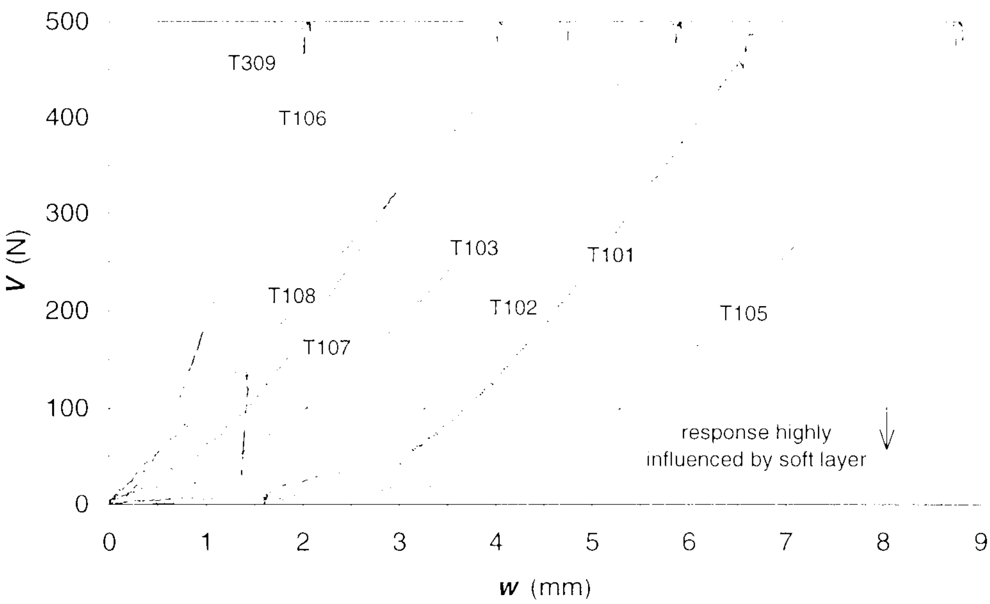


**Figure 6.1** Differences in the initial load:deformation response of the footing

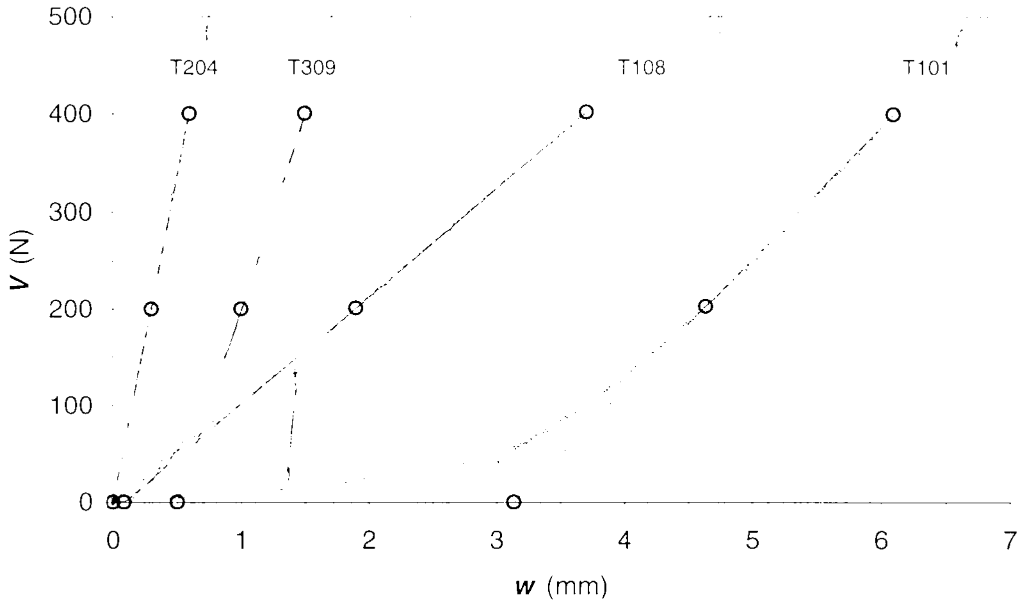


**Figure 6.2** Extrapolated origin of load:deformation curves

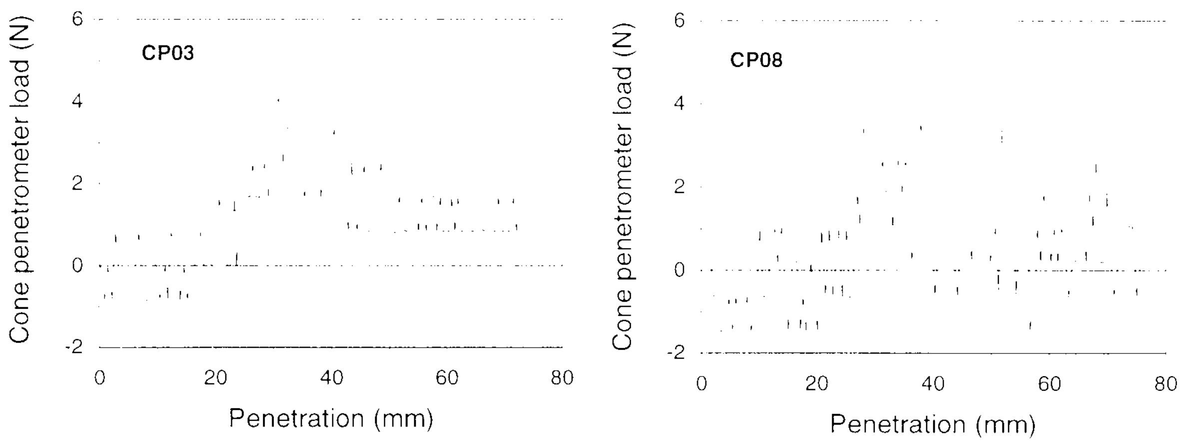


**Figure 6.3** Cone penetration tests at the centre of samples T103 and T108

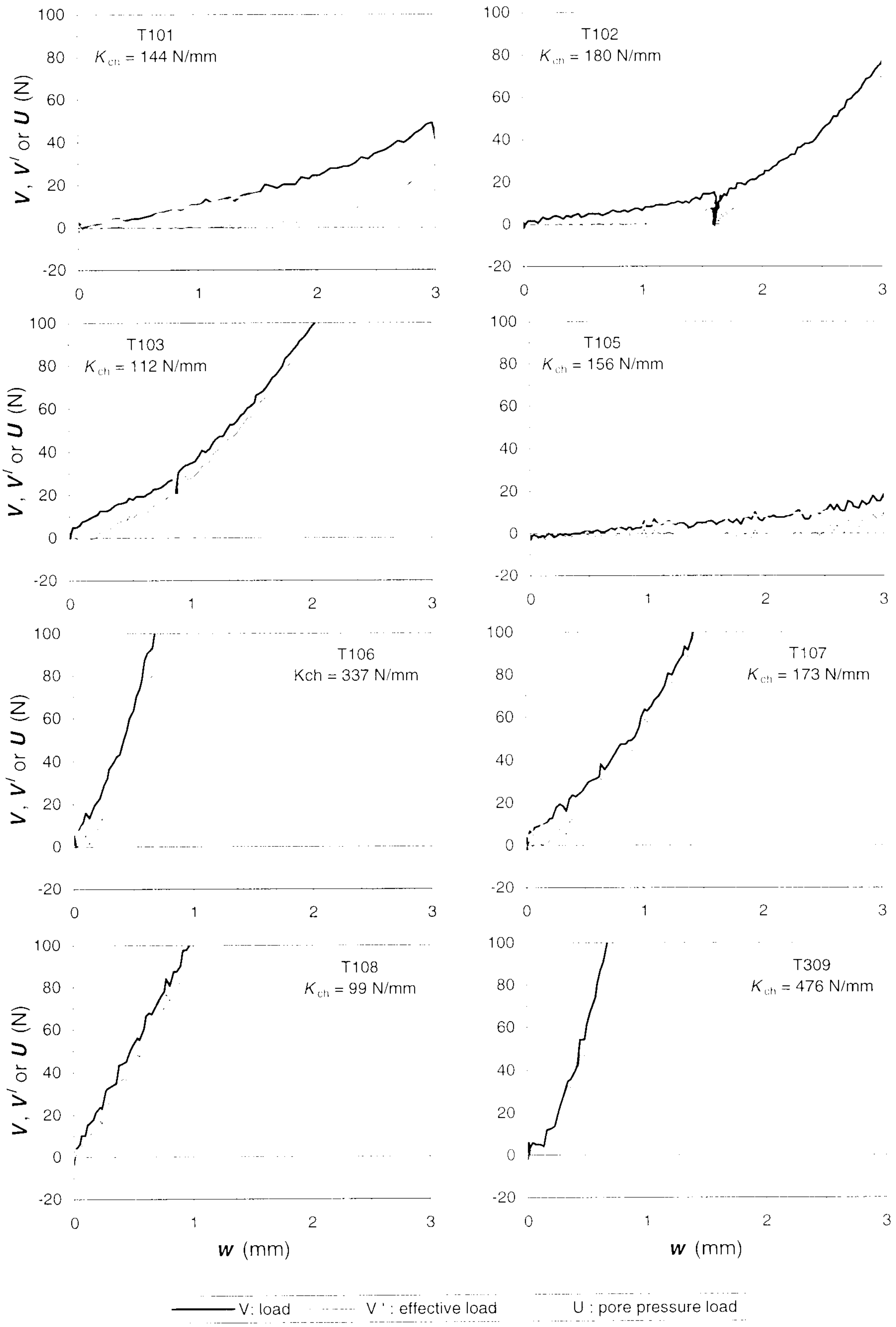


**Figure 6.4** Effect of loose layer of soil and pore pressures on initial load:deformation response

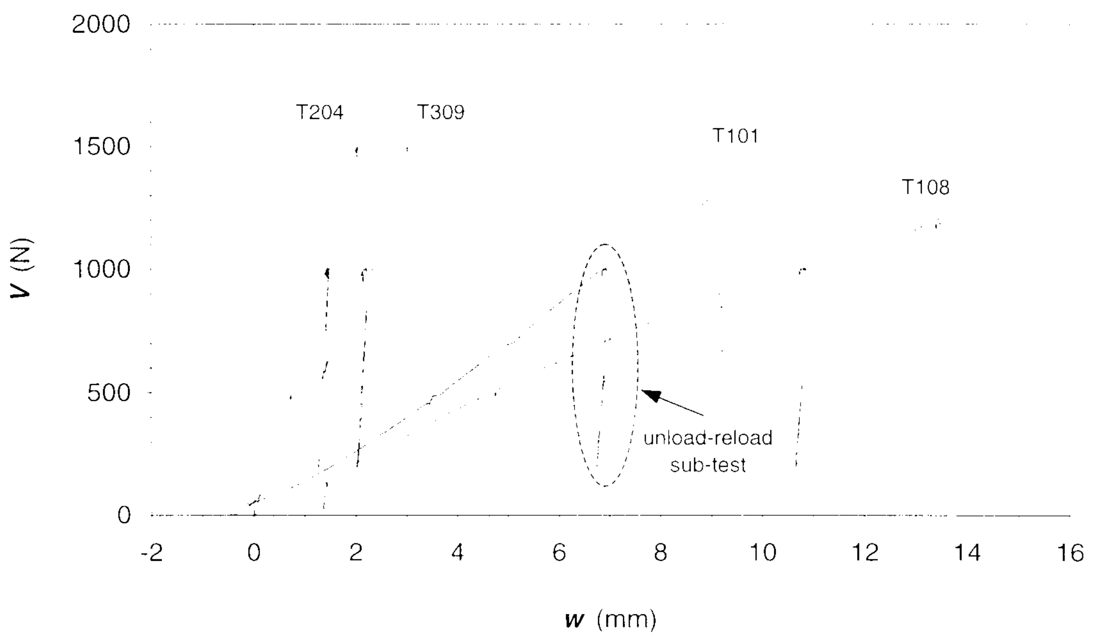


Note:
- The sideswipe sub-tests at end of virgin-penetration curves are not shown.

**Figure 6.5** Load:deformation curves of the tests that did not include partially-drained sub-tests

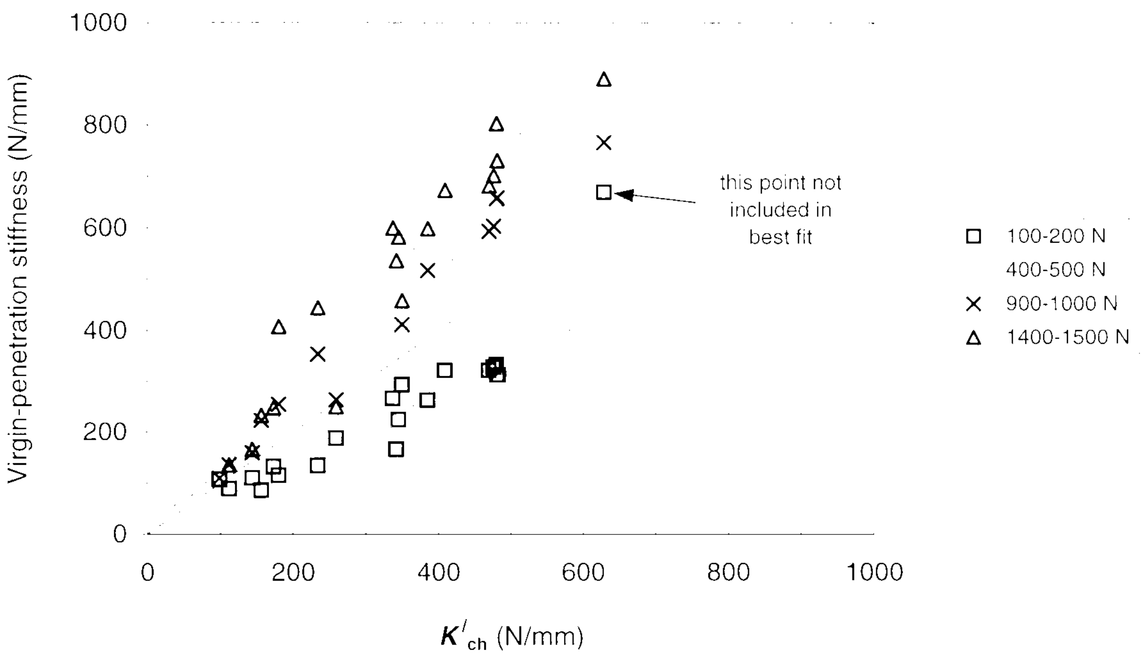


**Figure 6.6** The virgin-penetration stiffness values plotted against the characterisation stiffness

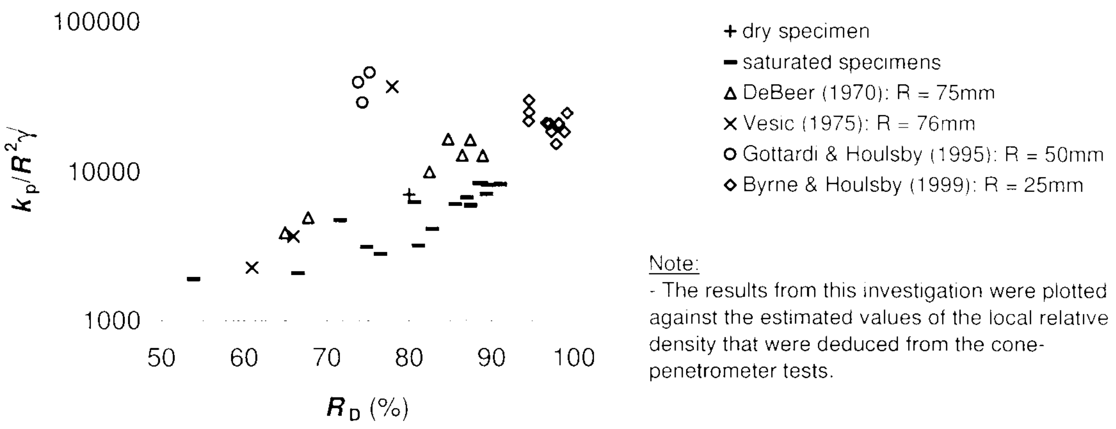


**Figure 6.7** The initial virgin-penetration stiffness versus the relative density; results from this investigation compared with some of those in the literature

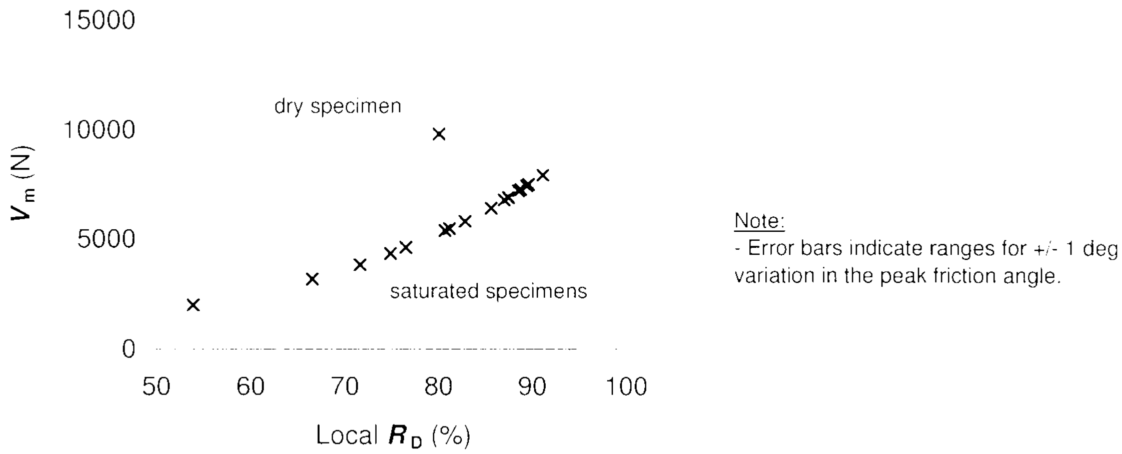


**Figure 6.8** Predictions of the bearing capacity plotted against the estimated values of the relative density in the top layer of the specimens

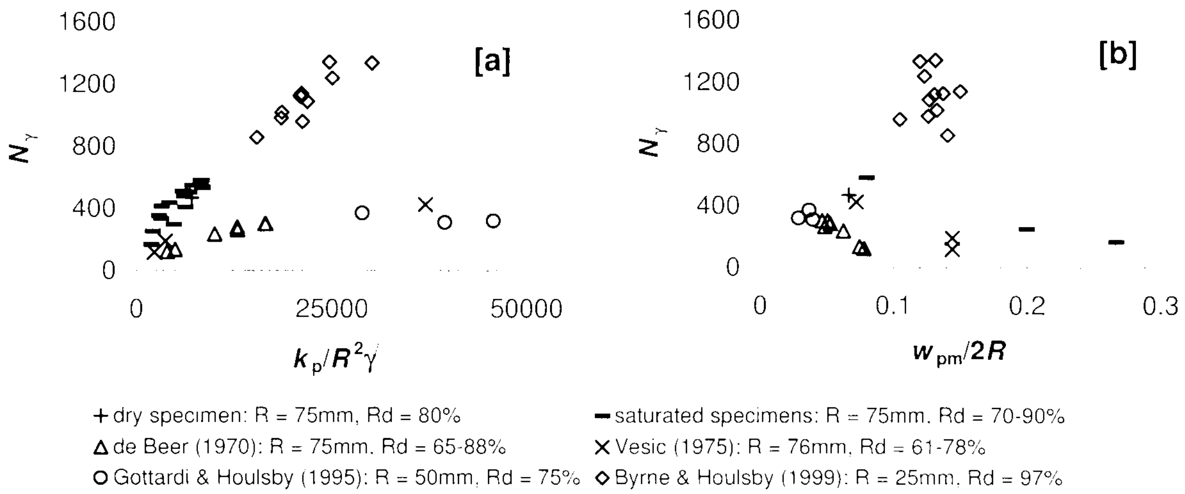


**Figure 6.9** Relationships between bearing capacity and initial stiffness parameters (estimated values from this investigation compared with some measured values from the literature):

**[a]** bearing capacity factor against initial stiffness; and

**[b]** bearing capacity factor against normalised displacement at failure

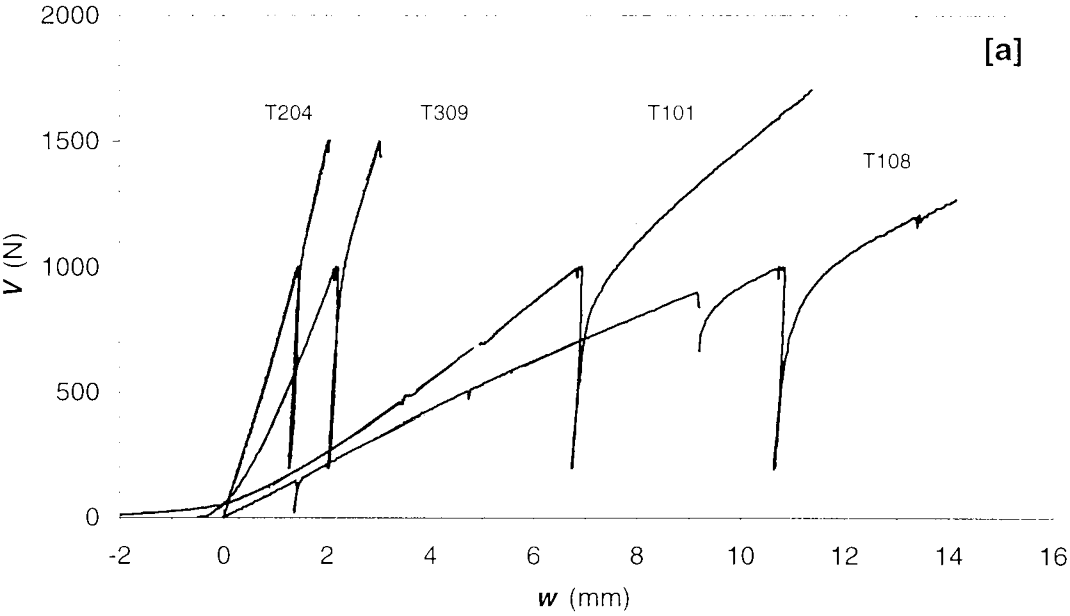


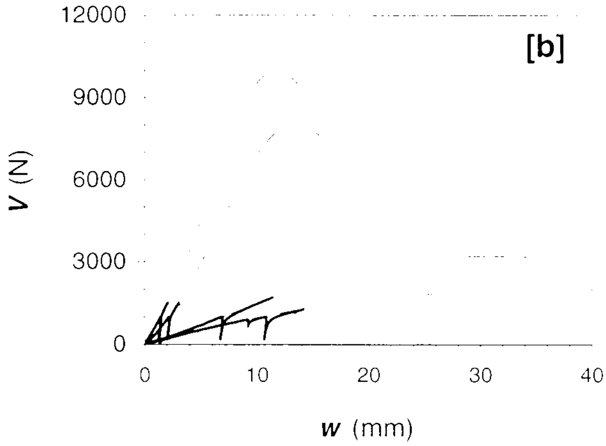


Fitting parameters:

| Test | $kp$ (N/mm) | $V_m$ (N) |
|---|---|---|
| T108 | 110 | 2000 |
| T101 | 130 | 3200 |
| T309 | 400 | 8000 |
| T204 | 650 | 10000 |

**Figure 6.10** Comparison of virgin-penetration curves and fitted curves: **[a]** at small displacement; and **[b]** large displacement

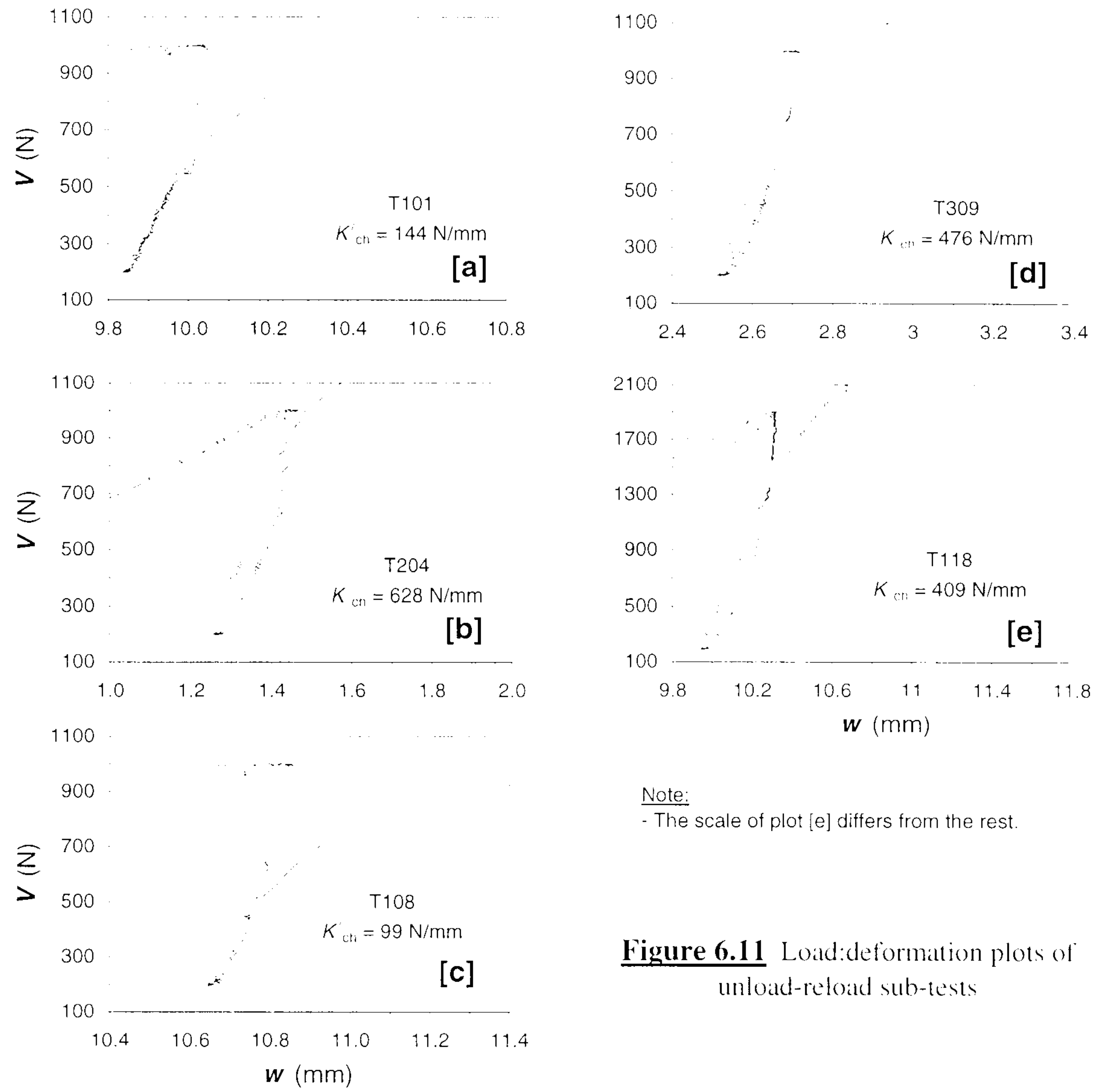


Note:
- The scale of plot [e] differs from the rest.

**Figure 6.11** Load:deformation plots of unload-reload sub-tests

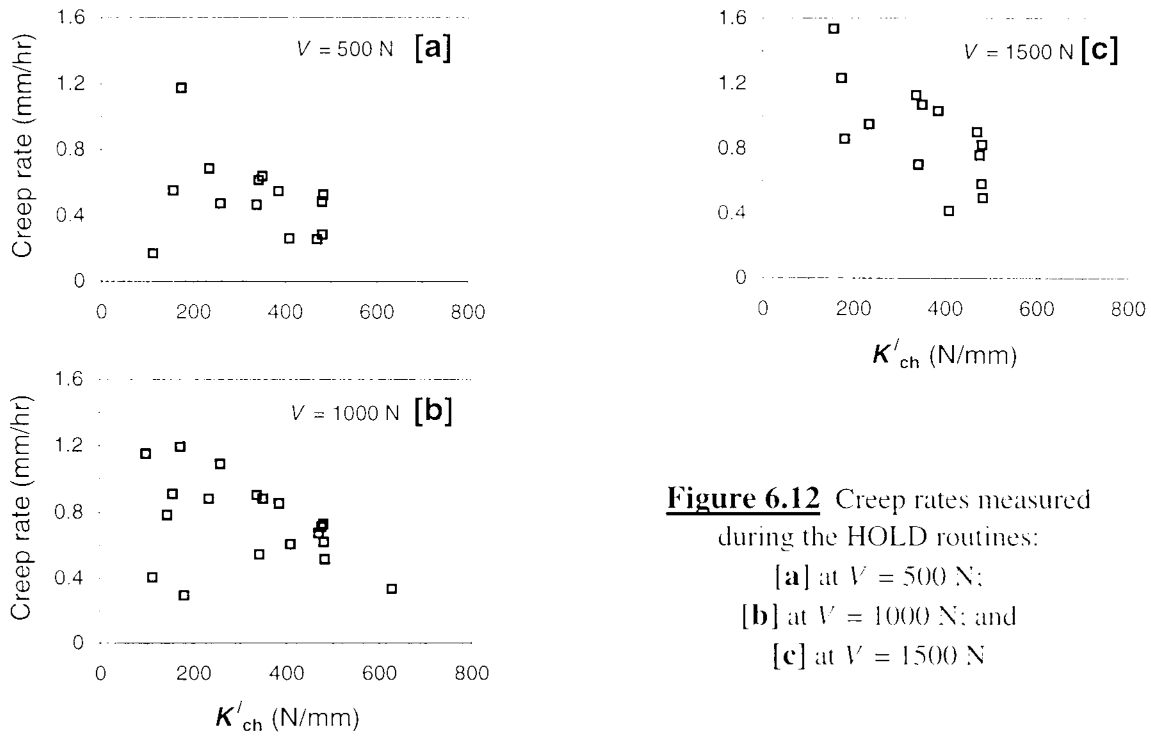


**Figure 6.12** Creep rates measured during the HOLD routines:
**[a]** at $V$ = 500 N;
**[b]** at $V$ = 1000 N; and
**[c]** at $V$ = 1500 N

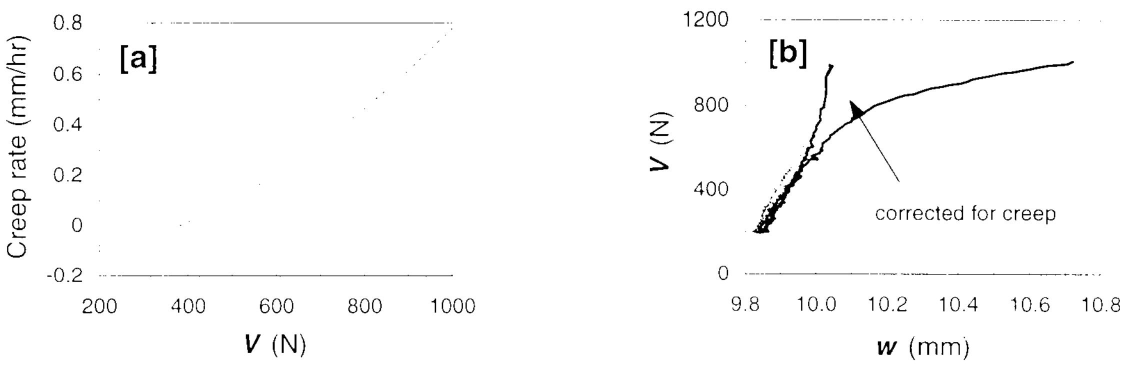


**Figure 6.13** The effect of creep on the unload-reload sub-test of T101: **[a]** assumed creep relationship; and **[b]** actual response compared with corrected response

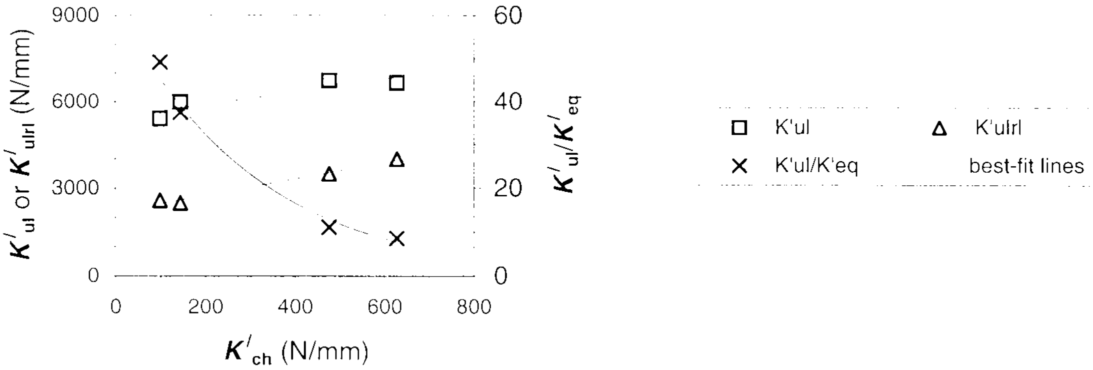


**Figure 6.14** Vertical stiffness parameters derived from the unload-reload footing tests

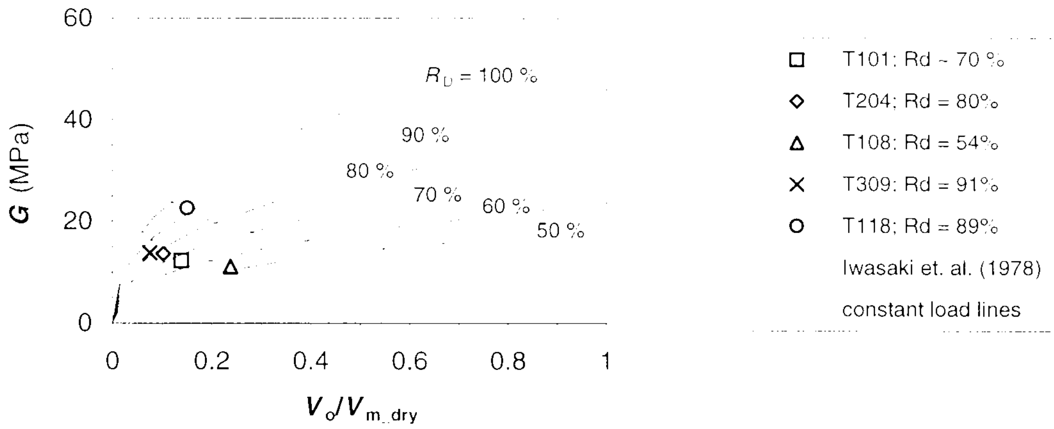


Note:
- See Figure 2.2 for Iwasaki *et. al*. relationship.
- In Iwasaki *et. al*., the effective mean stress was assumed equal to 0.53 times the contact stress on the footing ($K_o$ = 0.3) and the elastic shear modulus was taken as $0.2G_o$.
- The constant load lines represented $V_o$ = 1000 N and $V_o$ = 2000 N.
- The relative density measurements from the cone penetrometer tests were used, see Table 4.6.

**Figure 6.15** Elastic shear moduli from vertical unload-reload tests.

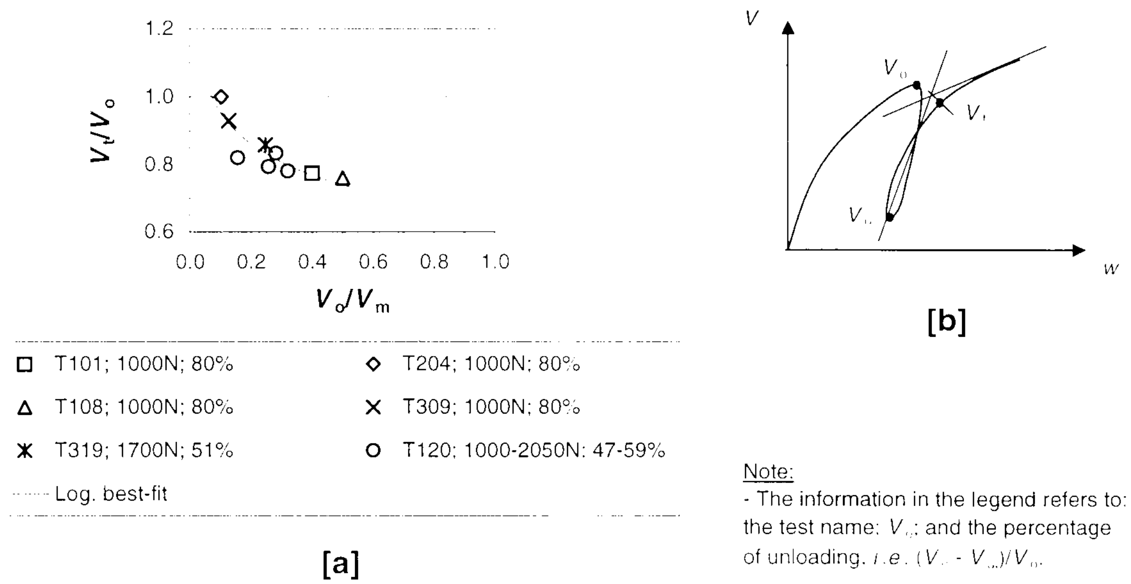


**Figure 6.16** Transition point of the reloading section of the vertical ULRL tests and after some of the sideswipe tests: **[a]** measured points; **[b]** diagram showning parameters involved

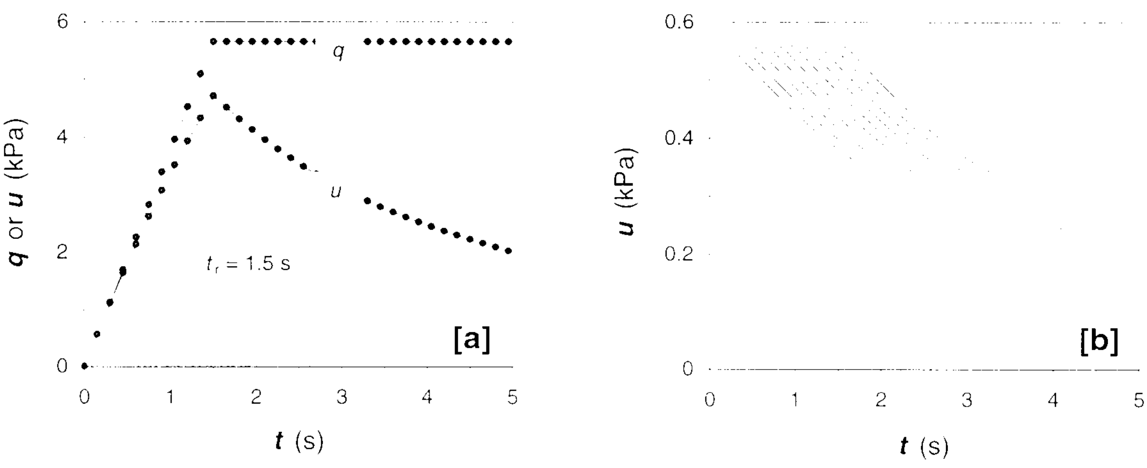


Note:
- $(du)_{t=0} = (dq)_{t=0}$
- Ten load increments.
- Dissipation of each increment given by relation in Figure 2.27.
- $dq = dV/(C_q \pi R^2)$ where $C_q = 2$.

**Figure 6.17** Illustration of partially-drained consolidation model: **[a]** total stress and sum of pore pressure increments at centre of footing; and **[b]** pore pressure increments

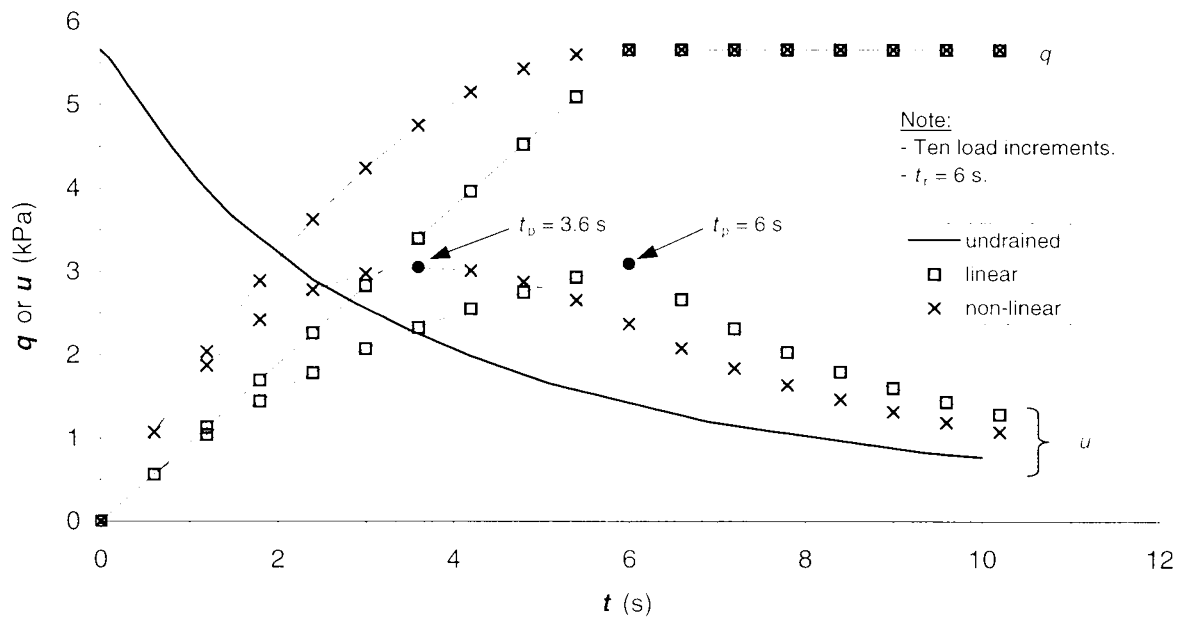


**Figure 6.18** Types of ramped loading and resulting pore pressures of partially-drained consolidation model

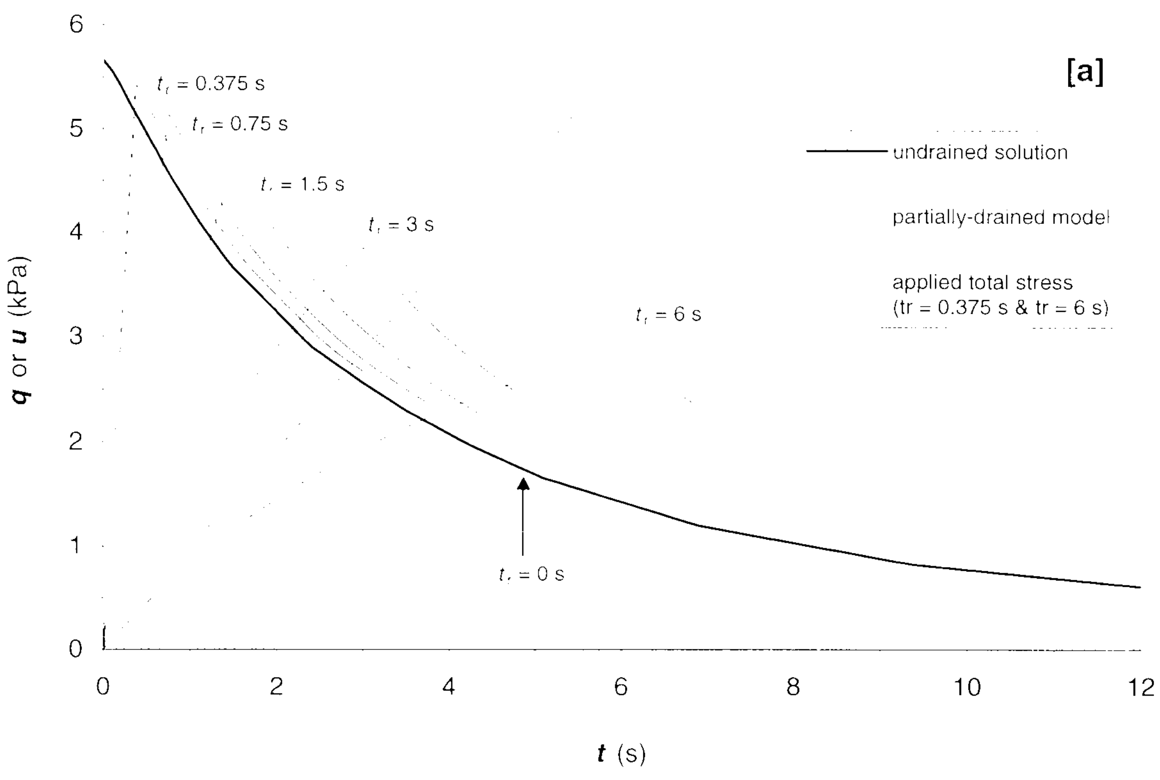


**Figure 6.19** Comparison of the Davis and Poulos (1972) undrained solution and partially-drained consolidation model: **[a]** $t:u$ space; and **[b]** $T_v:U'_p$ space

(continued on next page)

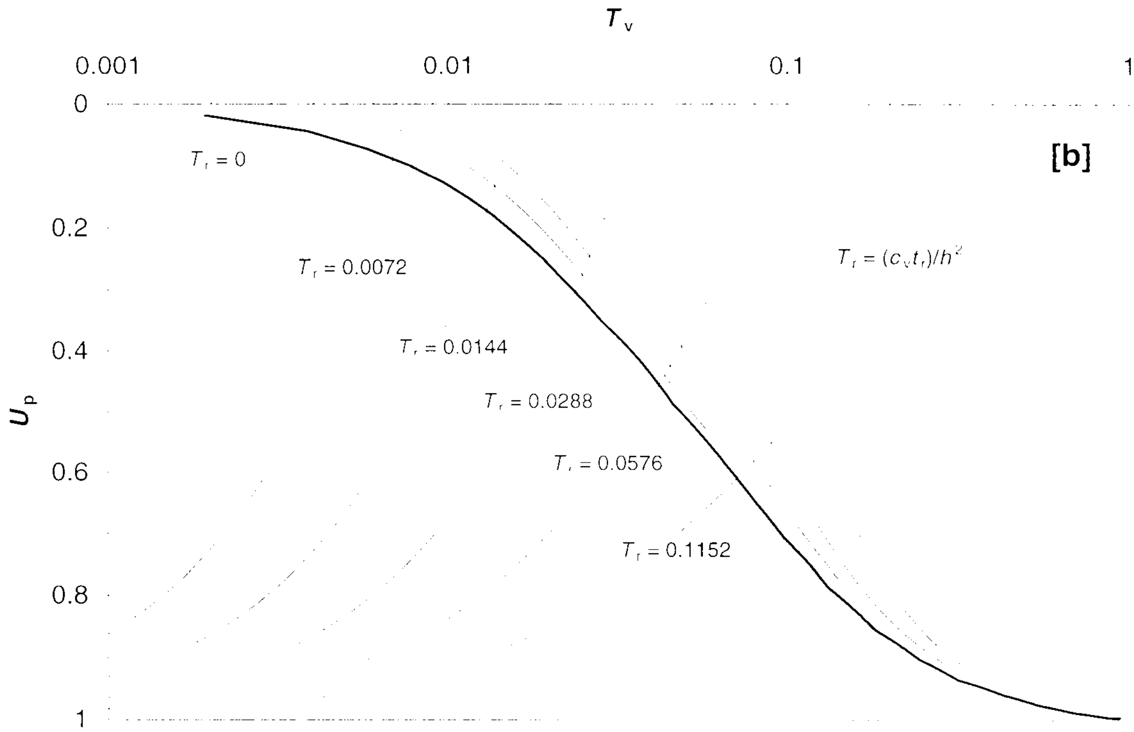


**Figure 6.19 (cont.)** Comparison of the Davis and Poulos (1972) undrained solution and partially-drained consolidation model: **[a]** $t:u$ space: and **[b]** $T_v:U_p$ space

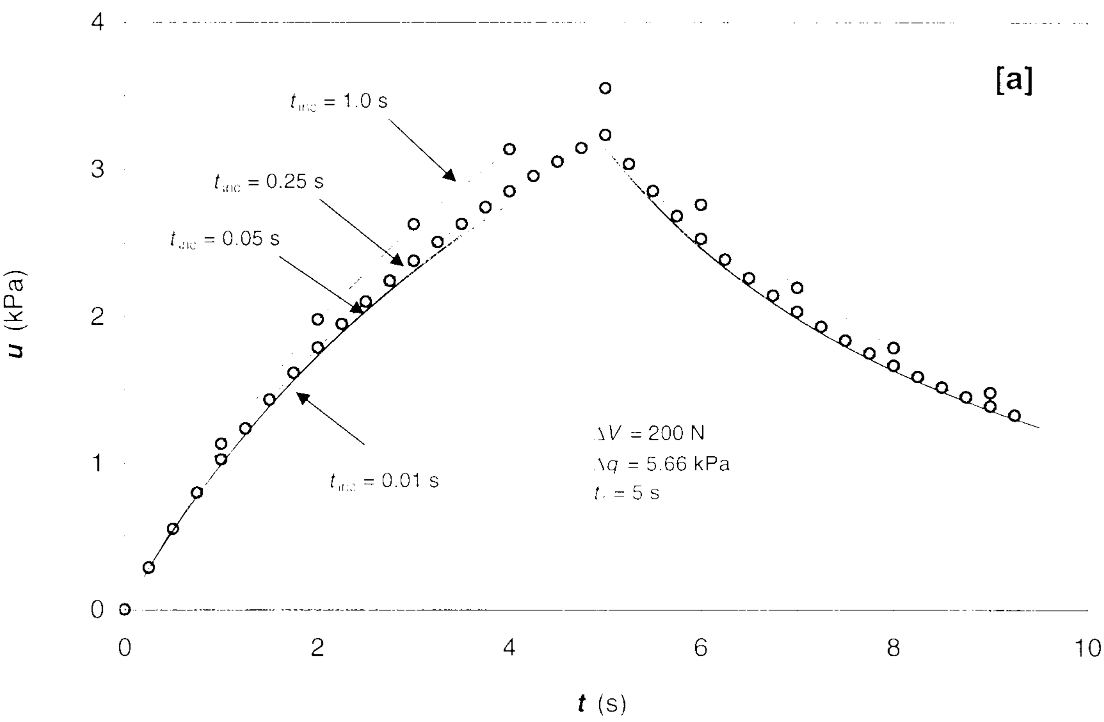


**Figure 6.20** Effect of the time increment on predictions of the partially-drained consolidation model: **[a]** trend of decreasing time increment: and **[b]** effect of time increment on different rise times

(continued on next page)

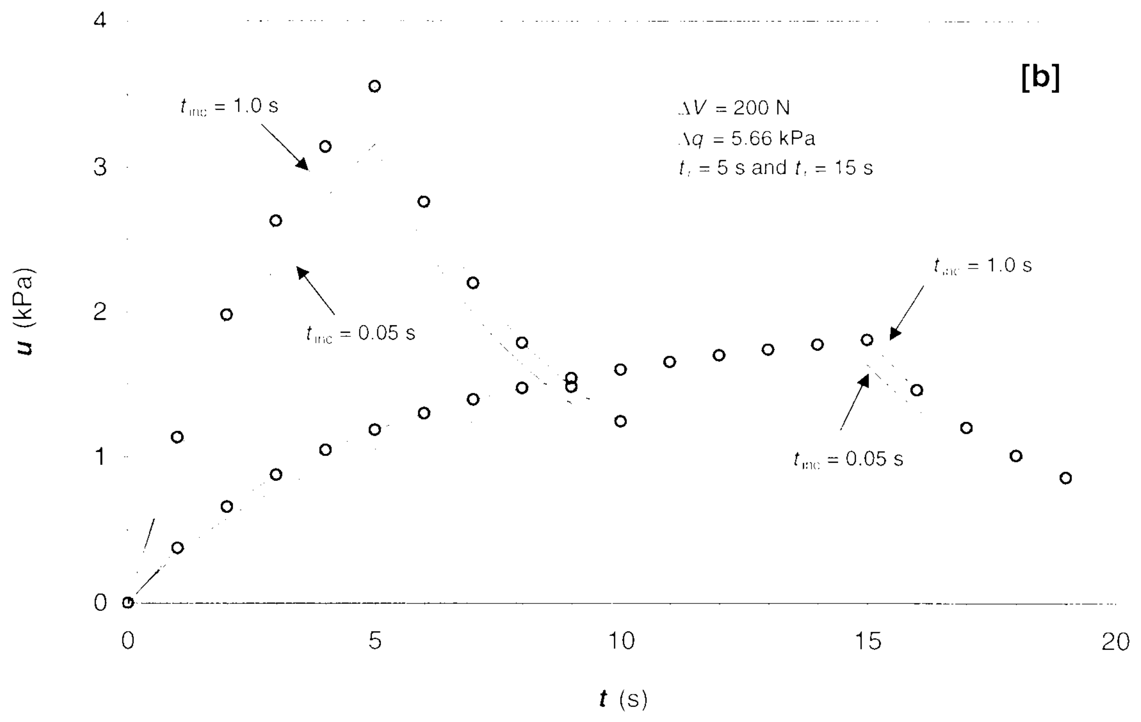


**Figure 6.20 (cont.)** Effect of the time increment on predictions of the partially-drained consolidation model: **[a]** trend of decreasing time increment; and **[b]** effect of time increment on different rise times

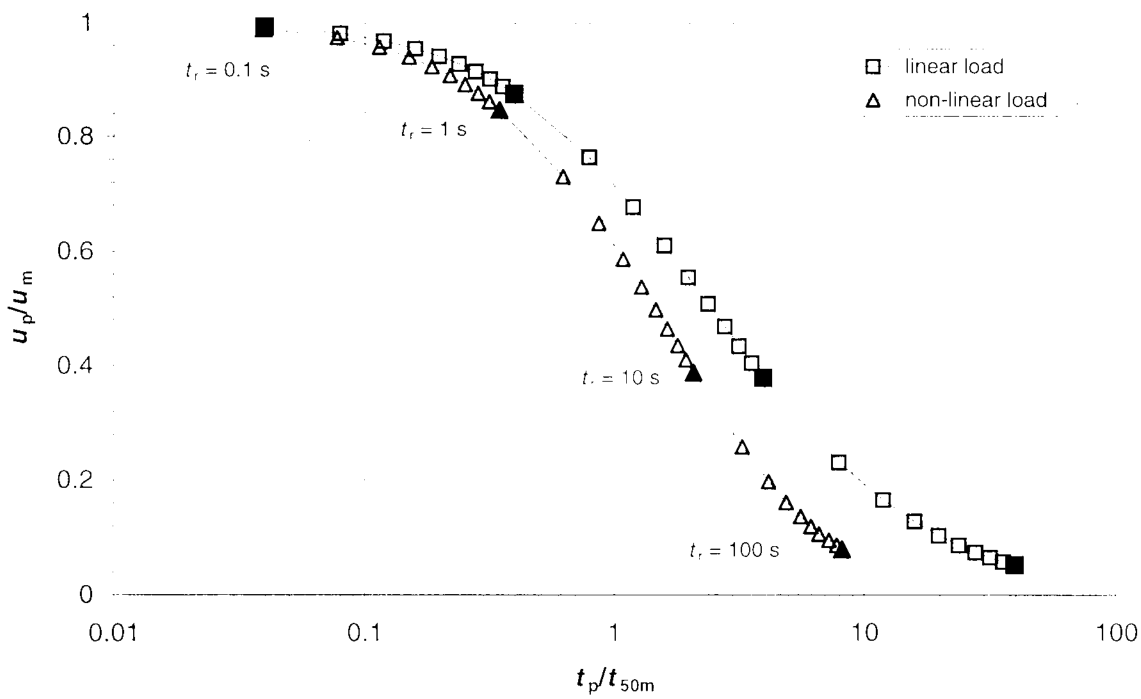


**Figure 6.21** Peak pore pressure as a function of time to peak, from partially-drained consolidation model

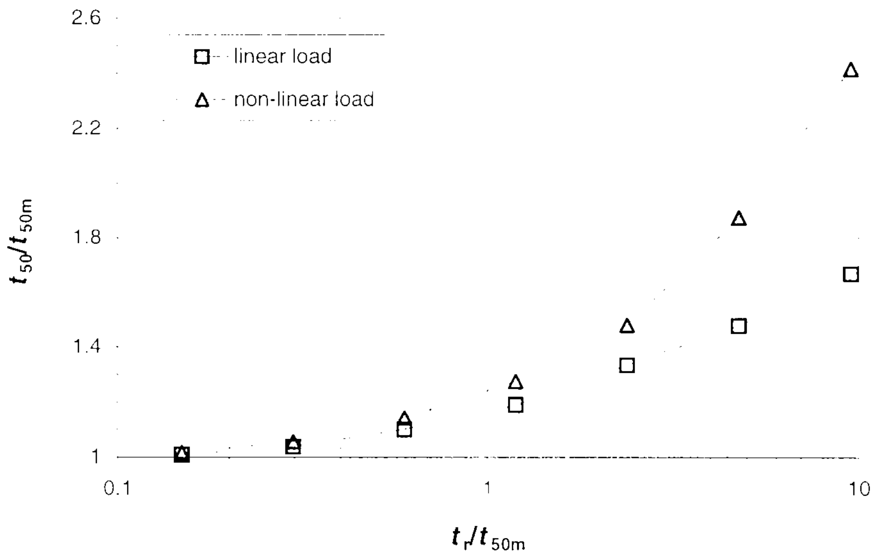


**Figure 6.22** Effect of rise time on $t_{50}$ time, from partially-drained consolidation model

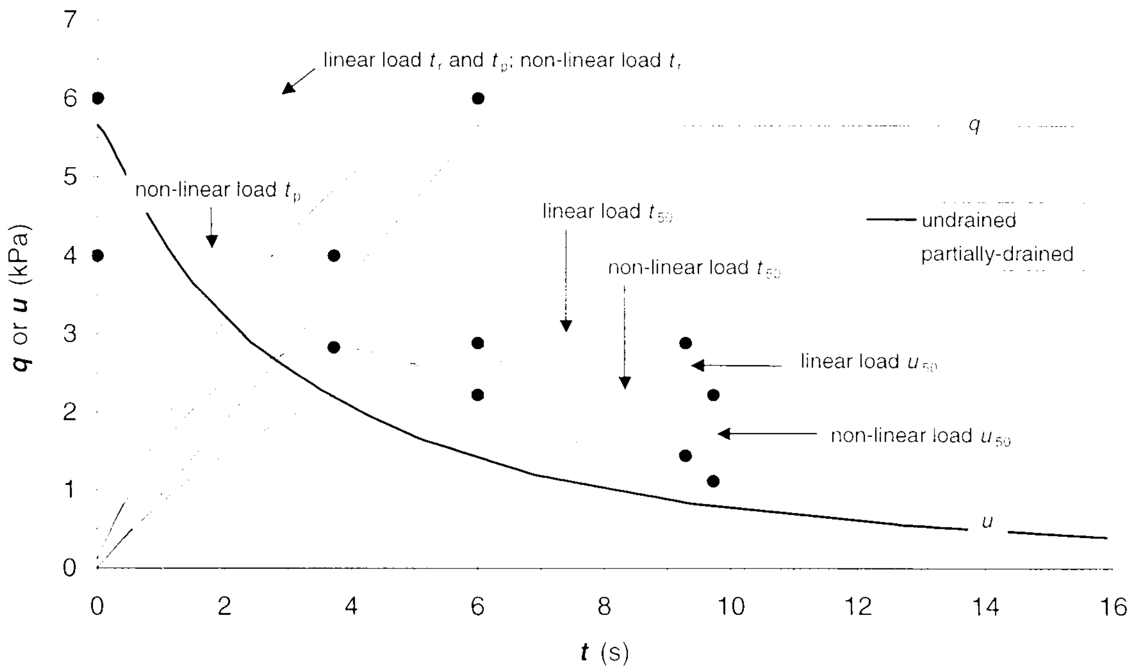


**Figure 6.23** Definition of $t_{50}$ time and $u_{50}$ pore pressure

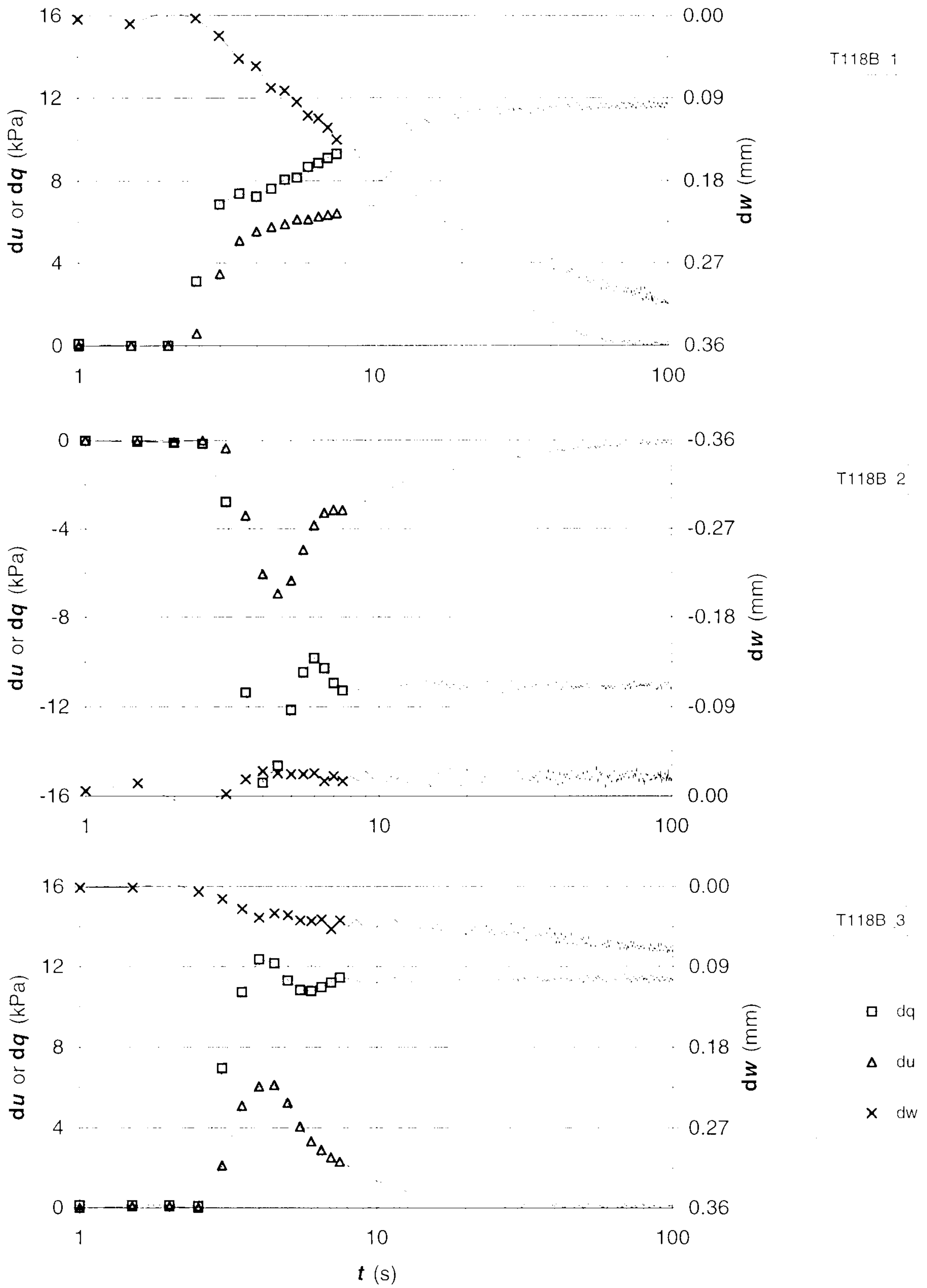


**Figure 6.24** Consolidation sub-tests of T118

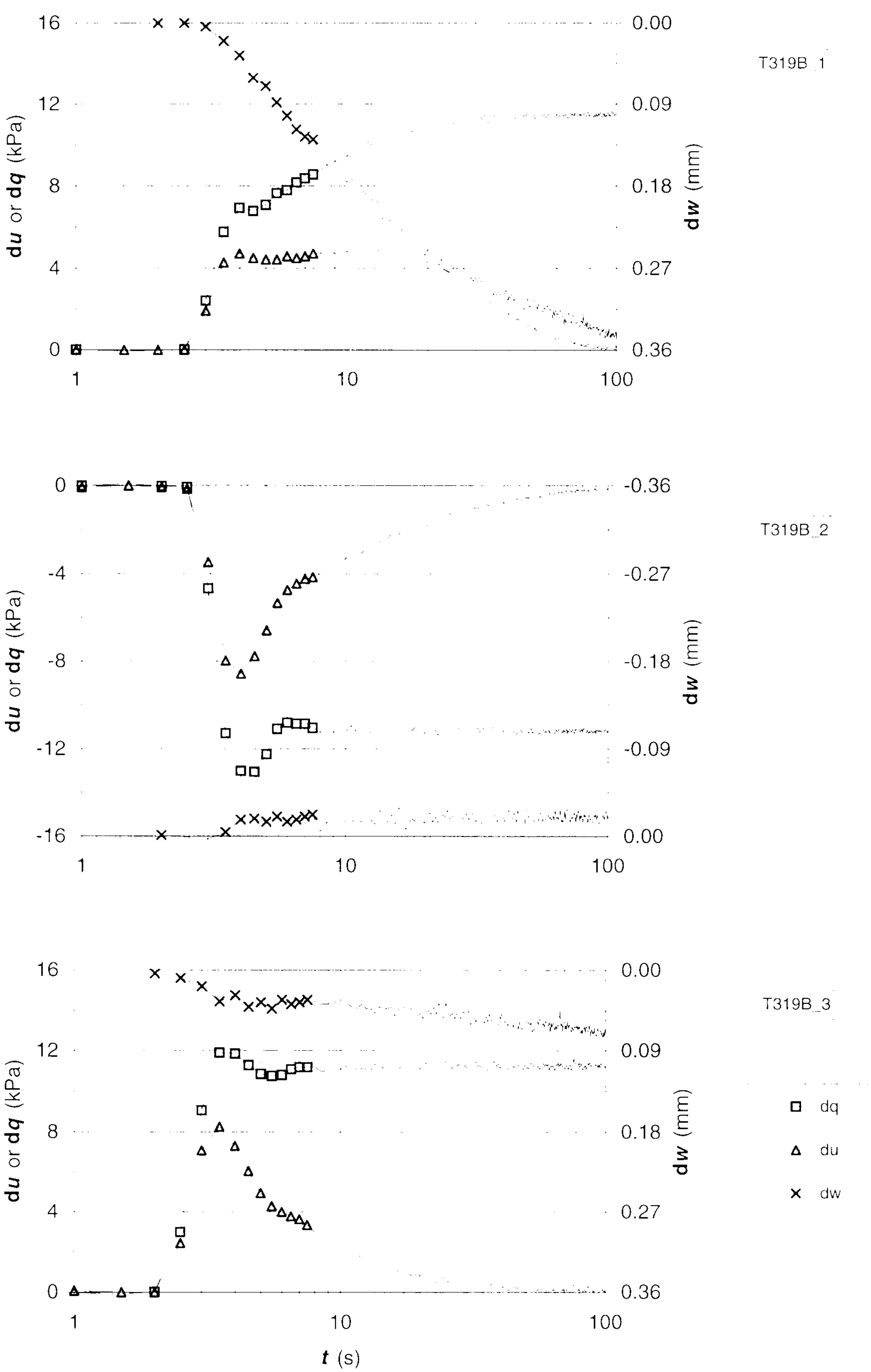


**Figure 6.25** Consolidation sub-tests of T319

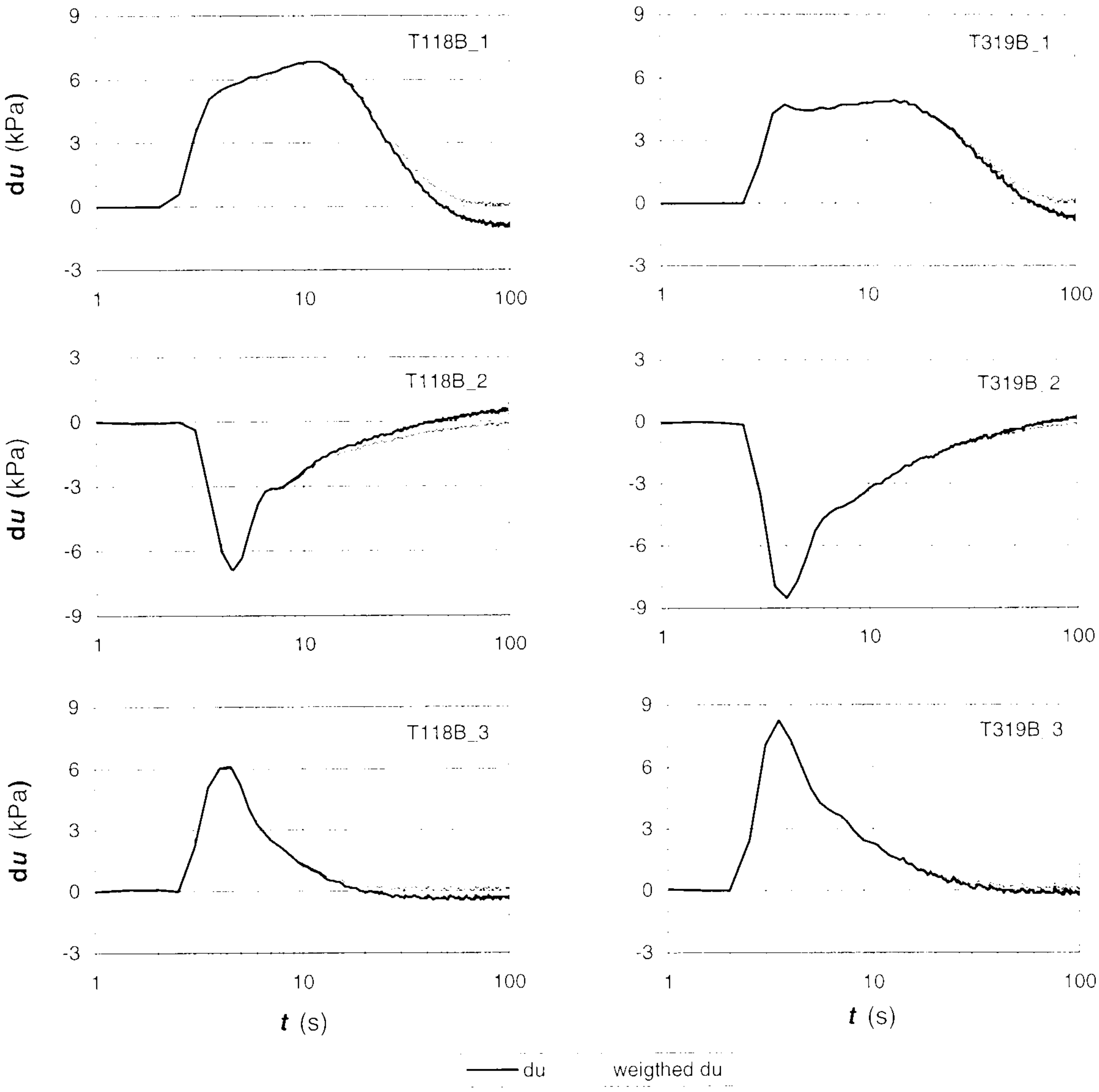


**Figure 6.26** Alteration of pore pressure measurements in consolidation tests

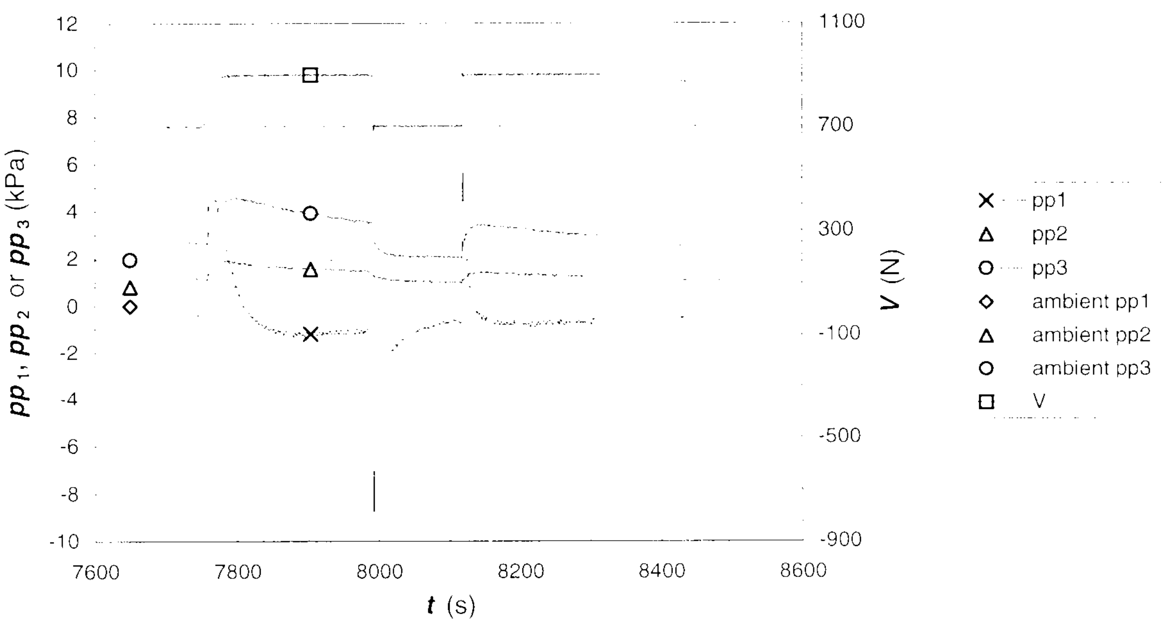


**Figure 6.27** Pore pressure measurements in footing and tank wall during consolidation tests of T319 (background logging only)

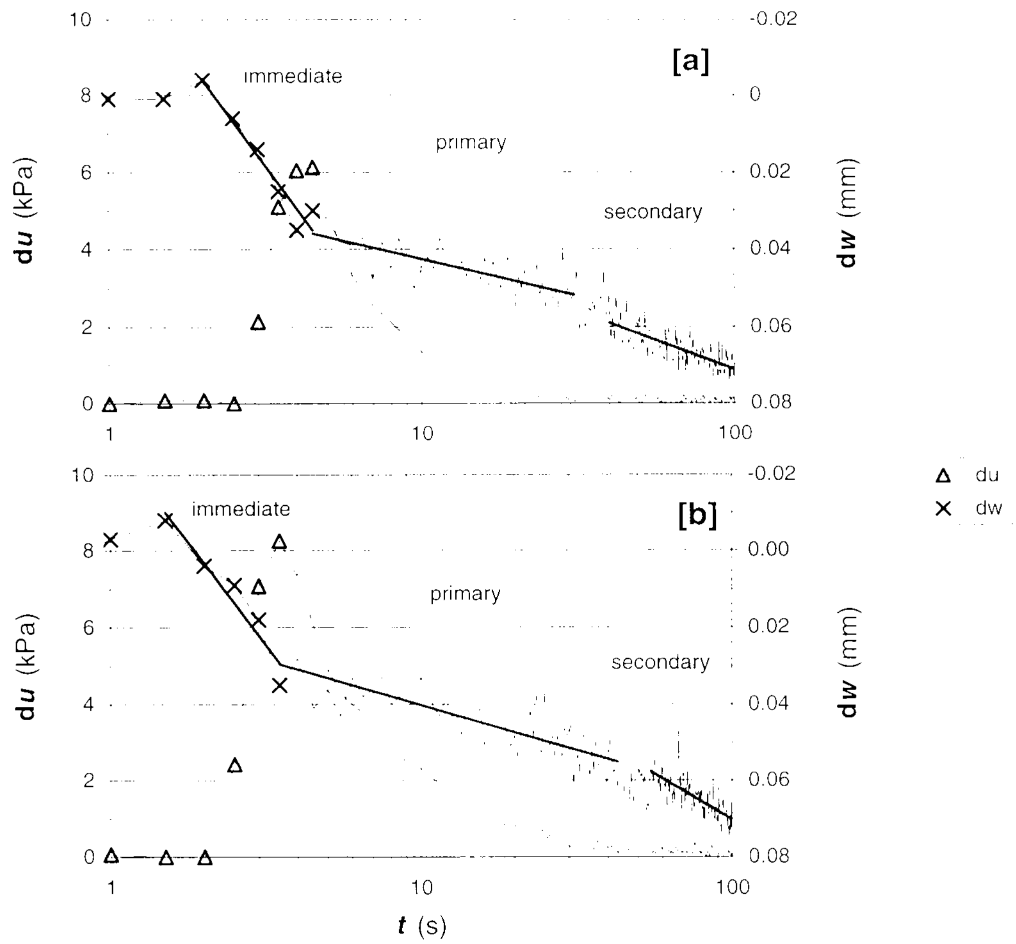


**Figure 6.28** The three stages of settlement in reloading consolidation tests: **[a]** test T118B_3; and **[b]** test T319B_3

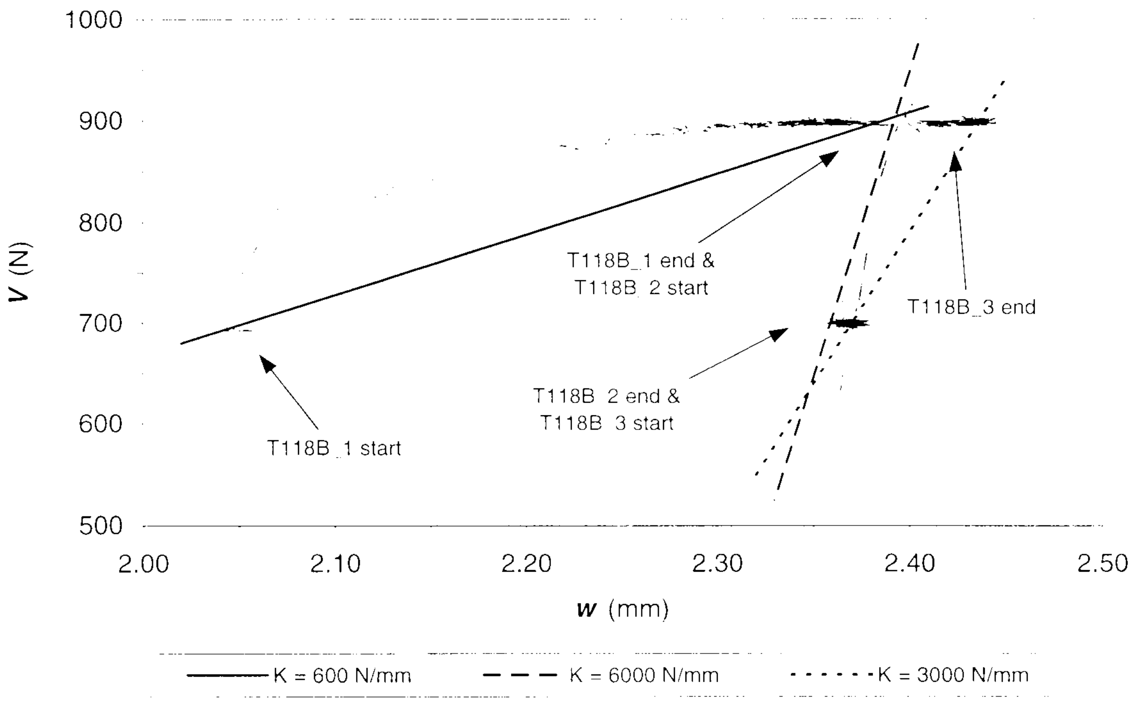


**Figure 6.29** Comparison of consolidation and drained load paths of test T118

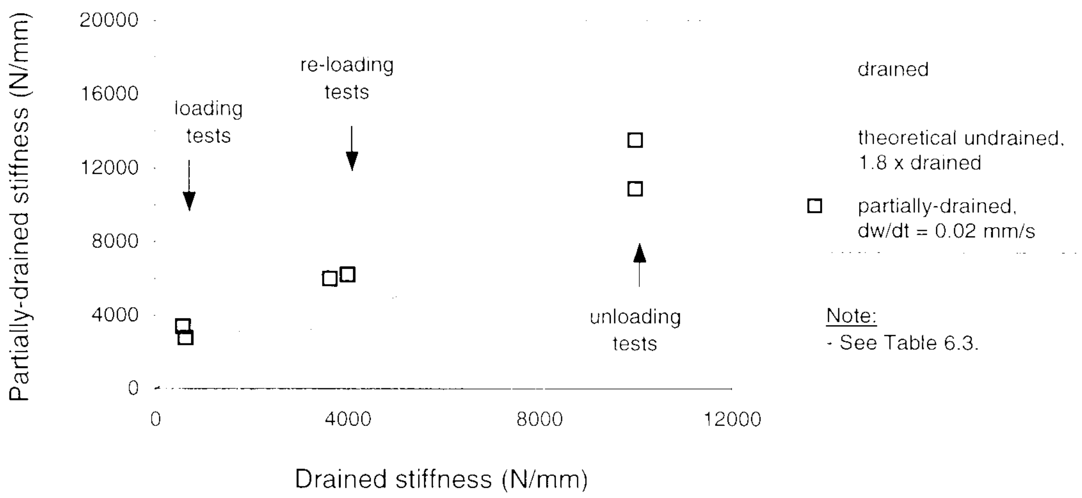


**Figure 6.30** Partially-drained (or immediate) vertical stiffness from the consolidation tests

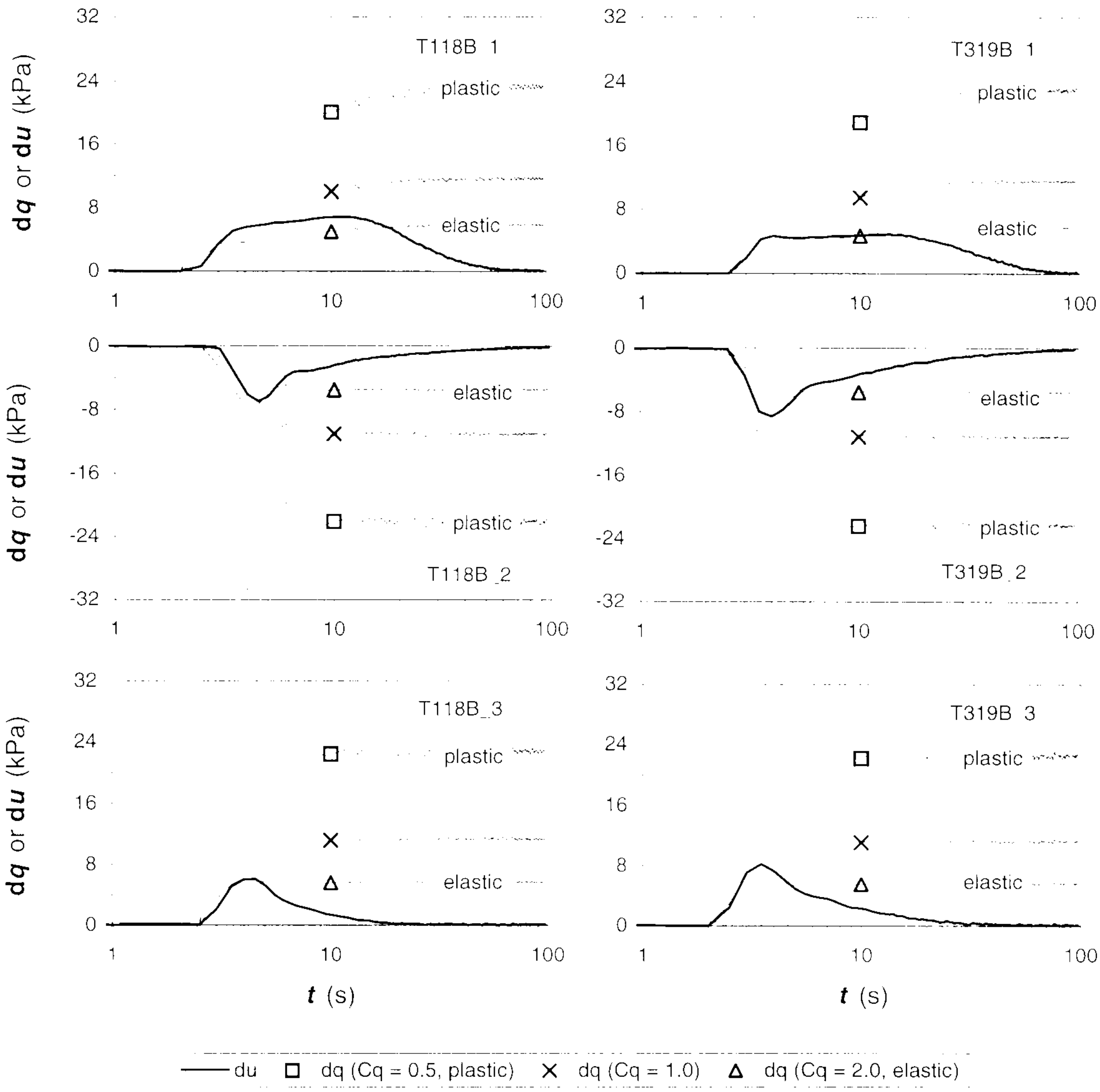


**Figure 6.31** Comparison of the measured pore pressure and the estimated total stress during the consolidation tests of T118 and T319
(at the centre of the footing for a range of total stress distributions)

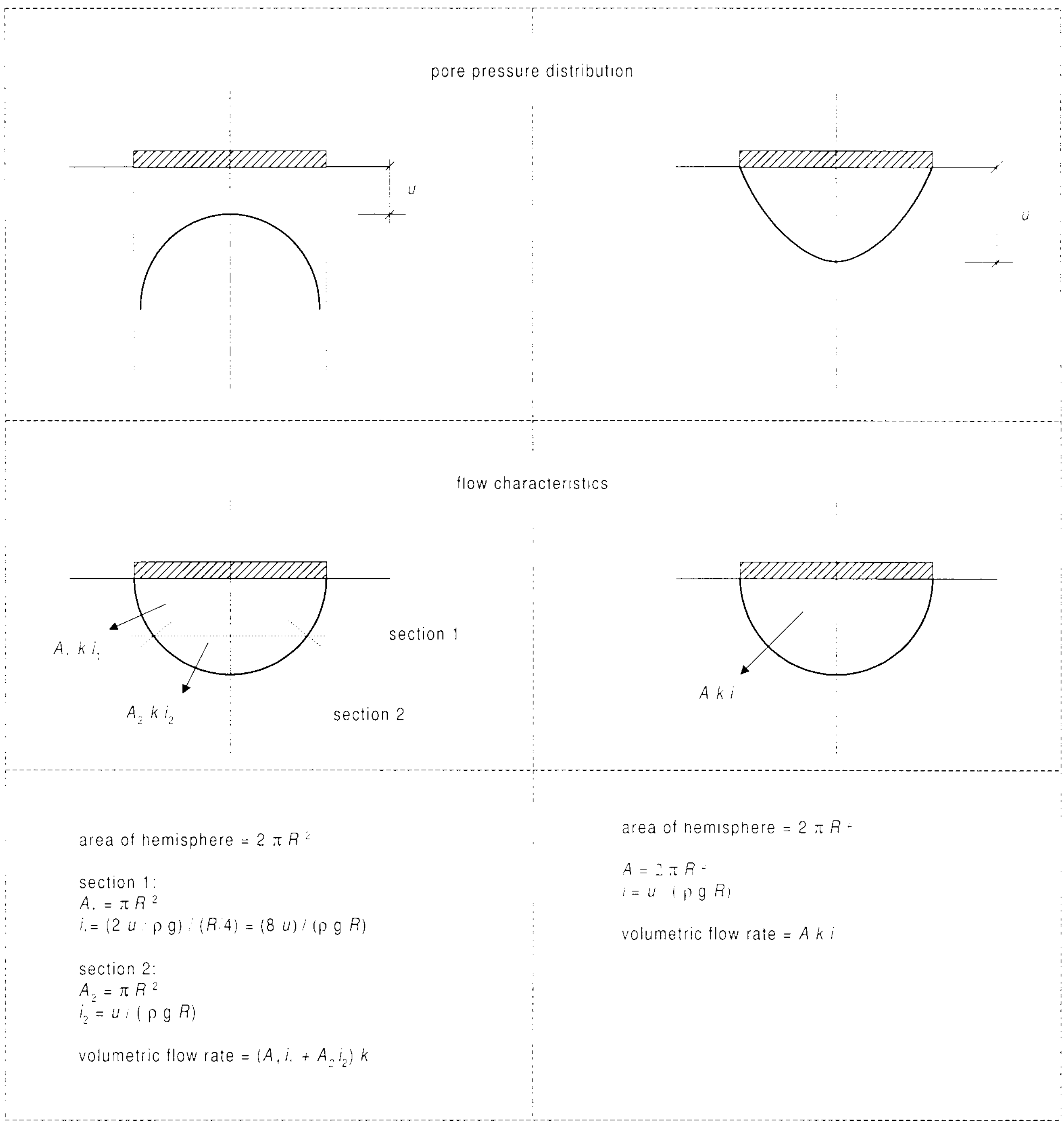


[a] [b]

**Figure 6.32** Definitions used in calculation of volumetric flow rate during consolidation: **[a]** immediate stage; and **[b]** primary stage

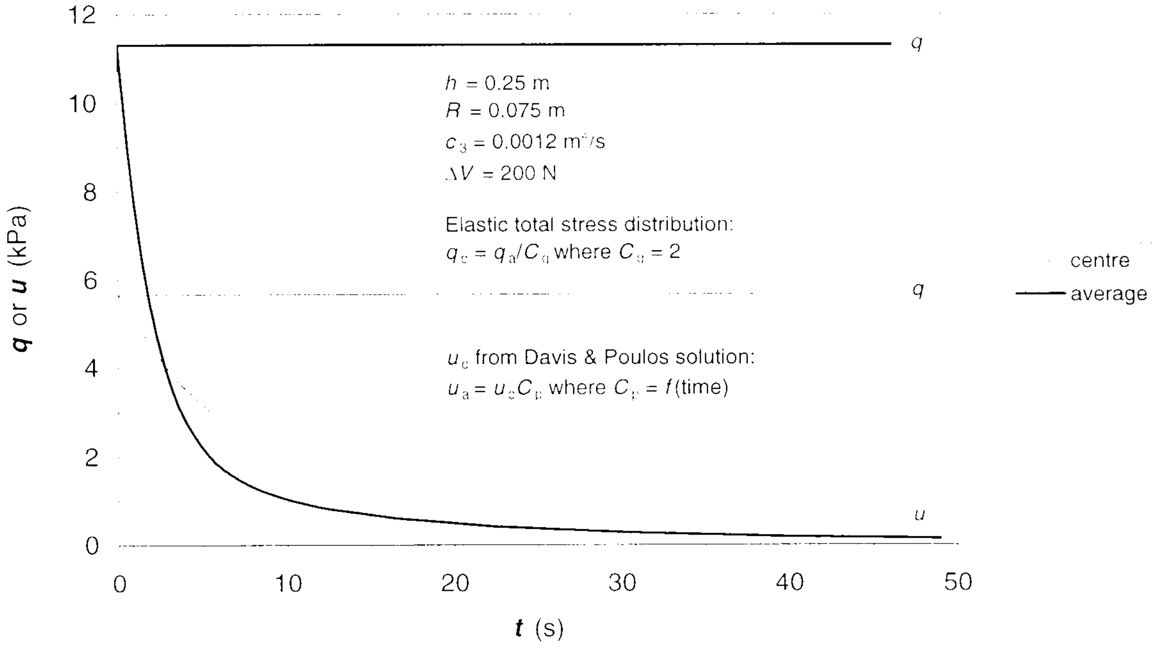


**Figure 6.33** Comparison of the pore pressure at the centre of a footing and the average pore pressure during consolidation

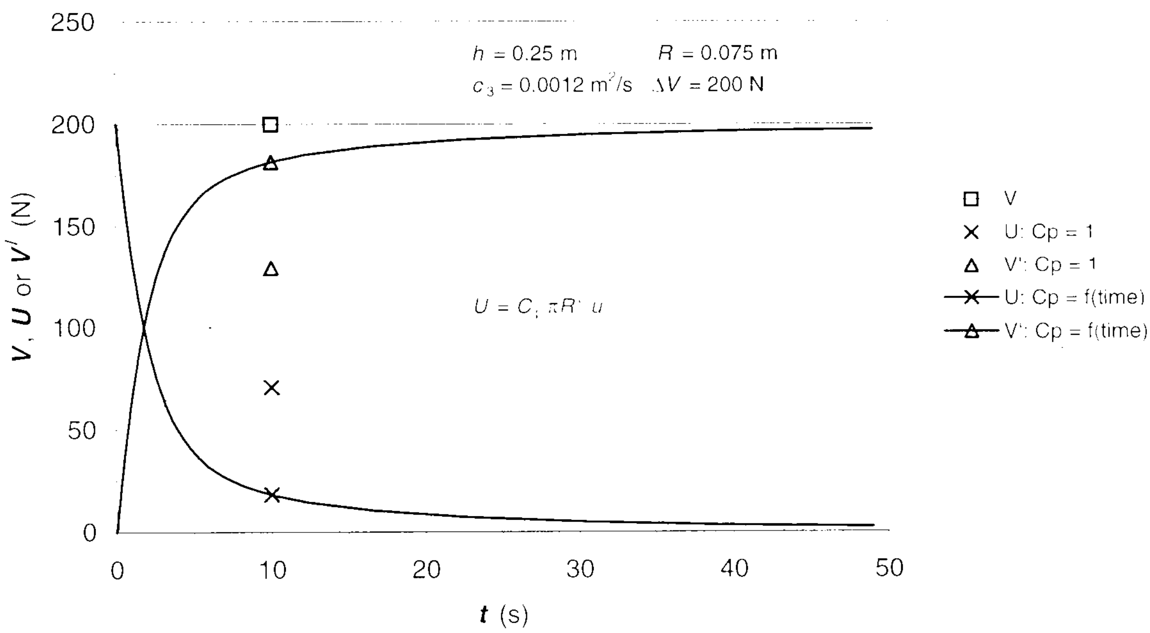


**Figure 6.34** Comparison of the effective load calculated assuming a uniform pore pressure distribution and a distribution that varies with dissipation

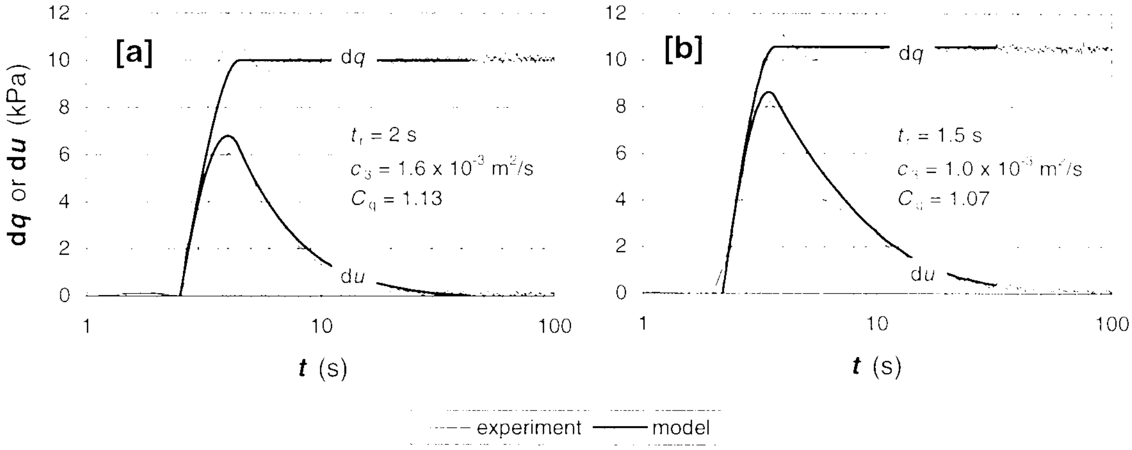


**Figure 6.35** Comparison of partially-drained consolidation model with tests: **[a]** with T118B_3; and **[b]** with T319B_3

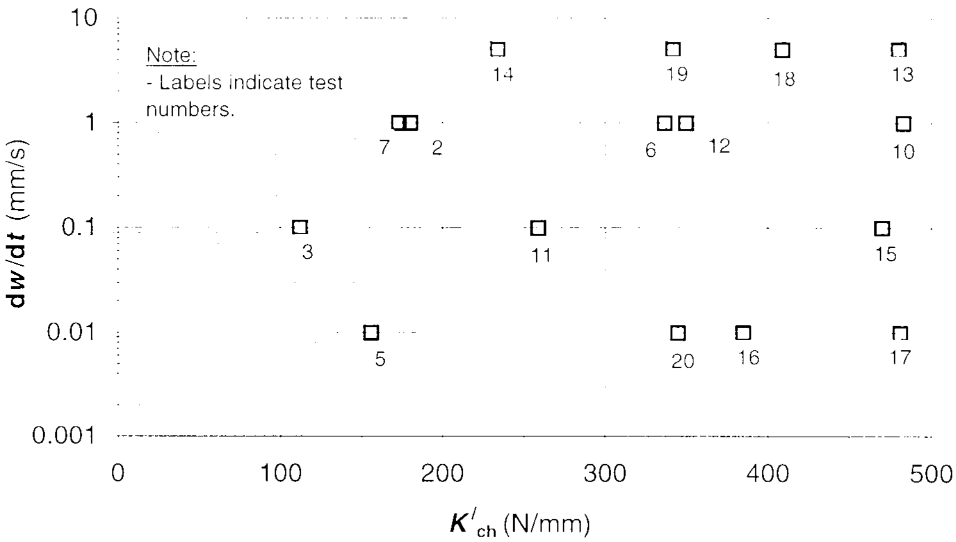


**Figure 6.36** Distribution of the displacement rate of the vertical partially-drained tests with the characterisation stiffness

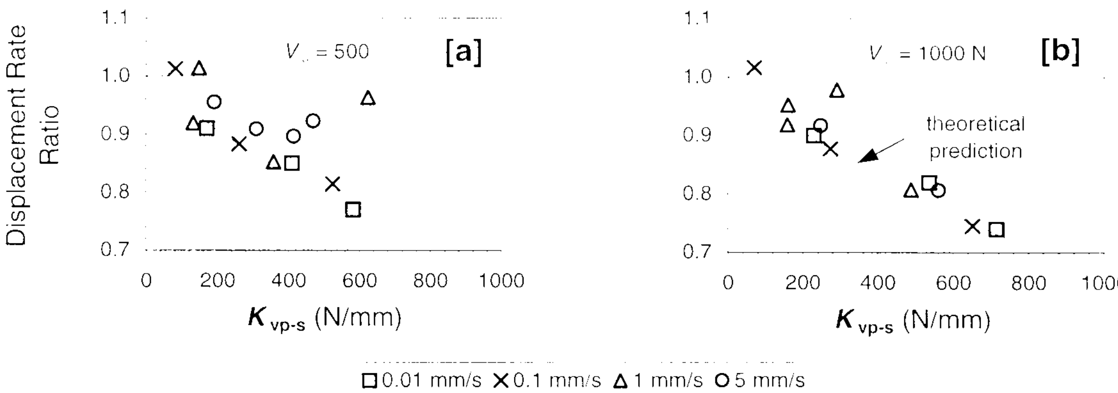


Note:
- Displacement ratio defined as measured displacement rate divided by intended displacement rate
- $K_{vp\text{-}s}$ was the stiffness of the secondary section of the partially-drained tests
- Theoretical prediction defined as $K_{rid}$ / ($K_{vp\text{-}s}$ + $K_{rid}$) where $K_{rid}$ was the rig stiffness measured between the stepper motor and the footing

**Figure 6.37** The variation of displacement rate ratio with stiffness from the vertical partially-drained tests: **[a]** tests from 500 N; and **[b]** tests from 1000 N

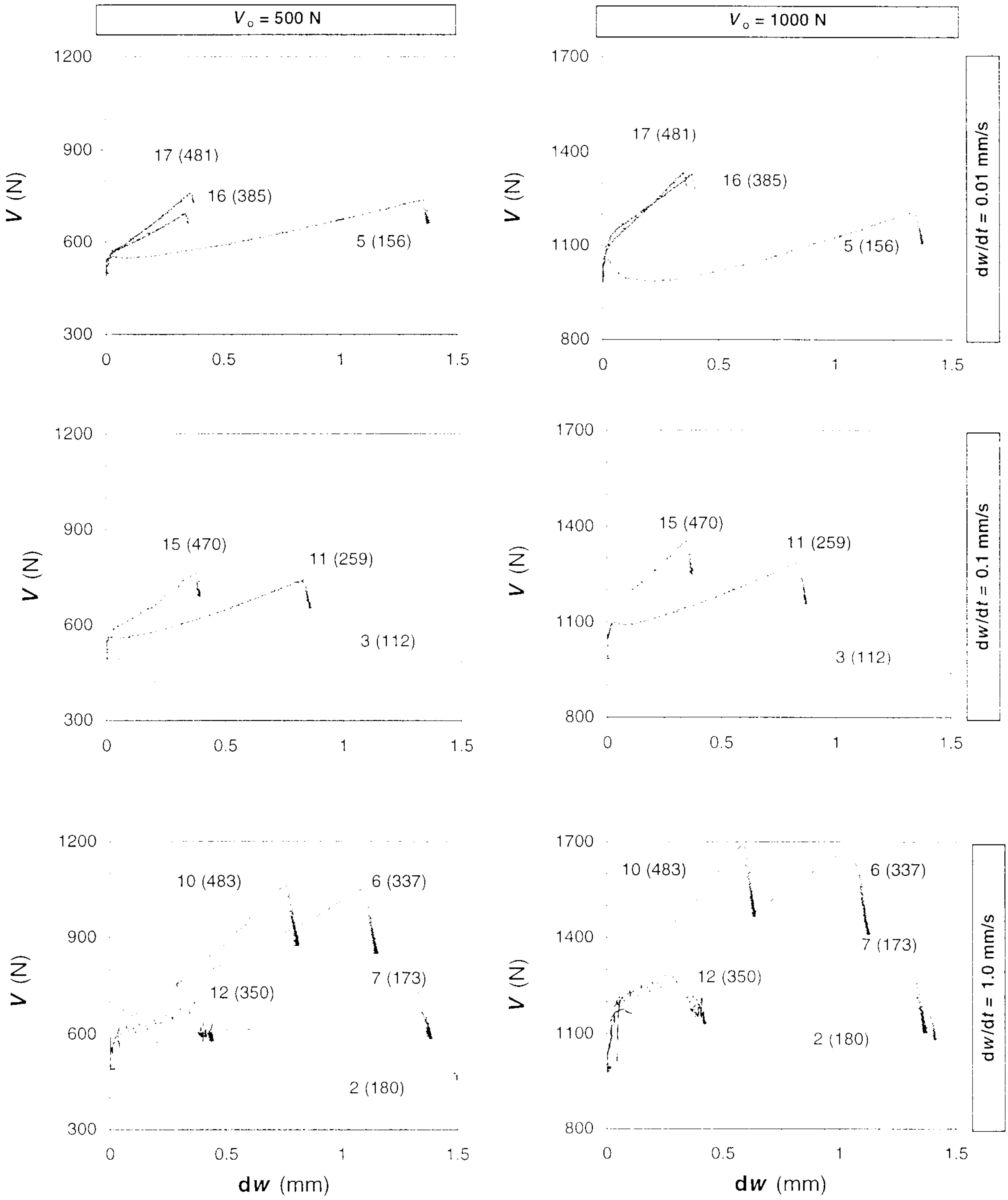


Note:
- Labels refer to the test number and the characterisation stiffness.

**Figure 6.38** Effect of characterisation stiffness on load:deformation response of the vertical partially-drained tests, at three different displacement rates

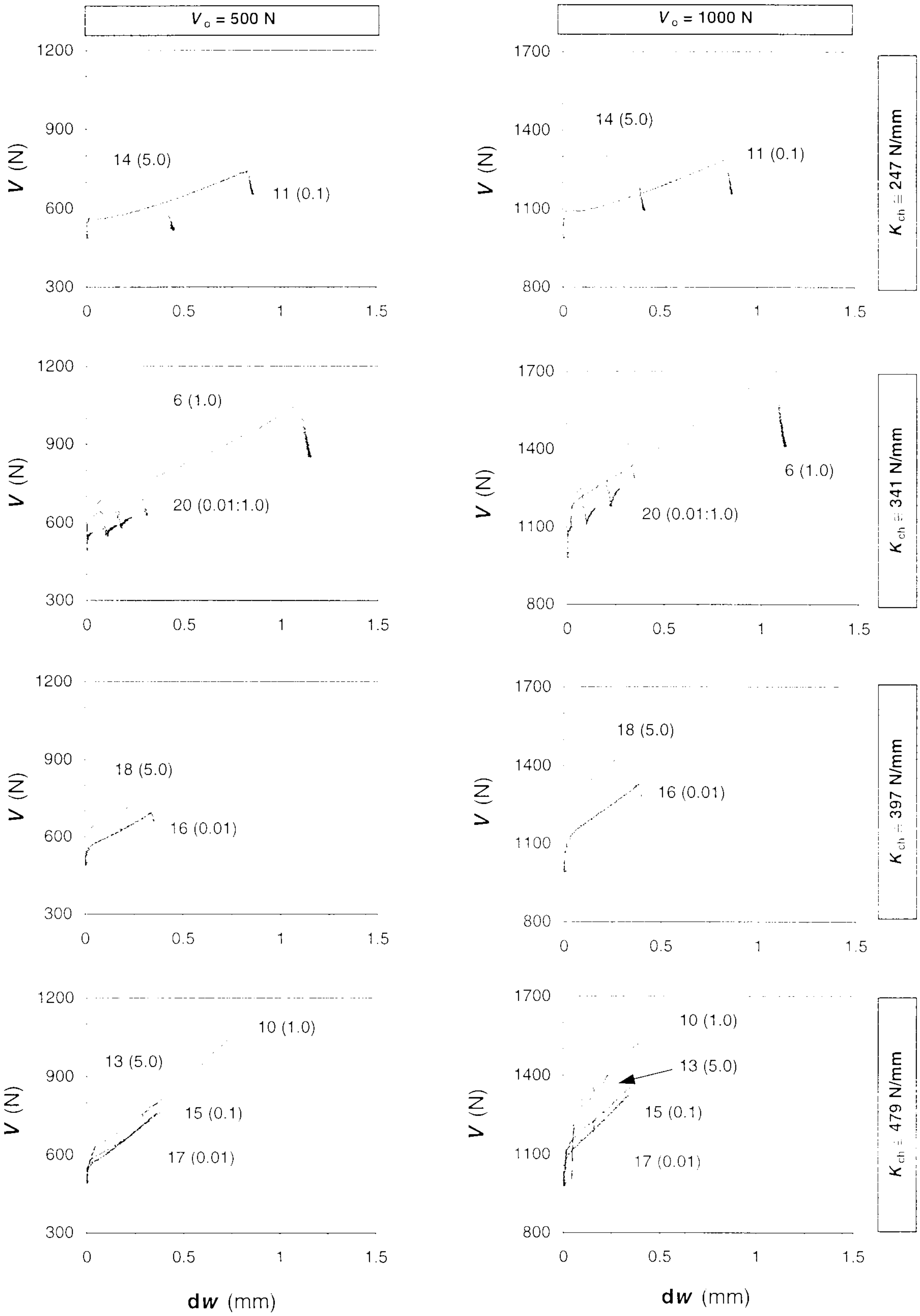


Note:
- Labels refer to the test number and vertical displacement rate.

**Figure 6.39** Effect of displacement rate on load:deformation response of vertical partially-drained tests, at four different values of characteristic stiffness

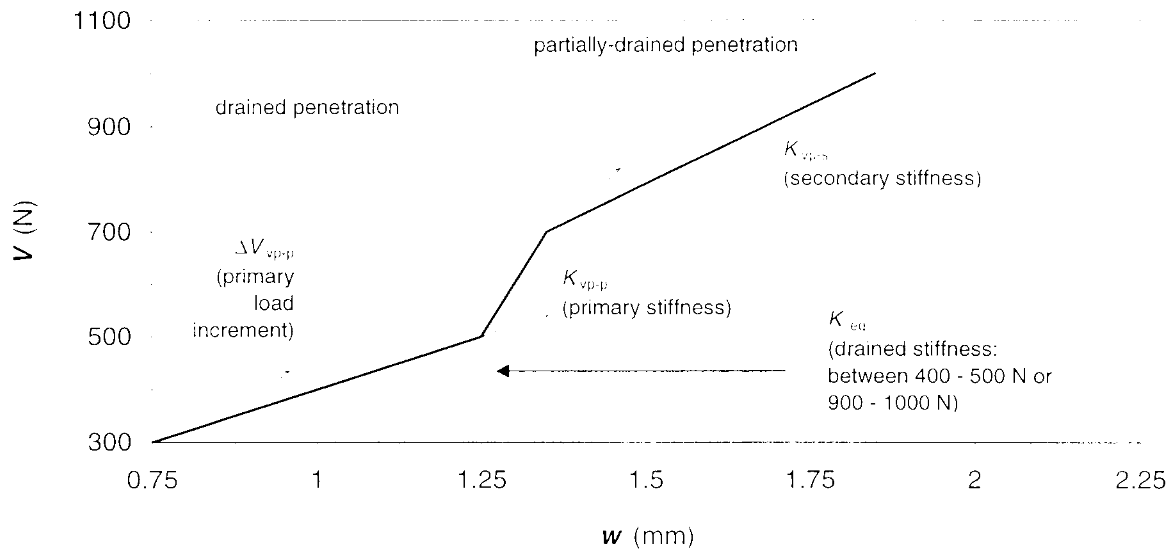


**Figure 6.40** Idealised load:deformation behaviour of vertical partially-drained tests

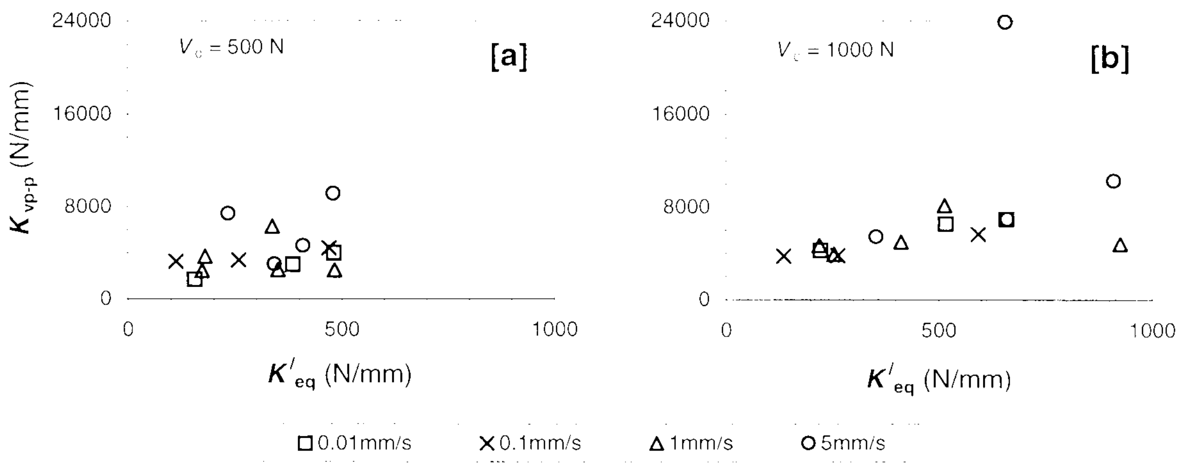


**Figure 6.41** The primary stiffness of the vertical partially-drained tests:
**[a]** from 500 N; and **[b]** from 1000 N

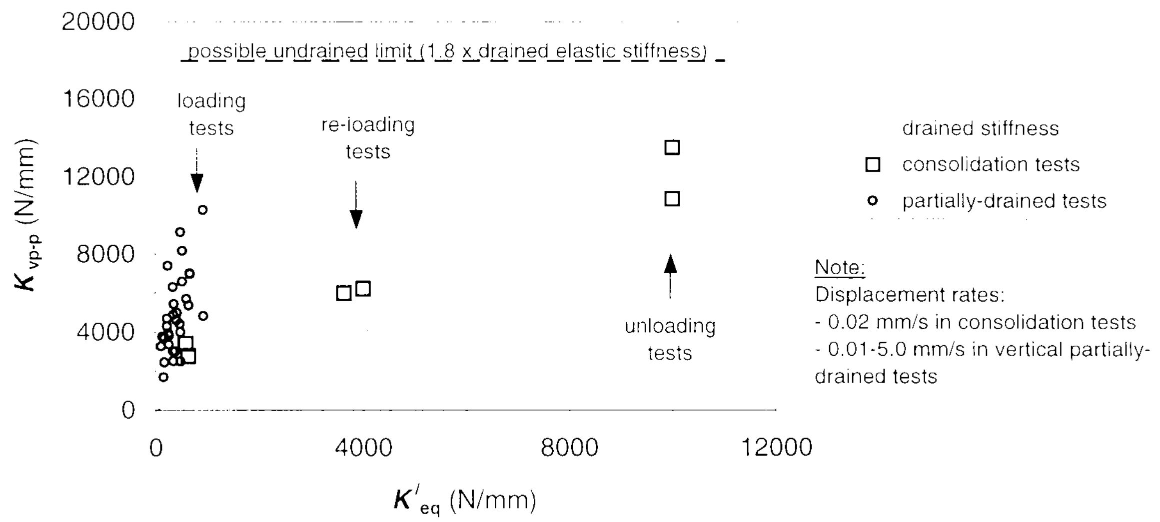


**Figure 6.42** Comparison of the partially-drained vertical stiffness from the consolidation tests and the vertical partially-drained tests

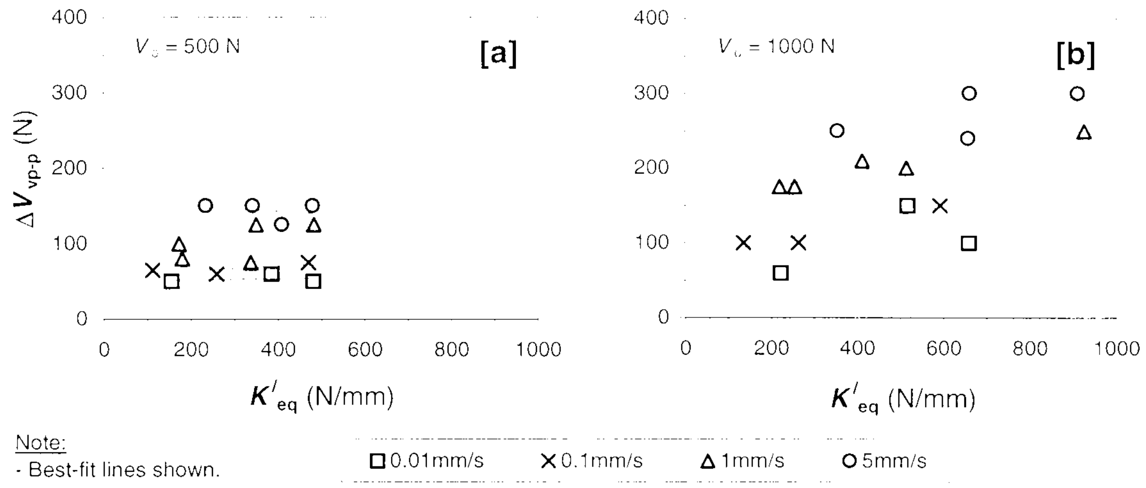


**Figure 6.43** The magnitude of the change in load over the primary section of the vertical partially-drained tests: **[a]** from 500 N; and **[b]** from 1000 N

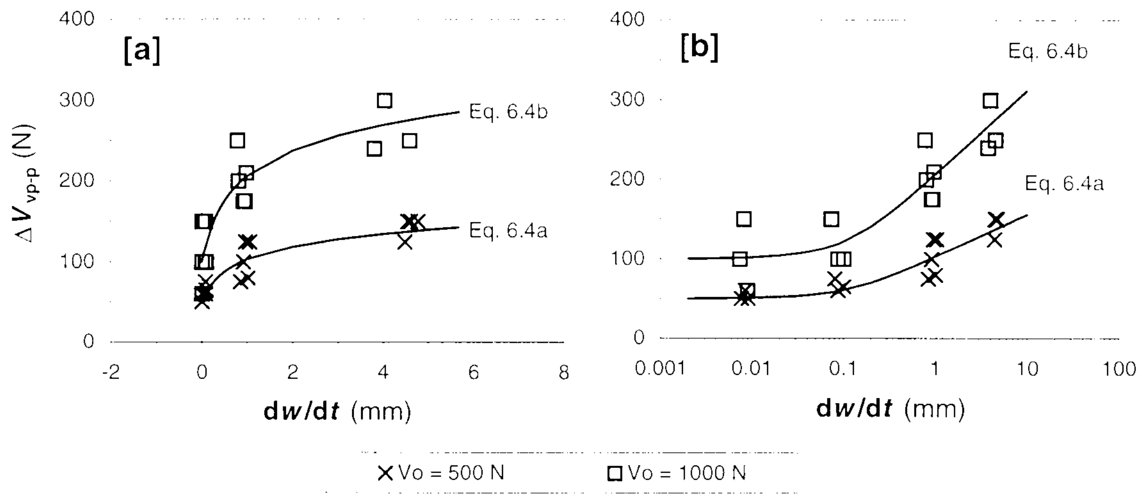


**Figure 6.44** The measured load increment during the primary stage of the vertical partially-drained tests versus the measured displacement rate: **[a]** normal $x$-axis; and **[b]** logarithmic $x$-axis

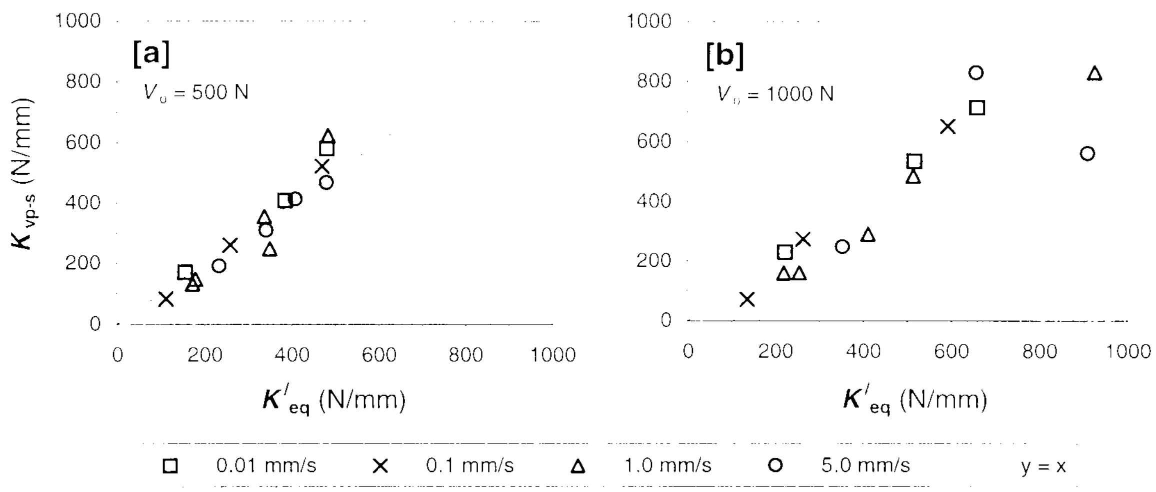


**Figure 6.45** The secondary stiffness of the vertical partially-drained tests: **[a]** from 500 N; and **[b]** from 1000 N

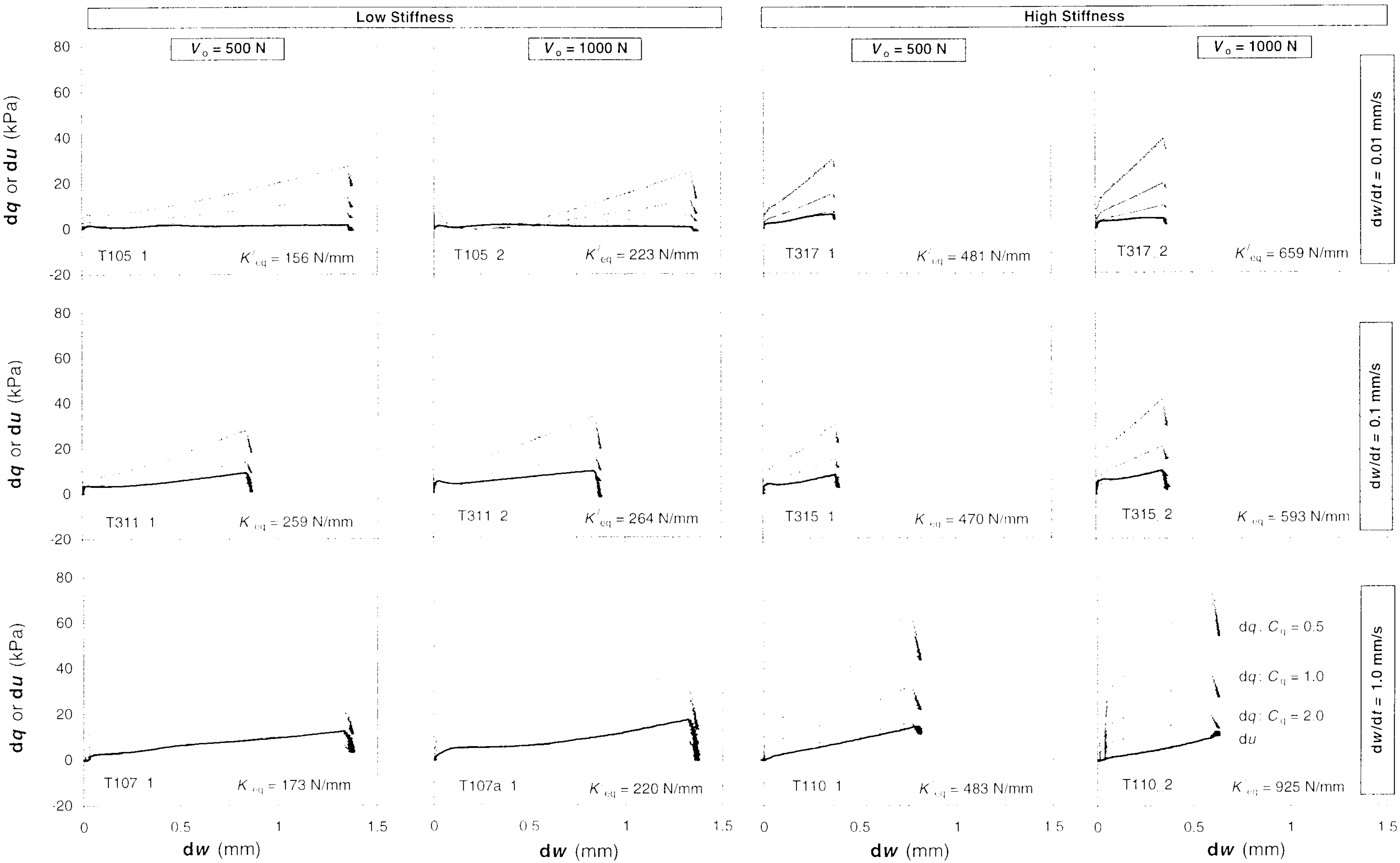


**Figure 6.46** Pore pressure response compared with total stress response at centre of footing (total stress for $C_q$ values of 2.0, 1.0 and 0.5)

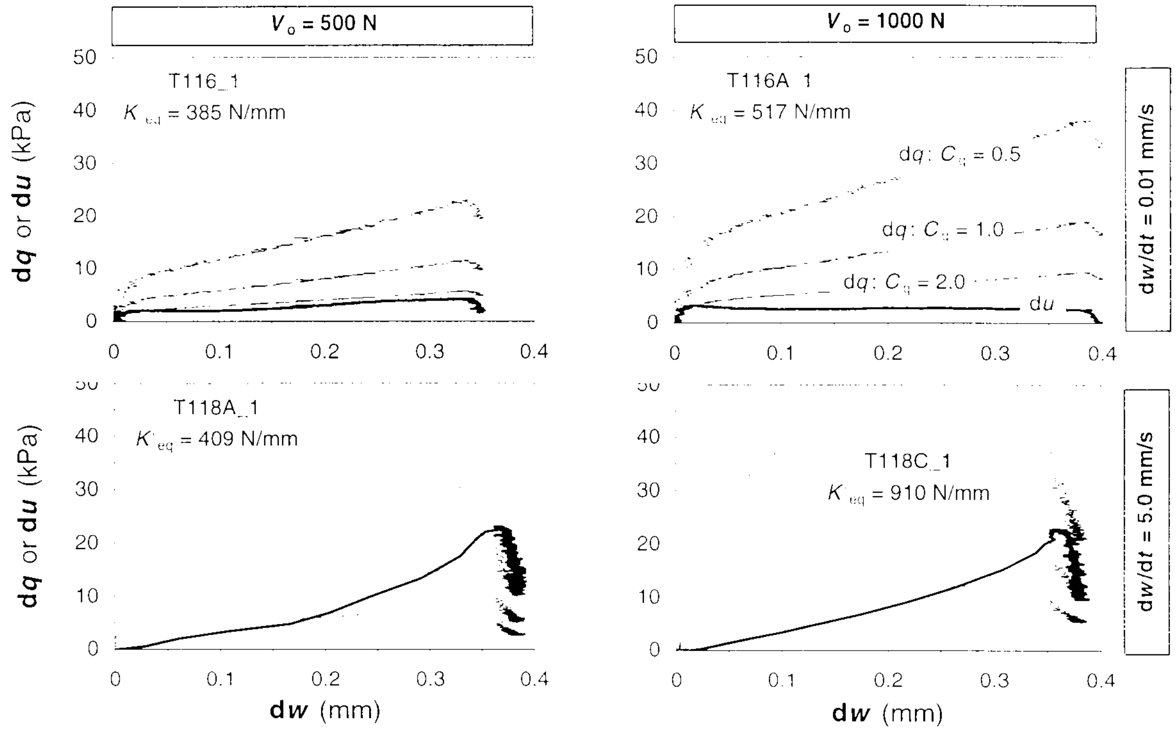


**Figure 6.47** Effect of a change in the displacement rate on the pore pressure response, in vertical partially-drained tests with similar sample stiffnesses (estimated total stress at the centre of the footing for $C_q$ values of 2.0, 1.0 and 0.5)

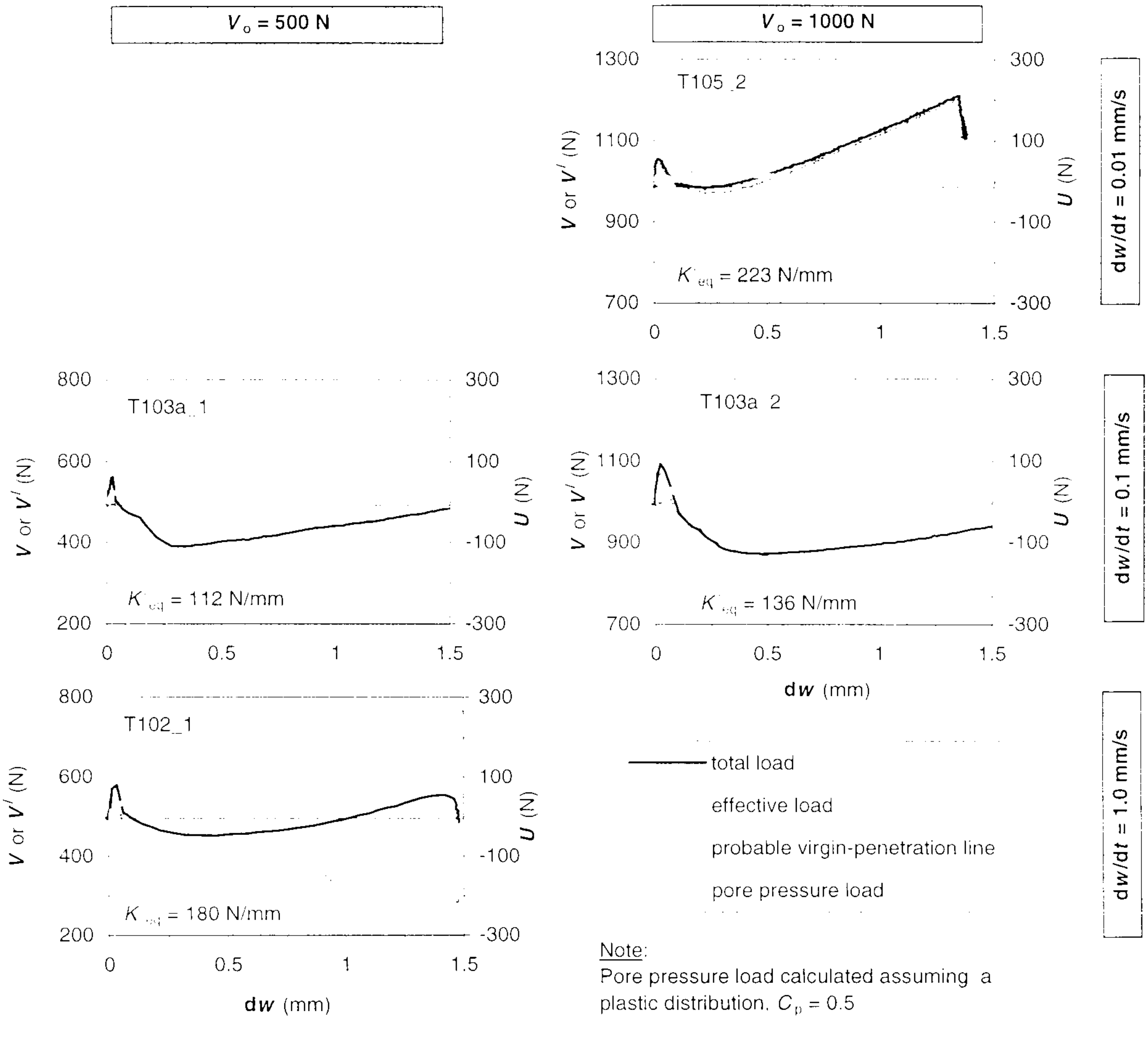


**Figure 6.48** Load:deformation behaviour of vertical partially-drained tests that exhibited evidence of liquefaction

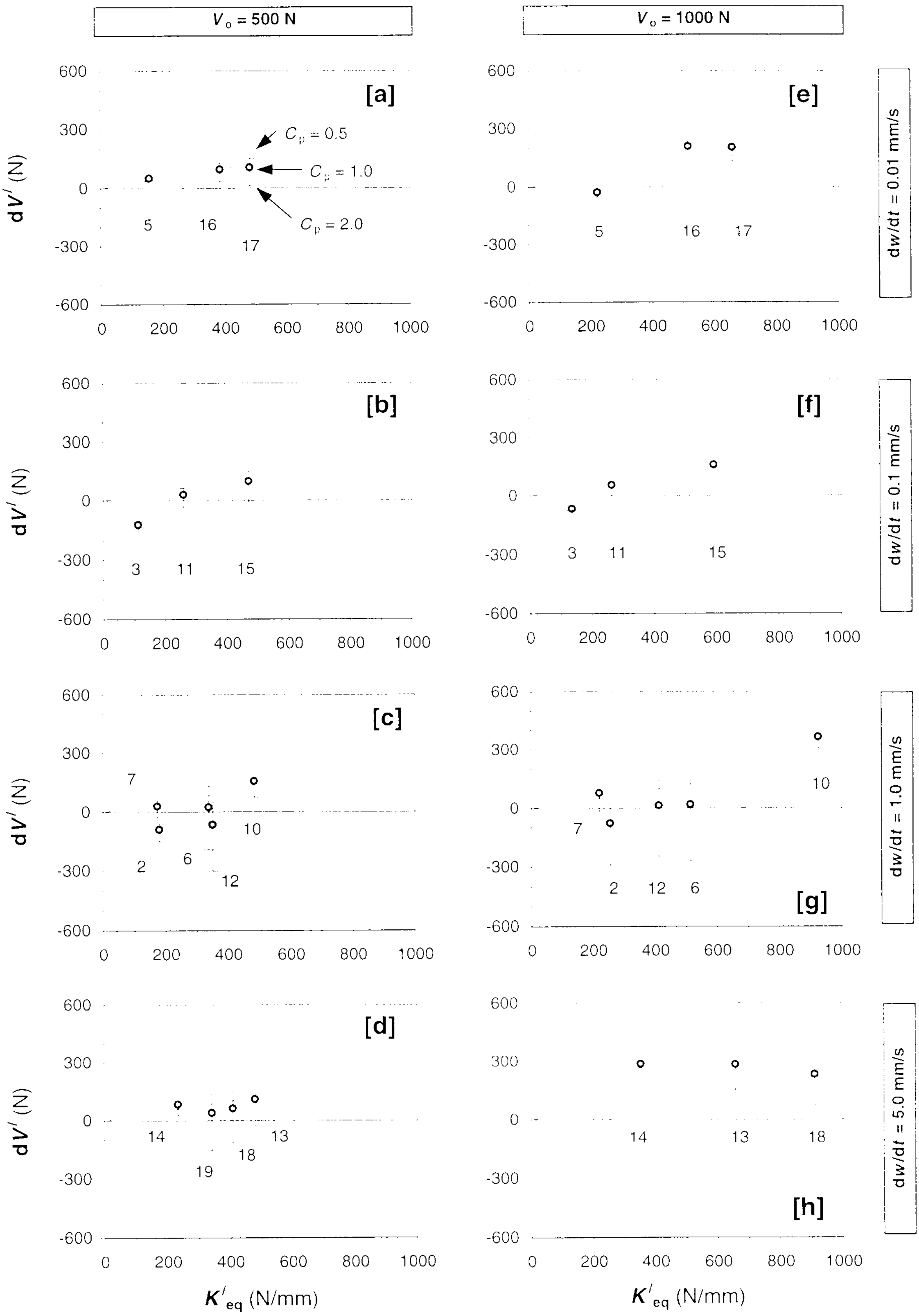


Note:
- The values of d$V$ were calculated for d$w$ approximately equal to 0.24 mm. The maximum and minimum values of d$w$ were 0.194 mm and 0.252 mm, and the standard deviation was 0.0147 mm.
- The dotted lines indicate the value of d$V$ for 0.24 mm of penetration at the equivalent effective stiffness.

**Figure 6.49** The range of possible values of the change in effective load in the vertical partially drained tests

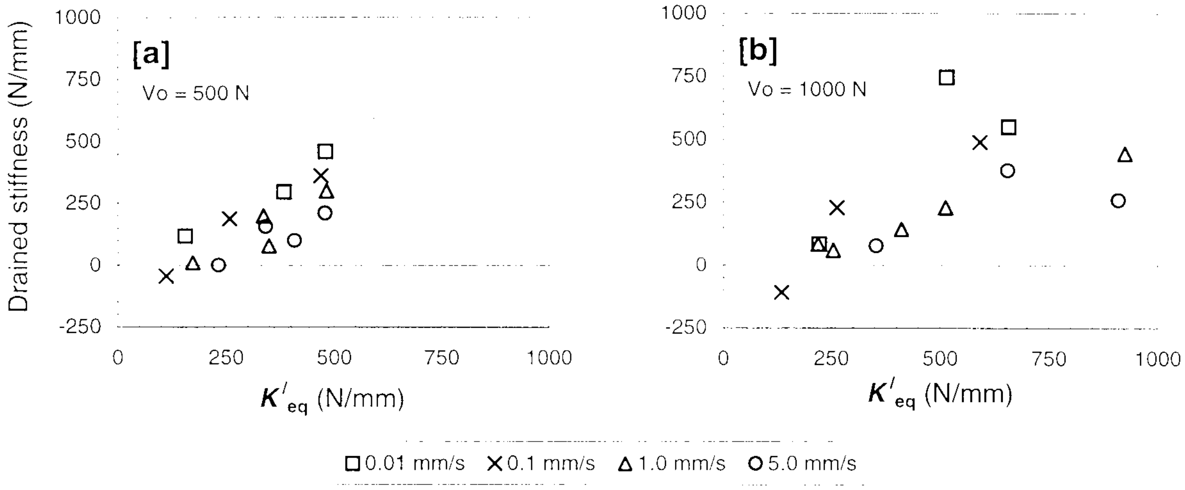


Notes:
- Drained stiffness measured from start of move to point after end of move at which the excess pore pressures were zero

**Figure 6.50** The overall drained stiffness of the vertical partially-drained tests: **[a]** from $V$ = 500 N; and **[b]** from $V$ = 1000 N

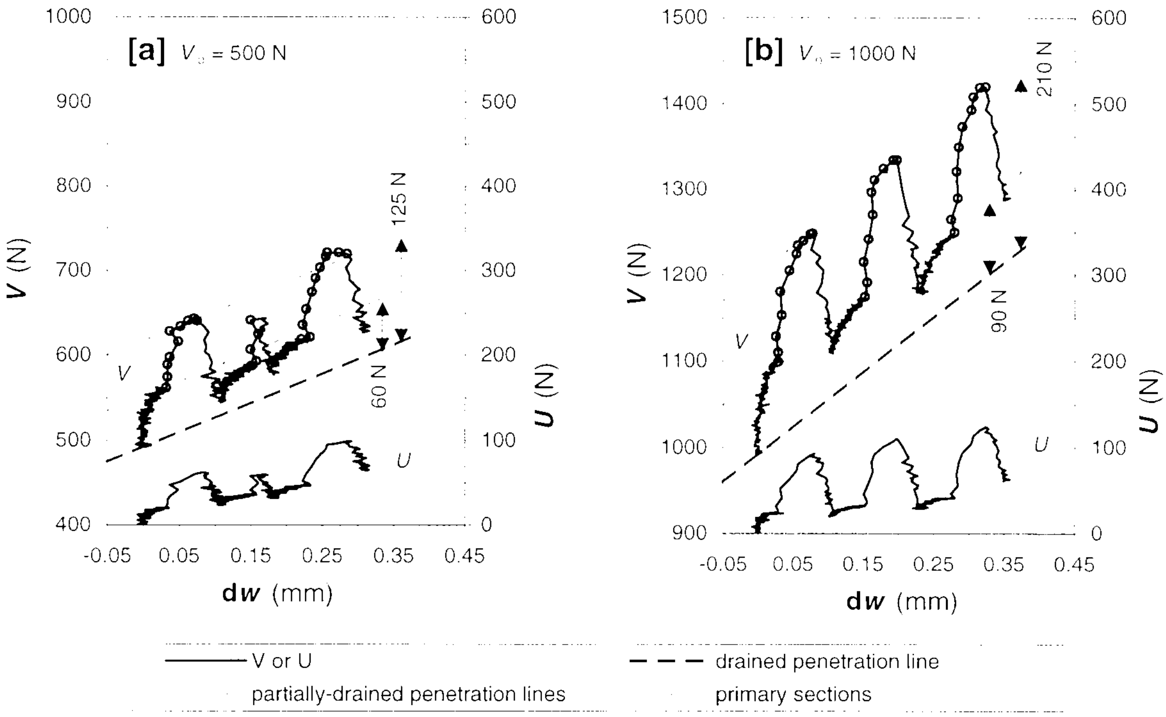


Note:
- Drained rate = 0.001 mm/s.
- Partially-drained rates = 0.01/1.00 mm/s.
- Drained stiffness equal to 350 N/mm at 500N and equal to 640 N/mm at 1000 N.

**Figure 6.51** The multi-rate vertical tests in T120: **[a]** from 500 N; and **[b]** from 1000 N

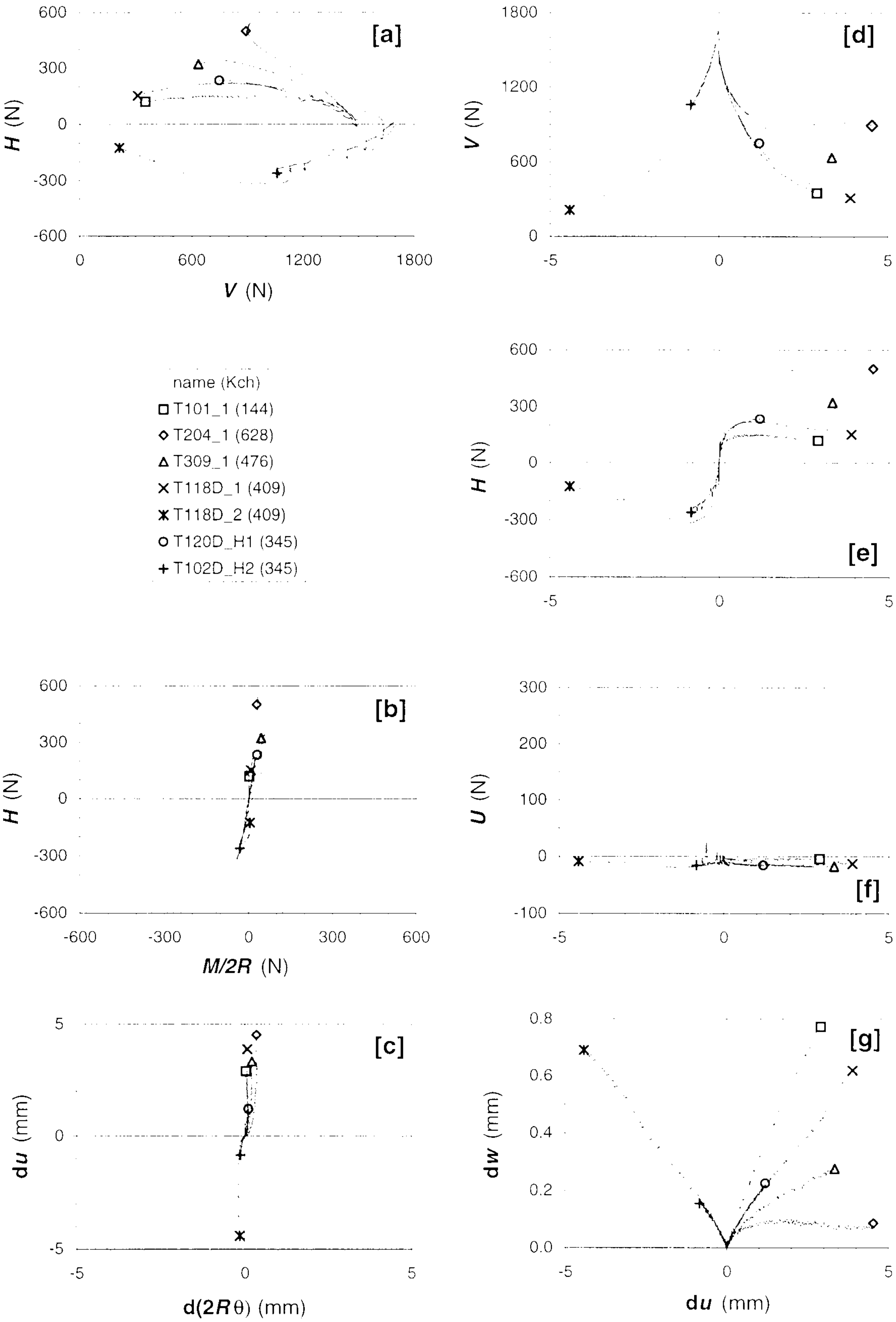


**Figure 7.1** Load and displacement interaction diagrams of the drained horizontal sideswipe tests (intended $du/dt$ = 0.001 mm/s)

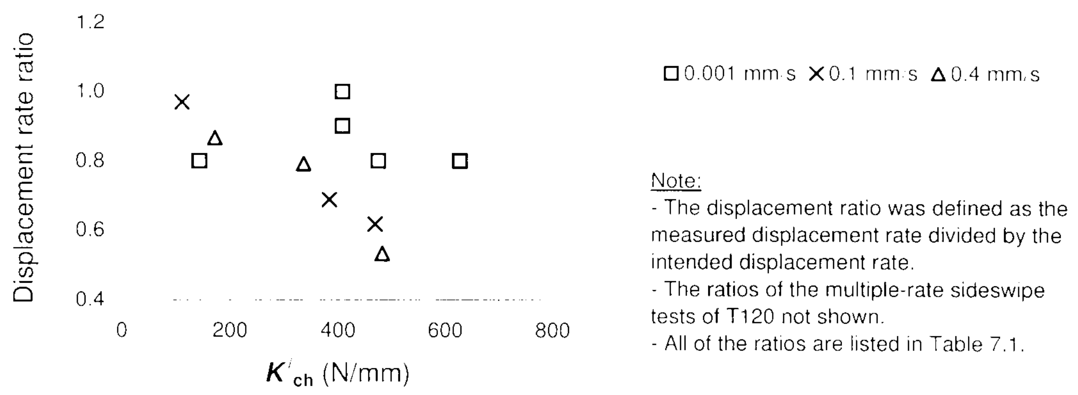


**Figure 7.2** The variation of the displacement rate ratio of the horizontal sideswipe tests with the characterisation stiffness

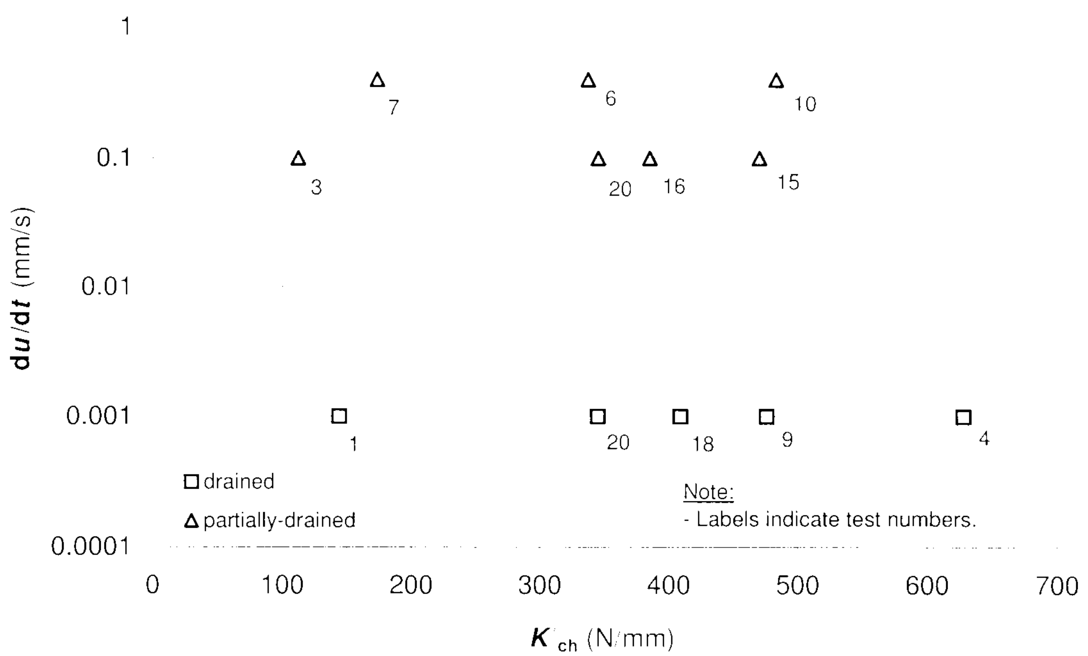


**Figure 7.3** Distribution of the displacement rate of the horizontal sideswipe tests with the characterisation stiffness

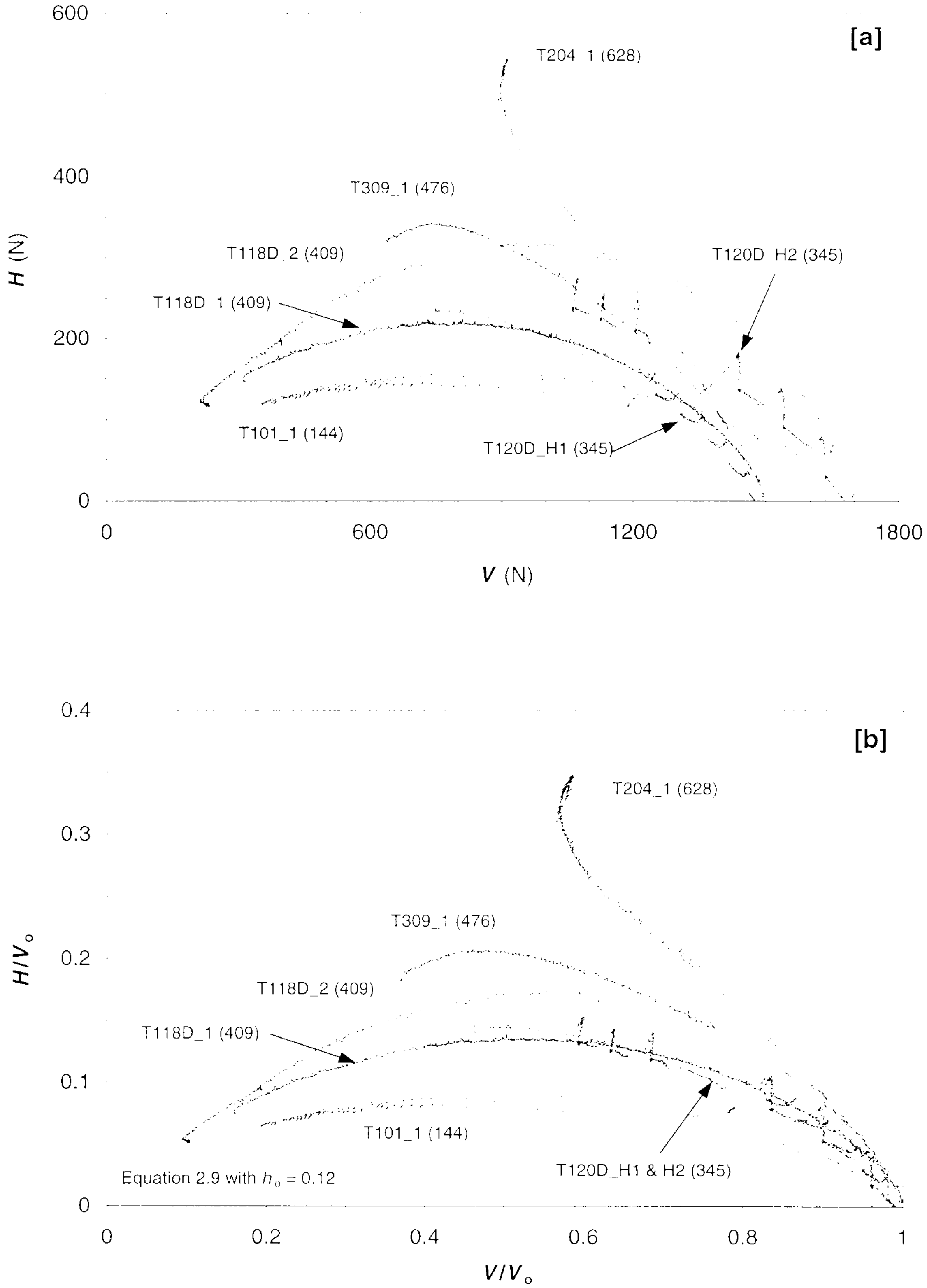


Note:

- Labels give test number and characterisation stiffness (in brackets).
- Tests T118D_2 and T120D_H2 were displaced in the negative horizontal direction.

**Figure 7.4** Drained horizontal sideswipe tests:
**[a]** in $V{:}H$ space; and **[b]** normalised by $V_o$

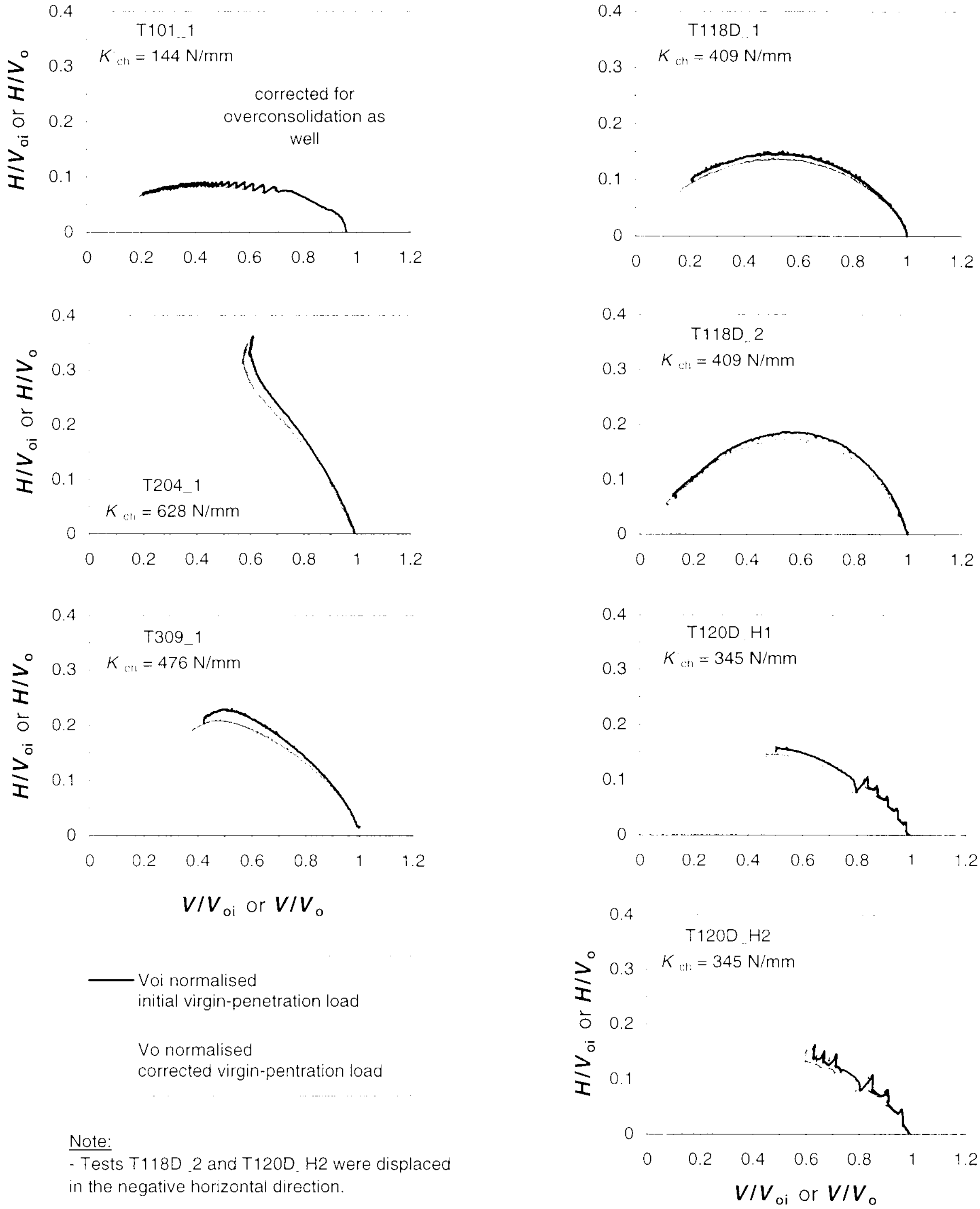


**Figure 7.5** Correction for vertical penetration of the drained horizontal sideswipe tests

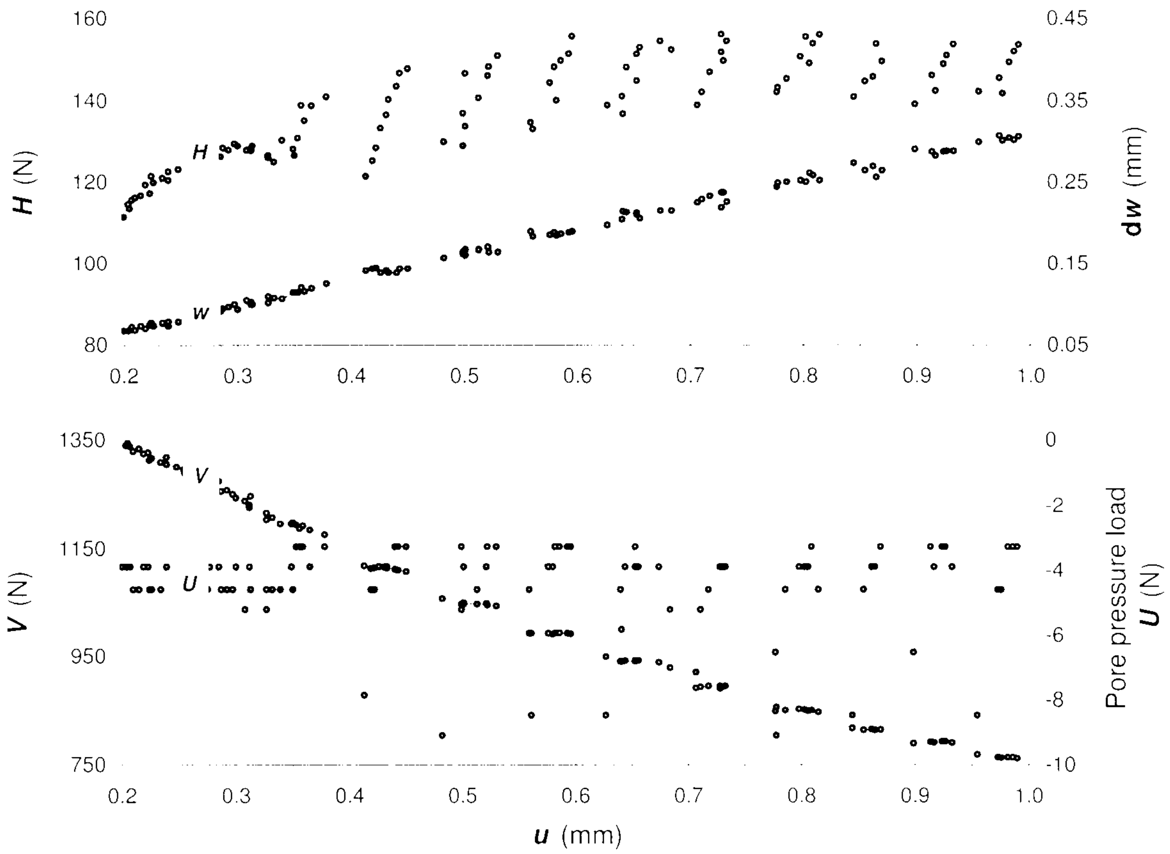


**Figure 7.6** Detail of the saw-tooth shaped sideswipe of test T101

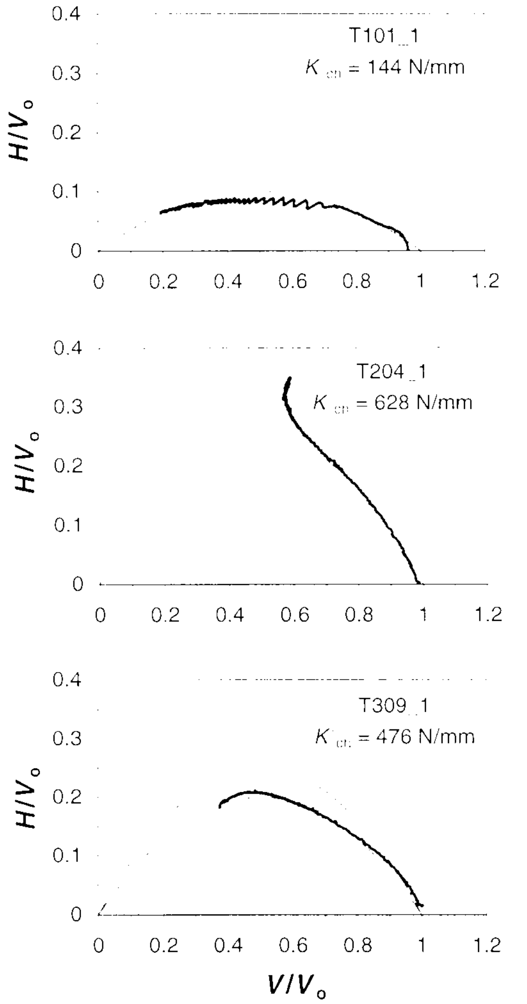


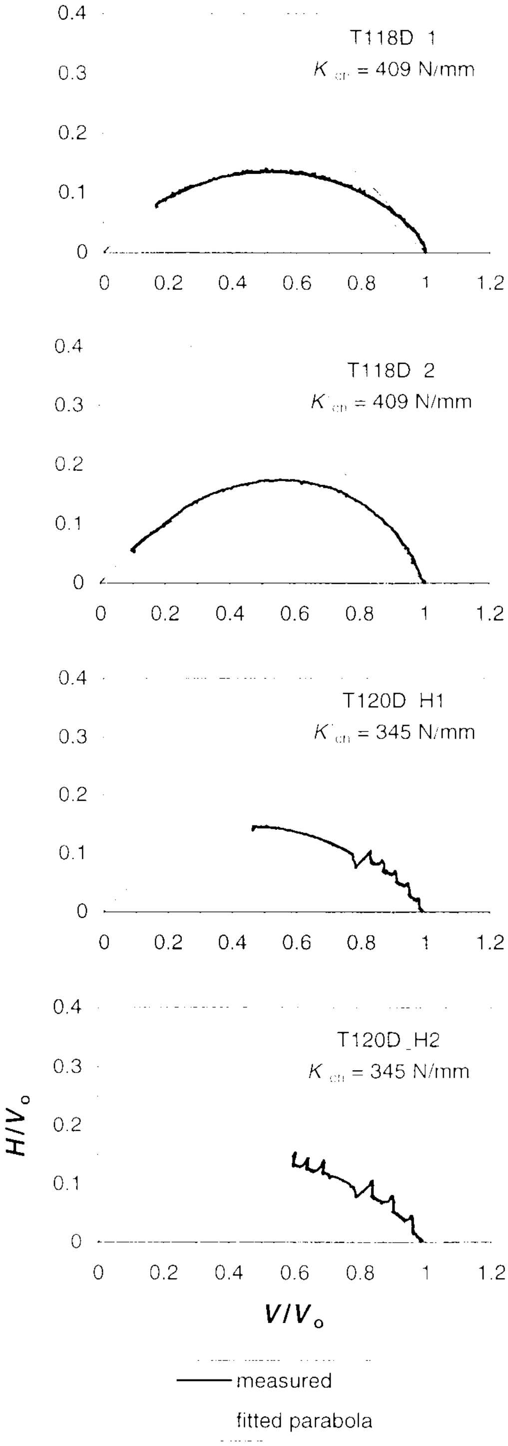


| Test | Position | $V_o$ | $V_o/V_m$ | $h_o$ |
|---|---|---|---|---|
| T101_1 | start | 1700 | 0.68 | 0.100 |
| | end | 1827 | 0.73 | |
| T204_1 | start | 1500 | 0.15 | 0.250 |
| | end | 1580 | 0.16 | |
| T309_1 | start | 1495 | 0.19 | 0.250 |
| | end | 1707 | 0.22 | 0.200 |
| T118D_1 | start | 1495 | 0.20 | 0.200 |
| | end | 1955 | 0.26 | 0.135 |
| T118D_2 | start | 1700 | 0.23 | 0.250 |
| | end | 2250 | 0.30 | 0.150 |
| T120D_H1 | start | 1489 | 0.23 | 0.145 |
| | end | 1623 | 0.25 | |
| T120D_H2 | start | 1693 | 0.26 | 0.140 |
| | end | 1790 | 0.28 | |

Note:
- Tests T118D_2 and T120D_H2 were displaced in the negative horizontal direction.

**Figure 7.7** Drained horizontal sideswipe tests and fitted parabolas

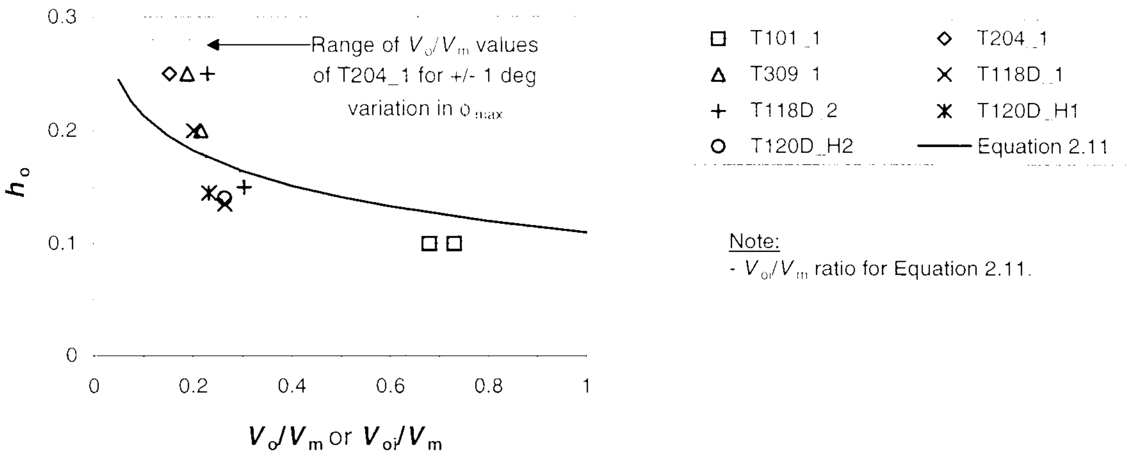


**Figure 7.8** Relationship between normalised peak horizontal load and $V_o/V_m$ ratio

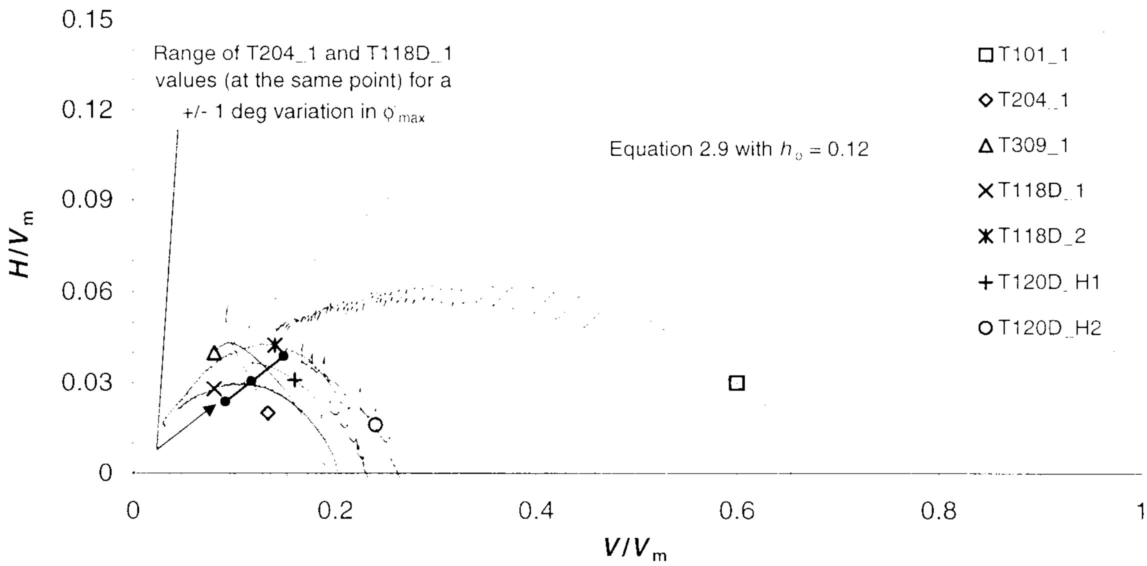


**Figure 7.9** Drained horizontal sideswipe tests normalised by estimated values of $V_m$

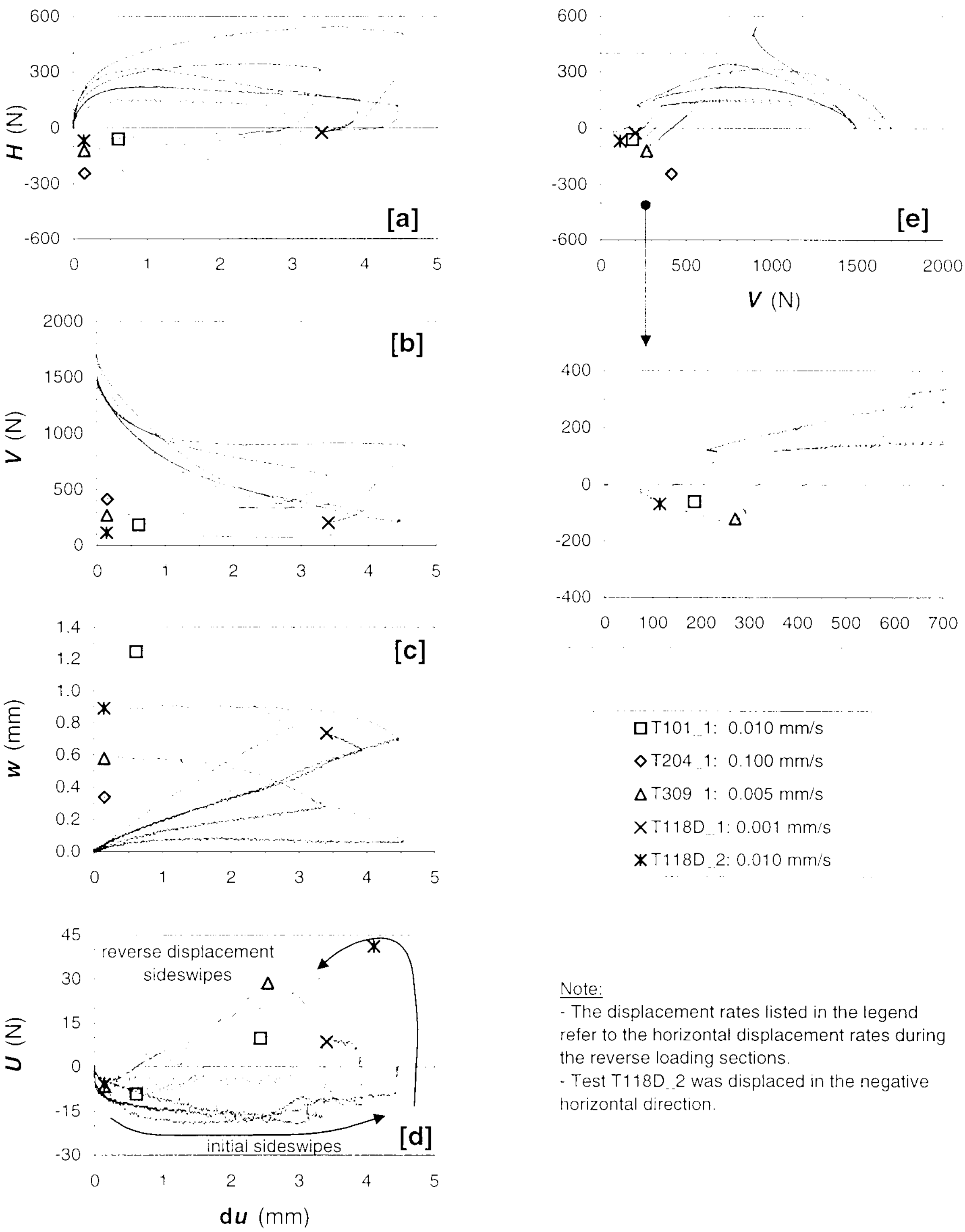


Note:
- The displacement rates listed in the legend refer to the horizontal displacement rates during the reverse loading sections.
- Test T118D_2 was displaced in the negative horizontal direction.

**Figure 7.10** The reverse displacement sections associated with the drained horizontal sideswipe tests

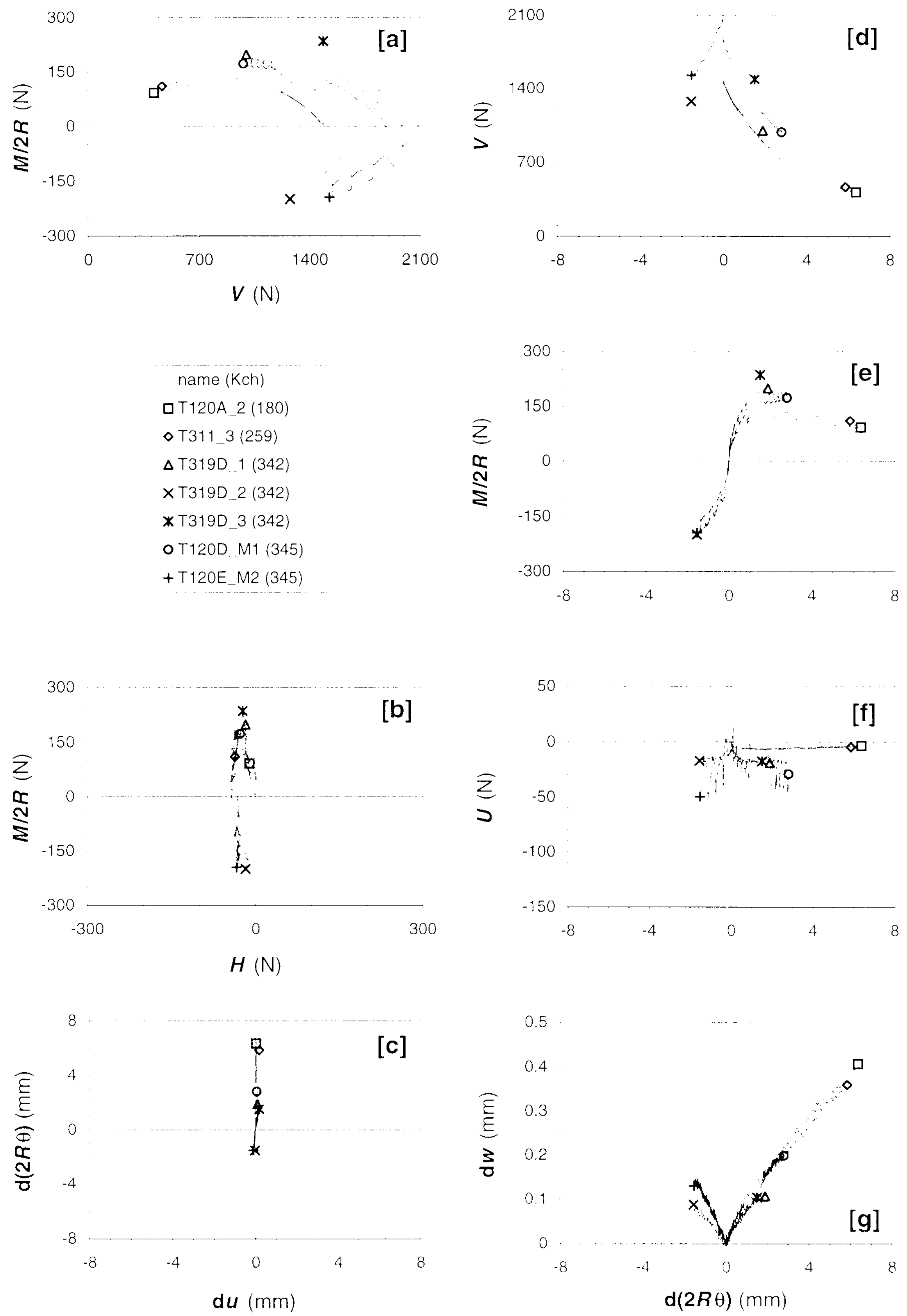


**Figure 7.11** Load and displacement interaction diagrams of the drained moment sideswipe tests (intended $d(2R\theta)/dt = 0.0026$ mm/s)

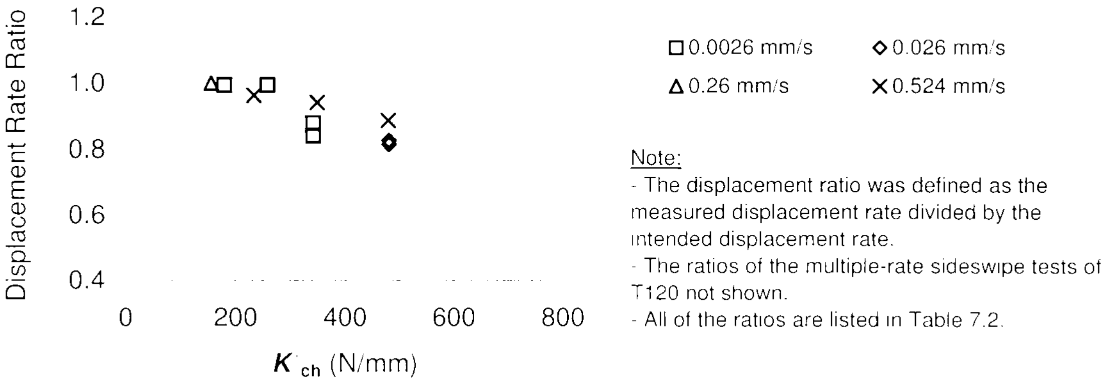


**Figure 7.12** The variation of the displacement rate ratio of the moment sideswipe tests with the characterisation stiffness

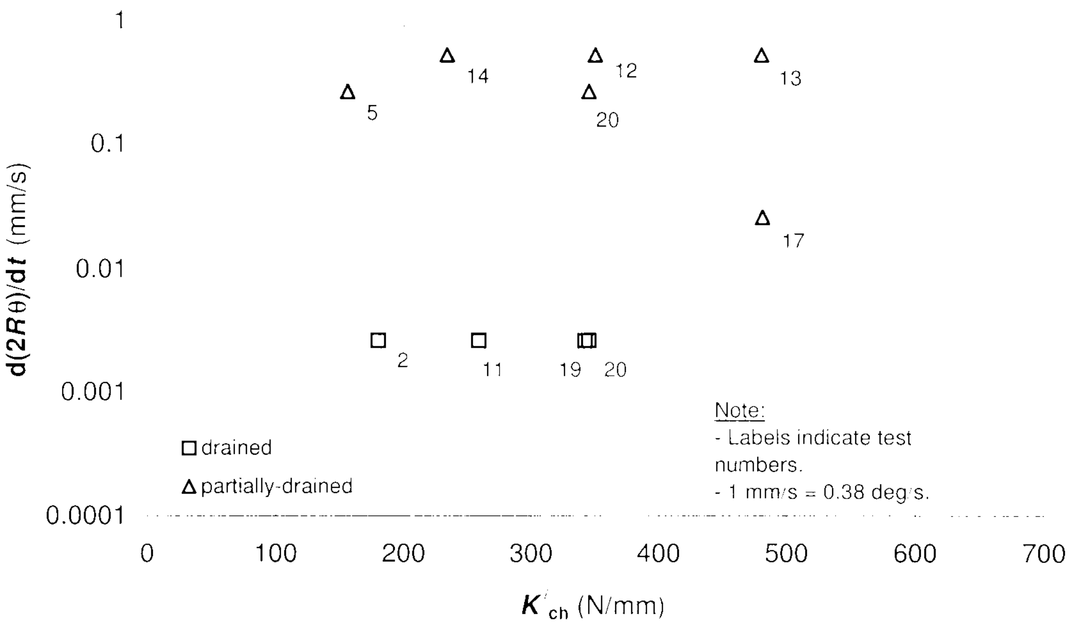


**Figure 7.13** Distribution of the displacement rate of the moment sideswipe tests with the characterisation stiffness

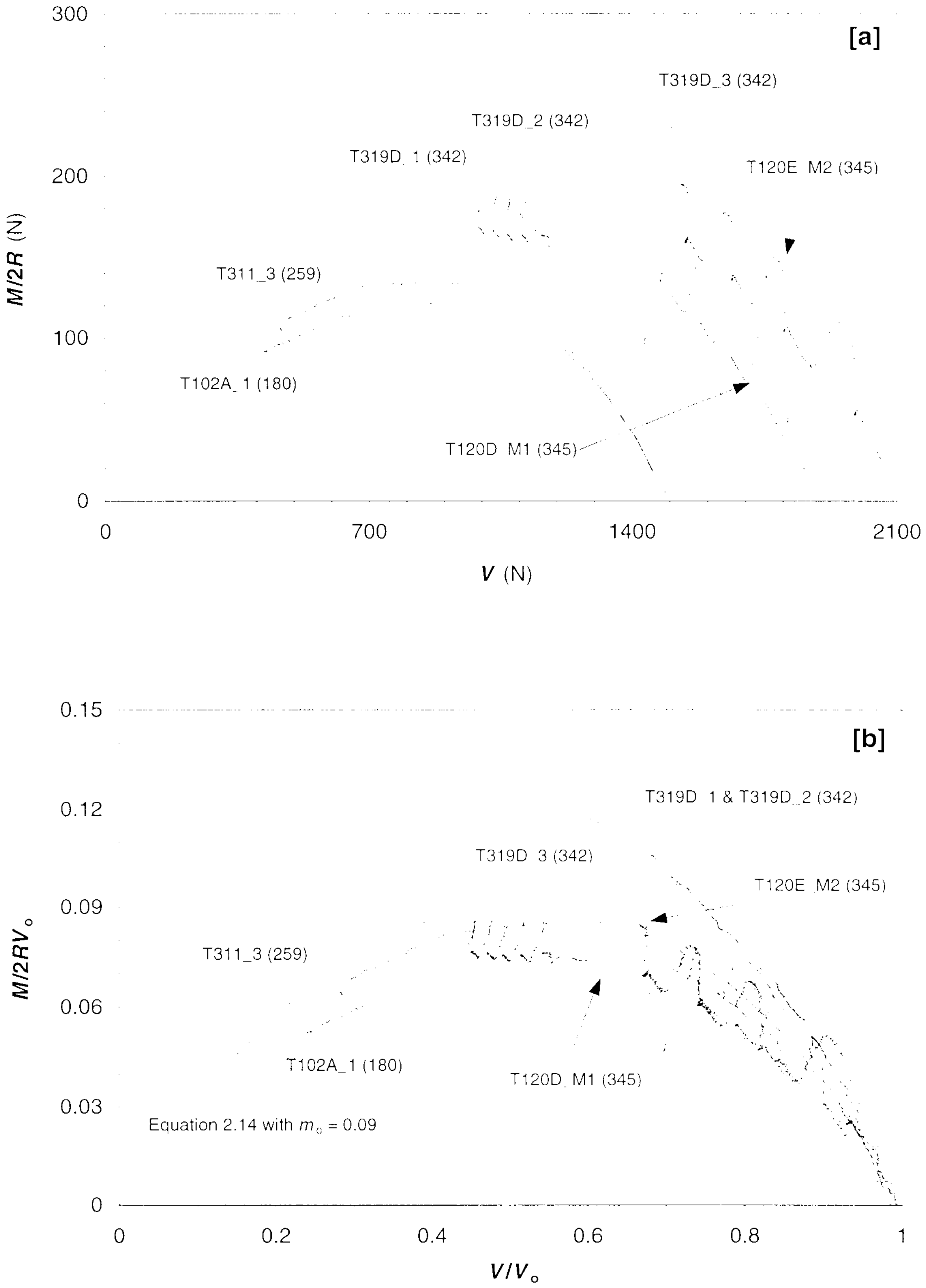


Note:
- Labels give test number and characterisation stiffness (in brackets).
- Tests T319D_2 and T120E_M2 were displaced in the negative horizontal direction.

**Figure 7.14** Drained moment sideswipe tests:
**[a]** in $V$:$M/2R$ space: and **[b]** normalised by $V_o$

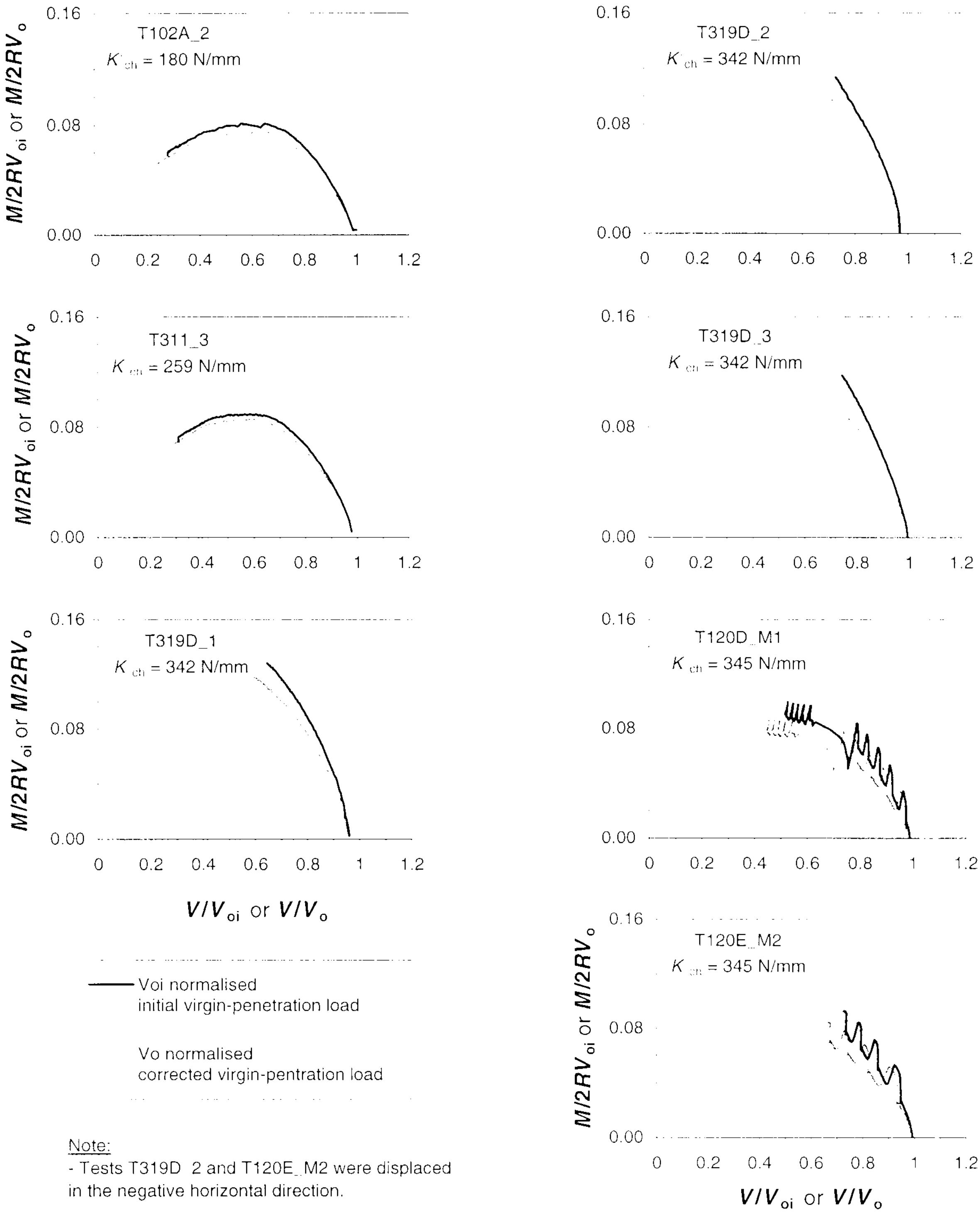


**Figure 7.15** Correction of the drained moment sideswipe tests for vertical penetration

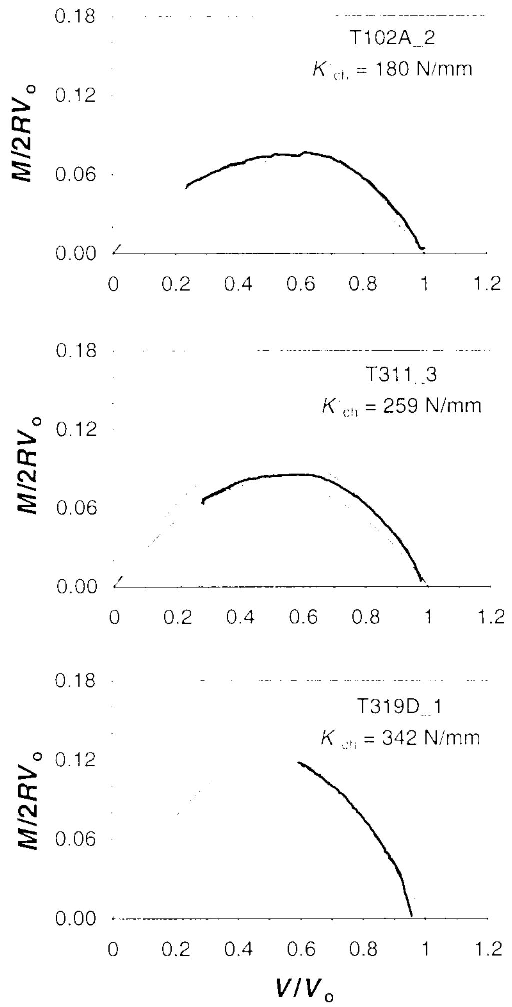


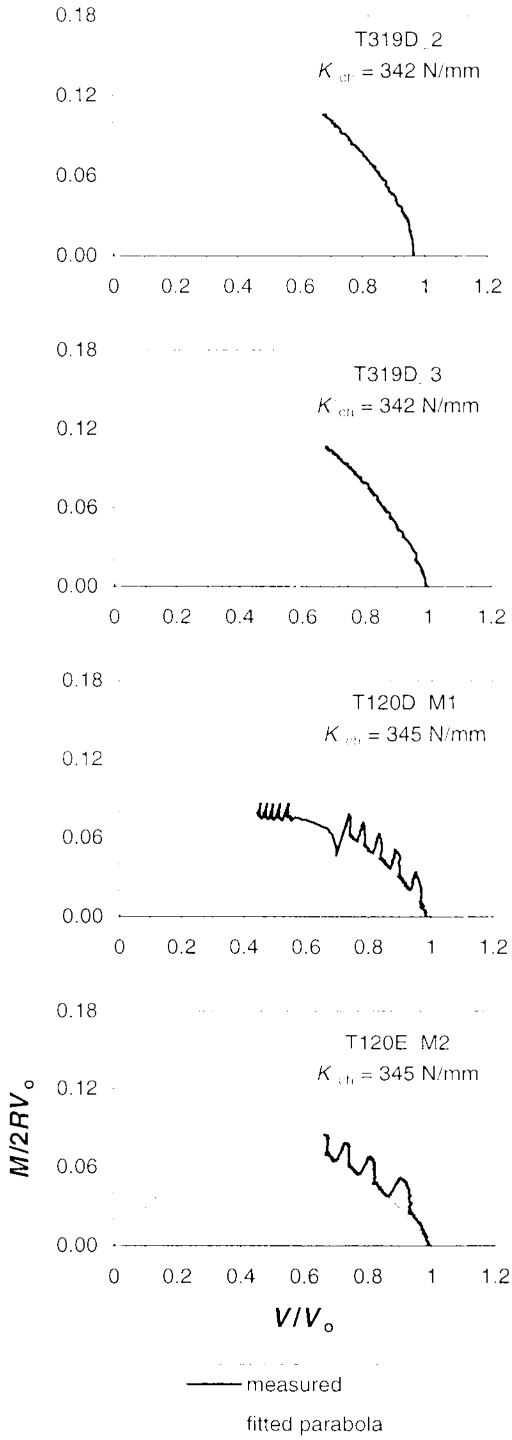


| Test | Position | $V_o$ | $V_o/V_m$ | $m_o$ |
|---|---|---|---|---|
| T102A_2 | start | 1500 | 0.27 | 0.09 |
| | end | 1752 | 0.32 | 0.07 |
| T311_3 | start | 1500 | 0.39 | 0.10 |
| | end | 1640 | 0.43 | 0.08 |
| T319D_1 | start | 1500 | 0.22 | |
| | end | 1627 | 0.24 | 0.12 |
| T319D_2 | start | 1700 | 0.25 | |
| | end | 1825 | 0.26 | 0.12 |
| T319D_3 | start | 2000 | 0.29 | |
| | end | 2200 | 0.32 | 0.12 |
| T120D_M1 | start | 1900 | 0.30 | 0.08 |
| | end | 2200 | 0.34 | |
| T120E_M2 | start | 2100 | 0.33 | 0.08 |
| | end | 2293 | 0.36 | |

Note:
- Tests T319D_2 and T120_M2 were displaced in the negative horizontal direction.

**Figure 7.16** Drained moment sideswipe tests and fitted parabolas

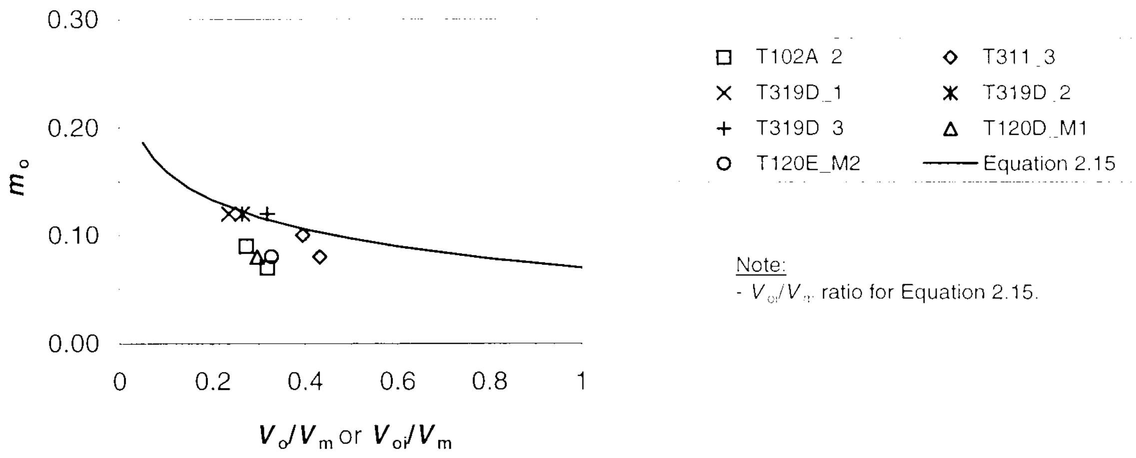


**Figure 7.17** Relationship between normalised peak moment load and $V_o/V_m$ ratio

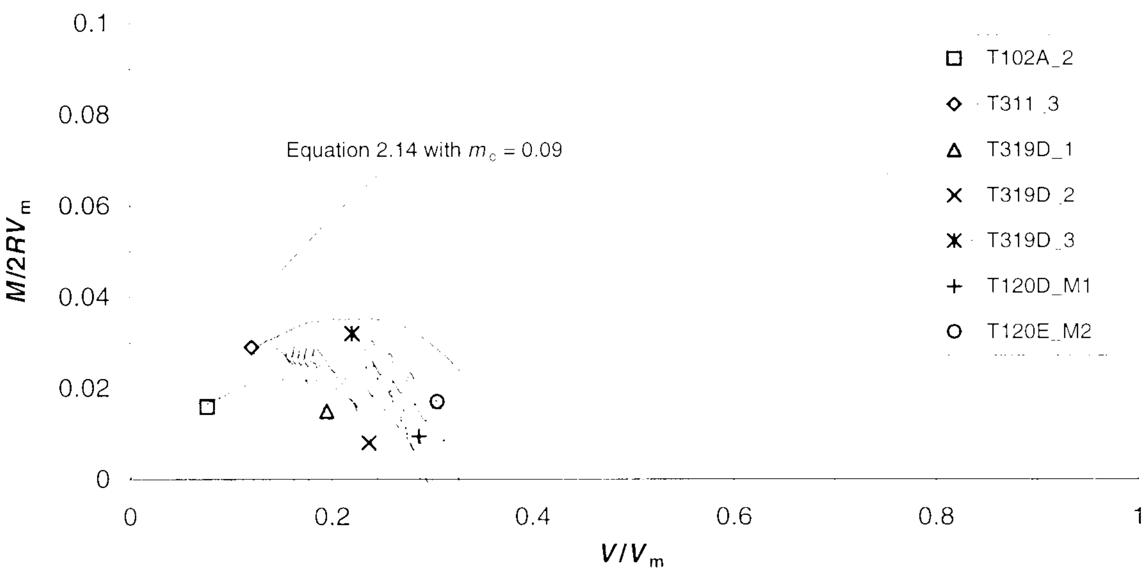


**Figure 7.18** Drained moment sideswipe tests normalised by estimated values of $V_m$

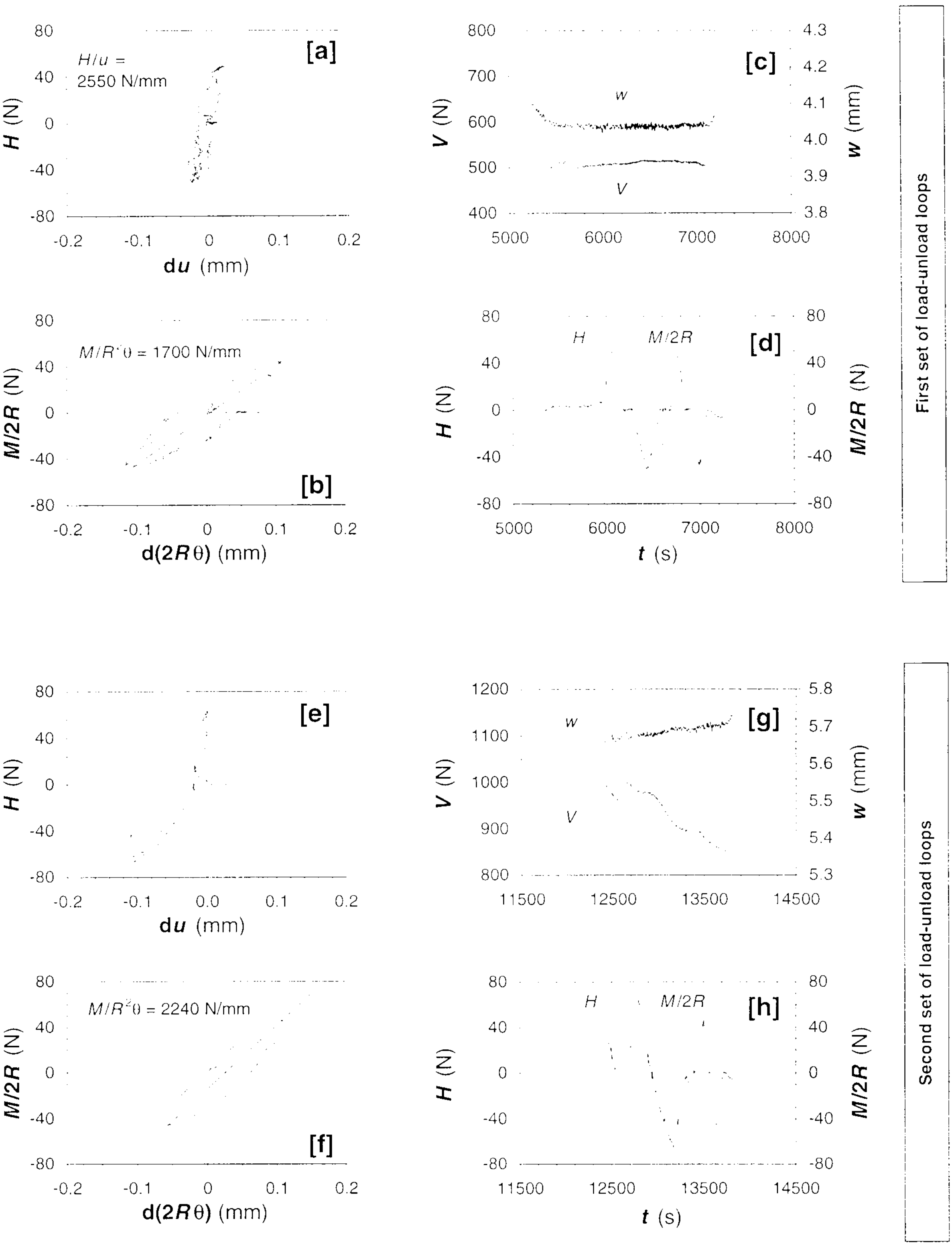


**Figure 7.19** Horizontal and moment load-unload loops and associated time histories

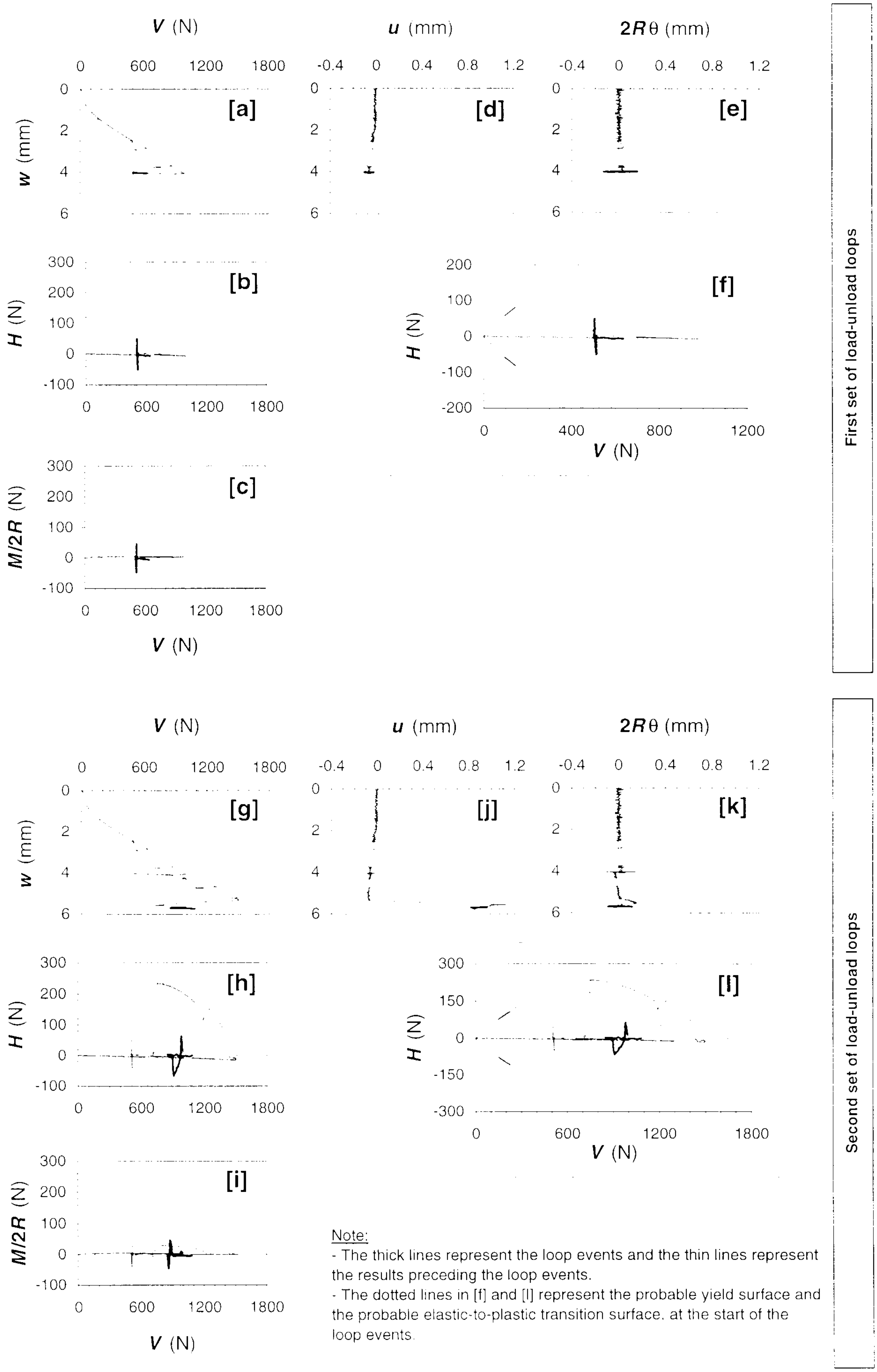


Note:
- The thick lines represent the loop events and the thin lines represent the results preceding the loop events.
- The dotted lines in [f] and [l] represent the probable yield surface and the probable elastic-to-plastic transition surface, at the start of the loop events.

**Figure 7.20** Load and deformation history of horizontal and moment load-unload loops

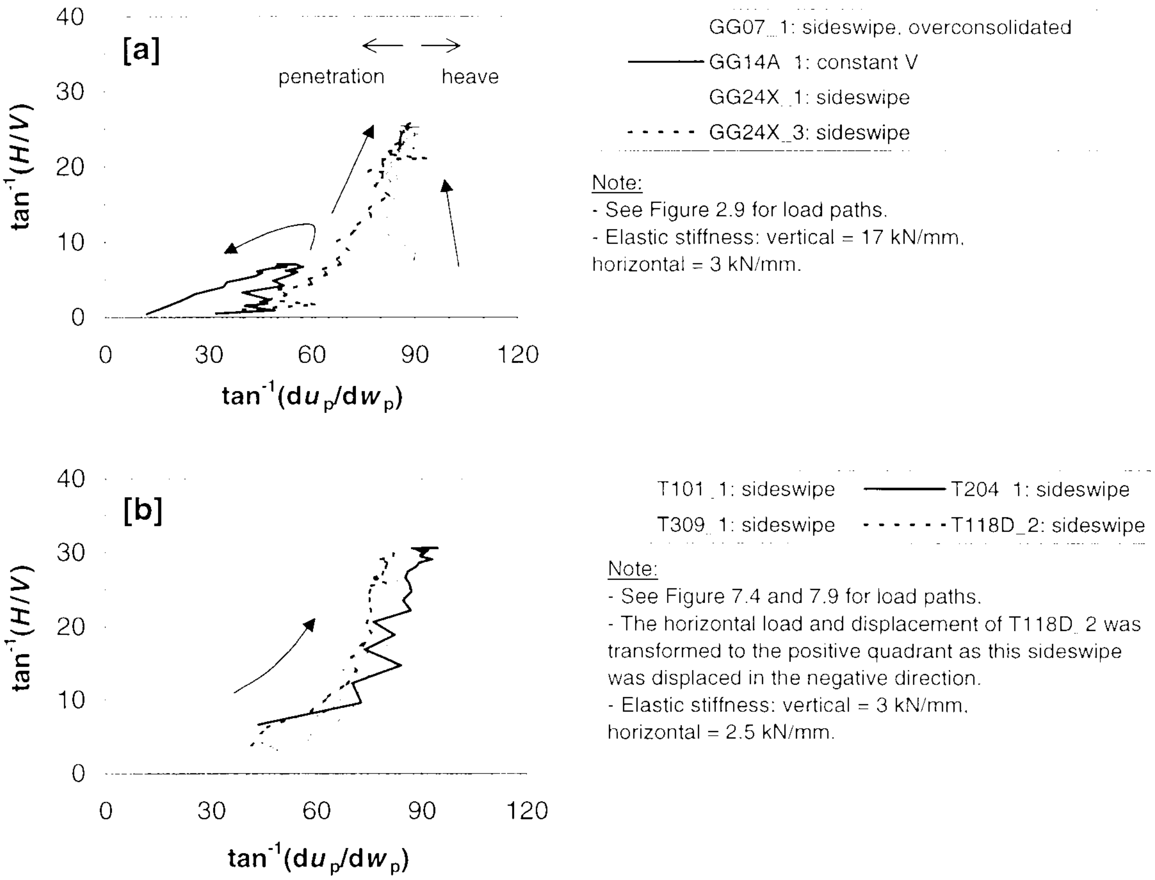


**Figure 7.21** The load and plastic displacement ratios from the horizontal sideswipe tests of this project compared with data from other tests in the literature:
**[a]** data from Gottardi and Houlsby (1995); and **[b]** data from this investigation

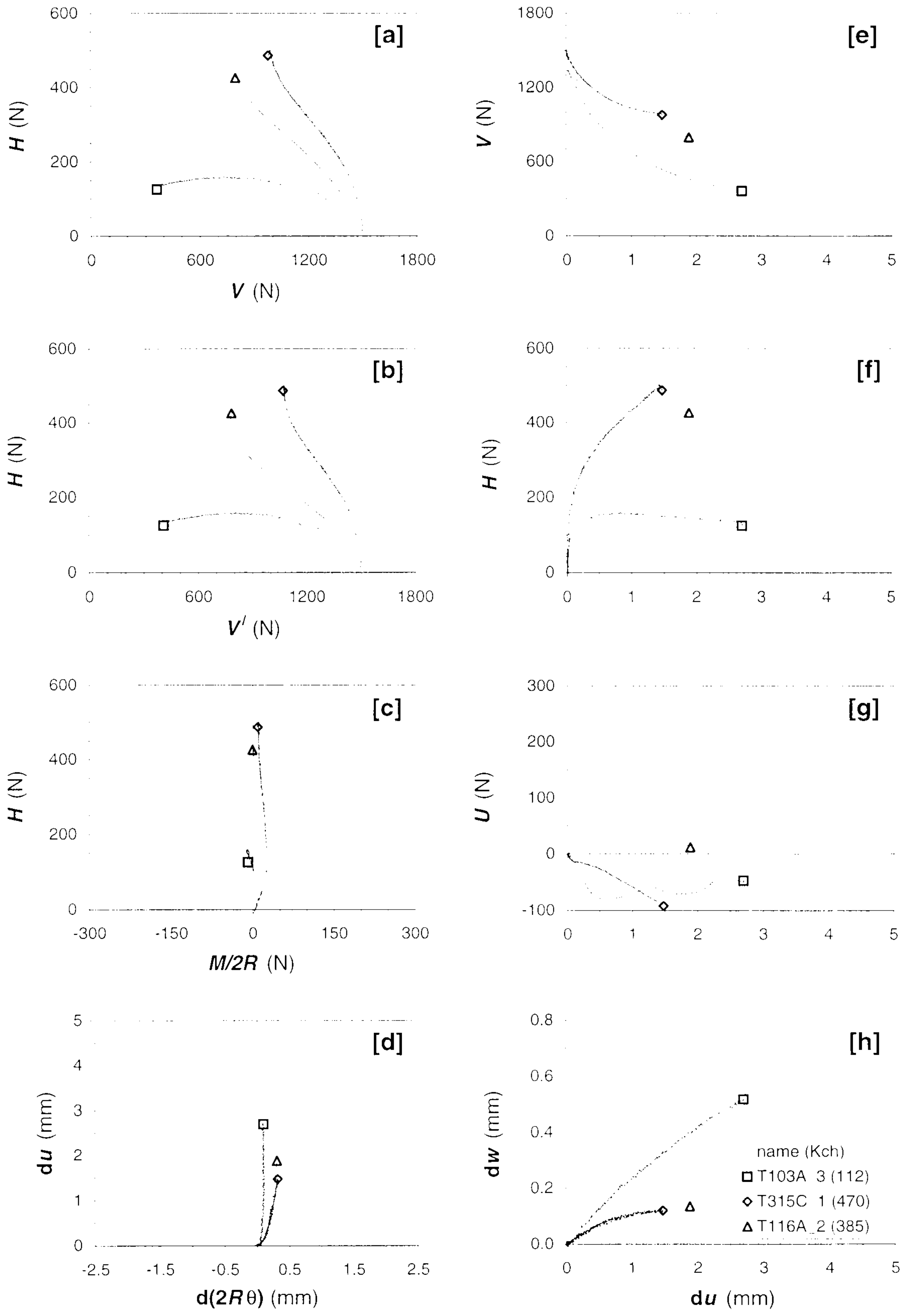


**Figure 7.22** Load and displacement interaction diagrams of the partially-drained horizontal sideswipe tests (intended $du/dt$ = 0.1 mm/s)

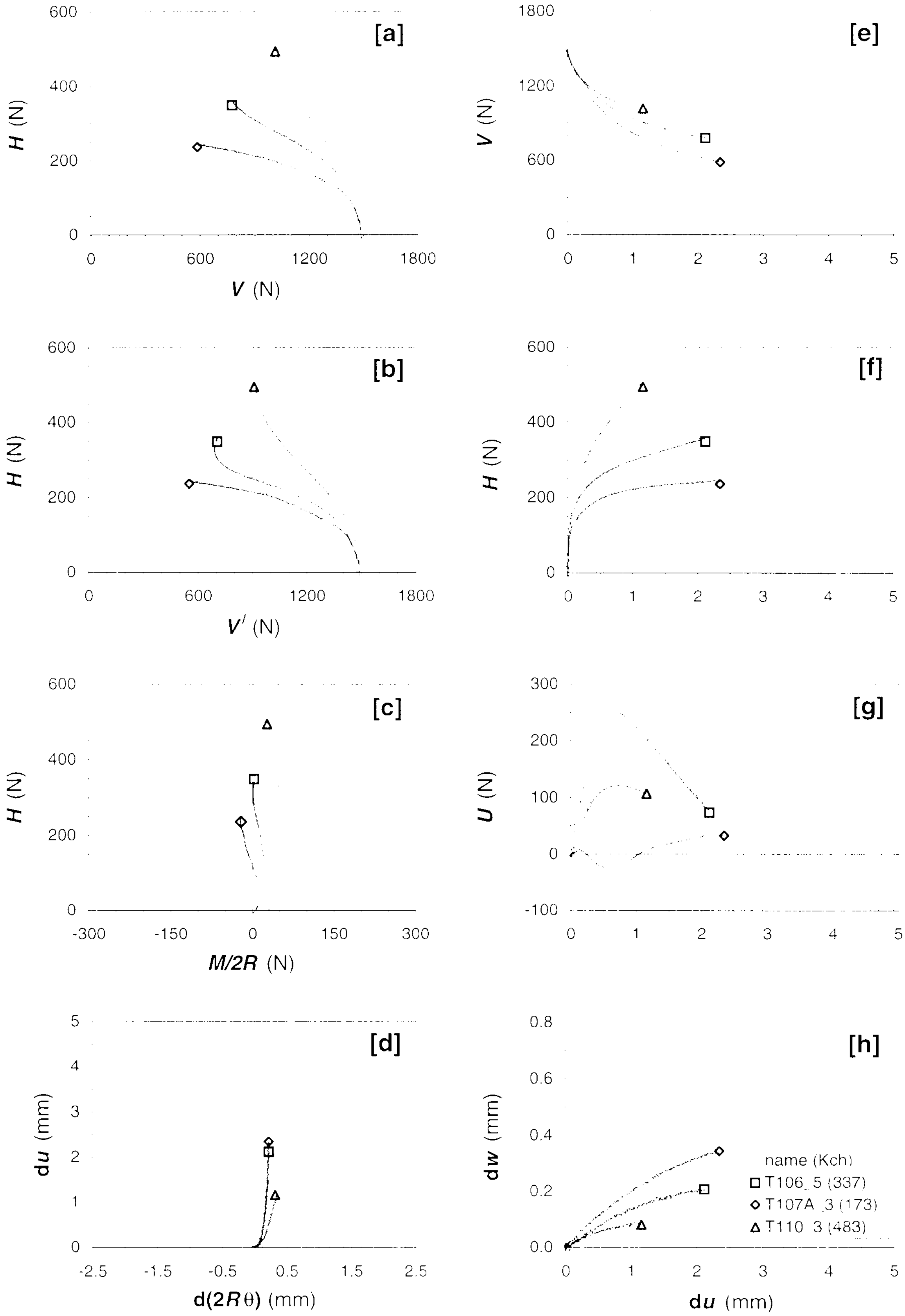


**Figure 7.23** Load and displacement interaction diagrams of the partially-drained horizontal sideswipe tests (intended $du/dt$ = 0.4 mm/s)

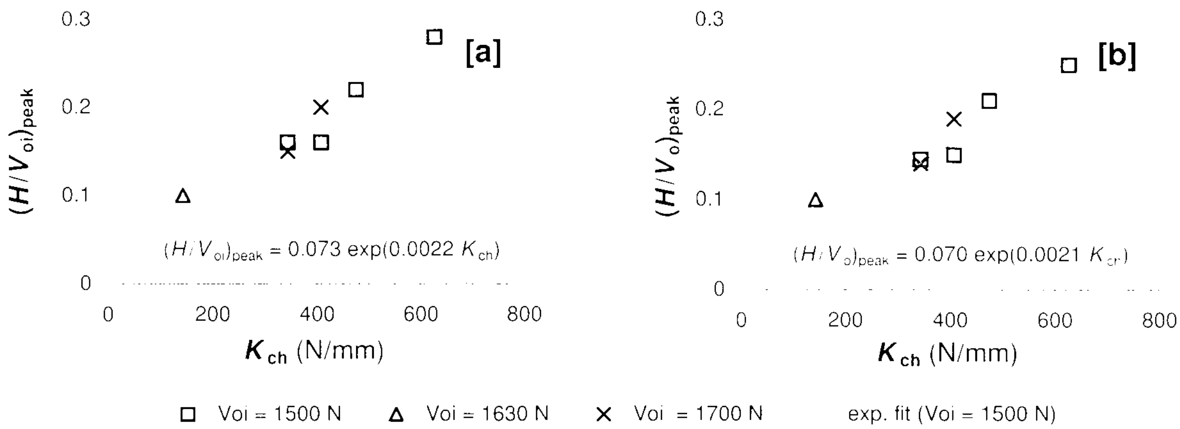


**Figure 7.24** Relationship between the normalised peak horizontal load and the characteriastion stiffness from the drained sideswipe tests:
**[a]** not corrected for vertical penetration; and **[b]** corrected for vertical penetration

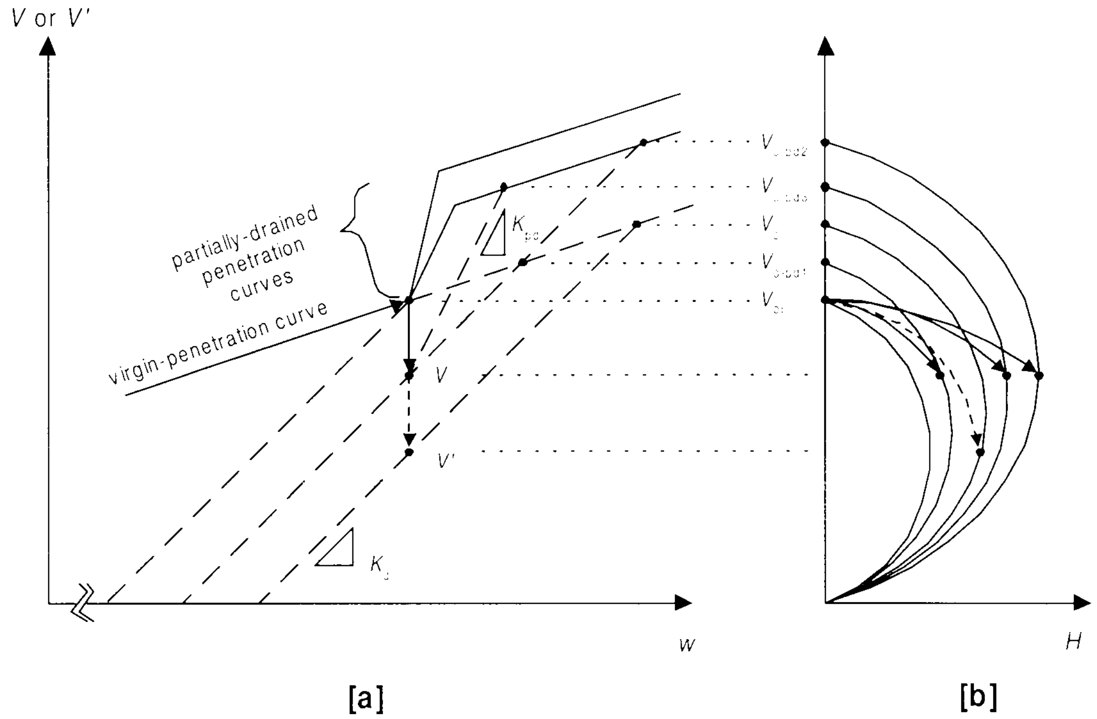


**Figure 7.25** Correction for the vertical penetration in a partially-drained sideswipe test:
**[a]** vertical load versus penetation; and **[b]** vertical load versus horizontal load

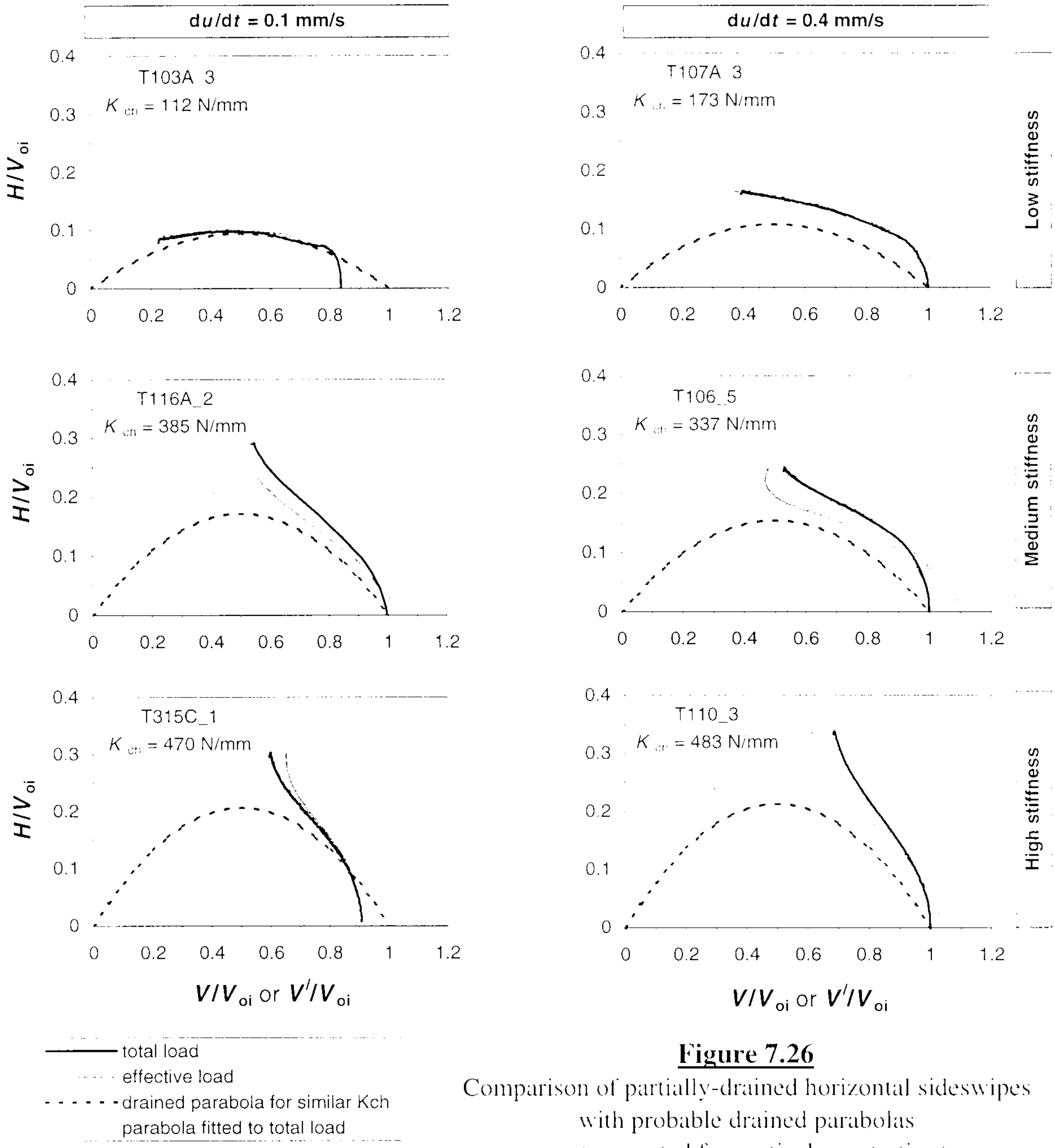


**Figure 7.26**

Comparison of partially-drained horizontal sideswipes with probable drained parabolas (not corrected for vertical penetration)

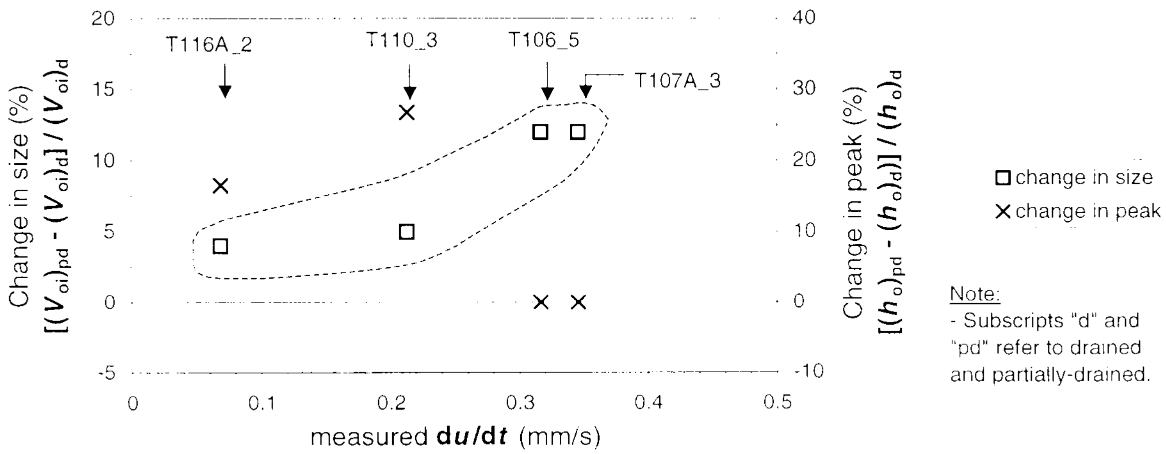


**Figure 7.27** The difference between the drained horizontal sideswipes and the parabolas fitted to the partially-drained sideswipes

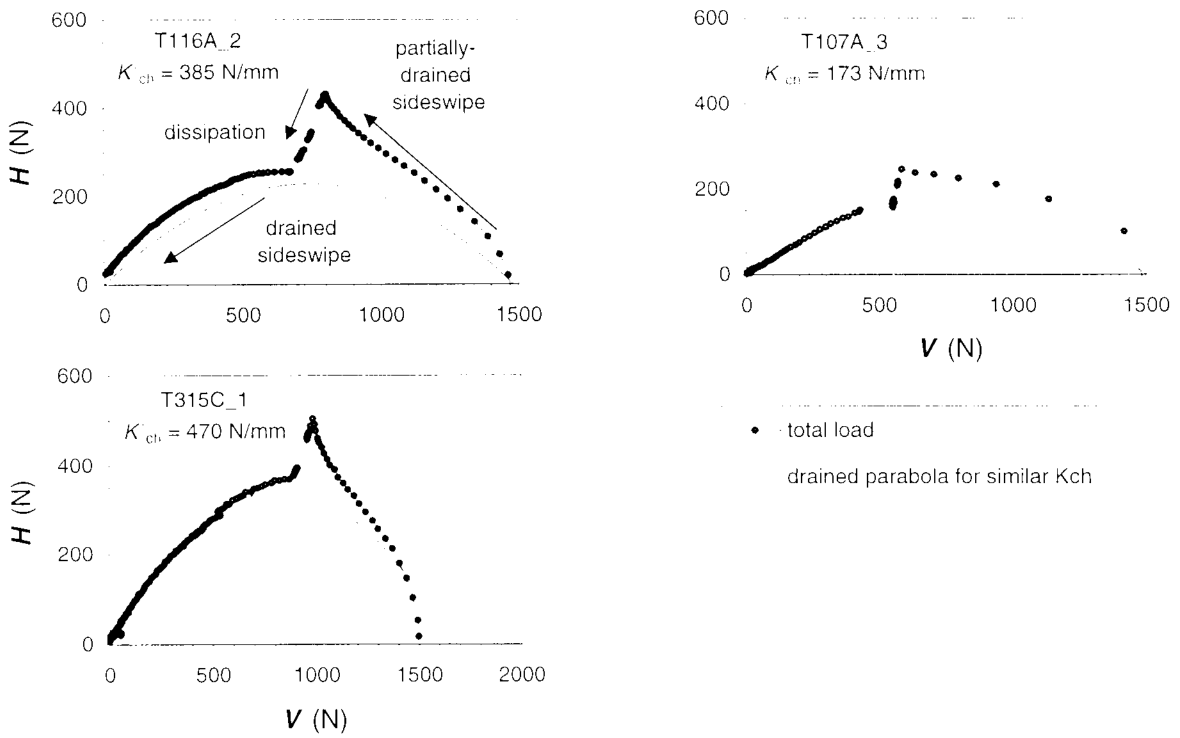


**Figure 7.28** Load paths after some of the partially-drained horizontal sideswipe tests

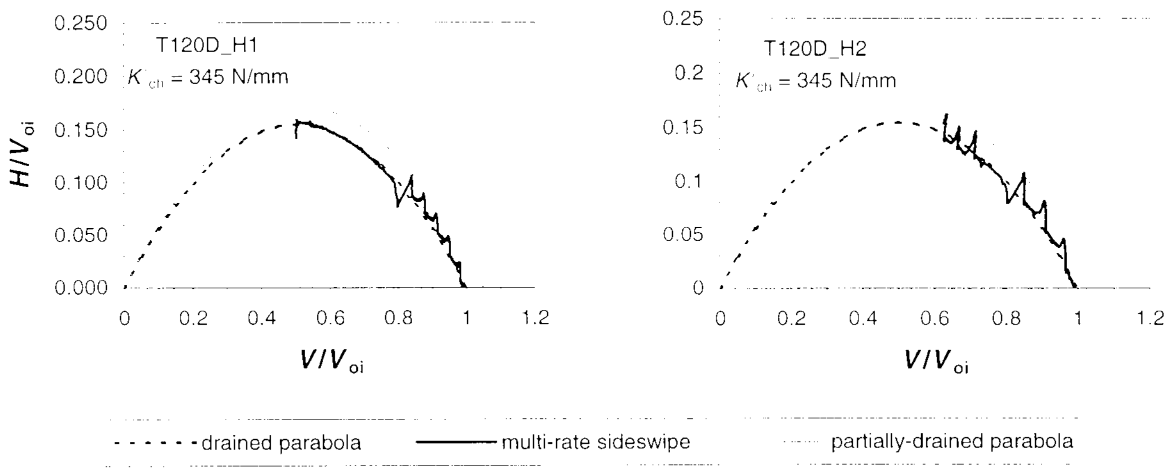


**Figure 7.29** The multi-rate horizontal sideswipe tests

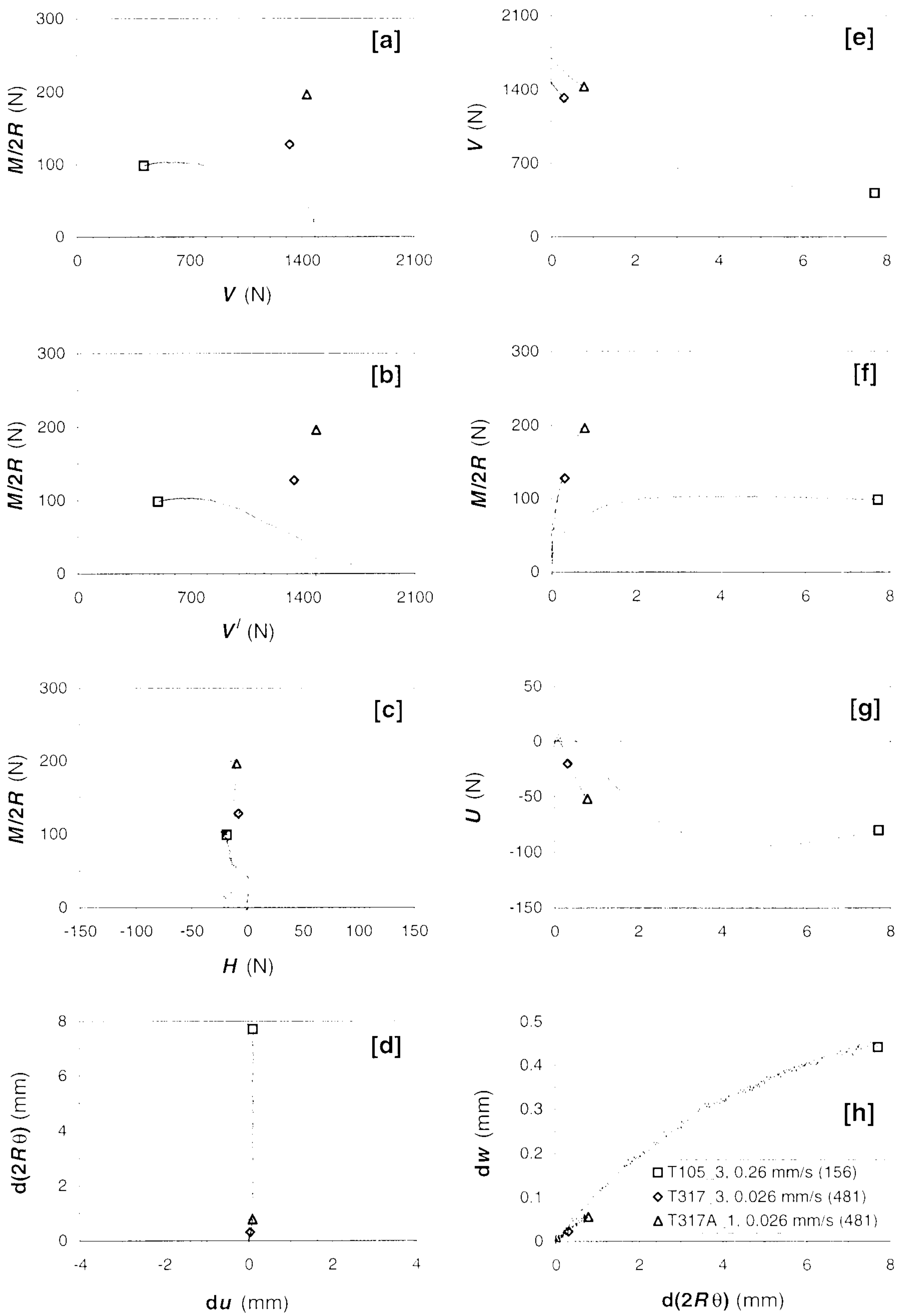


**Figure 7.30** Load and displacement interaction diagrams of the partially-drained moment sideswipe tests (intended $d(2R\theta)/dt$ = 0.26 mm/s and 0.026 mm/s)

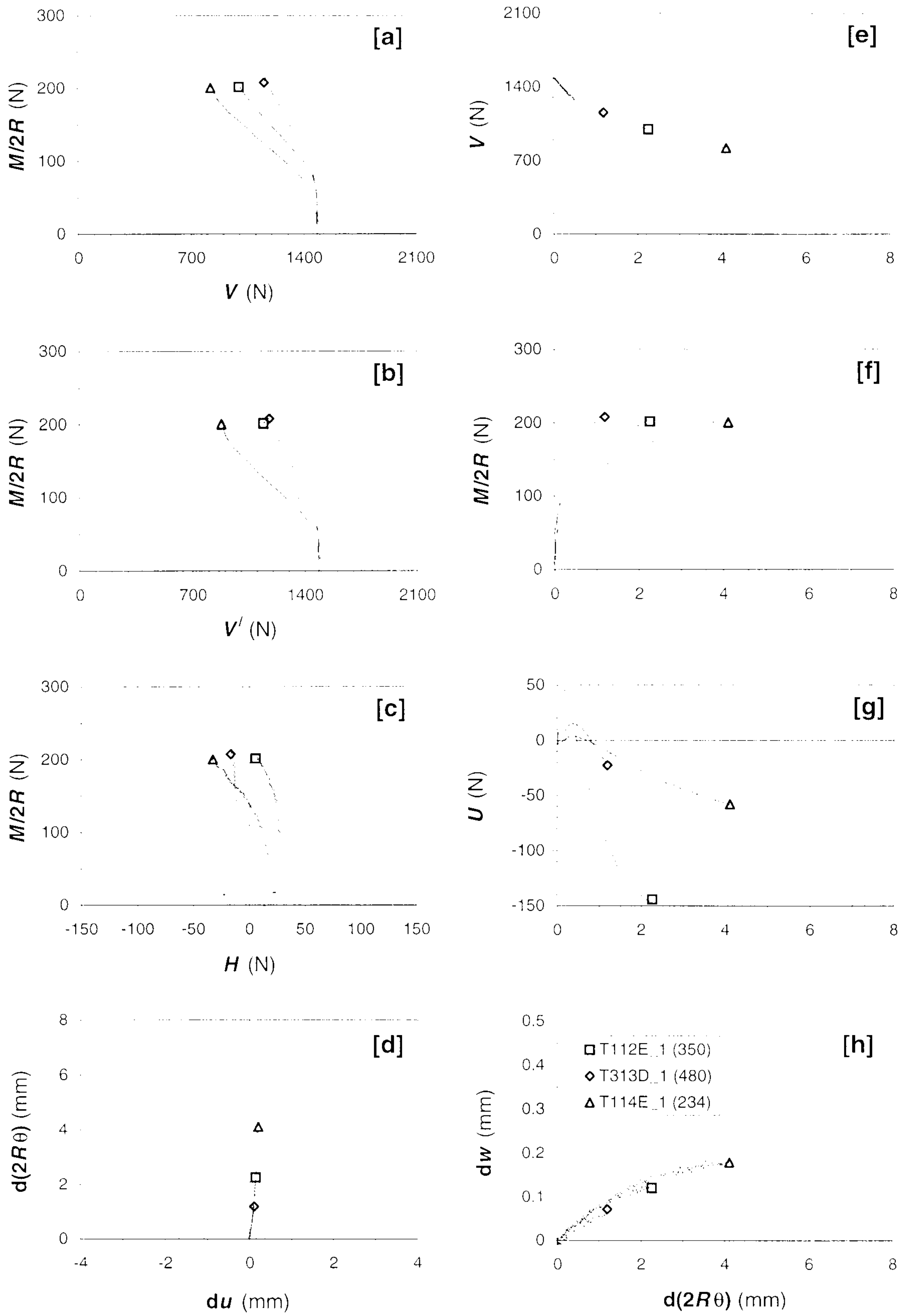


**Figure 7.31** Load and displacement interaction diagrams of the partially-drained moment sideswipe tests (intended $d(2R\theta)/dt = 0.524$ mm/s)

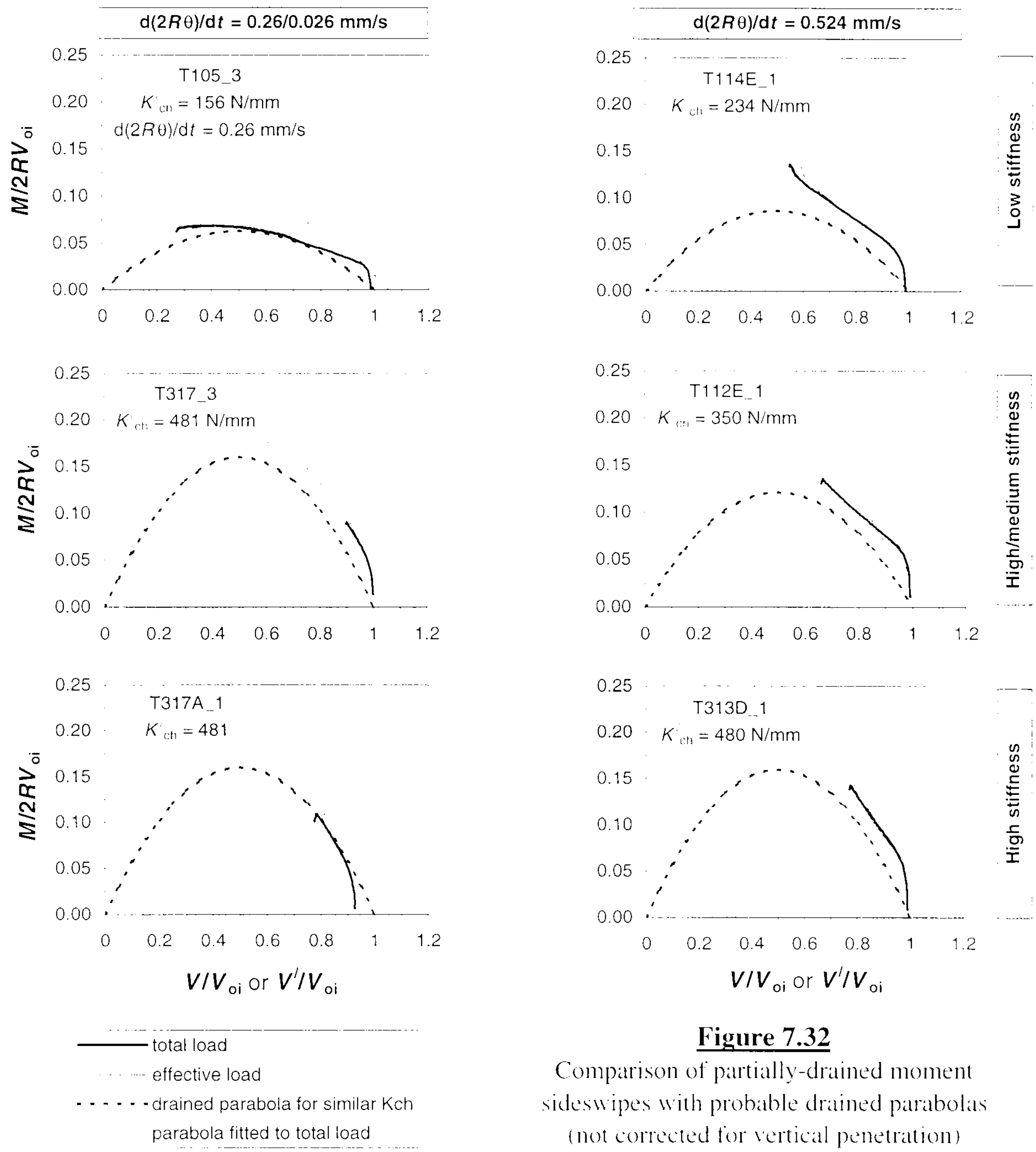


**Figure 7.32**
Comparison of partially-drained moment sideswipes with probable drained parabolas (not corrected for vertical penetration)

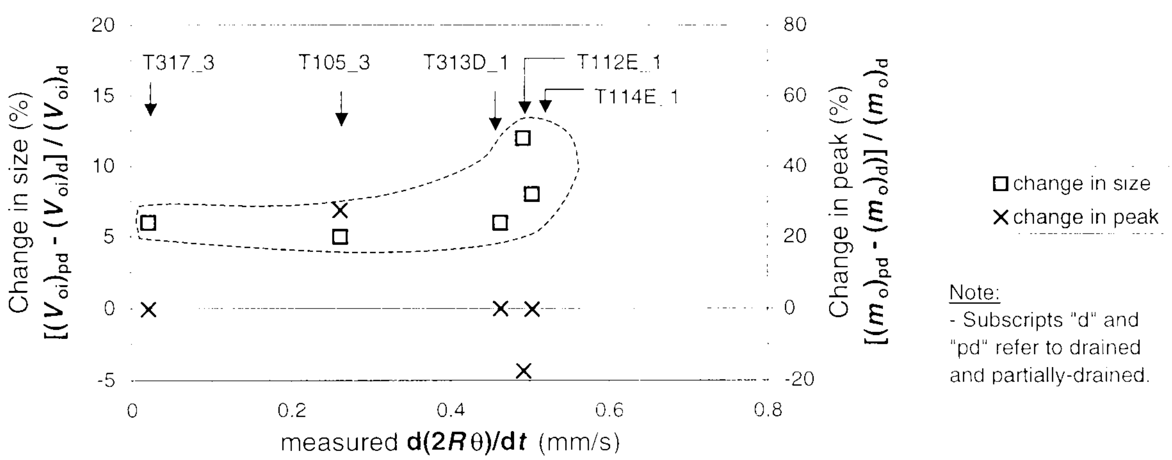


**Figure 7.33** The difference between the drained moment sideswipes and the parabolas fitted to the partially-drained sideswipes

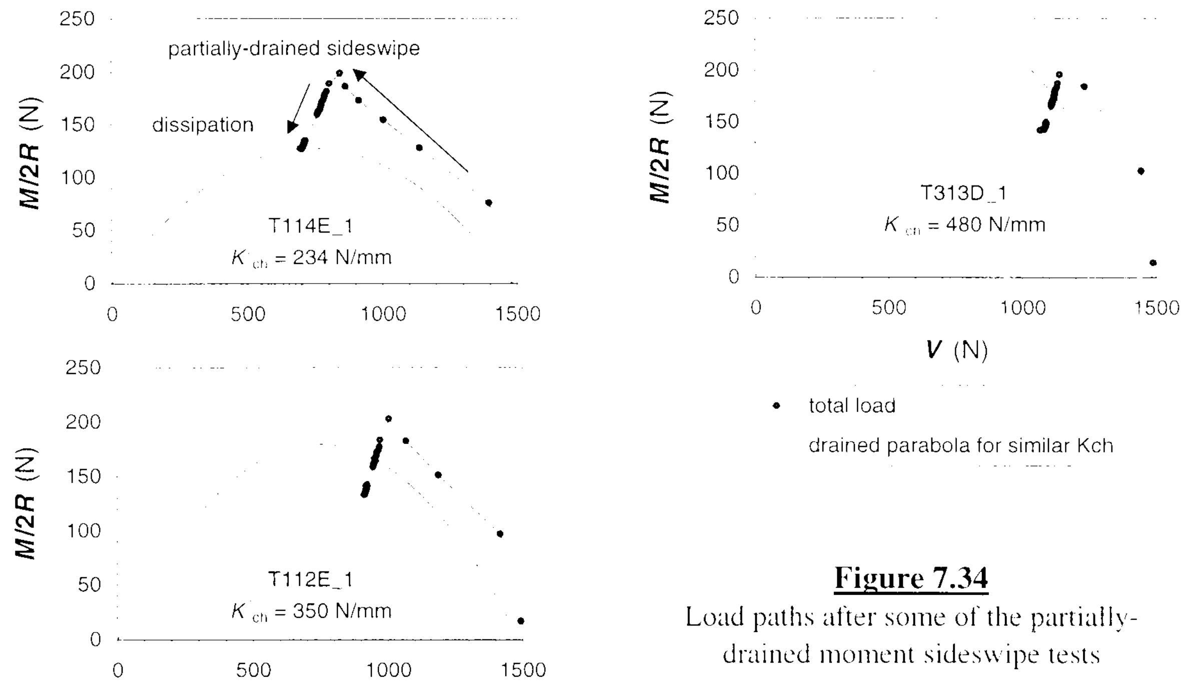


**Figure 7.34**
Load paths after some of the partially-drained moment sideswipe tests

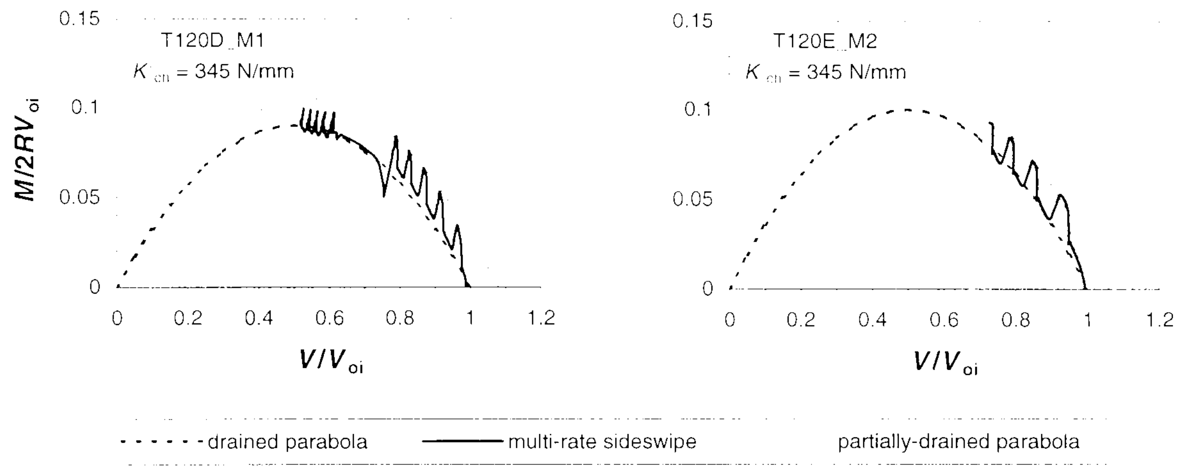


**Figure 7.35** The multi-rate moment sideswipe tests

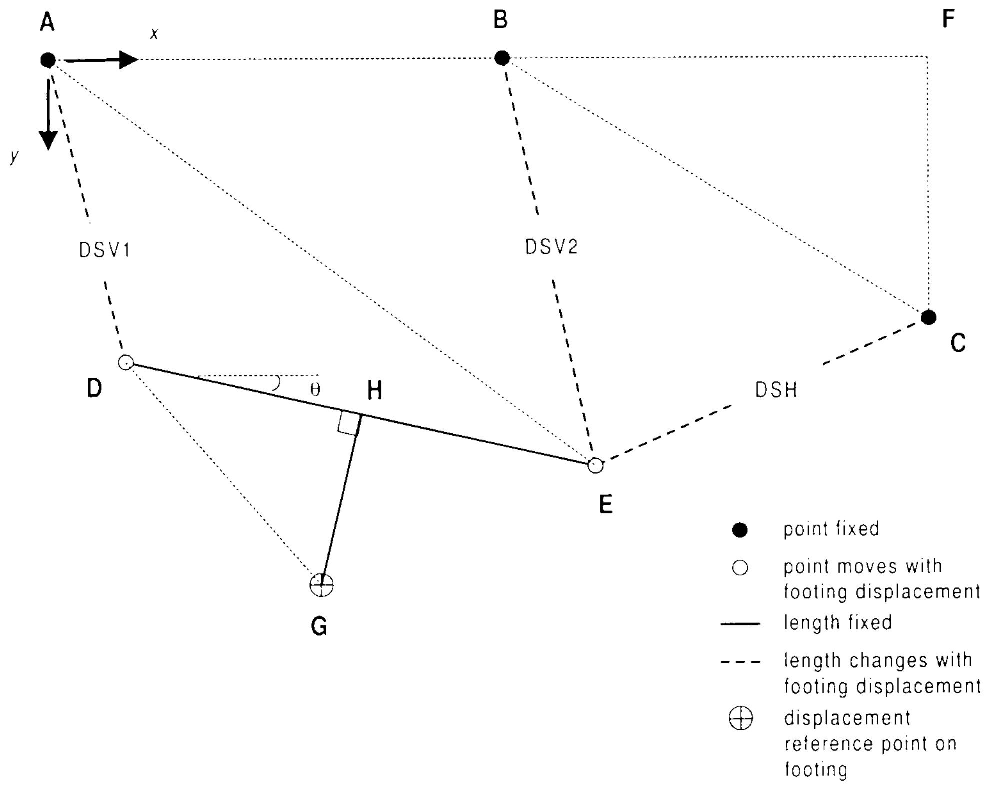


**Figure B.1** Parameters used in the derivation of the footing displacements from the small LVDTs